Title

TIME RESOLVED ELECTRON PARAMAGNETIC RESONANCE STUDIES ON THE LIGHT REACTIONS OF PHOTOSYSTEM 1

Author

McCracken, J.L.

Publication Date

1983-06-01

Lawrence Berkeley Laboratory
UNIVERSITY OF CALIFORNIA

CHEMICAL BIODYNAMICS DIVISION

TIME RESOLVED ELECTRON PARAMAGNETIC RESONANCE STUDIES ON THE LIGHT REACTIONS OF PHOTOSYSTEM 1

J.L. McCracken
(Ph.D. Thesis)

June 1983

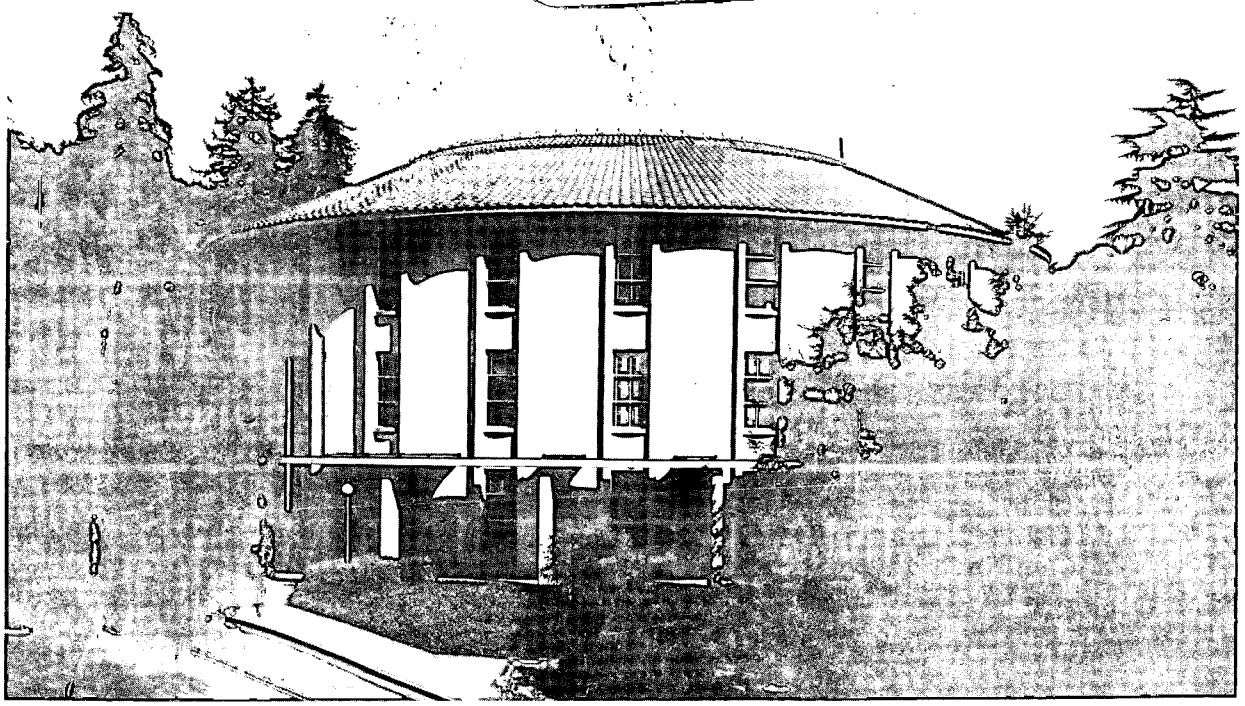

Prepared for the U.S. Department of Energy under Contract DE-AC03-76SF00098

DISCLAIMER

LBL-16251

TIME RESOLVED ELECTRON PARAMAGNETIC RESONANCE STUDIES ON THE LIGHT REACTIONS OF PHOTOSYSTEM 1

John L. McCracken
(Ph.D. Thesis)

Lawrence Berkeley Laboratory
University of California
Berkeley, California 94720

June 1983

This work was supported by the Office of Energy Research, Office of Basic Energy Sciences, Biological Energy Research Division of the U.S. Department of Energy under Contract Number DE-AC03-76SF00098.

TABLE OF CONTENTS

ABBREVIATIONS

A_0, A_1	primary electron acceptors of photosystem 1
ATP	adenosine triphosphate
CIDEP	chemically induced dynamic electron polarization
Chl a	chlorophyll a
DMSO	dimethyl sulfoxide
DPPH	diphenyl picryl hydrazyl
EDTA	ethylene diamine tetraacetic acid
EPR	electron paramagnetic resonance
Fd	ferredoxin
FWHM	full-width-half-maximum
G	gauss
$\hbar$	Planck's constant divided by 2π
P-700	primary electron donor of photosystem 1
PAS	principle axis system
PS1	photosystem 1
PS2	photosystem 2
Tris	Tris (hydroxymethyl) amino methane
X	secondary electron acceptor of photosystem 1

ACKNOWLEDGEMENTS

It is a pleasure to thank some of the people who have made a significant contribution to the work presented in this thesis.

My research director for the past five years has been professor Ken Sauer. I have benefited greatly from his considerable abilities as a scientist and a teacher. I thank him for giving me the freedom to pursue my own ideas, and for his support and encouragement during the course of this work. Thanks are also due to Dr. Melvin Klein of the Laboratory of Chemical Biodynamics for helping me to learn about magnetic resonance theory and instrumentation. His ideas concerning my research project always proved beneficial, even though it sometimes took weeks for me to fully understand them.

I also wish to thank Harry Frank who devoted much of his time to getting me started on research at Berkeley. Special thanks are due to Rich Friesner and Mary Blackwell for their help in learning magnetic resonance theory.

I would like to acknowledge the staff of the Laboratory of Chemical Biodynamics for their help over the past few years. I thank Gary Smith and Mike Press for building much of the electronic equipment that I worked with, and for their willingness to teach me about electronics. Additional help was provided by Dick O'Brien, Wally Erwin, Everett Harvey, Ken Wiley, Sheldon Wong, Beth Klingel, Lois Soule,

and many others. I also want to thank Howard Wood of the chemistry department for teaching me about machine tools and for his advice on the many machine shop projects that I undertook.

Many fellow graduate students and post-docs have also contributed to this work. They are D. Britt, D. Goodin, M. Boska, J. Casey, T. Pratum, W. Shih, J. Nairn, W. Haehnel, M. Crowder, R. Goldstein, K. Karukstis, P. Reisberg, F. Magnotta, G. Karczmar, C. Oshiro, and A. McGuire.

I would also like to thank my Mom and Dad for their love, support and encouragement over the past 26 years.

Most of all, I thank my wife, Gayle, for her love, understanding, and companionship during the past five years. Her contributions to this thesis are extensive and greatly appreciated.

This work was supported by the Office of Energy Research, Office of Basic Energy Sciences, Biological Energy Research Division of the U.S. Department of Energy under Contract Number DE-AC03-76SF00098.

TIME RESOLVED ELECTRON PARAMAGNETIC RESONANCE STUDIES ON THE LIGHT REACTIONS OF PHOTOSYSTEM 1

by

John L. McCracken

ABSTRACT

The investigations reported in this thesis involve time resolved EPR studies on the light-driven electron transport system of green plants known as photosystem 1. The primary goal of this work was to characterize the EPR properties of the primary electron acceptors of this photosystem and to learn about the nature of their interactions with the primary electron donor, P-700. Light excitation of plant material under reducing conditions at 10K gives rise to transient, spin-polarized EPR signals in the g 2.0 region. The lineshapes of these signals are dependent on the reduction state of photosystem 1 and on the orientation of the membrane bound photosystem in the DC magnetic field of the EPR spectrometer.

A model is presented that successfully predicts the spin-polarized lineshapes for both random and ordered samples. Some features of this model are: (a) there are two electron acceptor species that act in series between P-700 and X (a secondary electron acceptor also known as A_2), so that the organization of photosystem 1 can be viewed as P-

700 A_0 A_1 X ($Fd_{B,A}$); (b) the spin-spin interaction between P-700$^+$ and A_0^- is anisotropic involving electron-electron magnetic dipole coupling and isotropic exchange; and (c) spin polarization develops on A_1^- by a polarization transfer mechanism as a consequence of electron transfer from A_0^- to A_1. Use of this model to computer simulate the data provided information concerning the magnetic properties of A_0^-, A_1^-, and the spin-spin interactions between P-700$^+$ and these acceptor anions. Also, the orientation dependence of these magnetic parameters was analyzed, and information concerning the structure of the photosystem 1 apparatus relative to the thylakoid membrane normal was obtained.

In addition to analyzing the lineshape of spin-polarized, time-resolved EPR signals, analysis of the signal dynamics was carried out. Magnetic field modulation affects the dynamics of these signals and complicates the analysis. These complications may make analysis of the dynamics of spin-polarized EPR signals, obtained under conditions of magnetic field modulation and inhomogeneous broadening, intractable.

CHAPTER 1

INTRODUCTION TO PHOTOSYNTHESIS AND PHOTOSYSTEM 1 OF GREEN PLANTS

Photosynthesis is a process by which plants, and some bacteria and algae can utilize the energy from light to do the chemistry necessary to sustain life. The overall chemical equation for green plant photosynthesis is:

$$6\ CO_2 + 6\ H_2O \xrightarrow{\text{light}} C_6H_{12}O_6 + 6\ O_2$$

where the light energy is ultimately stored as chemical energy in the form of simple sugars represented by $C_6H_{12}O_6$. Most of the organic chemistry involved in the assimilation of CO_2 to form simple sugars is carried out by the so-called dark reactions. The reactions responsible for the conversion of light energy to chemical potential energy (stored as ATP or NADPH) are known as the light reactions.

1.1 The Light Reactions

In green plant photosynthesis there are two light reactions or photosystems. These photosystems are light-driven electron transport systems that are responsible for shuttling electrons from H_2O, to ultimately, $NADP^+$. A

convenient way to view the bioenergetics of this process is through the "Z-scheme" shown in Fig. 1-1 [1,2]. As this figure shows, photosystem 2 is associated with the water splitting or oxygen evolving capabilities of the photosynthetic apparatus, while photosystem 1 is primarily involved in the reduction of $NADP^+$ to NADPH. The constituents of these two photosystems are not just floating about inside plant cells, but are contained along with the rest of the photosynthetic apparatus in organelles called chloroplasts. Further, the components of the electron transport systems are organized into discrete units and bound within intracellular membrane sacks called thylakoids. An electron micrograph of a chloroplast is shown in Fig. 1-2; it shows an outer membrane defining the boundary of the organelle and the extensive network of thylakoid membranes. Figure 1-2 also shows that the thylakoid membranes are organized into stacked regions (known as grana) and unstacked regions (stroma).

There is evidence that the stromal regions are enriched in PS1, while the grana appear to contain most of the PS2 apparatus and very little PS1 [3,4]. Also, the stoichiometry between PS1 and PS2 is not 1:1. The ratio of PS2 to PS1 can vary from about three to less than unity depending on the developmental stage of the organelle and the conditions under which the plant is grown [5]. These last two findings point out that the Z-scheme picture of two light reactions acting in series is not completely correct

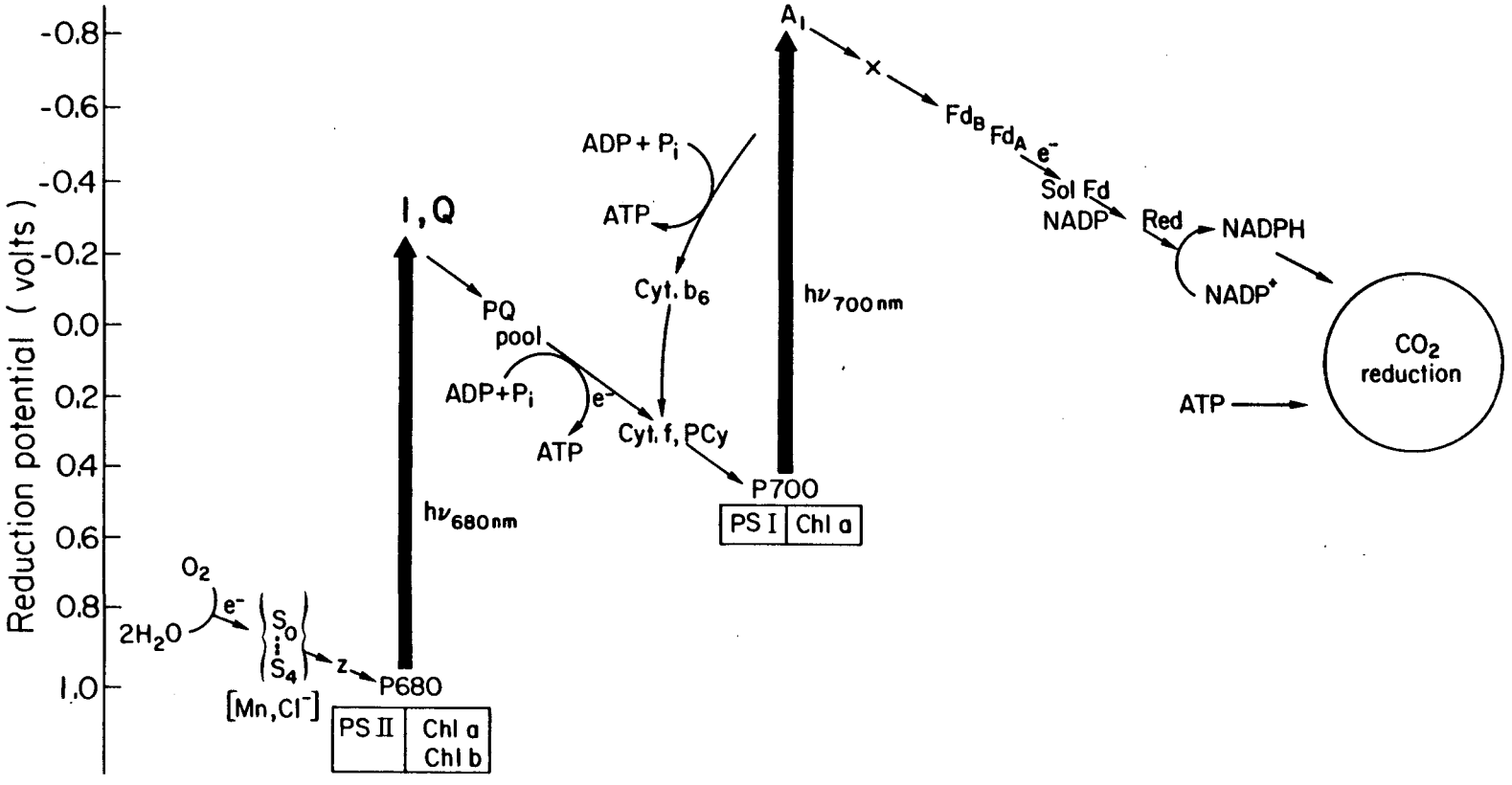

XBL 797-4937A

Fig. 1-1. The Z-scheme for electron transport in green plant photosynthesis.

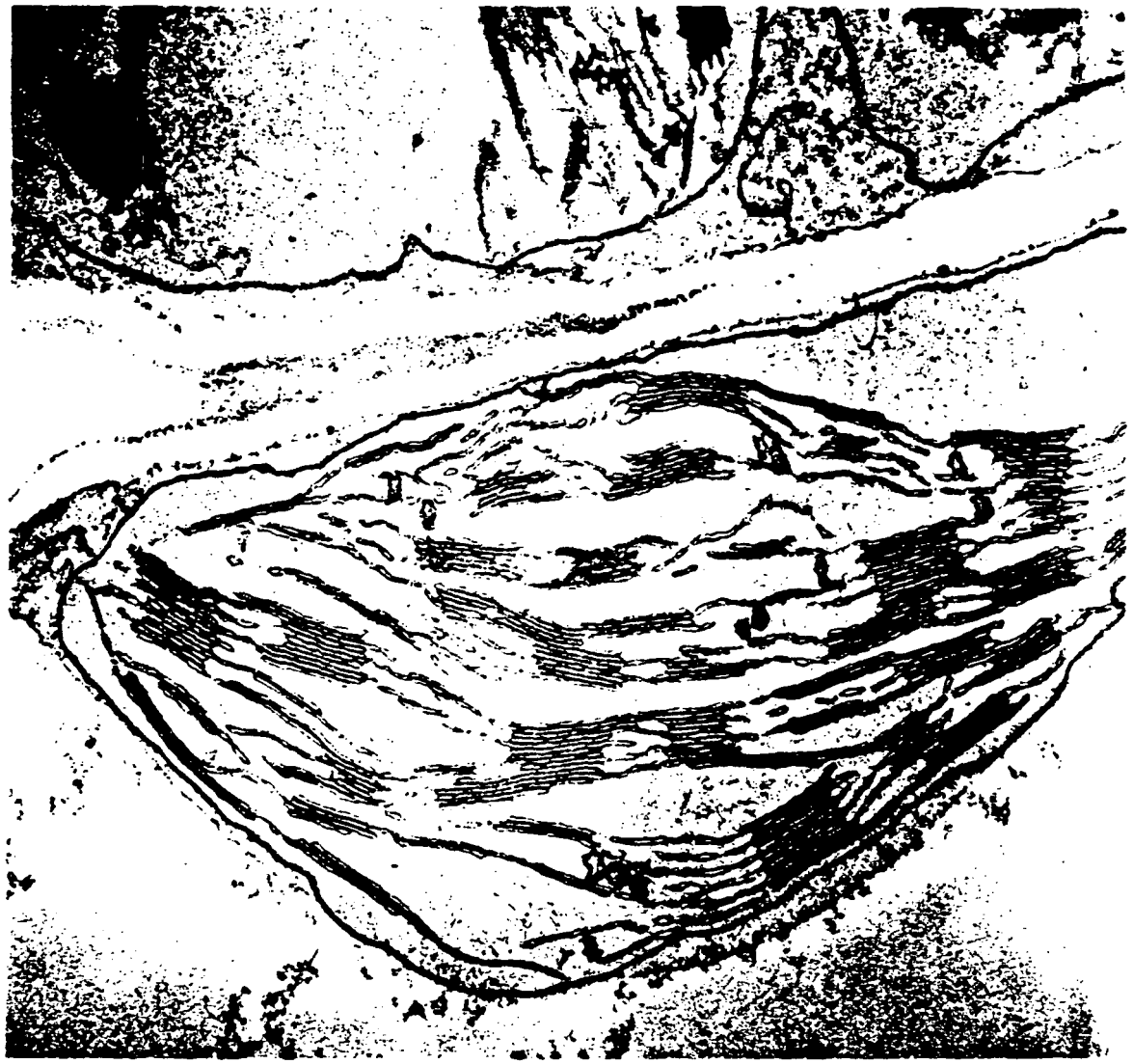

Fig. 1-2. Electron micrograph of a chloroplast displaying the arrangement of the thylakoid membranes (from R.B. Park, in "Plant Biochemistry," eds. Bonner, J. and Varner, J.E., Academic Press, NY, p.124, 1965).

and that the two photosystems function with less communication than the Z-scheme implies.

1.2 Photosystem 1

The research presented in this thesis involves studies of the light reactions of photosystem 1. The current view of the organization of PS1 electron transport is P-700 A_1 X ($Fd_{B,A}$), where P-700 is the primary electron donor of PS1; A_1, the primary electron acceptor; and X, Fd_B and Fd_A are stable secondary electron acceptors. The electron transport process in this system begins with the absorption of light by an array of antenna molecules consisting of various chlorophyll proteins. The excitation energy received by these antenna is transfered efficiently to the primary electron donor, P-700. Upon receiving this excitation energy, P-700 is excited to an excited electronic state, and within a few picoseconds it transfers an electron to A_1 [6]. The state of the PS1 reaction center is then $P\text{-}700^+$ A_1^- X ($Fd_{B,A}$). Subsequent electron transfer reactions serve to transfer the electron sequentially from A_1^- to X and from X^- to the bound Fe-S centers, Fd_B and Fd_A.

The function of PS1 in the chloroplast involves the reduction of $NADP^+$ to NADPH and the generation of ATP. PS1 plays a role in generating ATP by creating a trans-membrane electrochemical gradient during its normal operation. To accomplish this the electron donor and acceptors that comprise the PS1 reaction center have to be arranged in some

directional fashion across the membrane. A model for how the PS1 reaction center might be situated in the thylakoid membrane is shown in Fig. 1-3. It is similar to the model put forth by Sauer, et al. [7] and by Bengis and Nelson [8]. The model shows that the electron transport is directional and goes from the donor species, which is near the inside surface of the thylakoid, to the secondary electron acceptors, which are located near the opposite surface of the membrane. The important point here is that the constituents of PS1 are encased in proteins and bound in the thylakoid membrane at fixed orientations to one another so that electron transfer is efficient and directional.

Many of the details concerning the chemical identities and structural relationships within the membrane of the electron donor and acceptors of PS1 are not known. We will attempt below to give a brief summary of what is currently known about each component.

A. P-700

The primary electron donor of PS1, P-700, was first characterized optically by Kok [9]. The oxidation of P-700 can be achieved chemically or photochemically and gives rise to absorbance changes at 700, 685, and 435 nm. The midpoint potential of its oxidation has been measured to be between 0.43 and 0.53V [10-12]. The optical absorbance changes upon oxidation of P-700 point to its being a chlorophyll a-containing species. Using circular dichroism difference

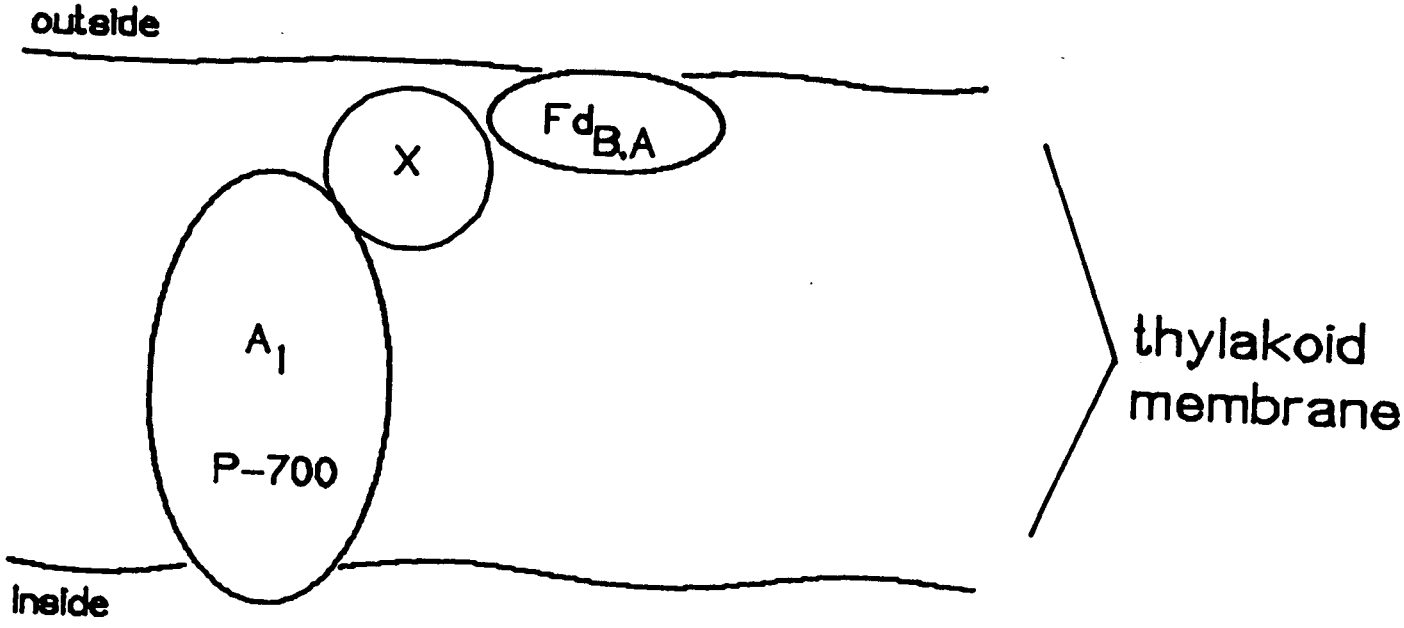

XBL 835-9829

Fig. 1-3. A model picturing how the photosystem 1 reaction center might be organized within the thylakoid membrane. The current view is that the PS1 reaction center consists of three proteins (A. McDermott, private communication).

spectroscopy, Philipson, et al. [13] found that the oxidation of P-700 caused changes in the CD spectrum near 700 nm indicative of an exciton interaction between two molecular species. They proposed that at least two Chl a molecules were responsible for the optical bleaching at 700 nm.

Oxidation of P-700 also gives rise to an EPR signal known as Signal 1. The signal was first observed by Commoner, et al. [14] and is characterized by a structureless gaussian lineshape centered at g 2.0026 having a peak-to- peak linewidth of 7-8 G. The linewidth of $P\text{-}700^+$ is narrowed by a factor of $\sqrt{2}$ from that of a Chl a monomer cation in vitro. This evidence, along with ENDOR data showing the differences between the hyperfine coupling constants of $P\text{-}700^+$ and Chl a^+ in vitro, led Norris, et al. [15,16] to propose that P-700 was a Chl a dimer species. More detailed ENDOR and EPR studies on $P\text{-}700^+$, ^{13}C enriched $P\text{-}700^+$, and several chlorophyll derivatives have been carried out by Wasielewski, et al. [17]. These authors indicate that there are several flaws in the dimer model and suggest that P-700 could be a monomeric Chl a-enol species. Thus, other than being a Chl a species, the chemical identity of P-700 remains unresolved.

B. The primary electron acceptor-A_1

The existence of an electron acceptor species more primary than X or bound Fe-S centers A and B was first

proposed by Sauer, et al. [7]. These authors monitored the kinetics of the re-reduction of P-700$^+$ in PS1 reaction center particles that had been poised at a redox potential so that secondary acceptors X, Fd_B, and Fd_A were reduced prior to application of an actinic flash. They found that at ambient temperature one could generate P-700$^+$ with an actinic flash under these redox conditions and that the signal had a lifetime of about 3 μsec. Other evidence that there was an electron acceptor more primary than X came from time-resolved EPR studies [18-20] which indicated that a species with EPR properties much different from those of X^- was participating in a radical pair interaction with P-700$^+$ immediately after application of an actinic flash.

Several investigators studying PS1 particle preparations poised at very low (< -750 mV) redox potentials have attributed an EPR signal appearing in the g 2.0 region to reduced A_1. Baltimore and Malkin [21] reported an EPR signal at g 2.0025 with a peak-to-peak linewidth of 12 G from reduced SDS PS1 particles which they attributed to A_1^-. Heathcote, et al. [22,23] reported a similar signal from PS1 particles prepared with Triton X-100 with g=2.0037 and a linewidth of 13.5 G. In all of these reports there was no attempt to quantitate the number of spins represented by this g 2.0 signal and to correlate it with the concentration of P-700 in the sample. Also, these authors did not demonstrate that the appearance of the g 2.0 signal affected the primary photochemistry of PS1.

Further characterization of the g 2.0 EPR signal attributed to A_1^- was done by McLean and Sauer [24]. They observed that in Triton PS1 particles the g 2.0 signal could represent as many as 12 spins per P-700. Further, these authors found that the appearance of the g 2.0 signal had little effect on the amplitude of a light-induced, spin-polarized triplet signal due to P-700 and indicative of the ability of the PS1 reaction center to perform its primary photochemistry [25]. They concluded that the g 2.0 signal was due to more radical species than just A_1^-. Similar experiments were carried out on PS1 particles prepared with lithium dodecyl sulfate (LDS) by Rutherford and Mullet [26]. These authors found that the appearance of the g 2.0 signal caused a corresponding decrease in the amplitude of the radical pair polarized triplet signal on P-700. Both of the above experiments were repeated by Gast, et al. [27]. These authors essentially reproduced the results of Rutherford and Mullet on LDS particles, but they also quantitated the number of spins giving rise to the g 2.0 signal. The results of this quantitation are that in Triton-treated PS1 particles, the g 2.0 signal corresponds to 2-3 spins per P-700 and that a change in amplitude of this signal only slightly affects the formation of the spin-polarized P-700 triplet. In LDS particles, two g 2.0 radicals are also produced by poising PS1 at low potentials. Gast, et al. conclude that the A_1 species is actually made up of two acceptors, A_0 and A_1, which operate in series between P-700

and X in the PS1 electron transport chain. They also state that A_0^- has a g-value of 2.0017 ± .0006 and a linewidth of 11.5 G and that A_1^- has a g-value of 2.0054 ± .0006 and a linewidth of 10.8 G. However, in LDS particles their data indicate that the g-value of A_0^- is 2.0033 and that the peak-to-peak linewidth is 8 G, a contradiction [27]. Bonnerjea and Evans [28] have also done a quantitative analysis of the g 2.0 signal in Triton-treated PS1 particles and found results similar to those of Gast, et al. [27]. One finding which should be kept in mind when considering the above data collected on Triton treated reaction centers of PS1, is that these studies have shown that the state of reduction of PS1, monitored via the integrated intensity of the g 2.0 EPR signal, only slightly affects the ability of P-700 to be photo-oxidized.

C. The secondary electron acceptor X

The secondary electron acceptor species known as X (or A_2 by optical spectroscopists) was first detected by EPR spectroscopy done at cryogenic temperatures on reduced PS1 particles by McIntosh, et al. [29]. The full spectrum was characterized more completely by Evans, et al. [30] and found to have an anisotropic g-tensor with principal g values of 2.08, 1.88, and 1.78. These g-values are consistent with X being an Fe containing species, but lie outside of the range normally found for Fe-S proteins [31].

X has also been characterized optically by Shuvalov, et

al. [32] and gives rise to a broad bleaching of an absorption band from 400-550 nm upon reduction. The midpoint potential of this species was determined at pH=10 to be -730 mV [33]. It has been shown that the EPR signal at g 1.78 decays with the same lifetime (130 msec) as the optical band at 430 nm in kinetic studies on PS1 particles that have secondary acceptors Fd_B and Fd_A reduced prior to application of an actinic flash at 5K [27,32]. The EPR signal of X^- has also been examined in oriented chloroplast samples and the g 1.78 component was found to be parallel to the thylakoid membrane normal [34].

D. Fe-S Centers A and B

Probably the best characterized electron acceptors of PS1 are iron-sulfur centers A and B. The participation of these bound Fe-S proteins in PS1 electron transport was first proposed by Malkin and Bearden [35]. These authors found that illumination of chloroplasts at cryogenic temperatures formed an irreversible EPR signal with g values of 2.05, 1.94, and 1.86. These g values are characteristic of a one electron reduction of an Fe-S protein [31]. If chloroplasts are illuminated in the presence of an electron donor at room temperature and then frozen and examined by EPR at cryogenic temperature, a second signal also indicative of an Fe-S protein is observed with g values of 2.05, 1.92, and 1.89 [36]. This signal is due to Fe-S center B. The EPR spectra of centers A and B have been studied in

oriented chloroplasts and a dramatic dependence of signal intensity at the various peak positions on orientation of the sample with respect to the DC field of the spectrometer was demonstrated [37].

Chemical analysis of reaction center particles shows that there are 10-12 non-heme Fe and up to 12 acid-labile sulfurs per P-700 [38,39]. It was suggested on the basis of some DMSO extraction work that PS1 contains two 4Fe-4S iron sulfur proteins and no 2Fe-2S Fe-S proteins [40]. However, given that there are 10-12 Fe and 12 acid-labile sulfurs in PS1 and that these iron containing species are in close proximity to one another, the analysis of these data is not straightforward. The question of whether centers A and B are 2Fe-2S or 4Fe-4S Fe-S proteins is unresolved. Another question that remains to be answered concerns whether electrons are transfered from X^- to centers A and B in parallel or in series.

1.3 Time-Resolved EPR Studies

The work presented in this thesis involves the study of the light reactions of PS1 using time-resolved EPR spectroscopy. The basic idea behind the experiments is simple. In the dark P-700 and the electron acceptor species are normally diamagnetic and do not give rise to EPR signals. When the sample is given a brief flash of actinic light, the excitation energy is funneled to the reaction center, P-700 is excited within 10 psec and electron

transfer occurs to form P-700$^+$ A_1^-. This species is a radical pair, and it should now be possible to observe an EPR signal from both P-700$^+$ and A_1^-. These signals are not long lived and must be observed with a spectrometer that has a fast time response. The time response of the EPR spectrometers used in this study is on the order of 1 μsec. Because the radical pair P-700$^+$ A_1^- is thought to have a lifetime of approximately 10 nsec, experimental parameters had to be adjusted to force the pair to live longer than it does under physiological conditions. These features of the experiments will be discussed in chapter 4.

As stated above, both P-700 and A_1 are thought to be Chl a species and have EPR spectra in the g 2.0 region. Treatments designed to poise PS1 in a redox state low enough to observe steady-state EPR signals from A_1^- (< -750 mV) usually result in the generation of g 2.0 signals which may have little to do with the primary photochemistry of PS1. These two problems have made steady-state investigations of the EPR properties of A_1^- difficult. Also, the steady-state investigations can be carried out only on PS1 particles that have been obtained by detergent treatment of the native system. These treatments may alter the local environments of the acceptor species significantly and thus affect the observed EPR spectra. The beauty of using time-resolved EPR methods to probe the EPR properties of the primary electron acceptors is that one looks only at radicals generated by the primary photochemistry of the reaction center. In

addition, these studies can be done on intact chloroplasts. In any case, experiments of this type were definitely needed to corroborate the results of the steady-state EPR work mentioned above.

Another interesting result of the time-resolved EPR experiments is that the signals arising from $P\text{-}700^{+}$ and the reduced primary acceptors are spin-polarized [18,19,20,41]. The polarization of the spin sublevels on each radical arises from the interplay of weak spin-spin interactions that are present in a radical pair and the difference in the local environment that each radical experiences [42-44]. Electron spin polarization makes experiments easier to accomplish (from the standpoint of signal-to-noise ratio), but also makes the analysis complicated because the spectra must be analyzed via computer simulation of the lineshapes before the magnetic parameters (g-values, linewidths, and spin-spin coupling constants) can be extracted from the data. The payoff in this instance is that the amount of information one can get from these data far exceeds that of the steady-state EPR experiment.

The drawing in Fig. 1-3 indicates that the photosystem is organized within the thylakoid membrane in a very specific manner. Thus, the spin-spin interaction for the radical pair species generated by the light flash should be anisotropic. Because these studies can be done on intact thylakoid membranes, one can orient the system [37,45] and study the spin-polarized lineshapes as a function of

orientation of the membranes with respect to the DC field of the spectrometer. The orientation effects on the time-resolved EPR data are large and will be discussed in chapters 4 and 5. The analysis of these effects gives information about the structural relation of the primary radical ion pair to the membrane normal. This analysis comprises a major portion of chapters 4 and 5.

REFERENCES

1. Clayton, R.K.,"Photosynthesis: Physical Mechanisms and Chemical Patterns," Cambridge University Press, Cambridge, 1980.
2. Govindjee, "Photosynthesis: Energy Conversion by Plants and Bacteria," vol. 1, Academic Press, NY, 1982, pp. 230-249.
3. Andersson, B. and Anderson, J.M. (1980) Biochim. Biophys. Acta 546, 426-439.
4. Anderson, J.M. (1981) FEBS Lett. 124, 1-10.
5. Melis, A. and Brown, J.S. (1980) Proc. Natl. Acad. Sci. USA 77, 4712-4716.
6. Shuvalov, V.A., Dolan, E., and Ke, B. (1979) FEBS Lett. 100, 5-8.
7. Sauer, K., Mathis, P., Acker, S., and Van Best, J.A. (1978) Biochim. Biophys. Acta 503, 120-134.
8. Bengis, C. and Nelson, N. (1977) J. Biol. Chem. 252, 4564-4569.
9. Kok, B. (1956) Biochim. Biophys. Acta 22, 399-401.
10. Kok, B. (1961) Biochim. Biophys. Acta 48, 527-533.
11. Knaff, D.B. and Malkin, R. (1973) Arch. Biochem. Biophys. 159, 555-562.
12. Ke, B., Sugahara, K. and Shaw, E.R. (1975) Biochim. Biophys. Acta 408, 12-25.
13. Philipson, K.D., Sato, V.L. and Sauer, K. (1972) Biochemistry 11, 4591-4595.

14. Commoner, B., Heise, J.J. and Townsend,J. (1956) Proc. Natl. Acad. Sci. USA 42, 710-718.

15. Norris, J.R., Scheer, H., Druyan, M.E. and Katz, J.J. (1974) Proc. Natl. Acad. Sci. USA 71, 4897-4900.

16. Norris, J.R., Scheer, H. and Katz, J.J. (1975) Ann. N.Y. Acad. Sci. 244, 261-280.

17. Wasielewski, M.R., Norris, J.R., Shipman, L.L., Lin, C.P. and Svec, W.A. (1981) Proc. Natl. Acad. Sci. USA 78, 2957-2961.

18. Blankenship, R., McGuire, A.E. and Sauer, K. (1975) Proc. Natl. Acad. Sci. USA 72, 4943-4947.

19. Dismukes, G.C., McGuire, A.E., Blankenship, R. and Sauer, K. (1978) Biophys. J. 21, 239-256.

20. Freisner, R., Dismukes, G.C. and Sauer,K. (1979) Biophys. J. 25, 277-294.

21. Baltimore, B.G. and Malkin, R. (1980) Photochem. Photobiol. 31, 485-490.

22. Heathcote, P., Timofeev, K.N. and Evans, M.C.W. (1979) FEBS Lett. 101, 105-109.

23. Heathcote, P. and Evans, M.C.W. (1980) FEBS Lett. 111, 381-385.

24. McLean, M.B. and Sauer, K. (1982) Biochim. Biophys. Acta 679, 384-392.

25. Frank, H.A., McLean, M.B. and Sauer, K. (1979) Proc. Natl. Acad. Sci. USA 76, 5124-5128.

26. Rutherford, A.W. and Mullet, J.E. (1981) Biochim. Biophys. Acta 635, 225-235.

27. Gast, P., Swarthoff, T., Ebskamp, F.C.R. and Hoff, A.J. (1983) Biochim. Biophys. Acta 722, 163-175.

28. Bonnerjea, J. and Evans, M.C.W. (1982) FEBS Lett. 148, 313-316.

29. McIntosh, A.R., Chu, M. and Bolton, J.R. (1975) Biochim. Biophys. Acta 376, 308-314.

30. Evans, M.C.W., Sihra, C.K., and Cammack, R. (1976) Biochem. J. 158, 71-77.

31. Sands, R.H. and Dunham, W.R. (1975) Q. Rev. Biophys. 7, 443-504.

32. Shuvalov, V.A., Dolan, E. and Ke, B. (1979) Proc. Natl. Acad. Sci. USA 76, 770-773.

33. Ke, B., Dolan, E., Sugahara, K., Hawkridge, F.M., Demeter, S. and Shaw, E.R. (1977) Plant Cell Physiol. Spec. Issue 3, 187-199.

34. Dismukes, G.C. and Sauer, K. (1978) Biochim. Biophys. Acta 504, 431-445.

35. Malkin, R. and Bearden, A.J. (1971) Proc. Natl. Acad. Sci. USA 68, 16-19.

36. Evans, M.C.W., Reeves, S.G. and Cammack, R. (1974) FEBS Lett. 49, 111-114.

37. Prince, R., Crowder, M.S. and Bearden, A.J. (1980) Biochim. Biophys. Acta 592, 323-337.

38. Golbeck, J.H., Lien, S. and San Pietro, A. (1977) Arch. Biochem. Biophys. 178, 140-150.

39. Golbeck, J.H. and Kok, B. (1978) Arch. Biochem. Biophys. 188, 233-242.

40. Cammack, R. and Evans, M.C.W. (1975) Biochem. Biophys. Res. Comm. 67, 544-549.

41. McIntosh, A.R., Manikowski, H., Wong, S.K., Taylor, C.P.S. and Bolton, J.R. (1979) Biochem. Biophys. Res. Comm. 87, 605-612.

42. Adrian, F.J. (1971) J. Chem. Phys. 54, 3918-3923.

43. Freed, J.H. and Pedersen, J.B. (1976) Adv. Magn. Res. 8, 1-84.

44. Friesner, R.,"Theoretical Studies of the Light Reactions of Photosynthesis," Ph.D. Thesis, University of California, Berkeley, 1979, Lawrence Berkeley Laboratory Report LBL-8953.

45. Geacintov, N.E., Van Nostrand, F., Becker, J.F. and Tinkel,J.B. (1972) Biochim. Biophys. Acta 267, 65-79.

CHAPTER 2

INTRODUCTION TO EPR AND THE THEORY OF CHEMICALLY INDUCED DYNAMIC ELECTRON POLARIZATION

The theory of Electron Paramagnetic Resonance (EPR) spectroscopy has been extensively covered in many books [1-4]. In this chapter, no attempt will be made to cover this vast field in any detail. However, the basic experiment as it pertains to the theory of Chemically Induced Dynamic Electron Polarization (CIDEP) will be discussed. Also, the standard theory of CIDEP and its adaptation to photosynthetic systems by Friesner, et al. [5] will be examined.

2.1 The Basic EPR Experiment - The Zeeman Interaction

Molecules or atoms with unpaired electrons possess a non-zero electron spin angular momentum. This causes the molecule to have a permanent magnetic dipole moment, $\underset{\sim}{\mu}$, given by

$$\underset{\sim}{\mu} = -g_e[e/(2m_e c)]\underset{\sim}{S} \qquad (2\text{-}1)$$

where g_e=2.0023, e is the charge on the electron, m_e is the electron mass, c is the speed of light, and $\underset{\sim}{S}$ represents the "spin" or intrinsic angular momentum of a species due to its

unpaired electrons. For a molecule with a single unpaired electron, S=1/2. In the presence of an external magnetic field, a torque will be exerted on the spin causing it to have a prefered orientation in the field. The interaction energy is $E=-\underset{\sim}{\mu}\cdot\underset{\sim}{H}$.

Because electrons obey quantum rather than classical mechanics, the interaction energy with the external magnetic field will be quantized. The number of different energy states will be 2S+1 so that an S=1/2 species will have two possible energy configurations when placed in an external magnetic field. The hamiltonian that describes this quantization of electron spin angular momentum is the Zeeman hamiltonian and is given by

$$H_{zee} = g_e \beta \underset{\sim}{H}\cdot\underset{\sim}{S} \; . \qquad (2\text{-}2)$$

In general, the Zeeman interaction is not the only interaction of the electron spin angular momentum with the environment. There may also be coupling with the orbital motion of the electron. The spin-orbit coupling hamiltonian is $H_{soc}=-\lambda \underset{\sim}{L}\cdot\underset{\sim}{S}$, where $\underset{\sim}{L}$ is the orbital angular momentum and λ is the spin-orbit coupling constant. The full hamiltonian describing the quantization of the electron spin angular momentum is then $H_{zee}+H_{soc}$. Normally these operators are combined by the introduction of a fictitious spin, and the effects of spin-orbit coupling are incorporated into a g-tensor so that the full hamiltonian is given by Eqn. 2-3.

$$H_{zee} = \beta \underset{\sim}{H} \cdot \underset{\approx}{g} \cdot \underset{\sim}{S}' \qquad (2\text{-}3)$$

In this thesis the molecules under study are, for the most part, organic free radicals with S=1/2 and isotropic g-tensors. Taking the direction of the Zeeman field (applied magnetic field) to be along the z axis, and the g-tensor to be a scalar quantity, the Zeeman hamiltonian reduces to $H_{zee}=g\beta H\hat{S}_z$. For an S=1/2 species, there will be two possible eigenstates of this hamiltonian with magnetic quantum numbers $m_s=\pm 1/2$. These two states are denoted $|\alpha\rangle$ for $m_s=1/2$ and $|\beta\rangle$ for $m_s=-1/2$. Physically, $|\alpha\rangle$ corresponds to an energy state where the bulk magnetization of a sample is aligned with the field and $|\beta\rangle$ corresponds to to a state where the magnetization is antiparallel to the field direction. An energy level diagram is shown below.

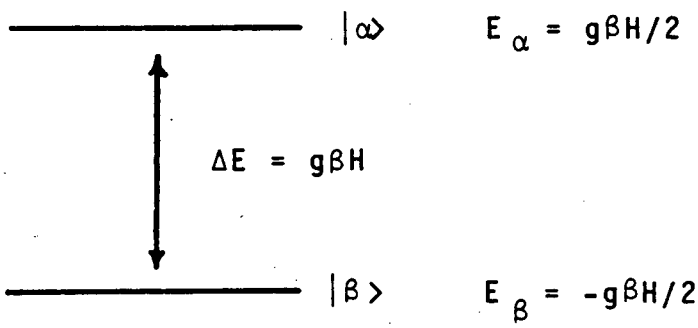

In an EPR experiment the sample is placed in an external magnetic field provided by an electromagnet and irradiated at a right angle to the DC field with a uniform oscillating microwave magnetic field of 9 GHz. The sample is irradiated at a fixed microwave frequency, and the DC

magnetic field is swept. When ΔE, the splitting between the energy levels, equals the energy of the incident microwave radiation, transitions between the two energy states are induced, and a change in the microwave power level returning from the sample to the detector is measured. For incident radiation of 9 GHz and g=2.0 this "resonance" occurs at a magnetic field strength of

$$H = h\nu/(g\beta) = 3215 \text{ Gauss.} \qquad (2\text{-}4)$$

If the sample is at thermal equilibrium in the spectrometer, the ratio of the populations of the spin sublevels will be given by the Boltzmann factor,

$$n_\alpha/n_\beta = e^{-\Delta E/(kT)} \qquad (2\text{-}5)$$

where n_α and n_β are the populations of the α and β sublevels, k is Boltzmann's constant and T is the temperature of the sample. At 10K, where most of the work in this thesis was done, this ratio is 0.96. This means that for every 100 molecules in the $|\beta\rangle$ state there are 96 in $|\alpha\rangle$. Therefore one will see a net absorption of microwave power when the sample is at thermal equilibrium.

2.2 Chemically Induced Dynamic Electron Polarization

In chapter 1 it was mentioned that the time-resolved EPR spectra reported on in this thesis are spin polarized. This means that the spin sublevels are populated in a non-Boltzmann manner so that there is an excess of spins in

either the $|\alpha\rangle$ or $|\beta\rangle$ state. The observation of electron spin polarization is common in instances where radicals are generated in solution via some chemical reaction and then examined by EPR spectroscopy on a time scale which is fast compared to the time required to attain thermal equilibrium.

A. History of CIDEP

The first observation of spin polarized EPR spectra was reported by Fessenden and Schuler in 1963 [6]. These authors were studying EPR properties of transient alkyl radicals in hydrocarbon solutions generated during irradiation of the sample with a 2.8 MeV electron beam. The spectra that they obtained had both emissive and enhanced absorptive components. A mechanism for explaining these results was developed by Adrian and is known as the radical-pair mechanism of chemically induced dynamic electron polarization (CIDEP) [7]. The theory of CIDEP is not due solely to Adrian; many authors have contributed to the understanding of this phenomenon [8-10].

The first observation of CIDEP in PS1 was made by Blankenship, et al. [11]. These studies were done on spinach chloroplasts at ambient temperature. The authors found that if the chloroplast sample was excited in the EPR cavity with a laser pulse, a fast (1 μsec) transient signal that was emissive could be observed in the g 2.0 region. Control experiments indicated that the signal was due to PS1 and probably $P\text{-}700^{+}$. Subsequent experiments [12] further

established that these signals were due to P-700$^+$ and it was noted that the lineshape was orientation dependent. The above data were analyzed by Friesner, et al. [5] using Adrian's radical pair formalism adapted to membrane bound chemical systems.

B. Mechanisms of CIDEP

Before describing the work of Friesner in detail, it should be mentioned that there are two mechanisms by which CIDEP can develop on a radical. These mechanisms are the radical-pair mechanism and the triplet mechanism. The development of spin polarization begins with the birth of a radical pair described by

$$D\ A \xrightarrow{h\nu} D^*A \rightarrow D^+A^-$$

where D represents an electron donor species and A an acceptor species. The triplet mechanism is operative if the precursor to the radical pair, D^*A, was a triplet species. The radical-pair mechanism is operative if the precursor was a singlet species. The evidence that the radical-pair mechanism describes the initial electron transfer event in PS1 comes from EPR studies done on the triplet P-700 species formed from a back reaction between P-700$^+$ and A_1^- after the initial electron transfer has occurred [13]. In these experiments, one blocks forward electron transfer to the secondary electron acceptors so that once the radical pair is generated the system will undergo a back reaction and

form ^{3}P-700.

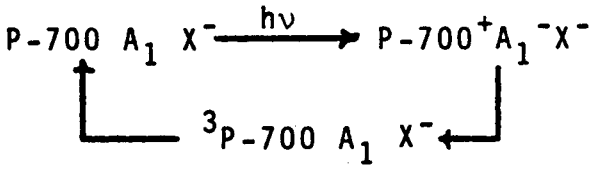

The lineshape of the ^{3}P-700 signal can be accounted for only if the triplet was generated from a radical pair that was created in a singlet state [14,15].

A good physical description of the development of electron spin polarization via the radical-pair mechanism is the vector model proposed by Syage [16]. The development of CIDEP on a radical involves three steps.

1. Generation of the radical pair - This occurs in PS1 when one excites the plant material with a brief flash of light. The absorption of light causes the excitation of P-700 and subsequent transfer of an electron to A_1. Thus, the radical pair P-700$^+A_1^-$ is born (in a singlet state).

2. Selective mixing of singlet and triplet states - The radical pair is born in a singlet state, but because the spins now feel different effective fields they precess at different frequencies about H_0 (the Zeeman field). This process causes selective mixing of $|S\rangle$ with $|T_0\rangle$.

3. Precession about a weak exchange field - A weak spin-spin interaction between P-700$^+$ and A_1^- sets

up an effective exchange field, perpendicular to H_0, about which the magnetization due to each radical can precess. This prepares the spin sublevels of each radical in a polarized state.

Steps 2 and 3 occur simultaneously.

The above description is summarized in the vector diagram of Fig. 2-1. The magnetization due to D^+ (the electron donor cation) is represented in Fig. 2-1 by the heavy arrows and the magnetization on A^- is represented by the lighter arrows. The radical pair starts out in a singlet state, which is represented vectorially by having the magnetization due to D^+ and A^- directly opposing one another (180^o apart), and precessing about H_0. Because the magnetization is localized on two different molecules, the precession rates differ. After a time, t, the magnetization vectors due to D^+ and A^- are no longer 180^o apart (the diagram shows them about 90^o apart). There is now a net magnetization on the radical-pair species and, as the diagram shows, it is perpendicular to H_0. This represents mixing of the singlet state with the high field triplet state commonly denoted as $|T_0\rangle$. The third step in Fig. 2-1 shows that if a weak spin-spin coupling exists between D^+ and A^- an exchange field, H_e will be set up perpendicular to H_0. The magnetization will precess about this exchange field during the radical pair lifetime. After these two processes have occurred for some time, the net magnetization on D^+ and

Fig. 2-1. Vector model for the development of CIDEP by the radical pair mechanism. The model is due to Syage [16] and a description is given in the text.

Vector Model for Radical Pair CIDEP

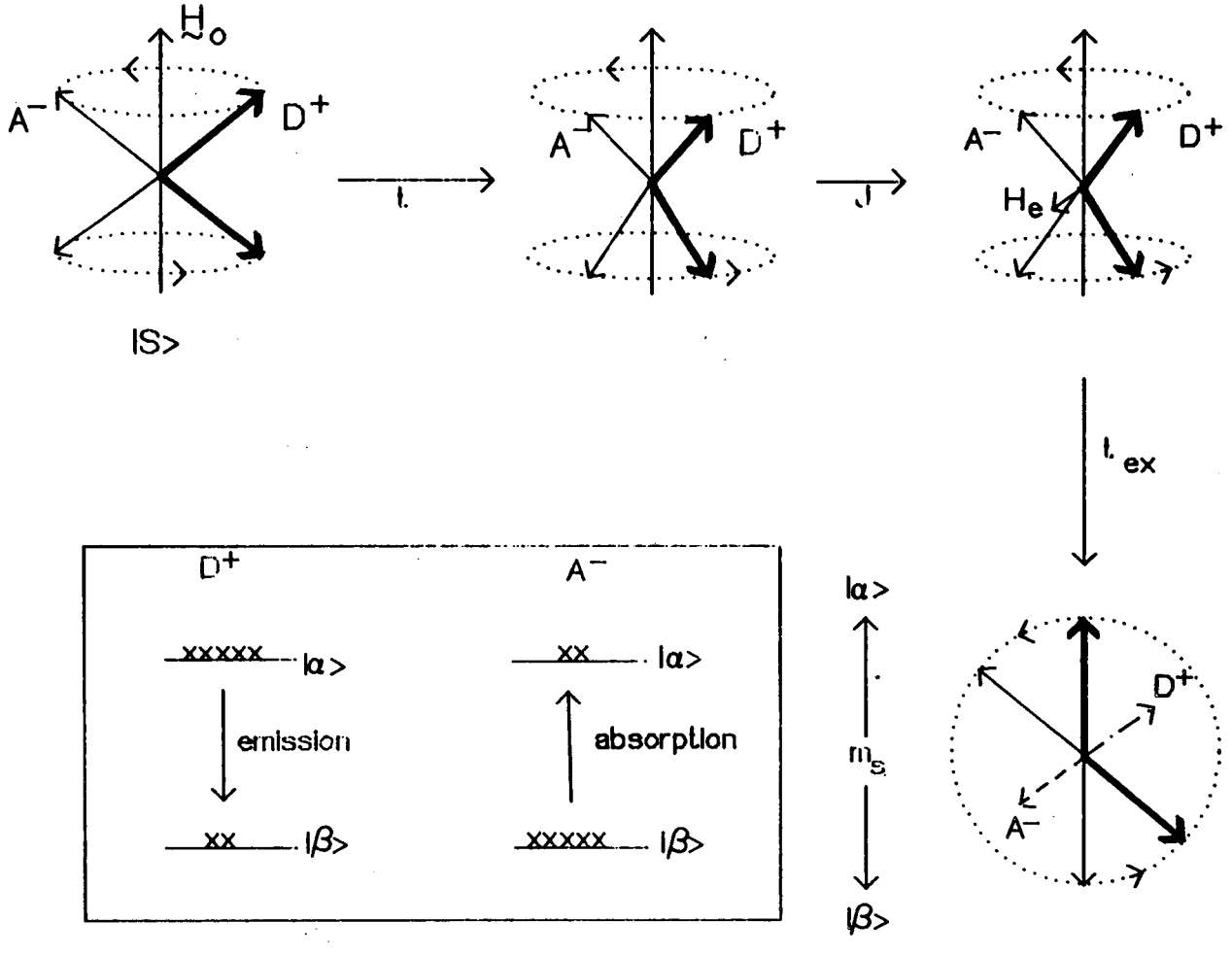

XBL 835-9821

A^- can be examined by projecting the vectors on to the plane of the paper (step four). Fig. 2-1 is drawn so that D^+ has a net magnetization aligned with H_o, meaning that there is an excess of spins in the $|\alpha>$ or high energy spin state. Therefore, the EPR signal due to D^+ will be emissive. The opposite situation is depicted for A^-; its spectrum will be enhanced absorptive.

At this point a fourth step in the development of CIDEP on a pair of radicals in a real system needs to be mentioned. That is the death of the radical pair. The lifetime of $P\text{-}700^+A_1^-$ in chloroplasts appears to be on the order of 10 ns. Its death comes about due to subsequent electron transfer from A_1^- to the secondary electron acceptors. The spin polarization developed on $P\text{-}700^+$ remains for its spin-lattice relaxation time or until it reacts with another species. The spin polarization that develops from this single radical-pair interaction can be large because the radical-pair lifetime is long compared to those encountered in solution work. In solution, the radical-pair lifetimes are much shorter because separation is brought about by diffusion. Therefore, little polarization develops due to the initial encounter of the pair. For a significant amount of polarization to develop, the radicals must undergo a re-encounter in a spin-selective reaction. Because development of CIDEP in solution systems involves inclusion of the diffusion process in the modeling, the calculations are much more complex [7,8].

C. Quantum mechanical treatment of radical pair CIDEP

In this section the standard radical-pair theory of CIDEP as developed by Adrian [7] and adapted by Friesner, et al.[5] will be given. Then the various categories of spectra predicted by this model will be discussed. One should keep in mind that this model was developed for radical-pair interactions occurring in solution and will require modification to describe the experimental data presented in chapters 4 and 5. The spin hamiltonian for a weakly coupled radical pair created by an electron transfer from a donor molecule (D) to an acceptor (A) is:

$$H_{RP} = H_{zee}^{(D)} + H_{zee}^{(A)} + H_{hf}^{(D)} + H_{hf}^{(A)} + H_{ex} \qquad (2\text{-}6)$$

where H_{zee}^{i} is the Zeeman hamiltonian for the i^{th} species, H_{hf}^{i} is the hamiltonian describing the nuclear hyperfine interaction for the i^{th} species, and H_{ex} represents an electron exchange interaction between D and A. The g-tensors for both donor and acceptor species are taken to be isotropic and the Zeeman field direction is chosen as the z axis. The Zeeman hamiltonians then have the form:

$$H_{zee}^{(D)} = g_D \beta H \hat{S}_{Dz} \qquad H_{zee}^{(A)} = g_A \beta H \hat{S}_{Az} \qquad (2\text{-}7)$$

where $\hat{S}_{Dz}$ and $\hat{S}_{Az}$ are the spin operators in the z direction for the donor and acceptor molecules. For the nuclear hyperfine interaction, only the first order contact terms

are considered.

$$H_{hf}^{(D)} = \sum_i A_i{}^{(D)}\hat{I}_{Dz}\hat{S}_{Dz}$$
$$H_{hf}^{(A)} = \sum_j A_j{}^{(A)}\hat{I}_{Az}\hat{S}_{Az} \qquad (2\text{-}8)$$

Finally, the exchange term is taken to be isotropic and has the form:

$$H_{ex} = -J(2\underset{\sim}{S}_D \cdot \underset{\sim}{S}_A + 1/2) \qquad (2\text{-}9)$$

where J represents the exchange integral. Because the above expression has a negative sign, a positive J indicates antiferromagnetic exchange and a negative J represents ferromagnetic exchange in our calculations.

The basis set used for this calculation is composed of the singlet and high-field triplet spin functions:

$$|S\rangle = 1/\sqrt{2}\,(|\alpha\beta\rangle - |\beta\alpha\rangle)$$
$$|T_0\rangle = 1/\sqrt{2}\,(|\alpha\beta\rangle + |\beta\alpha\rangle)$$
$$|T_{+1}\rangle = |\alpha\alpha\rangle$$
$$|T_{-1}\rangle = |\beta\beta\rangle\ . \qquad (2\text{-}10)$$

The hamiltonian matrix is:

$$\begin{array}{c} \\ \langle S| \\ \langle T_0| \\ \langle T_{+1}| \\ \langle T_{-1}| \end{array} \begin{array}{c} \begin{array}{cccc} |S\rangle & |T_0\rangle & |T_{+1}\rangle & |T_{-1}\rangle \end{array} \\ \begin{bmatrix} J & H_{AD} & 0 & 0 \\ H_{AD} & -J & 0 & 0 \\ 0 & 0 & E_{+1} & 0 \\ 0 & 0 & 0 & -E_{+1}-2J \end{bmatrix} \end{array} \qquad (2\text{-}11)$$

where H_{AD} is given by,

$$H_{AD} = \langle S|H_{RP}|T_0\rangle = 1/2[(g_D-g_A)\beta H + \sum_i A_i^{(D)} m_{iz}^{(D)} - \sum_j A_j^{(A)} m_{jz}^{(A)}]$$

and

$$E_{+1} = 1/2[(g_D+g_A)\beta H + \sum_i A_i^{(D)} m_{iz}^{(D)} + \sum_j A_j^{(A)} m_{jz}^{(A)}] - J \qquad (2\text{-}12)$$

where $m_{iz}^{(n)}$ is the z component of the nuclear spin of the i^{th} nucleus on molecule n. Diagonalization of this matrix yields the eigenvectors and corresponding eigenvalues.

$$|\phi_1\rangle = [(\omega+J)/2\omega]^{1/2}|S\rangle + [(\omega-J)/2\omega]^{1/2}|T_0\rangle$$

$$|\phi_2\rangle = [(\omega-J)/2\omega]^{1/2}|S\rangle - [(\omega+J)/2\omega]^{1/2}|T_0\rangle$$

$$|\phi_3\rangle = |T_{+1}\rangle \qquad (2\text{-}13)$$

$$|\phi_4\rangle = |T_{-1}\rangle$$

$$E_1 = \omega$$

$$E_2 = -\omega$$

$$E_3 = E_{+1}$$

$$E_4 = -E_{+1} - 2J \qquad (2\text{-}14)$$

ω is given by

$$\omega = (H_{AD}^2 + J^2)^{1/2} . \qquad (2\text{-}15)$$

The polarization, ρ , on either radical can be determined by computing the time evolution of the radical pair wavefunction and finding the expectation value of the spin angular momentum in the z direction for the species of interest. The polarization for the donor radical is given by:

$$\rho_D = 2\langle\psi(t)|S_{Dz}|\psi(t)\rangle \qquad (2\text{-}16)$$

where the factor of two is needed to normalize the polarization to ± 1 at its limits. Using the time-dependent Schroedinger equation, the form of $|\psi(t)\rangle$ is:

$$|\psi(t)\rangle = \sum_j \langle\phi_j|\psi(0)\rangle e^{-iE_jt/\hbar} |\phi_j\rangle \qquad (2\text{-}17)$$

where the $|\phi_j\rangle$ are the above eigenvectors. Because the radical pair is born in the singlet state, $|\psi(0)\rangle = |S\rangle$ and

$$|\psi(t)\rangle = [(\omega+J)/2\omega]^{1/2} e^{-i\omega t'} |\phi_1\rangle + [(\omega-J)/2\omega]^{1/2} e^{i\omega t'} |\phi_2\rangle \qquad (2\text{-}18)$$

where $t' = t/\hbar$. Using this result in Eqn. 2-16 yields:

$$\rho_D(t) = (2H_{AD}J/\omega^2) \sin^2\omega t \qquad (2\text{-}19)$$

The time-averaged polarization is the observable in an EPR experiment and is obtained by multiplying the above expression (Eqn. 2-19) by the probability that the radical pair will exist for a time, τ, and then by integrating over all time. The probability that the D^+A^- radical pair will exist for a time, τ, is given by $(dt/\tau)e^{-t/\tau}$. The time-averaged polarization is then:

$$\rho_D(\tau) = 4H_{AD}J\tau^2/(1+4\omega^2\tau^2) \qquad (2\text{-}20)$$

For calculation purposes, the value of H_{AD} for radical D^+ is a function of the particular hyperfine state, i, for which one is interested in calculating the polarization. Thus, Eqn. 2-20 should be rewritten:

$$\rho_D{}^i(\tau) = 4H_{AD}{}^iJ(\tau)^2/(1+4(\omega^i)^2\tau^2) \qquad (2\text{-}21)$$

and the intensity of a given hyperfine line, i, is:

$$I_D^{\,i}(H) = -\rho_D^{\,i}(\tau)P_i e^{(H-H_i^{\,o})^2/\delta^2} \qquad (2\text{-}22)$$

where $H_i^{\,o}$ is the center field position of hyperfine line i, δ is the intrinsic width of the resonance, and P_i is the probability of hyperfine state i. The minus sign in Eqn. 2-22 is needed because the situation where ρ=1 corresponds to all spins being in the $|\alpha\rangle$ spin state, which will give rise to an emissive or negative-amplitude signal.

D. Classes of lineshapes

The model presented above was refered to as a "one-site" model by Friesner, et al. [5] because the spin polarization develops due to a single radical pair interaction. Characterization of this model is simple and gives rise to three classes of lineshapes. From Eqn. 2-21, one finds that the polarization of a particular hyperfine line, i, on a radical is proportional to $H_{AD}^{\,i}$ which is the hamiltonian matrix element that describes the $|S\rangle$ - $|T_0\rangle$ mixing process.

$$\rho_D^{\,i}(\tau) \propto H_{AD}^{\,i} = 1/2[(g_D-g_A)\beta H+A_i^{\,(D)}m_{iz}-\sum_j A_j^{\,(A)}m_{jz}\,] \qquad (2\text{-}23)$$

Summing over j, the hyperfine states of A^-, yields

$$\rho_D^{\,i}(\tau) \propto H_{AD}^{\,i} = 1/2[(g_D-g_A)\beta H+A_i^{\,(D)}m_{iz}\,] \,. \qquad (2\text{-}24)$$

Likewise for the A^- species one obtains

$$\rho_A^{\,j}(\tau) \propto -H_{AD}^{\,j} = -1/2[(g_D-g_A)\beta H-A_j^{\,(A)}m_{jz}\,] \,. \qquad (2\text{-}25)$$

Using Eqns. 2-24 and 2-25 together with Eqns. 2-21 and 2-22, one can simulate both D^+ and A^- spectra. To illustrate the various classes of spectra, the following parameters will be used. The g-value of D^+ is set at 2.0026 and its hyperfine field consists of a 3.5G field generated by two protons. The g-value of A^- is varied to simulate the various classes of spectra, but its hyperfine field consists of a 5G interaction due to two protons. The exchange coupling constant is 9.0G, the radical pair lifetime is 2 μsec, and the microwave frequency is 9.222 GHz.

The first class of spectra are called "net effect" CIDEP spectra and occur when the $(g_D-g_A)\beta H$ term is large compared to the hyperfine fields of the radical. In this case the dependence of ρ on the hyperfine state of the radical is negligible and the entire spectrum of the species will be either emissive or absorptive. This is illustrated in Fig. 2-2 (note that these simulations are of derivative spectra). g_A was set at 2.01, so the resulting spectrum of D^+ is absorptive, centered at g 2.0026 and has a linewidth of 8 G. The spectrum differs from that obtained for D^+ under equilibrium conditions in that its intensity is increased by the polarization factor. The corresponding signal from A^- is emissive, centered downfield at g 2.01 and has a linewidth of 11 G. If the relaxation times associated with each species are similar, the integrated intensity of D^+ should be equal in magnitude, but opposite in sign to that of A^-. This is a result of conservation of spin angular momentum.

Fig. 2-2. Predicted spin-polarized EPR spectra for an electron donor cation species, D^+ (Fig. 2-2a), and an acceptor species, A^- (Fig. 2-2b), under conditions where "net effect" type spectra are observed. The parameters used in the simulations were: g_D, 2.0026; g_A, 2.01; J, 9.0 G; A_D, 3.5 G (2 protons); A_A, 5.0 G (2 protons); microwave frequency, 9.222 GHz; and τ, 2 μsec. The D^+ spectrum appears narrower than the A^- spectrum because of the smaller hyperfine coupling constant assigned to it.

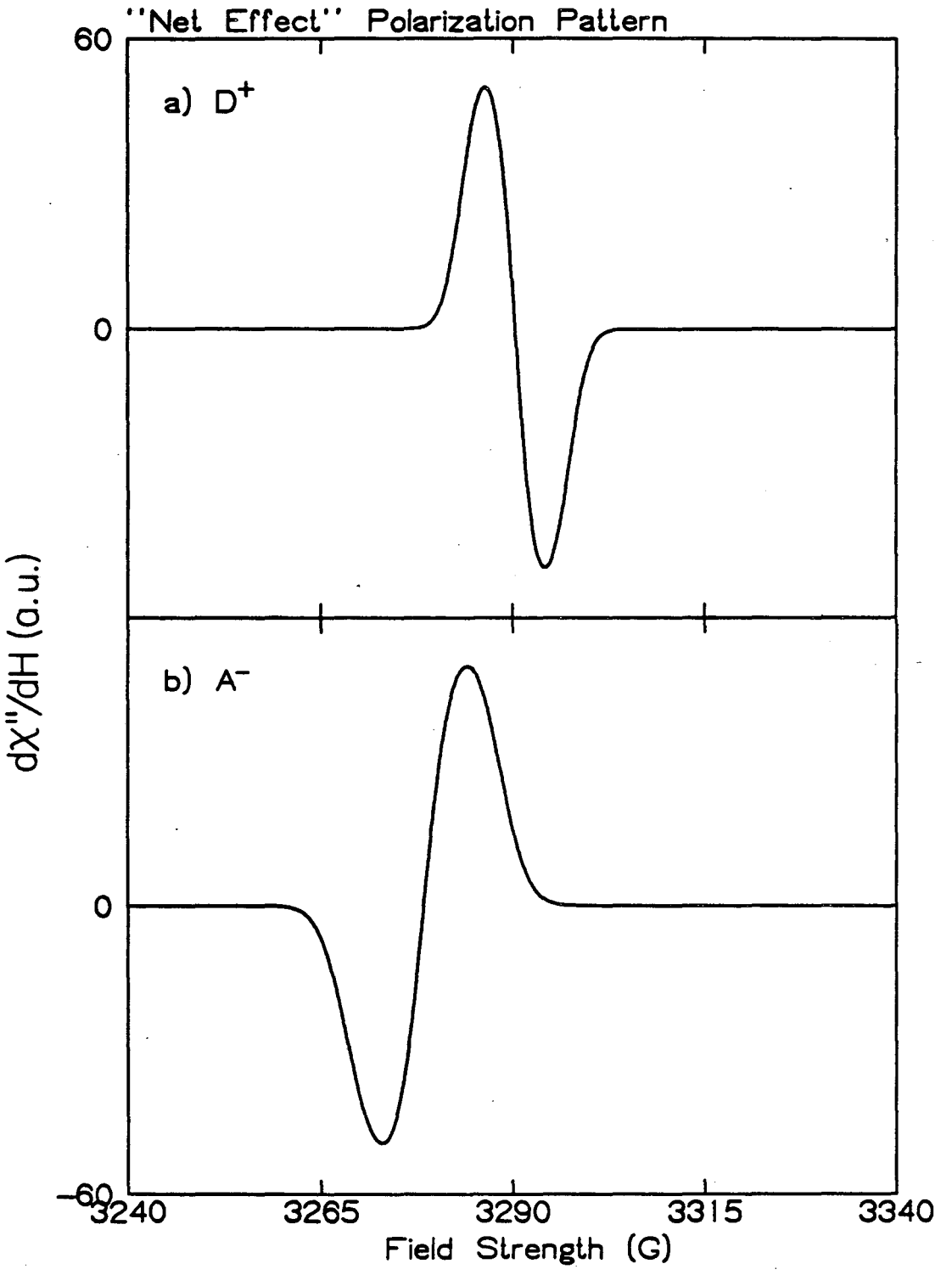
"Net Effect" Polarization Pattern
60
a) D^+
0
b) A^-
0
−60
dχ"/dH (a.u.)
3240
3265
3290
3315
3340
Field Strength (G)

XBL 835-9817

The second class of spectra are called "multiplet" effect spectra and occur when $g_D=g_A$. In this case only the hyperfine terms are considered in Eqns. 2-24 and 2-25 and to first order the spectra will be symmetric about the g-value of the radical of interest. The spectrum will be emissive on one side of the center field position and absorptive on the other side. This case is illustrated in Fig. 2-3 where g_A was set to 2.0026. The integrated or net polarization on each species in this case is zero.

The third class of spectra are "mixed multiplet" effect spectra and result when the $(g_D-g_A)\beta H$ term is comparable in magnitude to the hyperfine fields. This case is illustrated in Fig.2-4 where $g_A=2.0030$. Mixed multiplet effect spectra have both emissive and enhanced absorptive components, but are skewed so that there is some net polarization on each species. In Fig. 2-4 the g-values are such that the D^+ spectrum is emissive-absorptive and skewed towards absorption. The spectrum of A^- has the same overall polarization pattern, but is skewed in the opposite sense. Once again the net polarization on each species will be equal in magnitude, but opposite in sign.

E. Transfer of spin polarization

As mentioned above, the primary radical ion pair in PS1 is not long lived. Its death is brought about by either electron transfer from A_1^- to a secondary electron acceptor or a charge recombination reaction to form ^{3}P-700. If the

Fig. 2-3. Predicted spin-polarized EPR spectra for donor cation (D^+ - Fig. 2-3a) and acceptor anion (A^- - Fig. 2-3b) under conditions where "multiplet" effect spectra are observed. The parameters used in these simulations are identical to those of Fig. 2-2 except that g_A=2.0026.

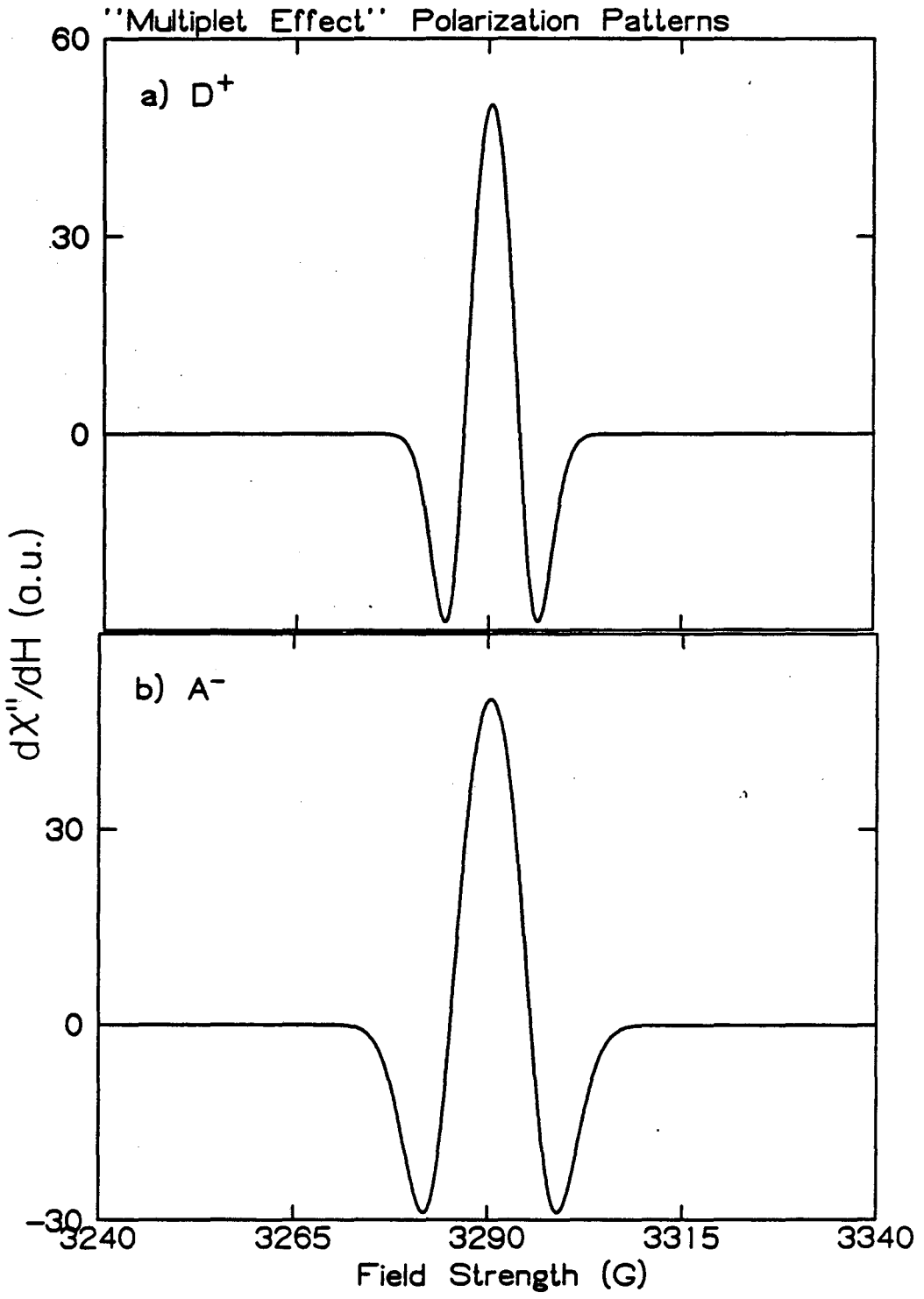
"Multiplet Effect" Polarization Patterns
a) D+
b) A−
60
30
0
30
0
−30
dχ''/dH (a.u.)
3240
3265
3290
3315
3340
Field Strength (G)

XBL 835-9818

Fig. 2-4. Predicted spin-polarized EPR spectra for donor cation (Fig. 2-4a) and acceptor anion (Fig. 2-4b) under conditions where "mixed multiplet" spectra are observed. The parameters used in these simulations are identical to those of Fig. 2-2 except that g_A=2.0030.

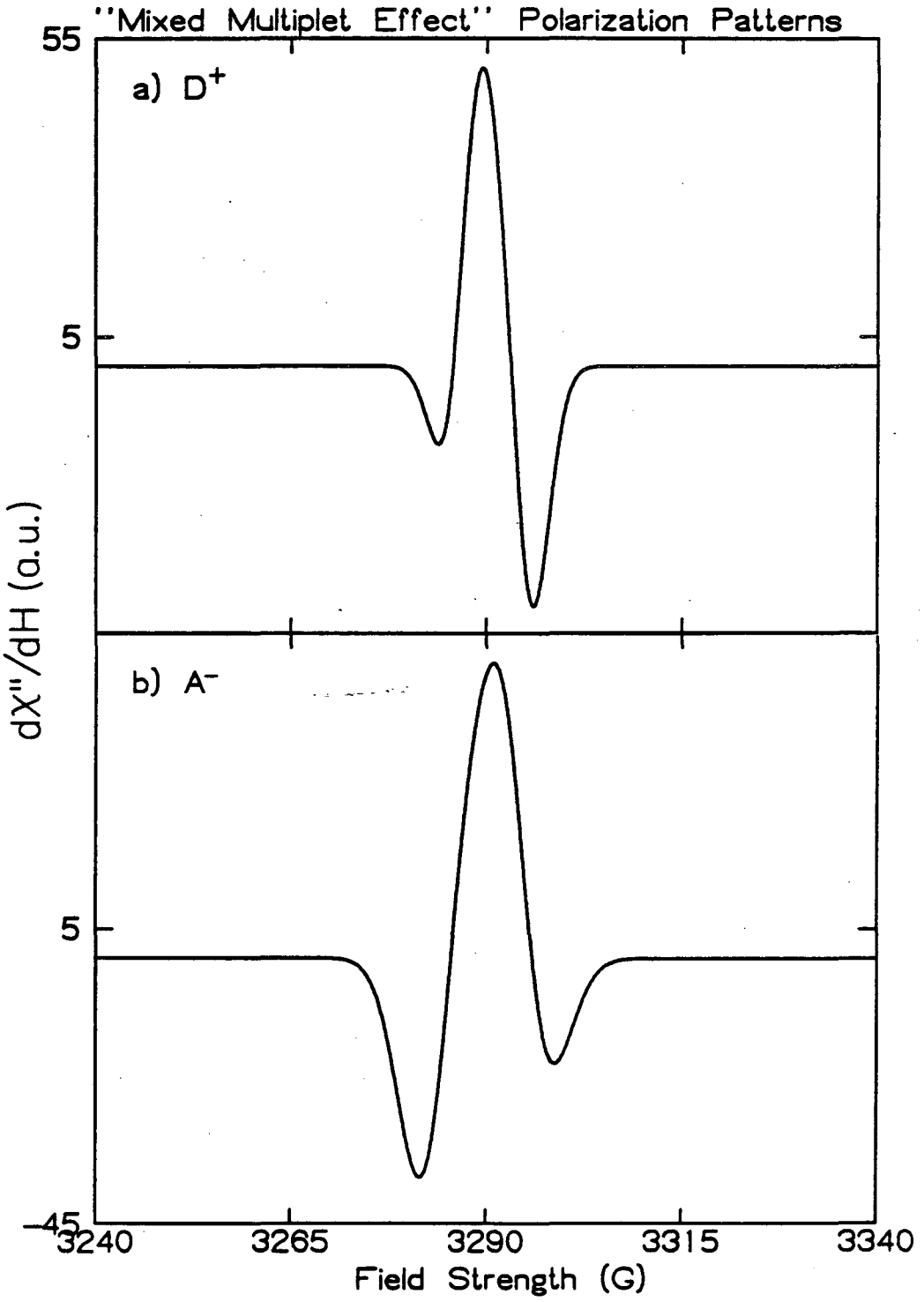
"Mixed Multiplet Effect" Polarization Patterns
55
a) D+
5
dX"/dH (a.u.)
b) A−
5
−45
3240
3265
3290
3315
3340
Field Strength (G)

XBL 835-9819

radical pair decays by forward electron transfer, the polarization on A_1^- at the time of the transfer will also be transferred to the next electron acceptor. This idea of transfer of electron spin polarization is due to Pedersen [17] who developed a "verbal" theory for the phenomenon. According to this theory polarization is transferred from the primary electron acceptor species to a secondary acceptor in a process that does not selectively involve the nuclear states of either radical. Thus, only the net polarization is transferred and it is spread uniformly over the hyperfine states of the secondary acceptor molecule. The situation can be described by a reaction sequence which proceeds as follows:

$$DA_1A_2 \xrightarrow{h\nu} D^+A_1^-A_2 \xrightarrow{\tau} D^+A_1A_2^- .$$

In this sequence D^+ and A_1^- give rise to the radical pair interactions described above and are spin polarized according to Eqn. 2-21. They are said to be statically polarized. Pedersen's proposal is that A_2^- will also be polarized, but that the polarization will be uniform across its spectrum. Only the net polarization on A_1^- will be transferred and only net effect type spectra will be observed for A_2^-. He distinguishes A_2^- from A_1^- and D^+ by calling it a dynamically polarized radical.

Experimental evidence to support this theory has been obtained by Gast, et al. [18-20] in studies on reaction centers of photsynthetic bacteria. Their findings support

Pedersen's idea in general. However, they have found some evidence that the transfer of polarization can be non-uniform [20]. The question of non-uniformly transferred polarization will be addressed in chapter 5.

F. Additional Interactions

The hamiltonian of Eqns. 2-6 through 2-9 is identical to that used by Adrian in his original formulation of the development of CIDEP in radical pair systems [7]. The interactions were all taken to be isotropic because he was modeling a chemical system where the radicals were diffusing about in solution. In contrast, the radicals of interest in PS1 are membrane bound and anisotropy, especially in the spin-spin interaction between the electron donor cation and the acceptor anion, is expected to be significant. Recently, evidence for anisotropy in the spin-spin interaction for the primary radical ion pair of bacterial photosynthesis has been obtained [21,22]. In both of these cases the interaction was interpreted with an isotropic exchange term and an electron-electron magnetic dipole interaction. This type of interaction would have a dramatic effect on the development of CIDEP in PS1 if present. To examine this possibility, studies were done on oriented thylakoid membranes, and a large effect of orientation on the observed CIDEP pattern was found. The data and interpretation of these effects are given in chapter 4 along with a discussion of the effects of dipolar coupling on the

development of CIDEP.

An additional anisotropic interaction that can play a role in the development of CIDEP is g-tensor anisotropy. Friesner, et al. [5] proposed a "two-site" model for the development of CIDEP in PS1 to explain the results of time-resolved EPR experiments done at ambient temperature [12]. This two-site model attributed the development of spin polarization on $P\text{-}700^+$ to radical pair interactions between $P\text{-}700^+$ and A_1^- and between $P\text{-}700^+$ and X^- after electron transfer from A_1^- to X^- had occurred. Because the g-tensor of X^- is anisotropic, this feature was incorporated into the model. In Chapters 4 and 5 the idea of g-anisotropy and the validity of the two-site model will be examined in detail.

A final source of anisotropy to be considered is that of the hyperfine fields of the radicals involved in CIDEP development. The hyperfine anisotropy of Chl a is thought to be small. However, the interactions that give rise to the polarization (Eqn. 2-23) are weak, possibly making anisotropy in the hyperfine fields important. An additional problem for the spectroscopist here is that little is known about hyperfine anisotropy of porphyrin systems. Therefore, the effects of anisotropic nuclear hyperfine coupling will not be considered in the work presented below.

REFERENCES

1. Carrington, A. and McLachlan, A.D.,"Introduction to Magnetic Resonance," Chapman and Hall, London, 1979.
2. Wertz, J.E. and Bolton, J.R., "Electron Spin Resonance," McGraw-Hill, NY, 1972.
3. Poole, C.P., "Electron Spin Resonance", Wiley-Interscience, NY, 1967.
4. Abragam, A. and Bleaney, B., "Electron Paramagnetic Resonance of Transition Ions," Oxford Univ. Press, Oxford, 1970.
5. Friesner, R., Dismukes, G.C. and Sauer, K. (1979) Biophys. J. 25, 277-294.
6. Fessenden, R.W. and Schuler, R.H. (1963) J. Chem. Phys. 39, 2147-2195.
7. Adrian, F.J. (1971) J. Chem. Phys. 54, 3918-3923.
8. Freed, J.H. and Pedersen, J.B. (1976) Adv. Magn. Reson. 8, 1-84.
9. Wan, J.K.S. and Elliot, A.J. (1977) Acc. Chem. Res. 10, 161-166.
10. Atkins, P.W. and McLauchlan, K.A. (1973) in "Chemically Induced Magnetic Polarization," Wiley-Interscience, NY, pp.41-94.
11. Blankenship, R., McGuire, A.E. and Sauer, K. (1975) Proc. Natl. Acad. Sci. USA 72, 4943-4947.
12. Dismukes, G.C., McGuire, A.E., Blankenship, R. and Sauer, K. (1978) Biophys. J. 21, 239-256.

13. Frank, H.A., McLean, M.B. and Sauer, K. (1979) Proc. Natl. Acad. Sci. USA 76, 5124-5128.

14. Kleibeuker, J.F., "The Molecular Photophysics of Chlorophyll," Ph.D. Thesis, Agricultural University, Wageningen, The Netherlands, 1977.

15. McLean, M.B. and Sauer, K. (1982) Biochim. Biophys. Acta 679, 384-392.

16. Syage, J.A. (1982) Chem. Phys. Lett. 91, 378-382.

17. Pedersen, J.B. (1979) FEBS Lett. 97, 305-310.

18. Gast, P. and Hoff, A.J. (1979) Biochim. Biophys. Acta 548, 520-535.

19. Hoff, A.J. and Gast, P. (1979) J. Phys. Chem. 83, 3355-3358.

20. Gast, P., Mushlin, R.A. and Hoff, A.J. (1982) J. Phys. Chem. 86, 2886-2891.

21. Roelofs, M., Chidsey, C.E.D. and Boxer, S.G. (1982) Chem. Phys. Lett. 87, 582-588.

22. Norris, J.R., Bowman, M.K., Budil, D.E., Tang, J., Wraight, C.A. and Closs, G. (1982) Proc. Natl. Acad. Sci. USA 79, 5532-5536.

CHAPTER 3

TIME-RESOLVED EPR INSTRUMENTATION

A difficulty with doing time-resolved EPR spectroscopy on spin-polarized radicals is that the polarization is often short lived, even at cryogenic temperatures. In photosynthetic systems, both the chemical lifetime of the radical species and their associated spin-lattice relaxation times can be on the order of microseconds. Thus, these processes can be much faster than the time resolution of commercially available EPR instruments (the intrinsic time constant of a Varian E-line series spectrometer is approximately 0.5 msec). In this chapter the experimental apparatus developed to study spin-polarized radicals in PS1 will be discussed with an emphasis on the EPR spectrometers used.

3.1 Overall System

A block diagram of the experimental apparatus is shown in Fig. 3-1. The heart of the system is an EPR spectrometer that differs from those normally used for steady state experiments in that it has faster time resolution. Two spectrometers were used in this work. One was a modified Varian E-109 spectrometer that employed 1 MHz magnetic field modulation and had a minimum time response of 2 μsec. The

Fig. 3-1. A block diagram of the time resolved EPR experimental, apparatus used in the studies presented in this thesis. The spectrometers are described in the text. The transient EPR signals were recorded on a Nicolet Explorer IIIA digital oscilloscope equipped with a model 204 plug-in; the computer was a Digital Equipment Corporation VAX 11/780; and the pulsed dye laser used in these experiments was a Phase-R DL-1400.

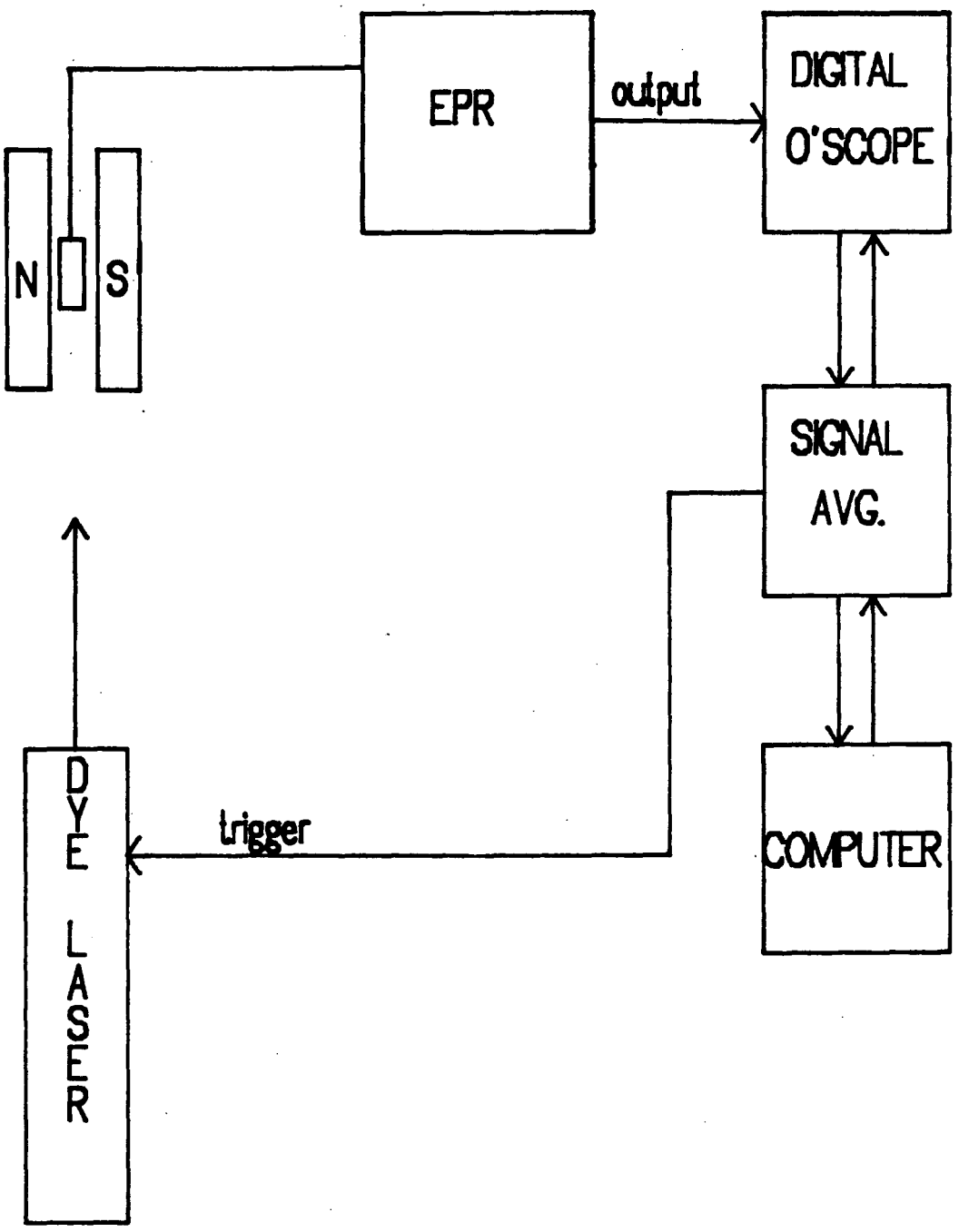
EPR
output
DIGITAL
O'SCOPE
N
S
SIGNAL
AVG.
DYE LASER
trigger
COMPUTER

XBL 835-9828

other was a superheterodyne spectrometer which did not employ magnetic field modulation and had a minimum time constant of approximately 300 nsec. These spectrometers will be discussed in more detail in the next section.

Control of the experiment is managed by a home-built signal averager. The averager begins the experiment by simultaneously triggering a pulsed dye laser (Phase-R model DL-1400) and the sweep of a digital oscilloscope (Nicolet Explorer IIIA with model 204 plug-in). After being triggered, the dye laser emits a laser pulse; the sample is excited; and EPR signals generated by the flash are recorded on the oscilloscope. The digitized spectrometer output is then read by the signal averager, and the sequence is repeated until good signal-to-noise for the transient signal at the field position of interest is obtained. After a specified number of passes has been completed, the data are transferred to a VAX 11/780 computer (Digital Equipment Corp.) for analysis and storage. The field position can then be changed and the above sequence repeated. The raw data consist of kinetic traces, each of which was collected at a fixed magnetic field strength, usually in the g 2.0 region.

An example of the raw data is shown in Fig. 3-2. The data are from chloroplasts at 9K and at a field position corresponding to g=2.0041. The laser pulse is delayed until about one-fifth of the way into the sweep. The flash produes a transient EPR signal that decays biphasically,

Fig. 3-2. Transient EPR signal from chloroplasts at 9K. The chloroplast sample was prepared so that Fe-S centers A and B were reduced prior to application of the actinic flash. The sample preparation involved treatment of the chloroplast suspension (approx. 3 mg/ml chl) with ascorbate and illumination while freezing. The details of this preparation are given in chapter 4. The laser flash energy was about 30 mJ/pulse. The conditions for this measurement were: microwave frequency, 9.147 GHz; microwave power, 50 μW; field position, 3261 G; modulation frequency, 1 MHz; and modulation amplitude, 2.5 G. The trace is the average of 500 events.

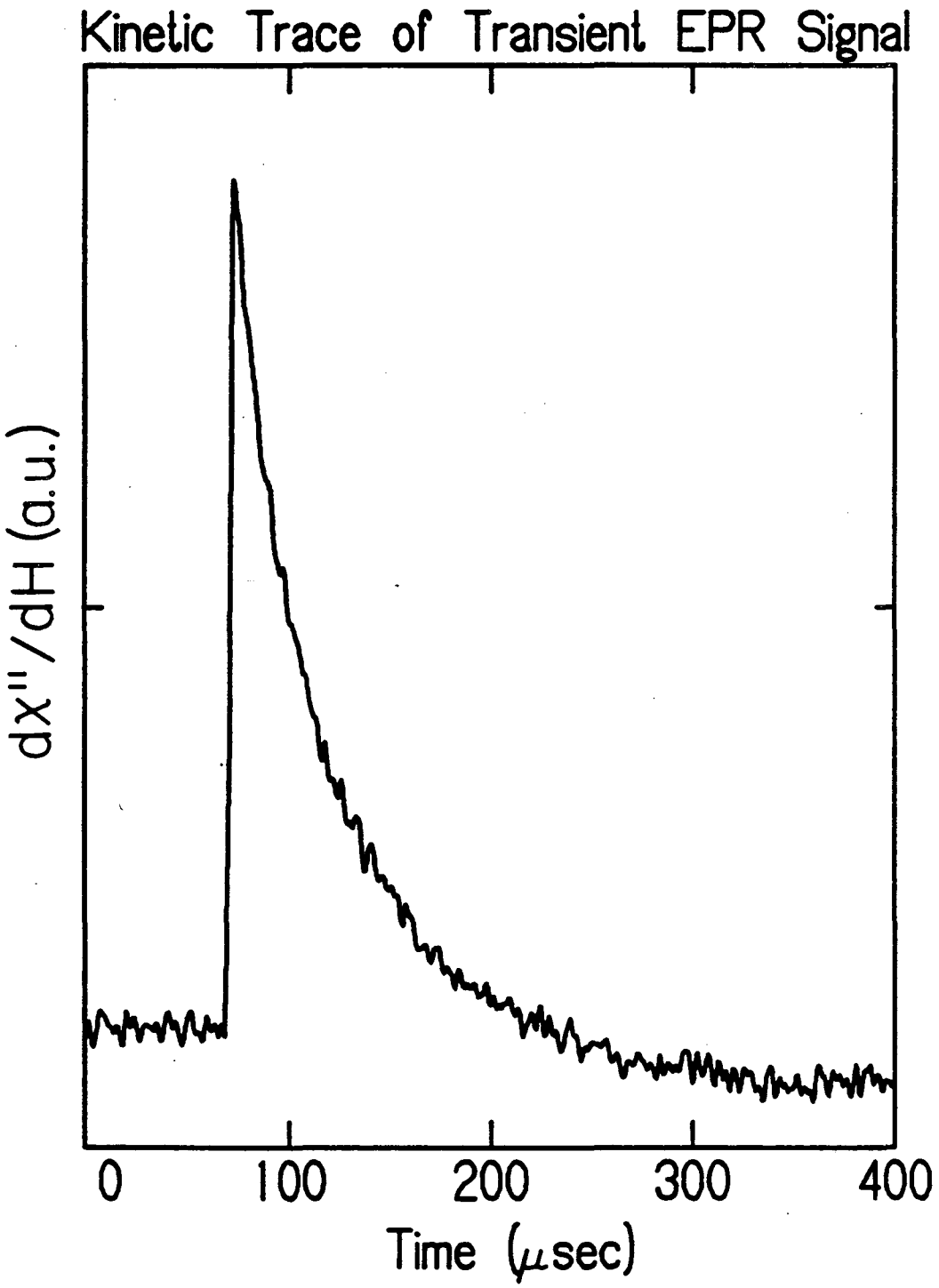
Kinetic Trace of Transient EPR Signal
dX''/dH (a.u.)
0
100
200
300
400
Time (μsec)

XBL 835-9827

with the major component having a lifetime (1/e time) of 50 μsec. The signal rises with the instrument response time, as is the case for all of the data presented in this thesis. In most experiments, kinetic traces were collected at about 30-40 different field positions in the g 2.0 region. Each trace was then fit with a one- or two-exponential decay model using a non-linear least squares computer routine (ZXSSQ of the International Math-Science Library). After fitting, the amplitudes of the various kinetic phases can be plotted as a function of magnetic field strength to generate a time-resolved EPR spectrum or field profile of the component. These field profiles will be the focus of chapters 4 and 5. Chapter 6 will deal with the dynamical information obtained from these measurements.

3.2 Spectrometers

Three basic techniques are utilized to do time-resolved EPR spectroscopy. Two of these approaches involve standard, continuous-wave microwave bridges; they differ in that one uses a more conventional magnetic field modulation scheme and the other involves 'direct' or wideband detection of the EPR output. Fast time-resolved EPR spectrometers that employ magnetic field modulation use high modulation frequencies (1-2 MHz) and have a time response of 1-2 μsec [1,2]. The time response in these systems is a property of the high frequency lock-in amplifier, which must integrate over at least two cycles of information before significant output

can be obtained. The major difficulty with this type of detection is that for the examination of fast transient signals the possibility of rapid passage distortion of the signal amplitude and dynamics is very real [3-6]. Examination of theoretical and experimental work done on rapid passage indicates that in many instances it may be difficult to test for its presence in the data. In these cases, the only definite test is to do the experiment without field modulation (direct detection). Therefore, the studies done in this thesis have utilized both techniques and both instruments will be described below.

A. 1 MHz System

The 1 MHz magnetic field modulation system used in this work is built around a Varian E-109 EPR spectrometer. The system consists of a separate 1 MHz field modulation and detection system which is substituted for the 100 KHz system during operation. The details of the 1 MHz lock-in amplifier and the conversion have been given in [1]. The modifications made to the Varian E-109 microwave bridge were: the bandwidth of the preamp had to be extended because its high frequency -3db point was only 800 KHz; and the bridge housing had to be shielded from radio-frequency radiation which is generated by the dye laser upon firing. The bandwidth of the preamp was extended by adding a second low gain (3db) amplifier stage to the preamp output line. This amplifier is used only when operating the system at 1 MHz so

that the normal, 100 KHz, operation is not affected. Shielding the system from RF generated by the dye laser was achieved by carefully shielding the dye laser system, the bridge housing, and their associated electronic components and cables. The measured time response of this system was 2 sec.

A nice feature of a field modulation detection scheme is that it is insensitive to non-resonant disturbances in the cavity after irradiation with the laser pulse. Light artifacts due to heating of the resonant cavity are always present, but they will not appear at the output of the 1 MHz lock-in amplifier because they do not have the proper carrier frequency associated with them. The beauty of a field modulation detection scheme is that only the sample resonance couples the carrier frequency to the spectrometer. A word of caution concerning this light artifact is in order. At high microwave power (above 1 mW) the 'glitch' created by the light flash is large enough to saturate the preamp of the E-102 microwave bridge. This causes the system essentially to shut down for as long as 100 μsec after the flash. Therefore, the light intensity at high microwave power must be kept low (approximately 10 mJ/pulse or less). Most of the work presented in this thesis was done at an incident microwave power of 50 μW or less. In this microwave power range, laser pulses of up to 100 mJ may be used without noticeable effects. In most of the experiments presented in this thesis, laser pulse

energies of about 30 mJ were utilized.

Another problem concerning high frequency field modulation is that only small modulation fields can be achieved in a conventional EPR cavity like the Varian E-231 (TE_{102} cavity). The standard approach to this problem is to lower the modulation coil impedence by connecting the two coils in parallel and capacitively matching them at 1 MHz. The impedence of the coils used in our system was about 120 Ω when matched. The coils were driven at 1 MHz with an ENI 420L 20 watt power amplifier. The problem here is that even with 1-2 A peak-to-peak current, the maximum modulation field in the cavity is only about 3 G. This significantly reduces the sensitivity of the system. Because the cavity wall thickness is much less than the skin depth of the material at 1 MHz, much of the energy is probably dissipated in the form of eddy currents set up in the cavity walls. This problem could possibly be alleviated by modifying the walls (perhaps breaking up the eddy currents with some type of slit pattern), or by introducing the modulation internally through a coil placed near the sample [7].

B. Direct Detection System

In the direct detection system, the output of the microwave detector is sampled directly via wideband amplification [8]. The spectrometer time response for this scheme is determined by the ring down time of the resonant cavity and is a function of the Q of the resonator and its

resonant frequency. The expression for the response time is: $t=Q/\omega$. For a typical cavity Q of 5000 and $\omega = 2\pi(9E+09\ s^{-1})$, one obtains t=100 nsec. In practice, response times of 200-400 nsec have been realized [8-10]. The price that one pays for increasing the time resolution by a factor of ten is the degradation of the instrument's sensitivity. The sensitivity decrease is due to an increase in system noise caused by the wider detection bandwidth, the increased sensitivity to source FM noise, and spectrometer microphonic noise in the output.

The problems stated above were encountered when initial attempts to do direct detection with the Varian E-109 system were made. Signals from concentrated reaction center preparations could be observed, but the sensitivity was low and the data were often masked by light and RF induced artifacts. A direct detection system is much more sensitive to RF artifacts because of the wideband nature of the detection. An additional sensitivity problem arises because, to keep the level of the light induced artifact low, the laser intensity had to be attenuated to the point where the sample was no longer saturated by the light flash. Thus, the number of spins that could be generated in the cavity was reduced. A final problem with using the Varian system was that the wideband output contained a considerable amount of 60 and 120 Hz noise (hum) and 70 KHz noise from the AFC system.

To get around the sensitivity problem and still achieve

200 nsec time resolution, a superheterodyne EPR spectrometer was constructed. Previous work done with this type of detection scheme [11] showed that relatively high sensitivity could be attained without the use of field modulation. Although light artifacts are still a problem with this system, noise due to RF artifacts could be easily eliminated and sensitivity gained. Diagrams for the superheterodyne microwave bridge constructed for the direct detection measurements are shown in Figs. 3-3 and 3-4. Fig. 3-3 is a conventional diagram and Fig. 3-4 is a block diagram intended to aid the reader in understanding the functions of the various 'arms' of this instrument. The design is a modern version of that built by Teaney, et al. [11].

As depicted in Fig. 3-3, radiation from the microwave source, a low-noise Gunn oscillator (Central Microwave), is sent to three different arms of the bridge. The bulk of the power is used to irradiate the sample, which is placed in a standard Varian TE_{102} reflection cavity. Reflected radiation from the cavity is mixed with radiation from the bucking arm, amplified by a low noise microwave GaAs FET amplifier (Narda model N6204S-78) and fed into the RF port of a balanced mixer (RHG model WM8.5-9.6/15A). The balanced mixer is biased with microwave radiation from a local oscillator (a varactor-tuned Gunn oscillator, Narda model 911-VGO-002) whose output frequency is displaced from that of the source by 60 MHz. Therefore, the mixer output is a difference or

Fig. 3-3. Schematic diagram of the superheterodyne microwave bridge used in direct detection measurements. A key for the various symbols used in this diagram is given below.

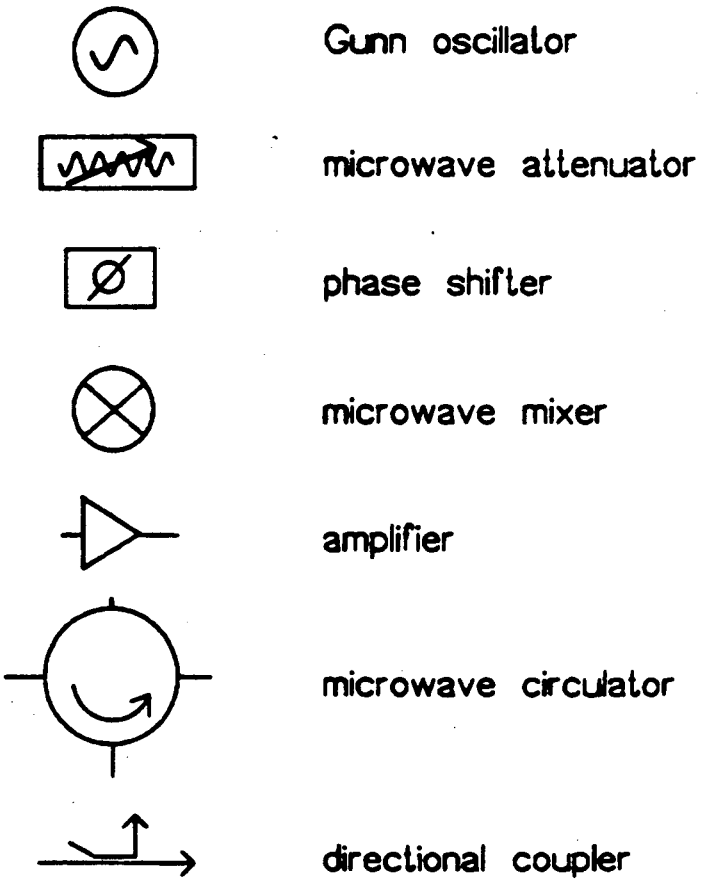

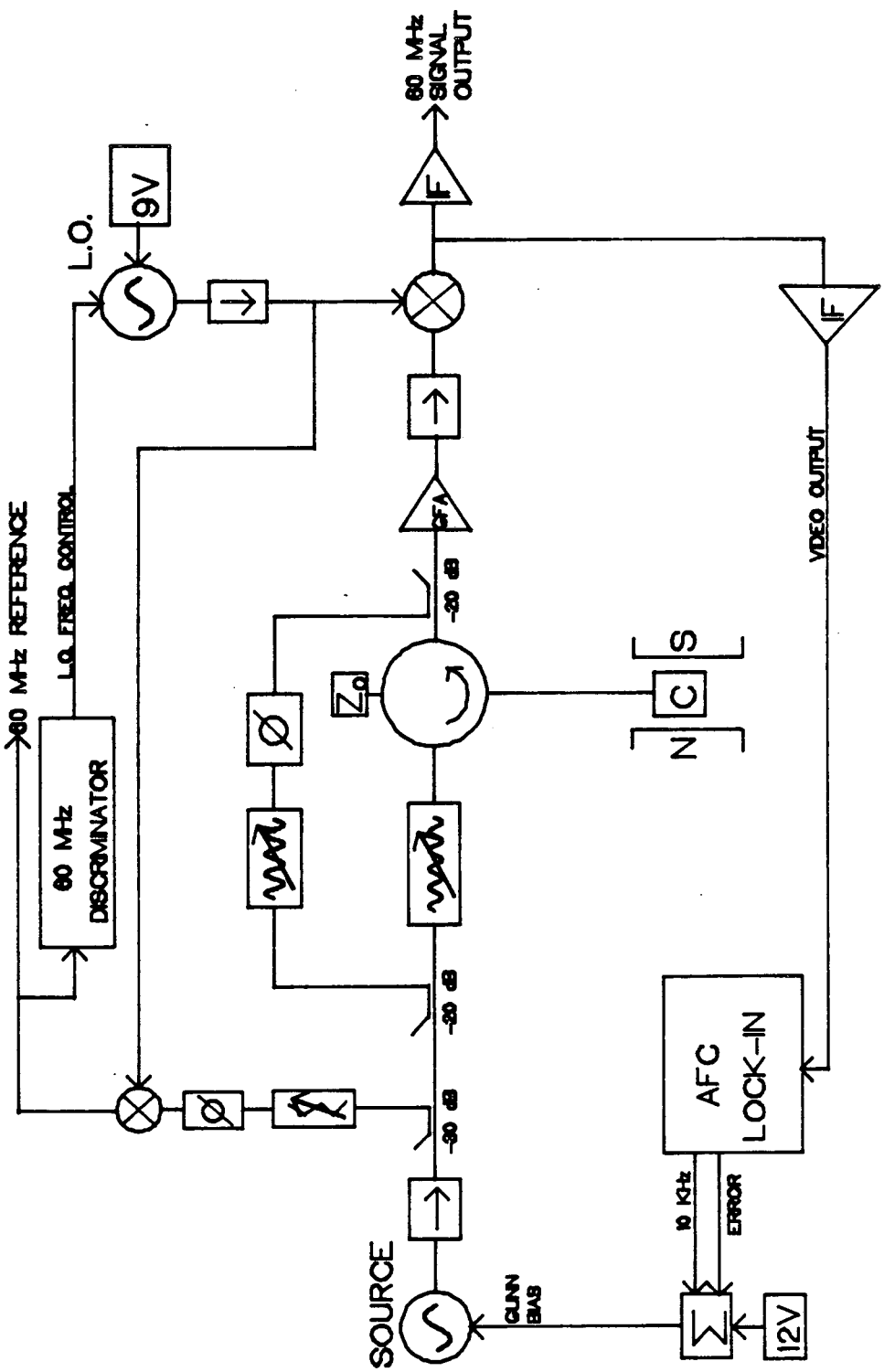
60 MHz SIGNAL OUTPUT
9V
L.O.
IF
IF
60 MHz REFERENCE
L.O. FREQ. CONTROL
60 MHz DISCRIMINATOR
VIDEO OUTPUT
-20 dB
-30 dB
-30 dB
S
C
N
AFC LOCK-IN
10 KHz
ERROR
SOURCE
GUNN BIAS
12V

XBL 835-9820

Fig. 3-4. Block diagram of the microwave bridge shown in Fig. 3-3.

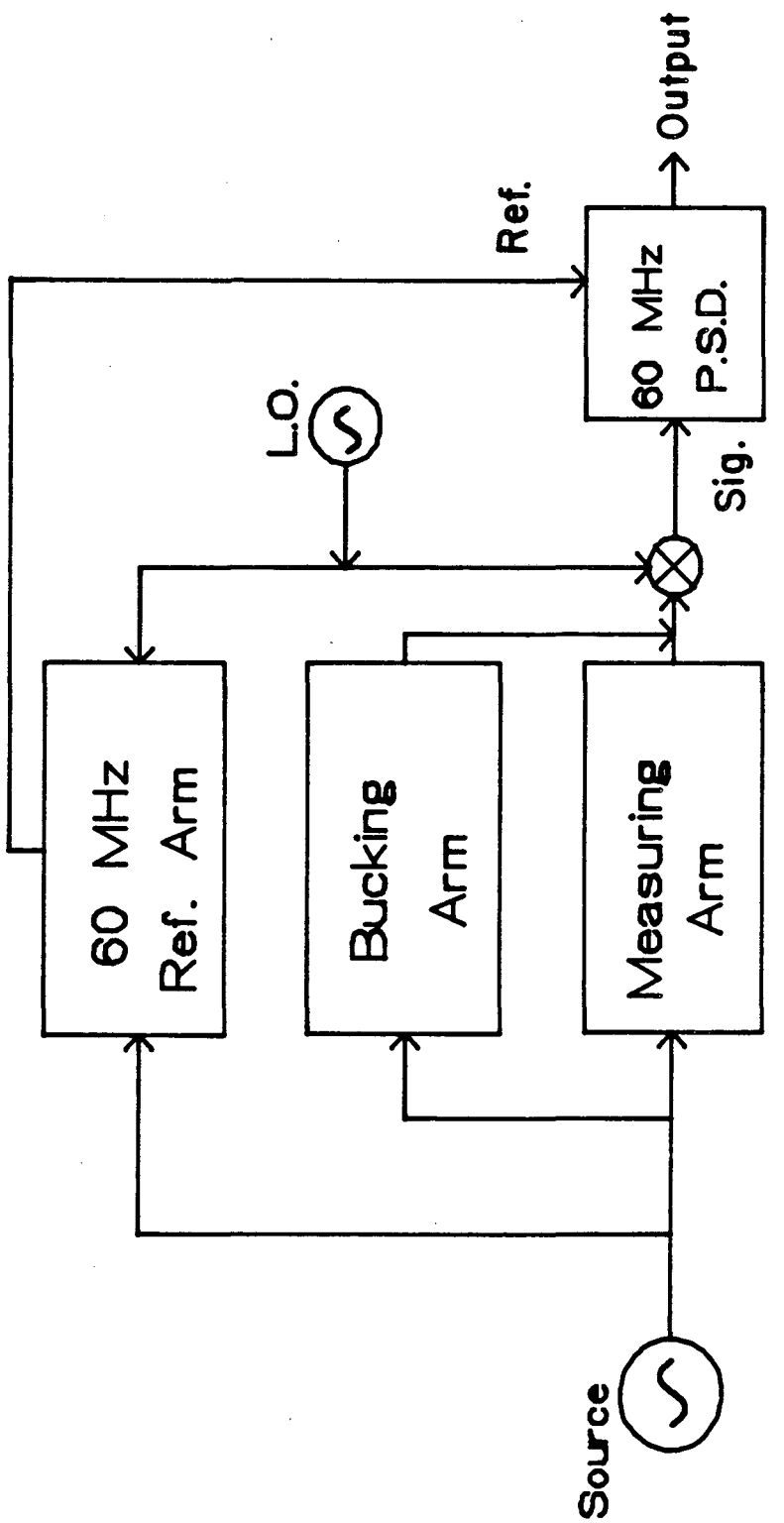
Output
Ref.
60 MHz
P.S.D.
L.O.
Sig.
60 MHz
Ref. Arm
Bucking
Arm
Measuring
Arm
Source

XBL 835-9845

intermediate frequency (IF) of 60 MHz. This output is then amplified by a narrow band 60 MHz IF amplifier (RHG Laboratories) and phase detected by a 2-phase, phase sensitive detector. The 60 MHz reference signal for the phase detection is generated by a second mixer on the bridge in the 60 MHz reference arm. The microwave phase shifter in this arm is used to adjust the phase of the 60 MHz reference signal relative to the IF signal from the signal mixer. The purpose of the bucking arm is to null the reflected radiation from the cavity and is used only when high output gains are required. Additional amounts of source radiation are used to monitor the microwave power and frequency. The frequency was monitored with a wavemeter (Hewlett-Packard model X532B), and the microwave power was measured with a Hewlett-Packard model 432A power meter.

The superheterodyne microwave bridge requires the use of two separate automatic frequency control (AFC) systems. One system is used to lock the source oscillator to the resonant frequency of the cavity and the other is needed to control the frequency of the local oscillator so that the IF is held at 60 MHz. The source AFC is of the conventional frequency modulation type [12]. As Fig. 3-3 indicates, the error signals generated by drifting of the source from cavity resonance are measured by a lock-in amplifier (Princeton Applied Research model HR-8). This error signal is summed with the source oscillator's dc bias voltage to alter the output frequency and to adjust the source

frequency to the cavity resonance frequency. The second AFC system consists of a finely tuned 60 MHz frequency discriminator which generates an error voltage when its input frequency is other than 60 MHz. The signal source for the discriminator is the 60 MHz reference signal for the phase sensitive detector. The error signal from this AFC is amplified, integrated and used to drive the varactor tuning port on the local oscillator. Frequency adjustment of the local oscillator is always done automatically.

Besides having a faster time response, the superheterodyne spectrometer allows one to conveniently check for the presence of rapid passage distortion of the time-resolved EPR data. The overall sensitivity is about ten fold less than that of the 1 MHz system, as can be seen from the comparison shown in Fig. 3-5. As stated above, the two major reasons for this are: the superheterodyne instrument has increased detection bandwidth, and the superheterodyne experiments must be run with laser pulse energies that are a factor of ten lower than those used in the 1 MHz experiments. At laser pulse energies of 5-10 mJ, the light artifact becomes small in comparison to the signals and the experiments can be accomplished. However, the number of spins that one is sampling is dimenished under these conditions. In Fig. 3-5 the transient signals are of opposite sign because the derivative trace, Fig. 3-5a, is taken at a field position where the signal is on the positive sloping side of an emission transient.

Fig. 3-5. A comparison of kinetic data obtained with the 1 MHz field modulation system (trace a) and the direct detection system (trace b). In both cases, the sample was chloroplasts prepared with Fe-S centers A and B reduced as described in chapter 4, which had been oriented and placed in the spectrometer so that the thylakoid membrane normals were parallel to the direction of the dc field. The conditions for the measurement of Fig.3-5a were: microwave frequency, 9.224 GHz; microwave power, 50 μW; sample temperature, 56K; field position, 3287 G; 1 MHz field modulation; modulation amplitude, 2.5 G; and laser pulse energy, 50mJ. The conditions for Fig. 3-5b were: microwave frequency, 9.225 GHz; microwave power, 50 μW; sample temperature, 62K; field position, 3291 G; direct detection of microwave power was utilized; and laser flash energy, 5mJ. Both traces represent the average of 500 events.

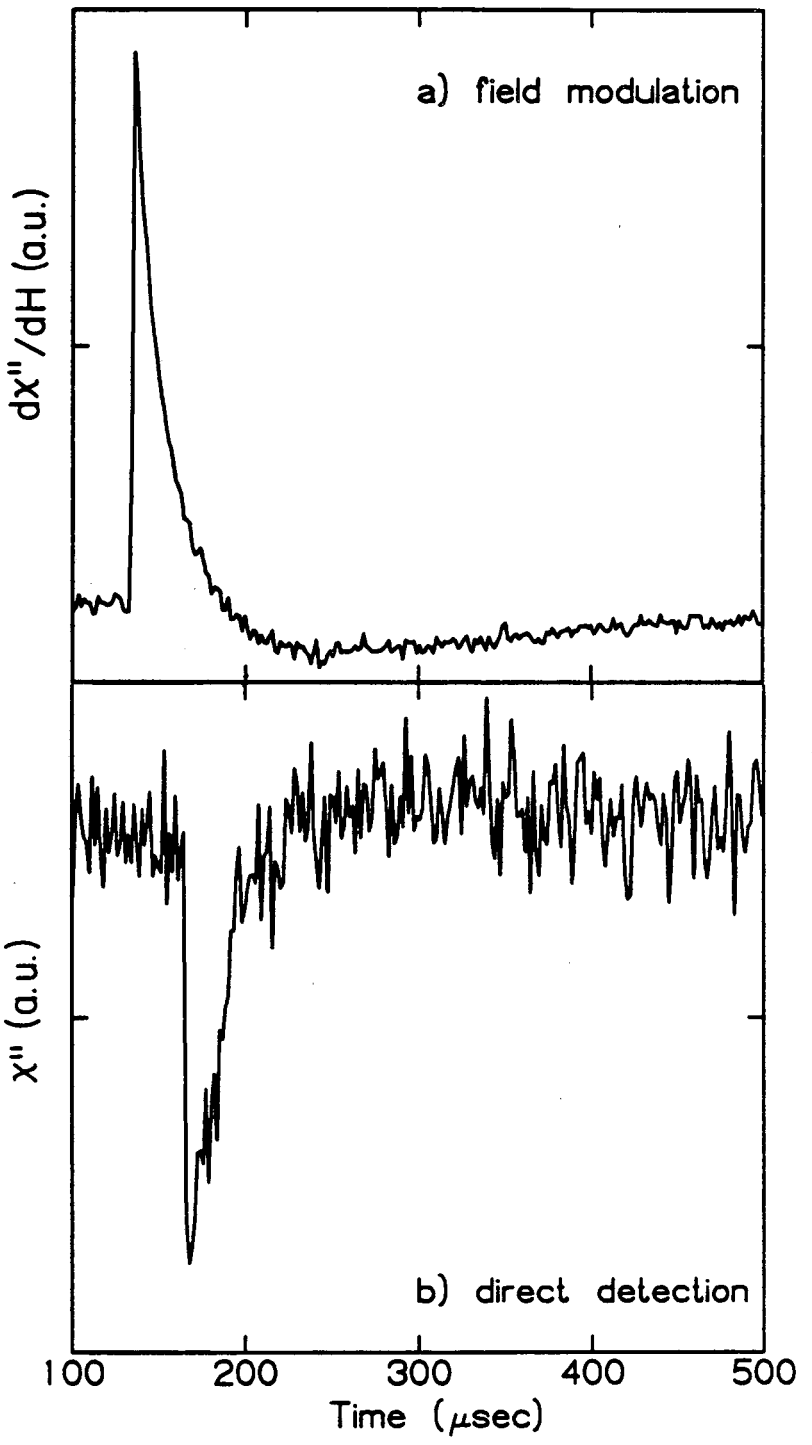
a) field modulation
dχ''/dH (a.u.)
χ'' (a.u.)
b) direct detection
100
200
300
400
500
Time (μsec)

XBL 835-9843

If the data of Fig. 3-5 are taken at similar light intensities, the 1 MHz system has a factor of only 3 to 5 better signal-to-noise ratio than the direct detection data. This difference can be accounted for by the increased detection bandwidth. Thus, the two spectrometers have comparable sensitivities for the detection of microsecond time-scale transient signals, but the effective sample size that one can achieve with the 1 MHz system is larger than that obtainable with the direct detection instrument.

REFERENCES

1. Smith, G.E., Blankenship, R. and Klein, M.P. (1977) Rev. Sci. Instrum. 48, 282-286.
2. Atkins, P.W., McLauchlan, K.A. and Simpson, A.F. (1970) J. Phys. E 3, 547-551.
3. Portis, A.M., "Magnetic Resonance in Systems with Spectral Distributions," Technical Note No. 1 of the Sarah Mellon Scaife Radiation Laboratory, University of Pittsburgh, Nov. 15, 1955.
4. Weger, M. (1960) Bell. Syst. Tech. J. 39, 1013-1112.
5. Pasimeni, L.J. (1978) J. Magn. Reson. 30, 65-73.
6. Friesner, R., McCracken, J.L. and Sauer, K. (1981) J. Magn. Reson. 43, 343-356.
7. Trifunac, A.D. and Thurnauer, M.C. (1979) in "Time Domain Electron Spin Resonance," Wiley-Interscience, NY, pp. 107-152.
8. Kim. S.S. and Weissman, S.I. (1976) J. Magn. Reson. 24, 167-169.
9. Trifunac, A.D., Thurnauer, M.C. and Norris, J.R. (1978) Chem. Phys. Lett. 57, 471-473.
10. Hore, P.J., "Electron Spin Resonance Studies of Polarized Species," Ph.D. Thesis, Oxford, England, 1980.
11. Teaney, D.T., Klein, M.P. and Portis, A.M. (1961) Rev. Sci. Instrum. 32, 721-729.
12. Poole, C.P., "Electron Spin Resonance," Wiley-Interscience, NY, 1967.

CHAPTER 4

LOW TEMPERATURE CIDEP FROM PHOTOSYSTEM 1 - PART 1

The first observation of CIDEP resulting from the primary photochemistry of PS1 was made by Blankenship, et al. [1]. These authors observed spin-polarized EPR signals in the g 2.0 region and attributed them to P-700$^+$. Subsequent experiments [2] supported this assignment and showed that the spin polarization pattern of P-700$^+$ was orientation dependent. Both of these reports were of experiments that were carried out at room temperature on untreated chloroplasts. Under these conditions the actinic flash generates the P-700$^+$ A_1^- radical pair, but the pair is short lived because electron transfer from A_1^- to X occurs in 200 psec [3]. The spin polarization on P-700$^+$ will be longer lived and will decay with T_1, the spin-lattice relaxation time of the molecule. Spin polarization on the primary acceptor species can never be observed in experiments of this design, because the species is too short-lived.

To analyze the data in [2], Friesner, et al. [4] used a "two-site" model for spin polarization development in PS1. In this model, polarization develops on P-700$^+$ due to radical pair interactions between P-700$^+$ and A_1^-, and between P-700$^+$ and X^- after electron transfer from A_1^- to X

has occurred. Because X^- has an anisotropic g-tensor, the $\Delta g\beta H$ term in Eqn. 2-23 is orientation dependent for the second radical-pair interaction. The inclusion of X^- was required in this model to describe the orientation dependence of the CIDEP of $P\text{-}700^+$. Both spin-spin interactions, that between $P\text{-}700^+$ and A_1^- and that between $P\text{-}700^+$ and X^-, were modeled with an isotropic exchange term.

In the work presented in this chapter and in chapter 5, an attempt is made to repeat the above experiments on spinach chloroplasts treated so that various acceptors of PS1 are reduced prior to application of the actinic flash. Specifically, the spin polarized spectra in the g 2.0 region are examined as a function of the oxidation-reduction state of PS1. The objectives of these experiments are given below.

1. To learn something about the chemical nature of the primary electron acceptor species. This can be achieved by blocking forward electron transfer so that the reduced primary electron acceptor becomes long-lived. The information obtained will be in the form of g-values and linewidths of the acceptor anion.

2. To test the one and two-site models proposed by Friesner, et al. [4] by creating situations where only one radical pair interaction can occur and situations where two radical pair interactions are possible. This is accomplished by:

a. Preparing samples in a redox state where X is reduced prior to flash stimulation, so that only the first radical pair forms:

$$\text{P-700 } A_1 \text{ } X^- \text{ } (Fd_{B,A})^= \xrightarrow{h\nu} \text{P-700}^+ \text{ } A_1^- \text{ } X^- \text{ } (Fd_{B,A})^=$$

Results from samples prepared in this state will be discussed in chapter 5.

b. Preparing samples in a redox state where only bound Fe-S centers A and B are reduced prior to flash stimulation, so that two successive radical pairs are formed:

$$\text{P-700 } A_1 \text{ } X \text{ } (Fd_{B,A})^= \xrightarrow{h\nu} \text{P-700}^+ \text{ } A_1^- \text{ } X \text{ } (Fd_{B,A})^=$$

$$\text{P-700}^+ \text{ } A_1 \text{ } X^- \text{ } (Fd_{B,A})^=$$

Results from samples prepared in this redox state will be examined in this chapter.

3. To study the orientation dependence of the CIDEP signals in the g 2.0 region in more detail to determine whether the g anistropy of X^- is responsible for the effects previously observed [2] or that the effects are due to some other orientation dependent interaction such as an anisotropic spin-spin interaction between P-700$^+$ and A_1^-. Analyses of these

effects give information concerning reaction center structure.

In addition to studying chloroplast samples under reducing conditions, data presented in this thesis were collected at cryogenic temperatures. This serves two functions: to ensure that, once samples are redox poised, they remain at that potential for the course of the experiment; and to slow down the decay processes so that the signals could be time resolved with our instruments.

4.1 Materials and Methods

Time-resolved EPR measurements were made at X-band with the experimental apparatus described in chapter 3. A TE_{102} cavity (Varian model E-231) was used for these measurements and was fitted with an optical transmission flange to allow 100% entry of the exciting light. For low temperature operation, the spectrometer was equipped with an Air Products Helitran Cryostat (model LTD-3-110), and temperature measurements were made with a gold-chromel thermocouple.

Microwave frequency measurements were made with a Hewlett-Packard model X532B wavemeter, and g-values were calibrated with 'weak pitch' (2.0028) and DPPH (2.0037). The field modulation amplitude was calibrated using an aqueous sample of Fremy's salt (ICN Pharmaceuticals/K+K Labs Inc.) [5] using the standard line broadening technique [6]. The

light source for these experiments was a Phase-R DL-1400 dye laser which was operated broadband at 640 nm (Rhodamine 101 in methanol (Exciton Chemical)). The laser pulse width was 400 nsec (FWHM), and saturating pulses of 30 mJ were utilized in field modulated experiments. In direct detection measurements, the laser pulse energy had to be kept below 5 mJ to avoid the light artifacts mentioned in chapter 3.

Broken spinach chloroplasts were prepared using a standard procedure [7] and then treated in one of two different ways:

a. Treatment with ascorbate. Broken chloroplasts were suspended in 50 mM Tris buffer (pH=8.0) containing 10 mM NaCl, 0.1 mM EDTA, and 50 mM sodium ascorbate.

b. Treatment with ferricyanide. Broken chloroplasts were suspended in 50 mM Tris buffer (pH=8.0) containing 10 mM NaCl, 0.1 mM EDTA, and 10 mM $K_3Fe(CN)_6$.

Orientation of the various chloroplast thylakoid suspensions used in these experiments was achieved by one of two different techniques: partial dehydration of the samples on mylar [8,9]; or alignment in a high magnetic field [10]. The procedure for orienting samples by partial dehydration on mylar is as follows. Mylar strips (approximately 2.5mm x 50mm; thickness, 0.25mm) were soaked in a solution containing 1% collodion (Mallinckrodt), 99% ethanol and allowed to dry. A thick chloroplast suspension

(approximately 3 mg/ml) was then pipetted onto the strips which were supported horizontally on a teflon drying rack. The rack was then placed in a 90% relative humidity environment or in a N_2 environment at 4^oC and allowed to dry. When drying was achieved by flowing N_2 gas over the strips, the flow rate was adjusted so that the process took about 4h. When drying was done in a 90% relative humidity environment, drying took about 36 h. In both cases, good orientation was obtained, and for most of this work the drying was done in a N_2 gas environment. After drying, approximately 5 strips were stacked into a "sandwich" and placed in a standard quartz EPR tube (3mm I.D.).

The other procedure for orienting chloroplasts involves freezing them in a 13.5 kG magnetic field. It has been shown that thylakoid membranes can be aligned in magnetic fields > 9kG so that the membrane normals are parallel to the direction of the alignment field [10]. When using this technique care was taken to ensure that the sample was a clear glass when frozen. This was done by preparing the chloroplast suspensions so that they were 60% ethylene glycol by volume. Orientation by field alignment gives lower ordering than that obtained with drying, but it will be used extensively in chapter 5 where many of the sample preparations are treated with sodium dithionite to poise them at low potential.

In many instances the samples were illuminated while being cooled to liquid N_2 temperature. The light source for

these treatments was a 400W tungsten lamp (Cary) filtered through a Calflex heat reflection filter (Balzers). The samples discussed in this chapter were illuminated at low intensity (6.2 W/m^2) for 20 sec at room temperature and then immediately placed in an optical dewar containing liquid N_2 and illuminated during another 20 sec.

4.2 Results

A. Steady state spectra

Prior to doing flash studies on the various samples studied in this work, the steady state EPR spectra of reduced Fe-S centers A and B and of reduced X (where applicable) were examined as a function of the angle between the normal to the mylar strips (coincident with the thylakoid membrane normal) and the direction of the spectrometer's DC magnetic field. For magnetically aligned chloroplasts, the membrane normals are coincident with the direction of the alignment field. These observations serve a dual function: (a) to determine the degree to which the thylakoid membranes were oriented in the sample; and (b) to determine the redox poise of PS1 as a result of the various sample treatments. For a review of these spectra and their orientation dependence see [8,11,12]. Fig. 4-1 shows the steady state EPR spectra (taken in the dark) from samples prepared so that Fe-S centers A and B are reduced. In the parallel orientation (membrane normal parallel to the

Fig. 4-1. Steady state EPR spectra of oriented spinach chloroplast thylakoids measured in the dark with: (a) the membrane normals parallel to the field direction; and (b) the membrane normals perpendicular to the field direction. Samples were suspended in 50mM Tris buffer (pH=8.0) containing 50mM ascorbate, 10mM NaCl and .1mM EDTA, then oriented by partial dehydration on mylar and illuminated while freezing to 77K. The spectrometer settings were: microwave frequency, 9.206 GHz; field modulation amplitude, 10G; modulation frequency, 100 KHz; microwave power, 10 mW; and sample temperature, 13K.

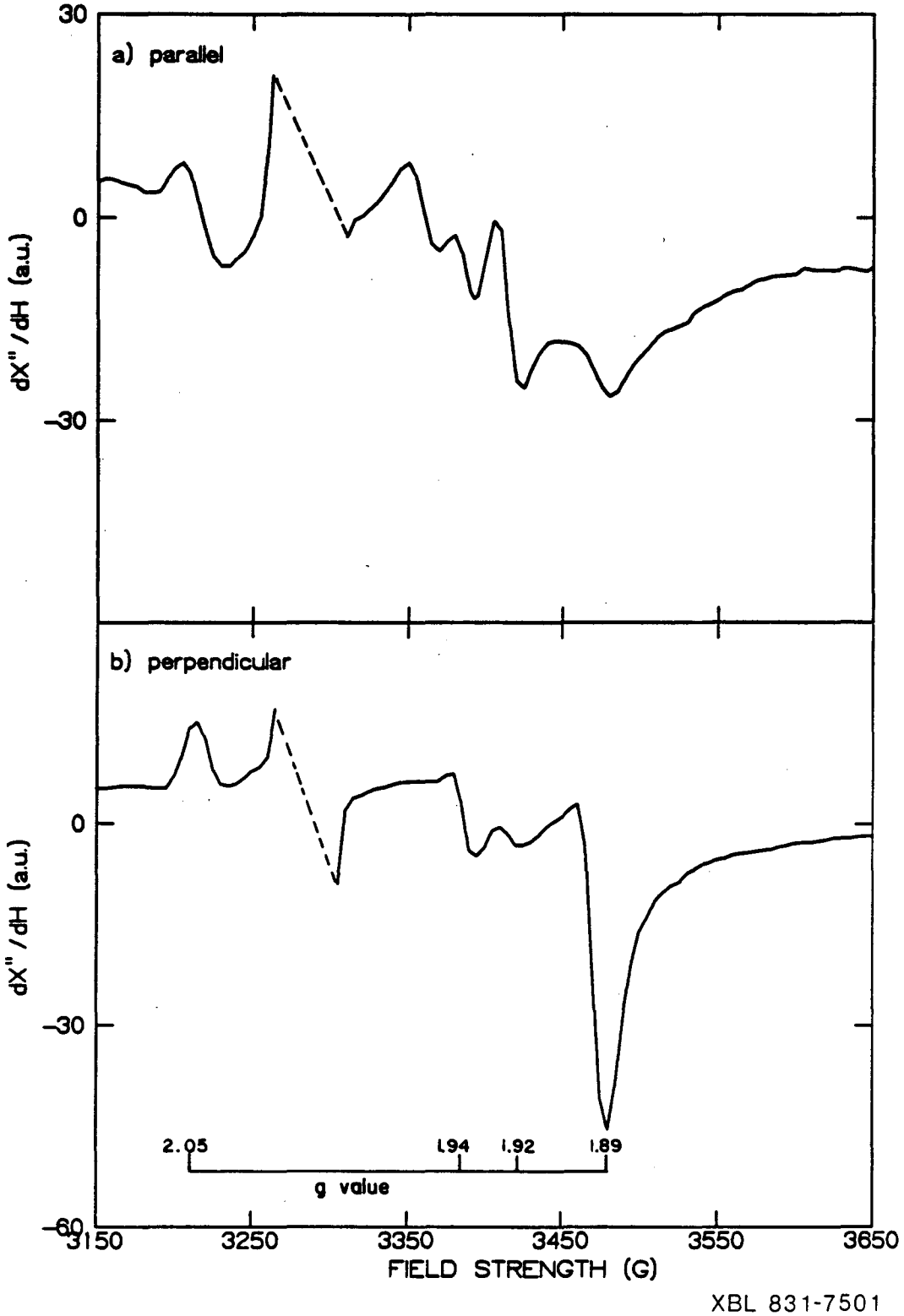
30
a) parallel
0
-30
dX"/dH (a.u.)
b) perpendicular
0
-30
-60
dX"/dH (a.u.)
2.05
1.94
1.92
1.89
g value
3150
3250
3350
3450
3550
3650
FIELD STRENGTH (G)

XBL 831-7501

magnetic field direction - Fig. 4-1a) the ratio of the amplitude (measured from the baseline) of the signal at g 1.89 to the signal at g 1.92 is nearly 1, while in the perpendicular orientation (Fig. 4-1b) this ratio is typically >6. The angular dependence of the relative peak intensities at g 1.89, 1.92, 1.94, and 2.05 found in all experiments was in good agreement with those previously reported [8]. In experiments where the species X was reduced, a large signal at g 1.77 was observed in the parallel orientation, in agreement with previous findings [12].

There are two experimental problems which arise when one studies EPR properties of samples dried on mylar strips.

1. Because the samples do not have cylindrical symmetry and the EPR cavity mode pattern is TE_{102}, the amount of sample in the maximum of the microwave magnetic field varies as one rotates the sample. This problem is alleviated somewhat by stacking of the sample strips in the EPR tube.

2. Because of the very high optical absorption of these dense chloroplast preparations, the fraction of sample that can be illuminated by the laser flash in the time-resolved measurements also depends on orientation.

Therefore, only the relative peak intensities at a given

sample orientation have quantitative significance.

B. Time-resolved EPR results

Oriented samples prepared so that Fe-S centers A and B were reduced prior to flash excitation gave rise to predominently monophasic transient EPR signals in the g 2.0 region at 10K and 50 μW microwave power. The lifetime of this decay component was approximately 50 μsec (1/e time) and independent of orientation. A slower component with a decay time of 150 μsec was also present at some field positions, but its presence seemed to vary with different sample preparations. Also, the lifetime of this component varies over a range 150-500 μsec as a function of field position for a given sample.

The lifetimes of both kinetic components are dependent on microwave power, and at high power levels (approximately 1 mW) an additional oscillation or component is observed. Gast, et al. [13] have also observed these effects and have postulated that they are due to a combination of spin-polarization, field modulation and transient nutation effects in inhomogeneously broadened lines. This problem has been examined theoretically [14] and the results of this work are presented in chapter 6. Thus, even under slow passage conditions the decay of polarized transient EPR signals can be complex, often appearing to have at least three different kinetic 'phases'. A conclusion of this work and that of others [15] is that any practical analysis of

these decays should be done using kinetic data obtained without magnetic field modulation.

The amplitude of the 50 μsec component is plotted versus magnetic field position in the g 2.0 region in Fig. 4-2 for randomly oriented thylakoids. The field profile shows that the low field portion of this spectrum is emissive, the center portion is absorptive, and the high field part is emissive. Figs. 4-3 through 4-5 show the field profiles for thylakoids oriented so that the membrane normals are parallel (Fig. 4-3), perpendicular (Fig. 4-4), and at 45^{o} (Fig. 4-5) to the DC magnetic field direction. These spectra were obtained for thylakoids oriented by partial dehydration on mylar and, as the data show, the amplitude of this kinetic component depends strongly on the orientation of the thylakoid membrane normals in the Zeeman field. In the perpendicular orientation (Fig.4-4), a mixed absorptive-emissive type signal centered at g 2.0026 is observed. When the sample is rotated 90^{o} to the parallel orientation, the polarization pattern is inverted and an appreciable amount of signal intensity grows in at low field causing the center of this pattern to shift to g 2.0034 (Fig. 4-3). The field profile obtained in the 45^{o} orientation (Fig. 4-5) is similar to that of the parallel orientation, except that the structure in the high field lobe of the spectrum is different. The trends seen in these field profiles are similar to those obtained for samples oriented in a high magnetic field (Fig 4-6), but the effects

Fig. 4-2. Plot of EPR transient signal amplitude (50 μsec component) versus magnetic field strength for randomly oriented chloroplasts. The sample was prepared as in Fig. 4-1, but was mixed with an equal volume of ethylene glycol before being placed in an EPR tube. The measurement conditions were: microwave frequency, 9.193 GHz; microwave power, 50 μW; modulation frequency, 1 MHz; modulation ampliude, 2.5G; sample temperature, 15K; and time constant, 2 μsec. Each point represents the average of 500 events.

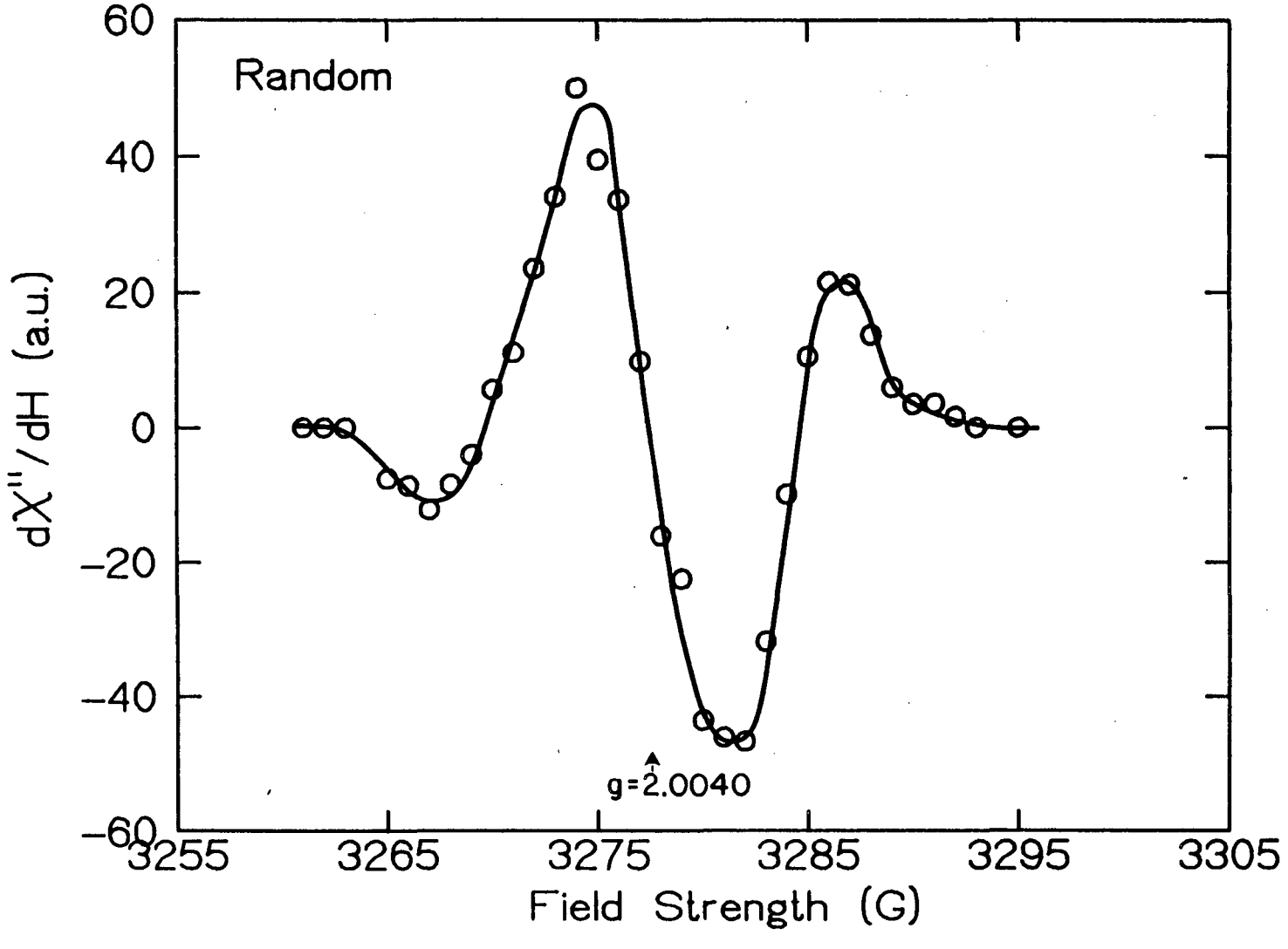
Random
60
40
20
0
-20
-40
-60
dχ''/dH (a.u.)
g=2.0040
3255
3265
3275
3285
3295
3305
Field Strength (G)

XBL 835-9823

Fig. 4-3. Plot of the amplitude of the 50 μsec component versus magnetic field strength for oriented thylakoids placed in the spectrometer so that the membrane normals are parallel to the direction of the Zeeman field. Thylakoids were prepared and oriented as in Fig. 4-1. Measurement conditions were identical to those of Fig. 4-2 except that the microwave frequency was 9.141 GHz.

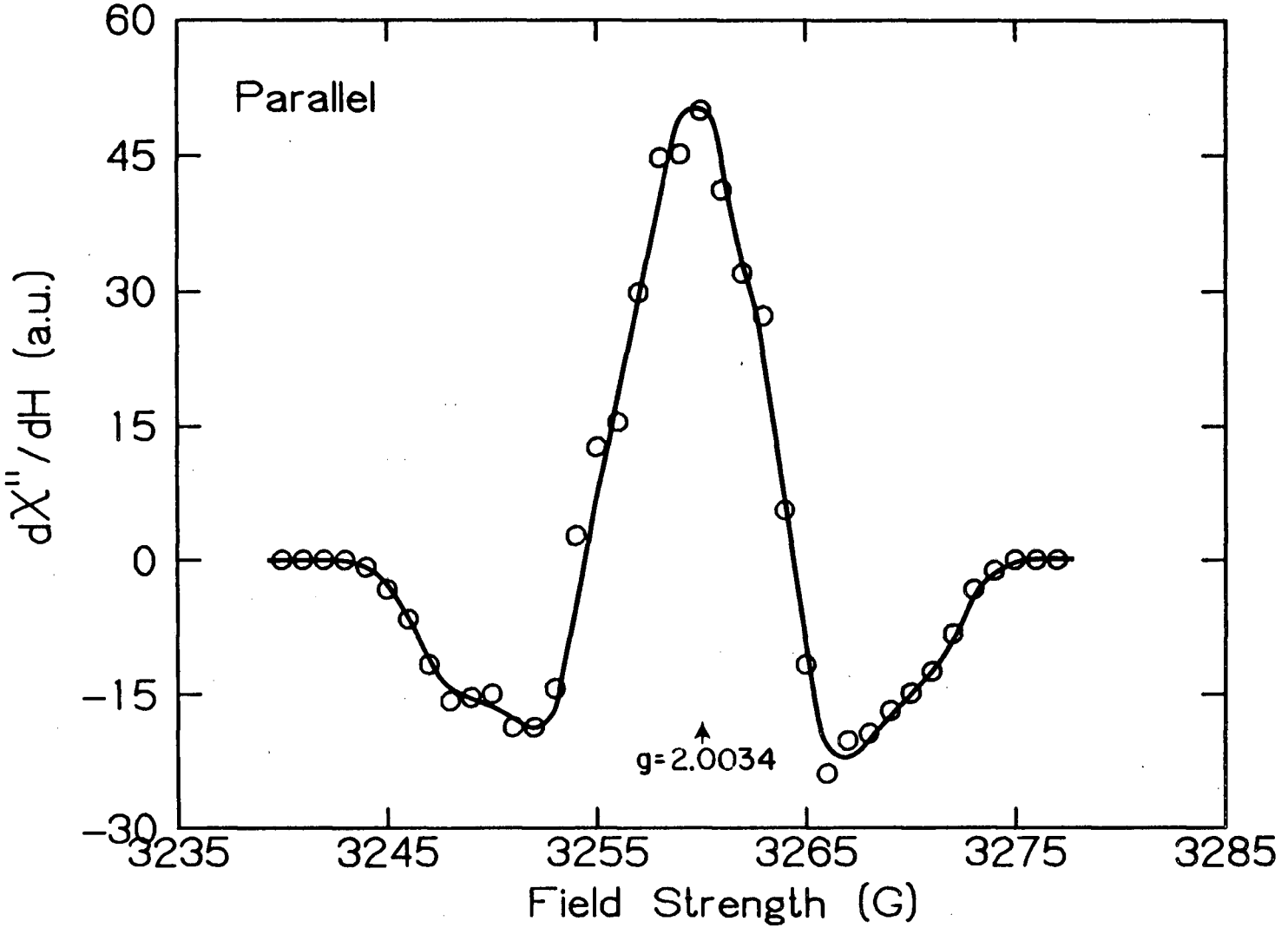
Parallel
60
45
30
15
0
−15
−30
dχ''/dH (a.u.)
g=2.0034
3235
3245
3255
3265
3275
3285
Field Strength (G)

XBL 835-9825

Fig. 4-4. Plot of the amplitude of the 50 μsec kinetic component versus field strength for oriented thylakoids in the perpendicular orientation. The sample preparation was as in Fig. 4-1. The measurement conditions were identical to those of Fig. 4-2 except that the microwave frequency was 9.143 GHz.

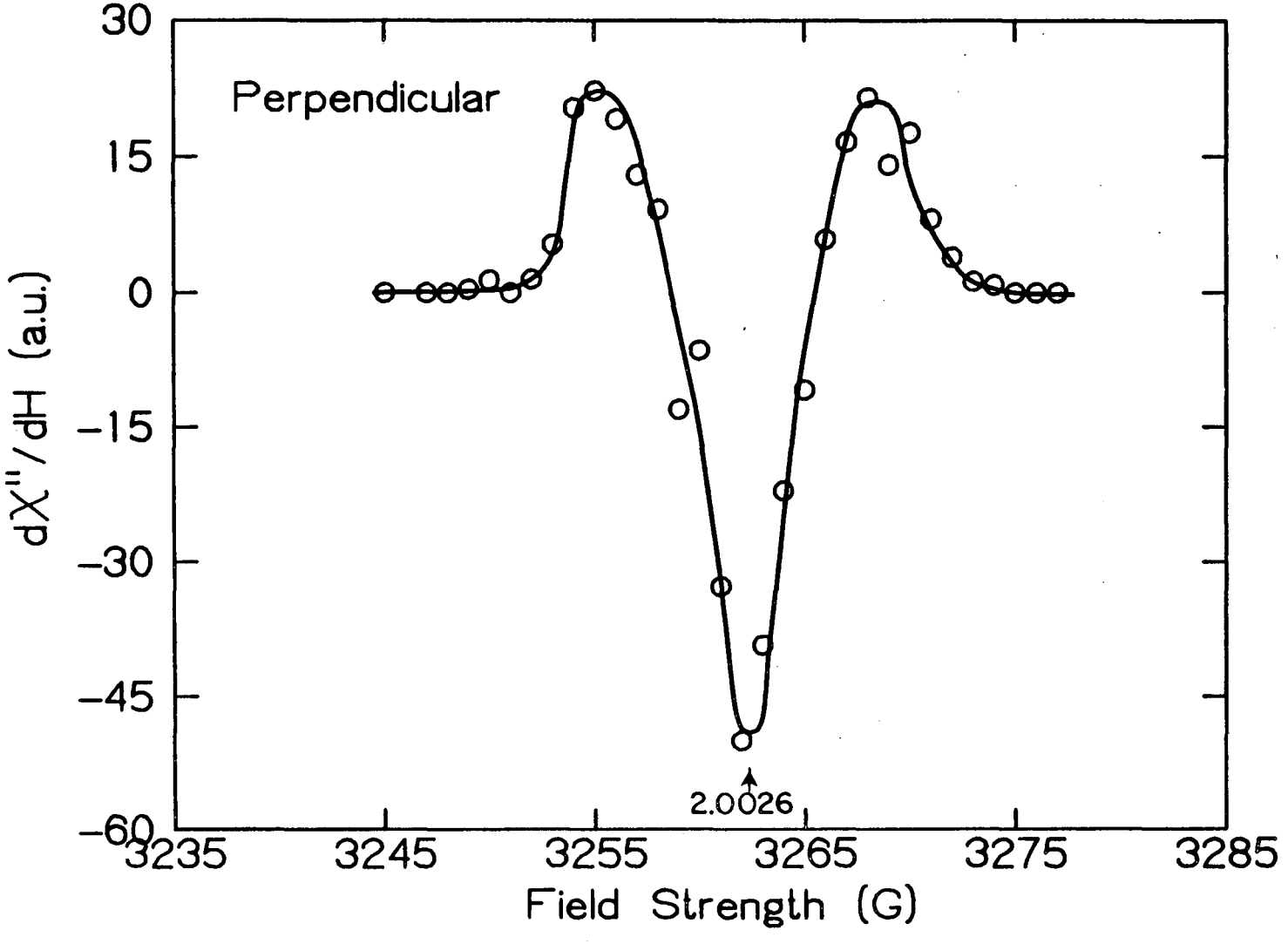
Perpendicular
30
15
0
−15
−30
−45
−60
dχ''/dH (a.u.)
2.0026
3235
3245
3255
3265
3275
3285
Field Strength (G)

XBL 835-9836

Fig. 4-5. Field profile for the 50 μsec kinetic component for oriented thylakoids placed in the spectrometer so that the membrane normals were at an angle of 45° from the direction of the Zeeman field. The sample preparation was identical to that of Fig. 4-1. Measurement conditions were identical to those of Fig. 4-2 except that the microwave frequency was 9.198 GHz.

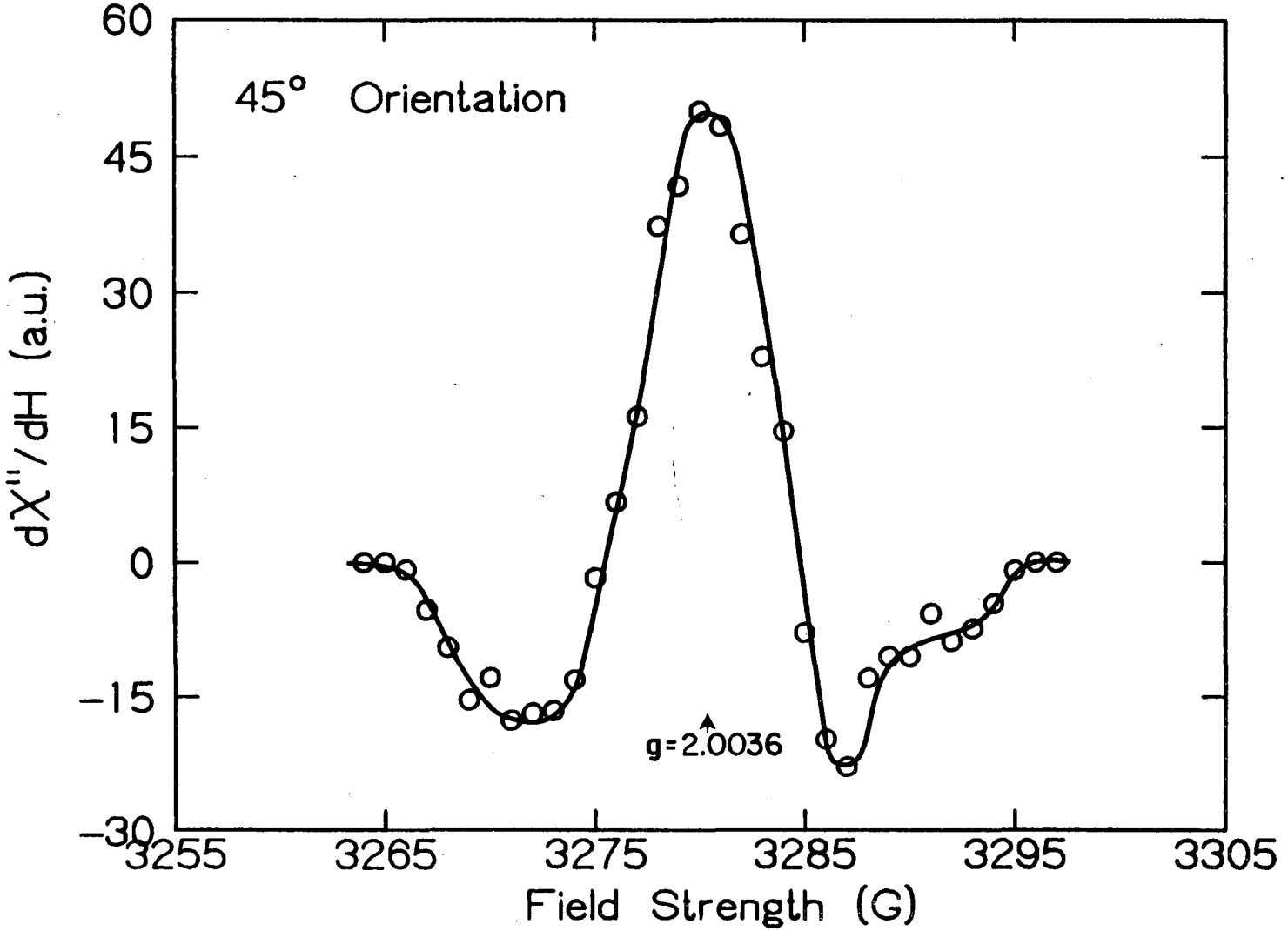
45° Orientation
60
45
30
15
0
−15
−30
dχ''/dH (a.u.)
g=2.0036
3255
3265
3275
3285
3295
3305
Field Strength (G)

XBL 835-9826

Fig. 4-6. Plots of EPR transient amplitude (50 μsec component) vs. magnetic field strength for magnetically aligned, broken spinach chloroplasts. Samples were prepared under N_2 gas in .2M glycine buffer, pH=10.1, treated with 50mM sodium dithionite, 10 μM methyl viologen, and mixed with an equal volume of ethylene glycol before freezing in the dark in a 10 kG alignment field. The spectrometer settings were: microwave power, 50 μW; sample temperature, 10K; field modulation frequency, 1 MHz; field modulation amplitude, 4G. Each point represents the average of 400 events. In (a) the sample was placed in the spectrometer so that the thylakoid membrane normals were parallel to the Zeeman field direction and in (b) the normals are perpendicular to the DC field.

Spinach Chloroplasts
Dithionite, Dark
10 °K

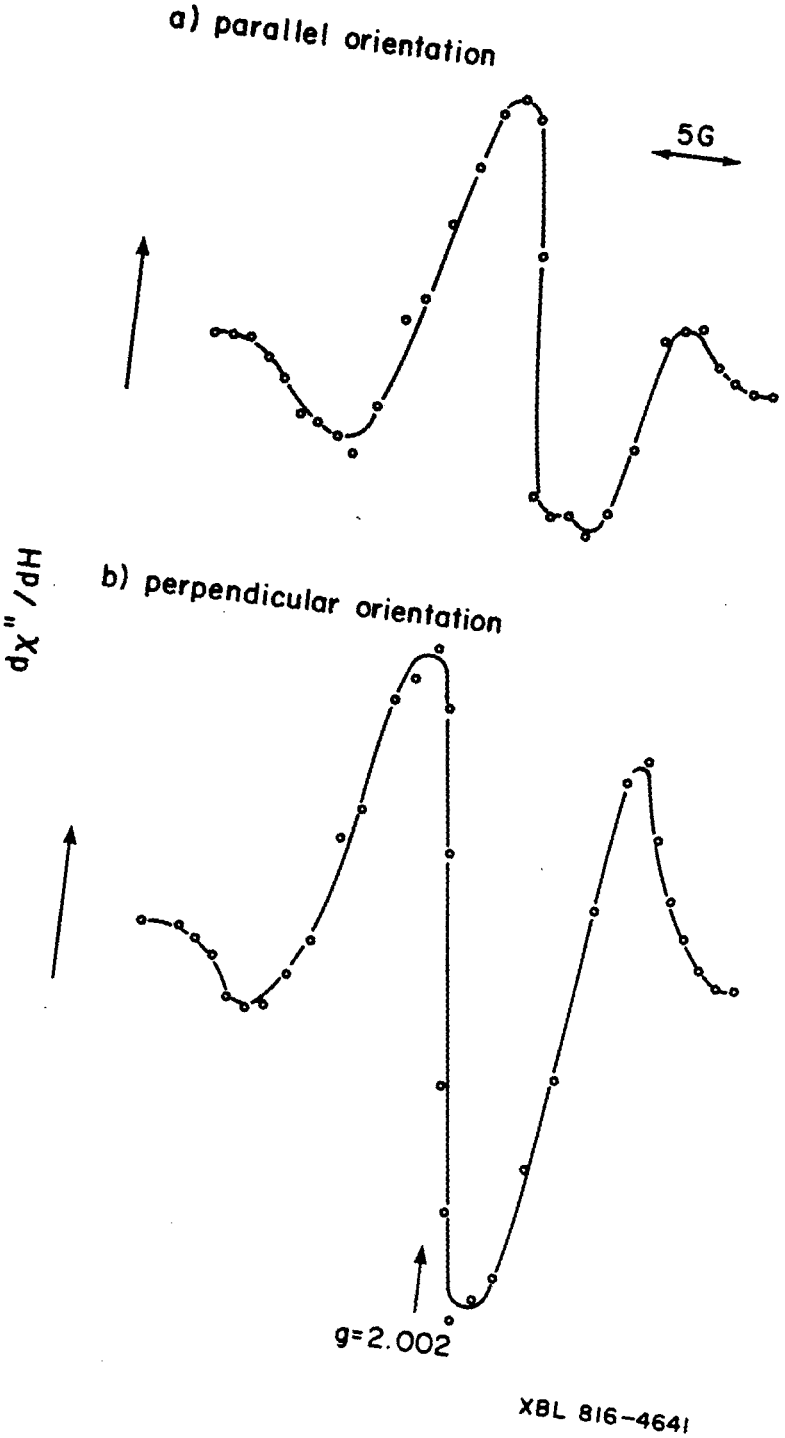

XBL 816-4641

shown in Figs. 4-3 through 4-5 are much more pronounced because of the higher degree of orientation obtained with the drying technique.

The possibility of distortion due to rapid passage in field modulation experiments was tested by repeating the above measurements using direct detection of resonance. The field profile recorded for oriented thylakoids in the parallel orientation (Fig. 4-7) yields a mixed emissive-absorptive lineshape identical to that obtained using field modulation (Fig. 4-3). The field profile obtained using direct detection for an oriented sample in the perpendicular orientation is also shown (Fig. 4-8). It has an absorptive-emissive lineshape in agreement with the field modulation data (Fig. 4-4). These experiments indicate that distortion of signal amplitudes due to rapid passage are not significant. The structure seen in the field-modulated data (the shoulders on the low- and high-field lobes of the spectra) is also observed in the direct detection measurements.

Time-resolved EPR data were also collected for randomly oriented PS1 particles prepared so that Fe-S centers A and B were reduced prior to flash stimulation. We found that in PS1 reaction centers prepared with digitonin [16] or Triton X-100 [17], results identical to those of Fig. 4-2 were obtained. Similar results have been reported by other researchers [13,18]. Measurements were done also on samples which had been treated with 10mM $K_3Fe(CN)_6$ before drying and

Fig. 4-7. A field profile of the 50 μsec component for oriented thylakoids prepared as in Fig. 4-1. The measurement conditions were: sample orientation, parallel; microwave frequency, 9.225 GHz; microwave power, 50 μW; time constant, 300 nsec; sample temperature, 15K; and the direct detection (superheterodyne) system was utilized. Each point is the average of 500 events.

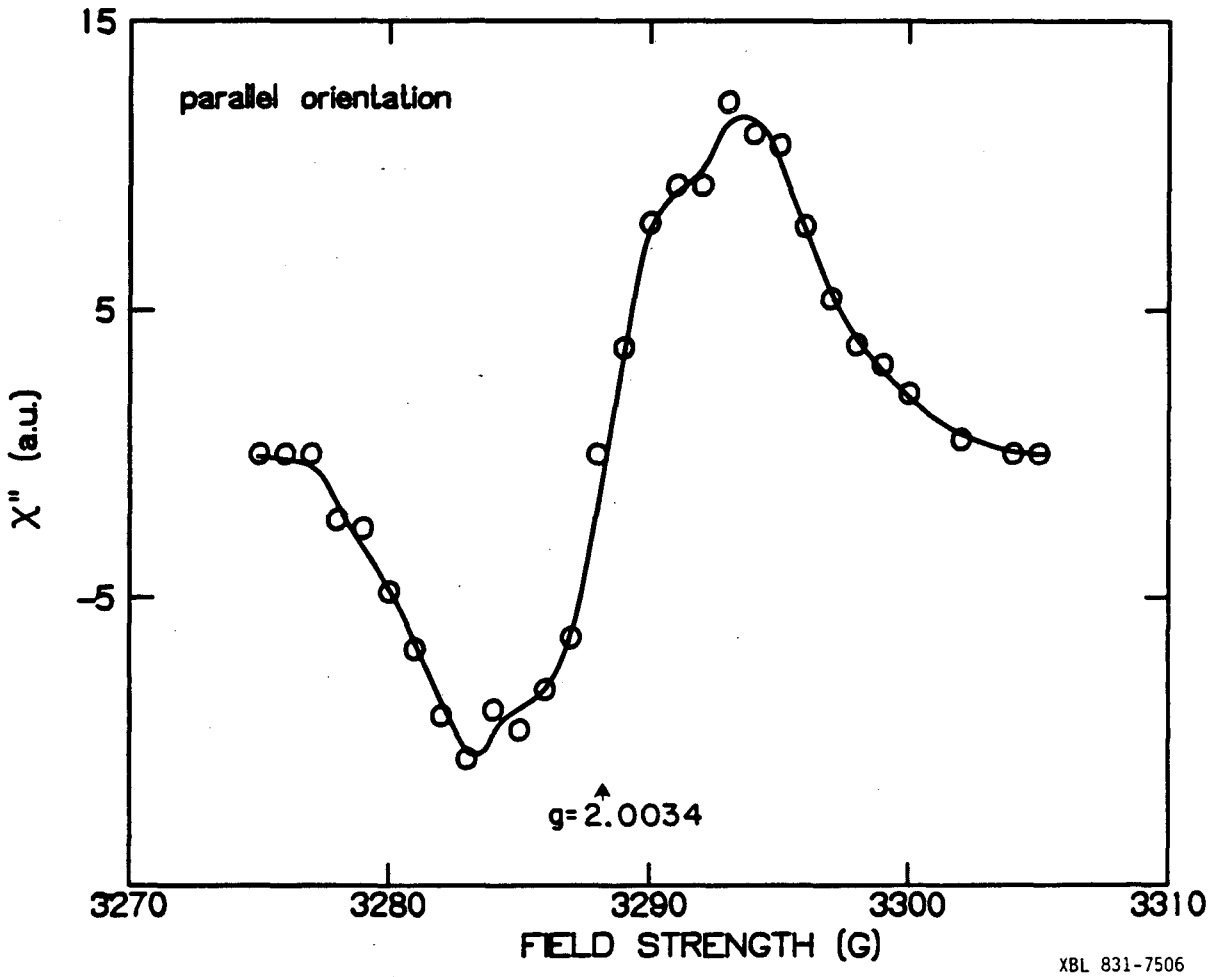
15
5
-5
χ'' (a.u.)
parallel orientation
g=2.0034
3270
3280
3290
3300
3310
FIELD STRENGTH (G)
XBL 831-7506

Fig. 4-8. A field profile of the 50 μsec component for oriented thylakoids prepared as in Fig. 4-1. The direct detection system was used for the measurements and the conditions were identical to those of Fig. 4-7 except that the microwave frequency was 9.226 GHz and the sample orientation was perpendicular.

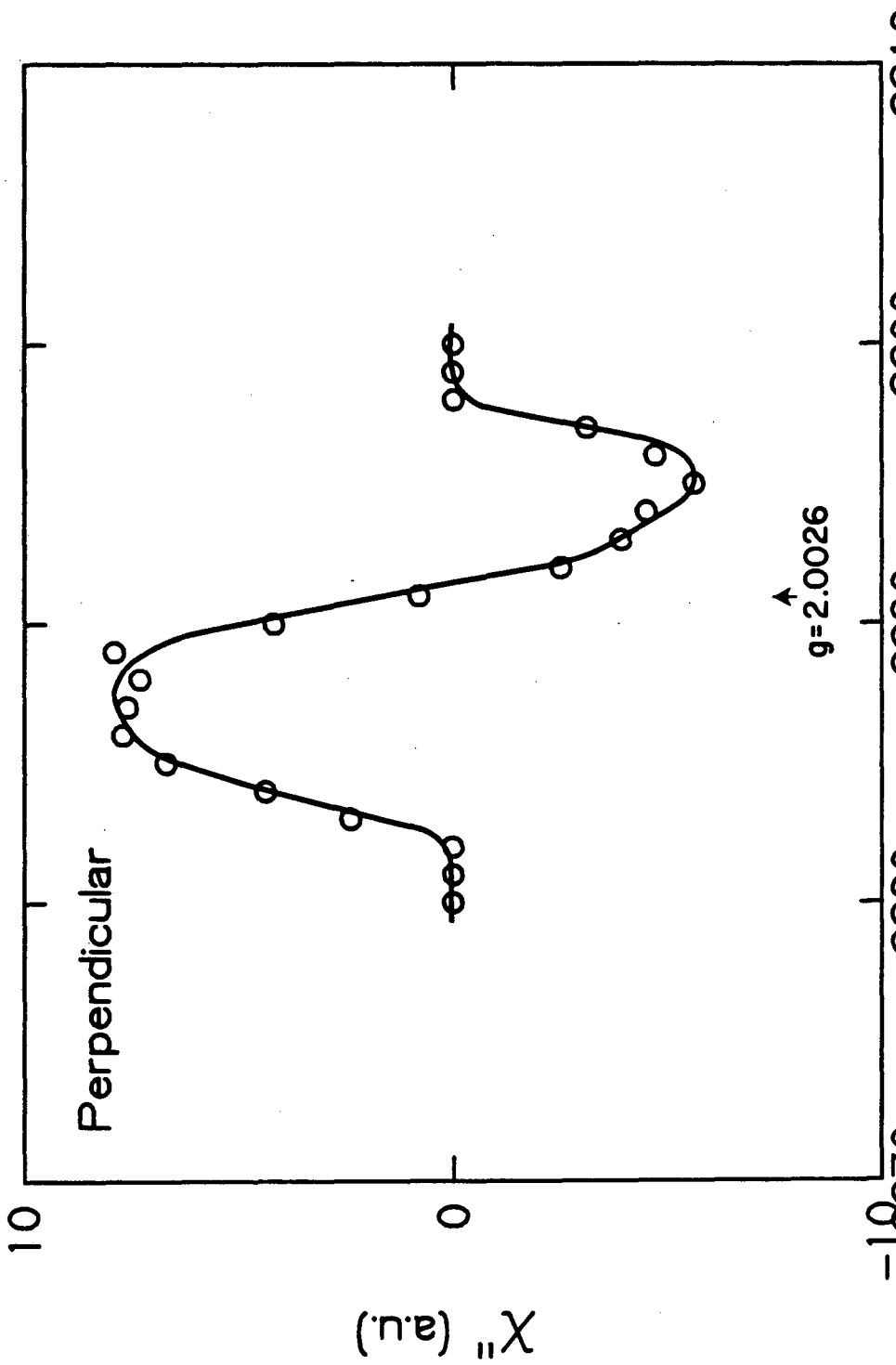
χ'' (a.u.)
10
0
-10
3270
3280
3290
3300
3310
Field Strength (G)
g=2.0026
Perpendicular

XBL 835-9846

freezing in the dark. Steady state EPR spectra showed that P-700, the primary donor of PS1, was oxidized and that Fe-S center A could not be reduced by steady illumination with white light at 10K. Under these conditions, no rapid (sub-millisecond) EPR transient signals were observed in the g 2.0 region. These control experiments confirm that the signals being studied above are due to PS1.

4.3 Discussion

A. The Model

Analysis of the spin polarized data presented above will allow one to extract information concerning both spectral properties of the radical pairs involved in PS1 photochemistry and information about the magnetic interactions between them. To accomplish this, a quantum mechanical model which is capable of predicting the polarization patterns for both random and oriented thylakoids prepared under the redox conditions given above must be formulated. In the remainder of this chapter, this model will be described, characterized, and its predictions discussed.

Fig. 4-2 shows the field profile obtained for randomly oriented thylakoids under conditions where Fe-S centers A and B are reduced prior to application of the actinic flash. If the model of PS1 electron transport given in chapter 1 is correct, the reaction sequence under these conditions would

be:

$$\text{P-700 } A_1 \text{ X } (Fd_{B,A})^{=} \xrightarrow{h\nu} \text{P-700}^{+} A_1^{-} \text{ X } (Fd_{B,A})^{=}$$

$$\text{P-700}^{+} A_1 \text{ X}^{-} (Fd_{B,A})^{=}$$

where the laser flash produces the first radical pair, P-700^{+} A_1^{-}, and then electron transfer produces the second radical pair, P-700^{+} X^{-}. The EPR spectrum of X^{-} is anisotropic with principal g-values of 2.08, 1.88, and 1.78 [19]. Because the polarization for this species will be spread out over 500 G, its contribution to the field profile in the g 2.0 region will be negligible. In contrast, both P-700 and the primary electron acceptor are thought to be Chl a species and will give rise to g 2.0 EPR signals in their oxidized and reduced states, respectively. A close examination of Fig. 4-2 shows that the center of the polarization pattern is g=2.0040. Because the EPR spectrum due to P-700^{+} is centered at g=2.0026 [20] and has a linewidth of 8 G, there must be another g 2.0 radical contributing to this spectrum. The dynamics of the transient signals obtained under these conditions are roughly the same across the entire spectrum (the decay times are between 40-50 μsec for the component plotted). This evidence indicates that the reaction scheme is probably not that given above, but

$$\text{P-700 } A_1 \text{ X } (Fd_{B,A})^{=} \xrightarrow{h\nu} \text{P-700}^{+} A_1^{-} \text{ X } (Fd_{B,A})^{=}$$

and that at 10K, under conditions where centers A and B are reduced, the back reaction between P-700$^+$ and A_1^- is more favorable than forward electron transfer from A_1^- to X. Under these conditions, one would see signals from two radicals in the g 2.0 region that would decay with similar kinetics as long as they were coupled to the lattice in a similar fashion.

Assuming this reaction sequence to be correct, P-700$^+$ and A_1^- will give rise to spin-polarized EPR lineshapes similar to the 'static' radical-pair polarization patterns illustrated in chapter 2. If one assumes that the two spectra are of the net effect type ($\Delta g \beta H$ > hyperfine fields - Fig. 2-2), there is no way that emissive and absorptive spectra (one centered at g=2.0026) can be added to give a profile similar to Fig. 4-2. Further, if the two spectra are considered to be of the multiplet type, simulation of the random spectrum (Fig. 4-2) is also impossible. This can be seen by examining Figs. 2-3 and 2-4. Pedersen [21] postulated that it was possible to obtain lineshapes like that of Fig. 4-2 if one of the radical species was dynamically polarized rather than statically polarized. In this picture, spin polarization would develop on P-700$^+$ due to radical pair interactions with the primary electron acceptor by the static mechanism presented in chapter 2. However, the primary acceptor anion would then decay via electron transfer to the next acceptor species. The net spin

polarization on the primary acceptor species at the time of this electron transfer would then be transferred to the secondary acceptor. This transfer would not involve the nuclear states of either radical selectively, and thus the net polarization would be spread out uniformly over the hyperfine states of the secondary acceptor anion. This picture involves the incorporation of a second electron acceptor species with a g-value in the free electron region that operates in series between P-700$^+$ and A_1^-. A similar hypothesis has been made by Bonnerjea and Evans [22] and by Gast, et al. [13]. The reaction sequence is then:

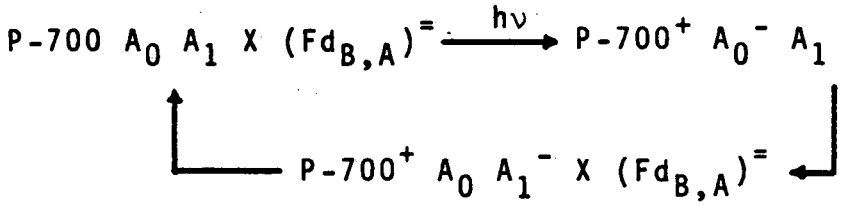

where the new species is denoted as A_0.

In addition to the existence of an A_0, the model required to predict the observations made above must provide for the orientation dependence of the spin polarization patterns. These orientation effects are dramatic, involving complete inversion of the polarization pattern as one goes from the parallel to the perpendicular orientation. Because the contributions from g-tensor anisotropy or anisotropy in the hyperfine fields of these radicals is expected to be small, the orientation dependence was modeled by considering the spin-spin interaction between P-700$^+$ and A_0^- to be anisotropic. The interaction chosen was the electron-

electron magnetic dipole interaction because recent reports indicate that this interaction is important in the primary radical ion pair of bacterial photosynthesis [23,24]. One should keep in mind that this interaction is mathematically isomorphic to an aniostropic exchange interaction.

Thus, the model used to describe the development of spin polarization in PS1 under these experimental conditions has the following three features.

1. It is a one-site model in that the spin polarization develops due to a single radical-pair interaction between P-700$^+$ and A_0^-.

2. The spin-spin interaction between P-700$^+$ and A_0^- is modeled with an isotropic exchange interaction and an electron-electron magnetic dipole interaction.

3. The polarization pattern observed in the g 2.0 region is due to contributions from two radical species: P-700$^+$, which is statically polarized; and A_1^-, which is dynamically polarized as a result of electron transfer from spin-polarized A_0^-.

B. Calculations

To calculate the spin polarization on P-700$^+$ one uses the same approach as that given in chapter 2. First, the time evolution of the radical pair wavefunction is determined. Then this wavefunction is used to calculate the

time dependence of the polarization of a given hyperfine state of the radical. This expression is then averaged over the radical pair lifetime and used to generate a stick spectrum of the polarized radical. The spin hamiltonian for the radical pair in this model is:

$$H_{rp} = H_{zee}^{D} + H_{zee}^{A} + H_{hf}^{D} + H_{hf}^{A} + H_{ex} + H_{dd} \qquad (4\text{-}1)$$

where the terms are identical to those used in chapter 2 (Eqn. 2-6) except that the dipolar coupling term has been added. Because the g-tensors, hyperfine tensors, and exchange interaction in the above equation are isotropic, the problem is best done in the principal axis system (PAS) of the dipolar coupling tensor. In general H_{dd} has the form:

$$H_{dd} = \underset{\sim}{S}_D \cdot \underset{\approx}{D} \cdot \underset{\sim}{S}_A \qquad (4\text{-}2)$$

where $\underset{\approx}{D}$ is the dipolar coupling tensor. In its PAS, the tensor is diagonal and the hamiltonian takes the form:

$$H_{dd} = -X\hat{S}_x^2 - Y\hat{S}_y^2 - Z\hat{S}_z^2 \qquad (4\text{-}3)$$

where $\hat{S}_x$, $\hat{S}_y$, and $\hat{S}_z$ are operators of the total spin ($S_x = S_{Dx} + S_{Ax}$). Since $\underset{\approx}{D}$ is traceless

$$-X-Y-Z = 0$$

and the dipolar hamiltonian can be rewritten in a form involving only two zero-field splitting parameters, D and E.

$$H_{dd} = D(S_z^2 - \underset{\sim}{S}^2/3) + E(S_x^2 - S_y^2) \qquad (4\text{-}4)$$

In terms of the elements of the D tensor, these zero field splitting parameters are given by:

$$D = -3Z/2$$

$$E = -(X - Y)/2. \qquad (4\text{-}5)$$

Using the singlet and high-field triplet basis set given in Eqn. 2-10, the hamiltonian matrix can be generated and is given in Fig. 4-9. H_x, H_y and H_z are the components of the Zeeman field along the x, y, and z axes of the dipolar coupling tensor and are given by:

$$\begin{aligned} H_x &= H_0 \sin\theta \cos\phi \\ H_y &= H_0 \sin\theta \sin\phi \\ H_z &= H_0 \cos\theta \end{aligned} \qquad (4\text{-}6)$$

where θ and ϕ describe the direction of H_0 in the PAS of the tensor. For a randomly oriented sample, θ and ϕ can take on all possible values.

Calculation of the time evolution of the radical pair wavefunction is not so straightforward as in chapter 2, because the eigenstates and eigenvalues must be found by numerical diagonalization of the matrix of Fig. 4-9. Because the dipole-dipole interaction mixes $|S\rangle$ with all three triplet sublevels, each of the four eigenstates will contribute to $|\psi(t)\rangle$. Just as before $|\psi(0)\rangle = |S\rangle$ and

Fig. 4-9. The hamiltonian matrix in the singlet-triplet basis for the hamiltonian of Eqn. 4-1. The model is a one-site polarization model with dipolar coupling and isotropic exchange interactions included.

	$\lvert S\rangle$	$\lvert T_0\rangle$	$\lvert T_{+1}\rangle$	$\lvert T_{-1}\rangle$
$\langle S\rvert$	J			
$\langle T_0\rvert$	$0.5\cdot[(g_D-g_A)\beta H_z + \sum_i A_i^{(D)} m_{iz} - \sum_j A_j^{(A)} m_{jz}]$	$-2D/3 - J$		
$\langle T_{+1}\rvert$	$\dfrac{[(-g_D+g_A)\beta(H_x-iH_y)]}{2\sqrt{2}}$	$(1/2\sqrt{2})\cdot[(g_D+g_A)\beta\cdot(H_x-iH_y)]$	$0.5\cdot[(g_D+g_A)\beta H_z + \sum_i A_i^{(D)} m_{iz} + \sum_j A_j^{(A)} m_{jz}] + D/3 - J$	
$\langle T_{-1}\rvert$	$(1/2\sqrt{2})\cdot[(g_D-g_A)\beta\cdot(H_x+iH_y)]$	$(1/2\sqrt{2})\cdot[(g_D+g_A)\beta\cdot(H_x+iH_y)]$	E	$-0.5\cdot[(g_D+g_A)\beta H_z + \sum_i A_i^{(D)} m_{iz} + \sum_j A_j^{(A)} m_{jz}] + D/3 - J$

XBL 835-9847

$$|\psi(t)\rangle = \sum_{j=1}^{4} \langle\phi_j|S\rangle\, e^{-iE_jt'}\, |\phi_j\rangle \qquad (4\text{-}7)$$

where the $|\phi_j\rangle$ are the eigenstates of the hamiltonian and E_j are the eigenvalues. The eigenstates will have the form

$$|\phi_j\rangle = C_{S,j}|S\rangle + C_{T_0,j}|T_0\rangle + C_{T_{+1},j}|T_{+1}\rangle + C_{T_{-1},j}|T_{-1}\rangle \qquad (4\text{-}8)$$

and

$$|\psi(t)\rangle = \sum_{j} C_{S,j}\, e^{-iEjt'}\, |\phi_j\rangle \qquad (4\text{-}9)$$

The spin polarization developed on the donor cation is obtained by plugging Eqn. 4-9 into Eqn. 2-16. The solution has the form,

$$\rho_D(t) = X_1 + \sum_{j=2}^{7} [(X_j + X_j^*)\cos\omega_j t + i(X_j - X_j^*)\sin\omega_j t] \qquad (4\text{-}10)$$

where the X_j are linear combinations of the eigenvector coefficients (the $C_{x,y}$ in Eqn. 4-8) and are obtained by doing massive amounts of algebra. A detailed description of this algebra problem is given in appendix A. Time averaging Eqn. 4-10 in a manner analogous to that used in chapter 2 yields the time averaged polarization:

$$\bar{\rho}_D(\tau) = X_1 + \sum_{j=2}^{7} [X_j + X_j^* + i(X_j - X_j^*)\omega_j\tau]/(1 + \omega_j^2\tau^2) \qquad (4\text{-}11)$$

where τ is the radical pair lifetime. As with the expressions for the polarization developed in chapter 2, Eqn. 4-11 must be evaluated for each hyperfine state of D^+. The time averaged polarization expressed by Eqn. 4-11 is

actually a function of hyperfine states on both donor and primary acceptor species; and θ and ϕ, the angles which describe the orientation of H_0 in the PAS of the dipole-dipole coupling tensor. Thus, the spin polarization on hyperfine line i of D^+ in a randomly oriented sample is:

$$\rho_D{}^i(\tau) = \int_0^{\pi/2}\int_0^{\pi/2}\left(\sum_j \rho_D{}^{(ij)}(\tau)\right)\sin\theta d\theta d\phi \ . \qquad (4\text{-}12)$$

The spin polarization which develops on a given hyperfine state of A_1^- is determined using Pedersen's description of polarization transfer [21]. Because A_1^- will be dynamically polarized, only the net polarization that developed on A_0^- will be transferred to A_1. Further, the polarization will be spread uniformly over the hyperfine states of A_1^- so that the spectrum of this species will be either emissive or absorptive, but not mixed. Experimental evidence in support of this idea has been obtained in studies on bacterial reaction centers [25,26]. The net polarization transferred to A_1^- will be equal in magnitude, but opposite in sign to that developed on P-700$^+$. The procedure for determining the polarization weighting for the hyperfine states of A_1^- is to first compute the polarization pattern for P-700$^+$ and find the net polarization on the species. Then this net polarization can be divided equally among the hyperfine states of A_1^- and its spectrum computed. The spectra due to each radical are then added to give the predicted output.

Fig. 4-10. A flow diagram for the computer program used to simulate spin-polarized EPR spectra in the g 2.0 region.

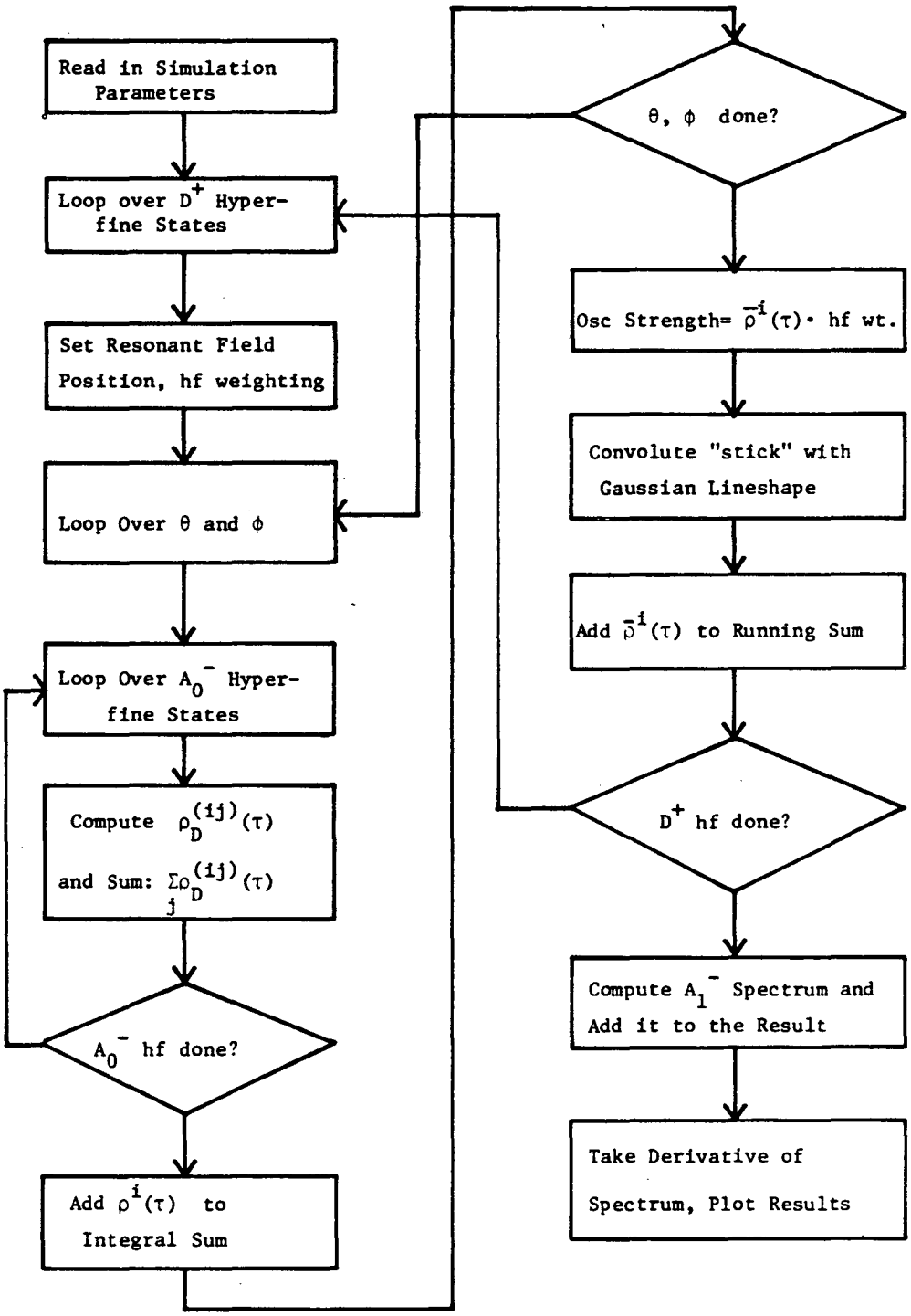
Read in Simulation Parameters
Loop over D^+ Hyperfine States
Set Resonant Field Position, hf weighting
Loop Over θ and φ
Loop Over A_0^- Hyperfine States
Compute $\rho_D^{(ij)}(\tau)$ and Sum: $\Sigma_j \rho_D^{(ij)}(\tau)$
A_0^- hf done?
Add $\rho^i(\tau)$ to Integral Sum
θ, φ done?
Osc Strength= $\bar{\rho}^i(\tau)$ · hf wt.
Convolute "stick" with Gaussian Lineshape
Add $\bar{\rho}^i(\tau)$ to Running Sum
D^+ hf done?
Compute A_1^- Spectrum and Add it to the Result
Take Derivative of Spectrum, Plot Results

XBL 835-9848

Fig. 4-11. A flow diagram for the subroutine used to compute the static polarization due to the hamiltonian of Eqn. 4-1. The matrix diagonalization is done by the routine EIGCH of the International Math Science Library.

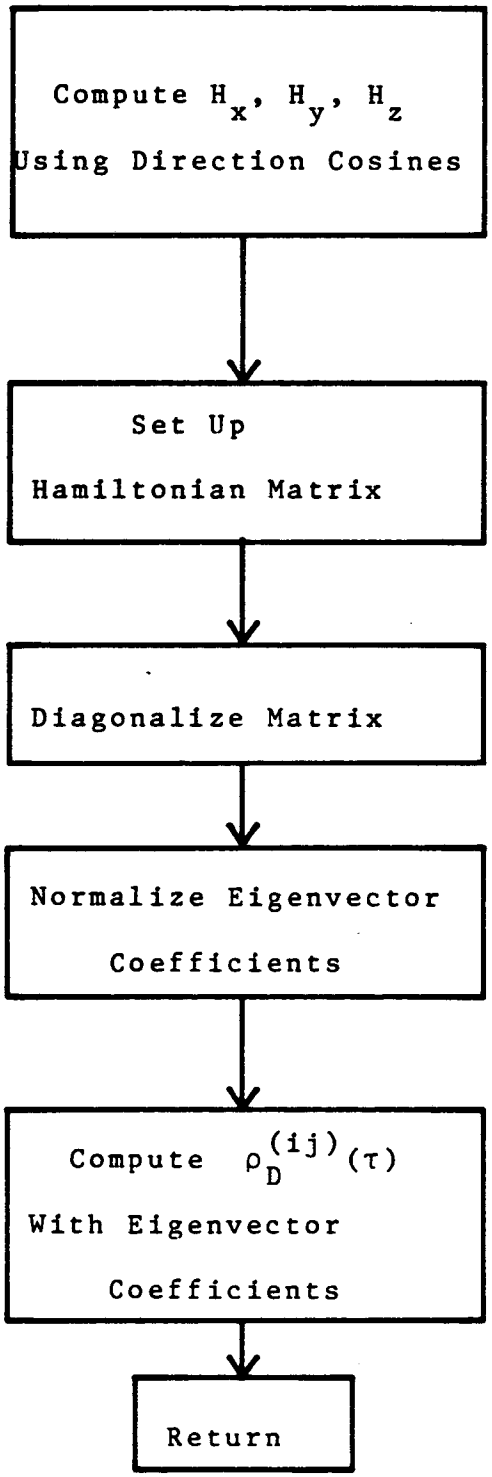
Compute H_x, H_y, H_z
Using Direction Cosines
Set Up
Hamiltonian Matrix
Diagonalize Matrix
Normalize Eigenvector
Coefficients
Compute $\rho_D^{(ij)}(\tau)$
With Eigenvector
Coefficients
Return

XBL 835-9849

C. Simulation Routine

A flow diagram for the computer routine used to do the simulations described above is given in Fig. 4-10. The calculation of the spin polarized P-700$^+$ spectrum is done first and begins by looping over the hyperfine states of the donor species. The resonant field strength of the hyperfine component of interest is calculated, and the oscillator strength for this hyperfine state under normal conditions is determined (for protons this weighting is given by the coefficients of the binomial expansion of $(1+x)^n$). The DO loops for performing the integration over θ and ϕ in Eqn. 4-12 are then started. The integration is done using Simpson's Rule and θ is usually divided into 30 equal cosine intervals while ϕ is divided into 20 equal intervals over the range from 0^o to 90^o. The calculation of the integral of Eqn. 4-12 involves first setting θ and ϕ and then looping over the hyperfine states of the acceptor anion species (A_0^- in this case) to compute the integrand. The actual values of $\rho_D^{(ij)}(\tau)$ are calculated by a subroutine which sets up the hamiltonian matrix for each set of θ, ϕ, and hyperfine parameters on P-700$^+$ and A_0^-. This routine then diagonalizes the matrix, normalizes the eigenvectors and uses them along with the eigenvalues to compute the polarization. The expressions used for this calculation are given in appendix A, and a flow diagram for this subroutine is given in Fig. 4-11. After performing the integration of Eqn. 4-12, the

oscillator strength for the hyperfine state of P-700$^+$ being considered is multiplied by the polarization weighting. The contribution of this hyperfine component to the spectrum is then added to a spectral array by convoluting the "stick" at the resonant field position with a gaussian lineshape of fixed width. This convolution is done using Eqn. 2-22. Before considering the next hyperfine component of P-700$^+$, the polarization weighting is added to a running sum which will represent the net polarization on the radical when all the hyperfine states have been considered.

After the spin-polarized spectrum of P-700$^+$ has been computed, the net polarization is divided equally among the hyperfine states of A_1^-. This weighting is then corrected for possible differences in intrinsic linewidth between P-700$^+$ and A_1^-, and the stick spectrum of A_1^- is computed. As with P-700$^+$, this stick spectrum is convoluted with a gaussian lineshape and added to the spectral array. Before exiting from the routine, the spectrum may be differentiated so that the output can be compared with the data taken using field modulation.

The validity of the numerical calculations was checked by comparing the results obtained numerically with those predicted by analytical expressions which can be derived in limiting cases. These cases were: when D and E go to zero, the polarization is given by the expressions developed in chapter 2; and the z canonical orientation ($H_0=H_z$, $H_x=H_y=0$ - see section 4.4A).

D. Random Spectrum Simulation

Computer simulation of the random spectrum shown in Fig. 4-2 requires the specification of several parameters. These parameters are: the g-values of P-700$^+$, A_0^- and A_1^-; the peak-to-peak linewidths of P-700$^+$ and A_1^-; and the spin-spin coupling constants for the interaction between P-700$^+$ and A_0^-, J, D, and E. The linewidths of P-700$^+$ and A_1^- enter into the calculation through the specification of the hyperfine coupling constants and the number of contributing nuclei on each molecule. In the work presented here, these properties are described by assuming that there are two protons on each radical with some hyperfine coupling constant. The coupling constants were chosen so that simulation of the steady state spectrum would give a structureless gaussian lineshape with the desired peak-to-peak linewidth. This approximation is necessary for describing the hyperfine fields of A_0^- and A_1^-, because very little information is known about these radicals. ENDOR data for P-700$^+$ does exist [27,28], but it was found that explicit inclusion of the larger coupling constants from these results in our calculations made negligible differences in the convoluted output spectra.

For the calculations presented below, the g-value of P-700$^+$ was set at 2.0026 and its linewidth at 8 G, while the g-values of A_0^-, A_1^- and the linewidth of A_1^- were allowed

to vary. It was found that the values of D and J were dependent on one another to the extent that for a given value of D, J could be adjusted to give good simulations of the data. Therefore, the values of D and J used in the simulations were chosen so that they fell into the range of D and J values given for the primary radical ion pair of bacterial reaction centers [24]. The general approach for doing these simulations was to fix D at -50G and then vary J, the g-values of the acceptors, the linewidth of A_1^-, and E to predict the random spectrum. Several parameter sets that gave good simulations were found.

The parameters that can be accurately set by prediction of the random spectrum alone are the g-value of A_1^- and its linewidth. A typical simulation for this spectrum is shown in Fig. 4-12 (upper trace). The range of acceptable g-values for A_1^- was 2.0054 ± .0010 and the peak-to-peak linewidth must be between 8-10.5 G. These values are in good agreement with those reported by Gast, et al. [13] and by Bonnerjea and Evans [22]. The acceptable range of J values (if D=-50 G) was from -8 G to -10.5 G (antiferromagnetic) depending on the g-value chosen for A_0^- which was found to have a range of acceptable values from 2.0027 to 2.0040. The effects of E on the random spectrum are slight, and good simulations could be obtained for the full range of values from zero to D/3. The lower trace in Fig. 4-12 shows the contribution of $P\text{-}700^+$ alone to the random spectrum simulation.

Fig. 4-12. A comparison of the calculated and experimental EPR spectrum for randomly oriented thylakoids prepared as in Fig. 4-2. The lower trace represents the contribution to the spectrum made by spin-polarized P-700$^+$ alone. The parameters for the simulation were: g-value of P-700$^+$, 2.0026; linewidth of P-700$^+$, 8G; g-value of A_0^-, 2.0031; g-value of A_1^-, 2.0054; linewidth of A_1^-, 9.0G; J=-9.35G (antiferromagnetic); D=-50G; E=0G; microwave frequency, 9.193 GHz.

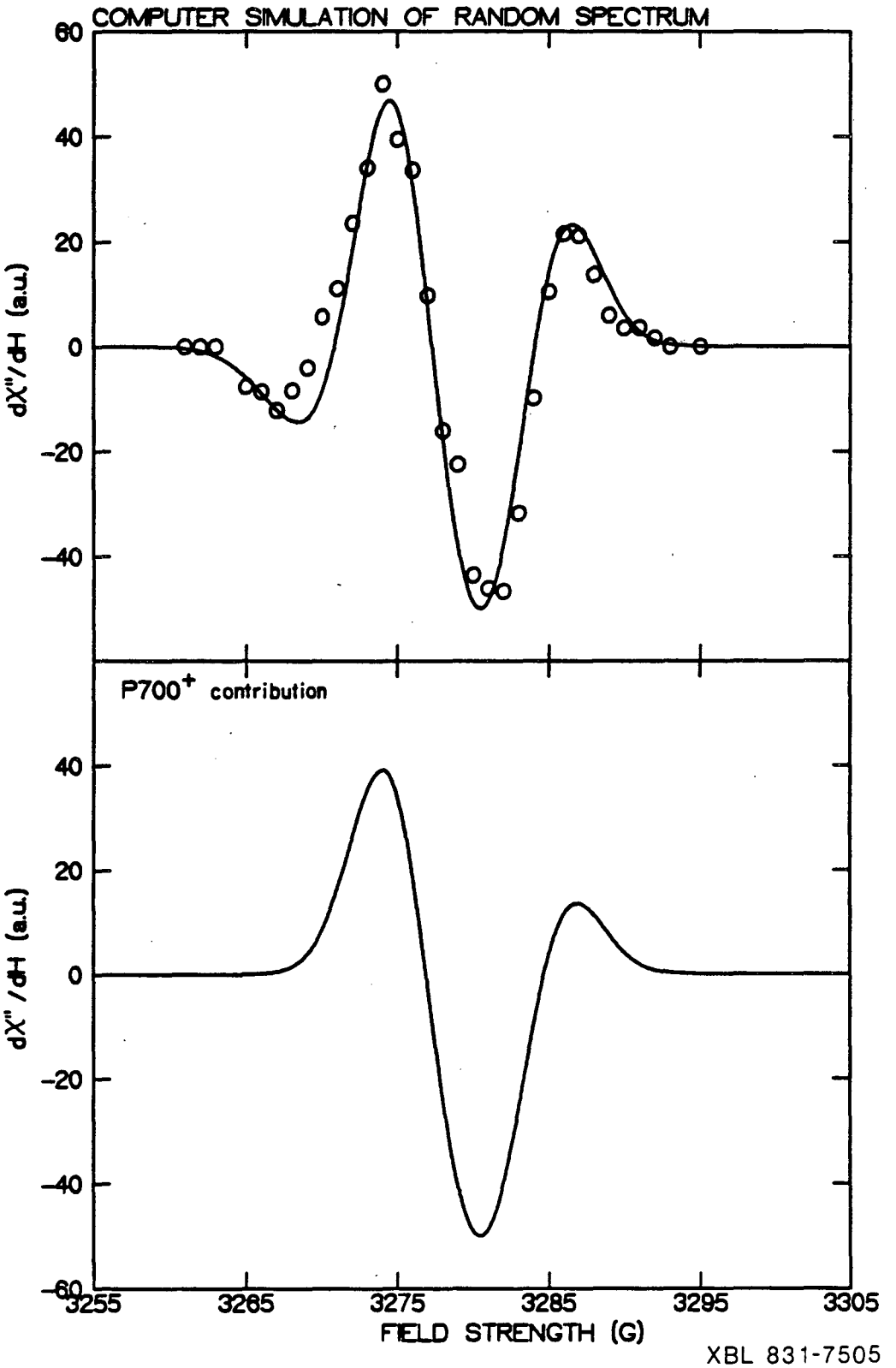
COMPUTER SIMULATION OF RANDOM SPECTRUM
60
40
20
0
-20
-40
dX"/dH (a.u.)
P700+ contribution
40
20
0
-20
-40
-60
dX" /dH (a.u.)
3255
3265
3275
3285
3295
3305
FIELD STRENGTH (G)
XBL 831-7505

E. Simulation of Oriented Spectra

The constraint that the above parameters, which allow satisfactory fits to the random spectrum, must also provide good fits to the oriented spectra narrows the range of acceptable parameter values considerably. Calculation of spectra obtained for oriented samples differs from that described for randomly oriented samples in that in the evaluation of the integral of Eqn. 4-12 the various values of θ and ϕ (the angles that describe the direction of H_0 in the PAS of the dipolar coupling tensor) are no longer weighted by just a $\sin\theta$ term. For the simulations in this work, the orientation averaging technique of Blum, et al. [29] developed for systems of partially ordered membrane multilayers is used to weight various field directions with respect to the PAS of the dipolar coupling tensor. This procedure involves relating the PAS of the tensor to a lab axis system described by the membrane normal via an Euler angle rotation. Various orientations of the magnetic field vector can be weighted according to the known orientation of the vector in the lab axis system and then related to the PAS of the tensor in question.

The relation between the lab axis system and the PAS of the dipolar coupling tensor is depicted in Fig. 4-13. The procedure described above requires the use of four angle parameters: θ and ϕ which describe the position of the membrane normal in the PAS of the dipolar coupling tensor;

Fig. 4-13. A sketch depicting the relation between the principal axis system of the dipolar coupling tensor, the membrane normal, and the direction of H_0. θ and ϕ define the orientation of the membrane normal in the PAS, while ω and α define the direction of H_0 in the lab axis system. Because there is no ordering in the membrane plane, α is measured from an arbitrary axis. The mosaic spread in the membrane normals is modeled as a cone about H_0. (The figure is taken from ref. [29].)

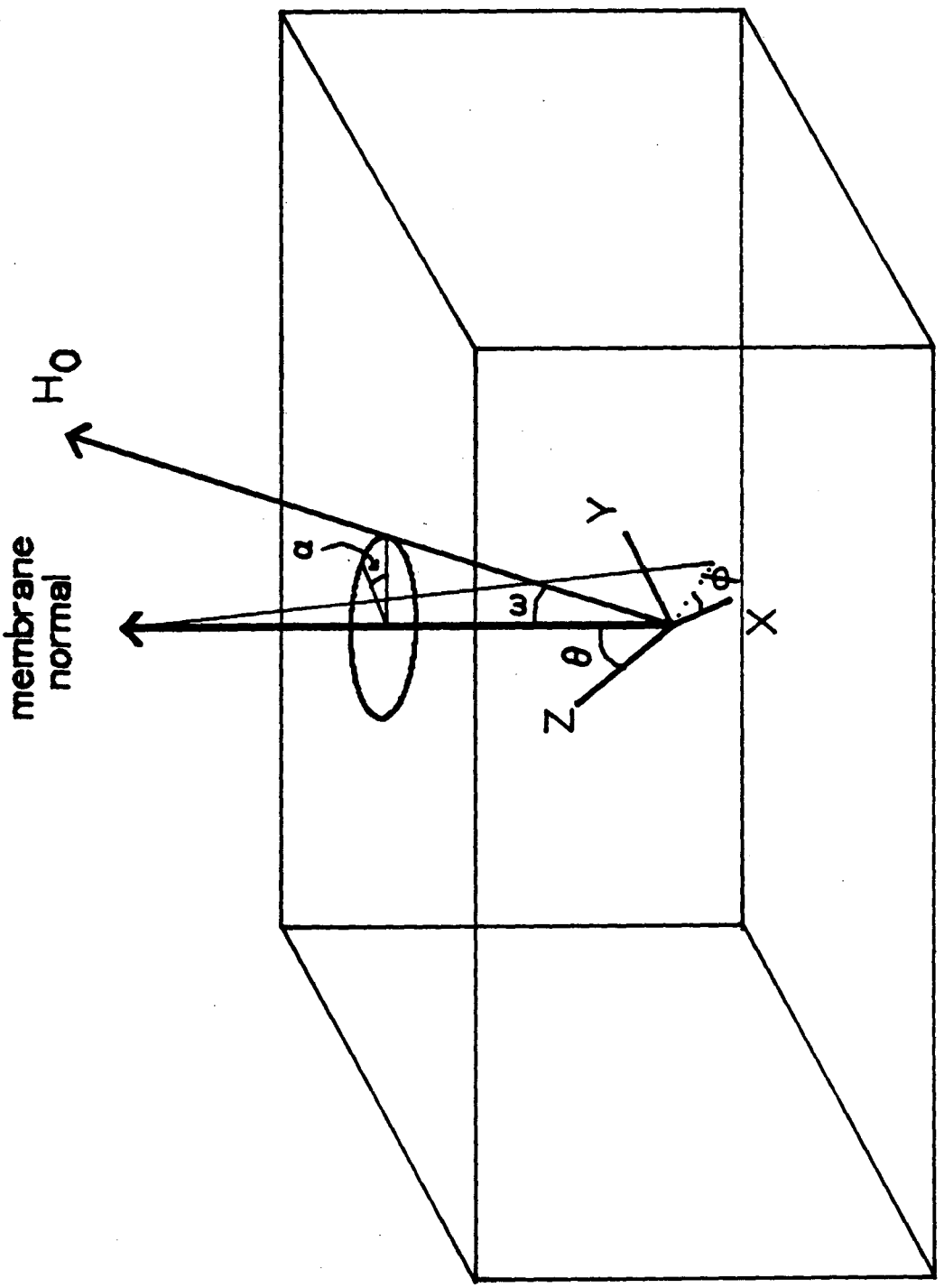

XBL 835-9824

and ω and α which describe the position of the magnetic field vector, H_0, in the lab axis system. θ and ϕ are a property of the sample and are fixed for a given calculation. ω is the angle between the membrane normal and the direction of the Zeeman field and is known from the experiment. Because there is no preferential ordering of the membranes in the plane transverse to the membrane normal, α must be averaged over 360^{o}. In the procedure for calculating the polarization above, the direction of H_0 in the PAS of the dipolar coupling tensor was specified using a set of direction cosines. For the randomly oriented sample these were given by Eqn. 4-6. For the oriented samples described in Fig. 4-13, the direction cosines must be obtained by relating the direction cosines that describe the position of H_0 in the lab axis system to the PAS of the dipolar coupling tensor using an Euler angle transformation. The relation is fairly simple and the direction cosines are given by:

$$H_x = H_0 l_x \quad , \quad H_y = H_0 l_y \quad , \quad H_z = H_0 l_z \qquad (4\text{-}13)$$

where

$$l_x = \cos\omega\sin\theta\cos\phi + \sin\omega(\sin\alpha\sin\phi - \cos\alpha\cos\theta\cos\phi)$$
$$l_y = \cos\omega\sin\theta\sin\phi - \sin\omega(\sin\alpha\cos\phi + \cos\alpha\cos\theta\sin\phi)$$
$$l_z = \cos\omega\cos\theta + \sin\omega\cos\alpha\sin\theta$$

The Euler angle transformation described above involves only two rotations because the axis from which α is measured is arbitrary. This effectively removes one degree of freedom

Fig. 4-14. Artist's view of membranes partially dehydrated on a mylar strip. The drawing illustrates the wobble or mosaic spread in the membrane normals. (Taken from Crowder, M.S., "The Photophysics and Photochemistry of Green Plant Photosystem 1," Ph.D. Thesis, University of California, Berkeley, 1981.)

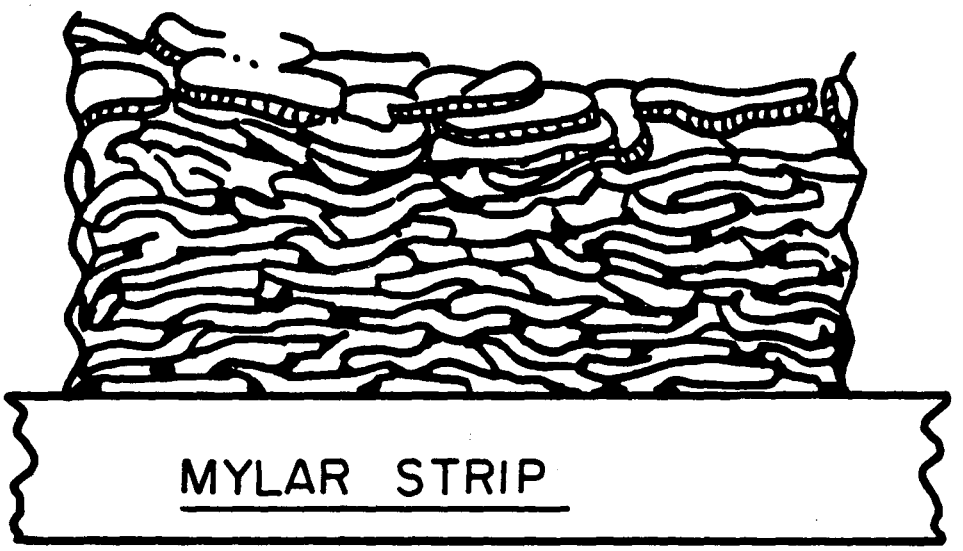

XBL816-3934

from the problem.

Because a rather thick suspension of thylakoid membranes is used in the drying procedure to orient samples, there is considerable disorder, or spread, in the alignment of the membrane normals. This spread is illustrated in Fig. 4-14. This disorder was referred to as the mosaic spread by Blum, et al. [29] and is incorporated into the orientational averaging scheme by the introduction of a weighting factor to the integrand of Eqn. 4-12. This factor is given by:

$$W = \Omega^{-1} \, e^{[-\ln 2 \cdot (\omega - \omega_o)^2 / \Omega^2]} \qquad (4\text{-}14)$$

where Ω is the half-width of the gaussian distribution used to weight the direction of H_0 which is ω away from the membrane normal. ω_o is the angle that the membrane normals make with H_0 and is known from the experiment.

The differences in the simulation routine for doing calculations on oriented samples are given below.

1. Four angle parameters must be specified: θ, ϕ, ω_o and Ω, the mosaic spread.

2. The integration of Eqn. 4-12 is done over a 0 to 90^o interval of ω and a 0 to 360^o interval of α. The weighting factor of Eqn. 4-14 is included in the integrand and used to account for the spread in membrane normals.

3. The direction cosines of Eqn. 4-6 are replaced by

those of Eqn. 4-13 for the calculation of the hamiltonian matrix elements at a given ω and α.

Computer simulations of the three oriented spectra examined above are plotted in Fig. 4-15 along with the experimental data. These spectra were simulated assuming that the A_0^- species had a slightly anisotropic g-tensor so that: (a) the g-value of A_0^- is $2.0031 \pm .0002$ for the parallel and 45^o orientations; and (b) the g-value of A_0^- is $2.0026 \pm .0001$ for the perpendicular orientation. This slight amount of g anisotropy is needed to make the low field portion of the spectrum, due to A_1^-, go to zero in the perpendicular orientation (Fig. 4-15b). When there is no net polarization on $P\text{-}700^+$ (which occurs when $\Delta g \beta H = 0$ in the primary radical pair - see Fig. 2-3 and the associated discussion), there is no polarization transferred to A_1^- and the low-field contribution to the spectrum is minimized. Thus,the spectrum observed in the perpendicular orientation covers a narrower width of field values and is centered at g=2.0026, the g-value of $P\text{-}700^+$. Evidence for small g anisotropy of the primary acceptor in bacterial photosynthetic reaction centers has recently been reported by Boxer, et al. [30]. A second way in which the spectrum in the perpendicular orientation can be simulated is if the g-value of A_0^- is fixed at $2.0031 \pm .0002$, and g anisotropy and/or hyperfine anisotropy on A_1^- is incorporated into the model, so that the contribution to the spectrum due to A_1^-

Fig. 4-15. A comparison of calculated and experimental EPR spectra for oriented thylakoids prepared as in Fig. 4-1. The g-values and linewidths of $P\text{-}700^+$ and A_1^-, as well as the values of J, D, and E were identical to those used to simulate the random spectrum (Fig. 4-12). The microwave frequency used in simulating each spectrum was identical to that used in the experiment (Figs. 4-3 through 4-5). Other simulation parameters were: (a) sample orientation, parallel; g-value of A_0^-, 2.0031; (b) sample orientation, perpendicular; g-value of A_0^-, 2.0026; and (c) sample orientation, 45^o; g-value of A_0^-, 2.0031. The mosaic spread of the membrane normals was 20^o, θ was set at 90^o, and ϕ was 10^o.

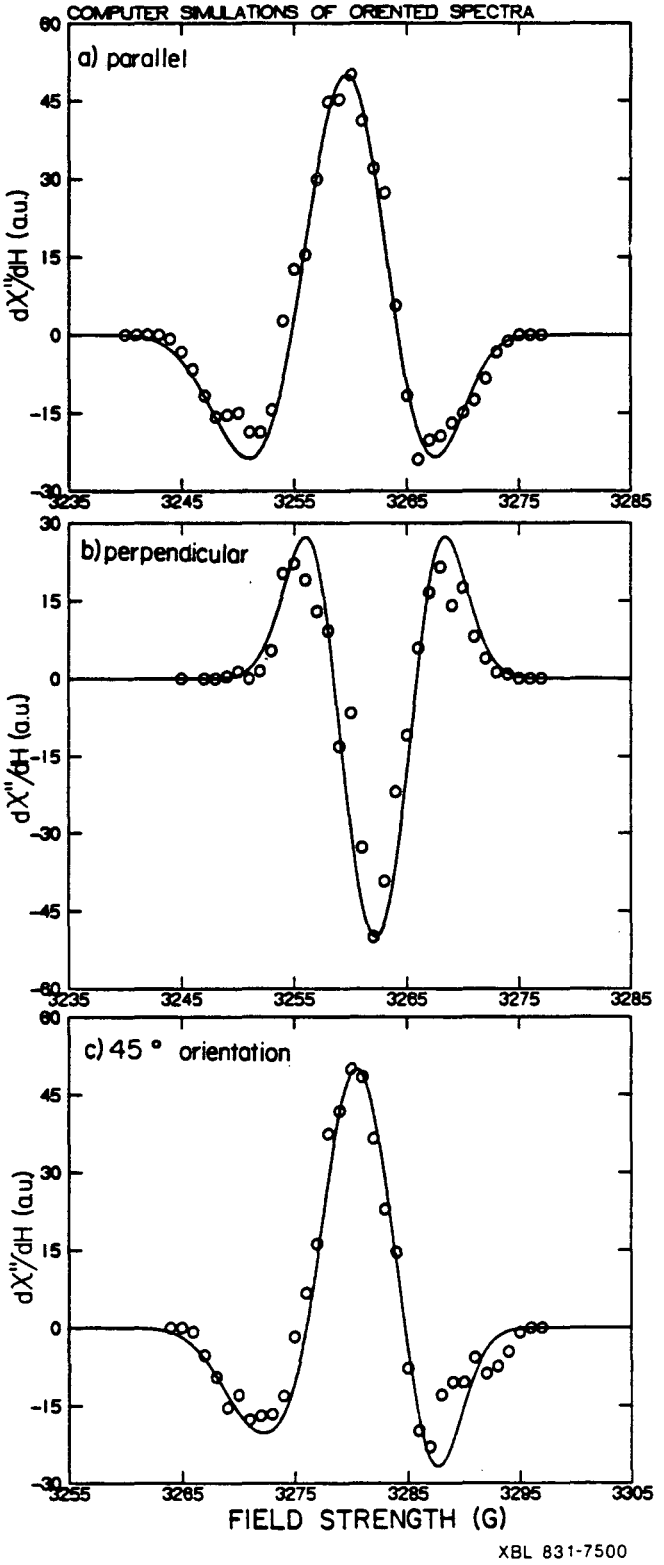
COMPUTER SIMULATIONS OF ORIENTED SPECTRA
a) parallel
b) perpendicular
c) 45 ° orientation
dX''/dH (a.u.)
FIELD STRENGTH (G)
XBL 831-7500

lies precisely on top of that due to $P\text{-}700^{+}$. This possibility is explored in detail in chapter 5.

As stated above, the random spectrum is only slightly sensitive to the value of E. Simulation of the spectra of the oriented samples requires that E be between 0 and -8 G. When the dipolar coupling tensor is made more rhombic, it is no longer possible to predict the peak positions of the spectrum obtained for the 45^{o} orientation. Because the range of acceptable g-values for A_0^{-} is narrowed by the oriented spectra simulations, the range of J values (assuming D= -50 G) is also narrowed to J = -9.5 G ± 1.0G.

Of the angle parameters used to perform the orientational averaging, the simulations are most sensitive to the values of θ and the mosaic spread. It was found that θ, the angle between the membrane normal and the z axis of the PAS of the dipolar coupling tensor, must be very close to 90^{o} (the lower limit is 85^{o}) to predict the spectra successfully at all three orientations. Further, the mosaic spread cannot be greater than 20^{o}. Because the best simulations were obtained with the dipolar coupling tensor nearly axial and a θ of 90^{o}, the dependence of the predicted spectra on ϕ (the angle between the x axis of the PAS and the membrane normal) was slight.

One shortcoming of the model presented here is that, although it is successful in predicting the peak positions and relative peak amplitudes of the random and oriented spectra, it does not predict the structure in some of the

oriented spectra (Figs. 4-12 and 4-15). It is possible that the structure in these spectra is due to spectral properties of A_1^- that are difficult to extract from these experiments because the spectra from $P\text{-}700^+$ and A_1^- overlap extensively at X-band. Because little is known about the A_1^- species, it was assumed in our simulations that it has no g-tensor or hyperfine tensor anisotropy. Inclusion of either one or both of these properties in the model presented above could account for the structure in the data. Recently, Bonnerjea and Evans [22] have obtained steady-state EPR spectra from chloroplasts that they attribute to A_1^- and A_0^-. The spectrum that they assign to A_1^- has a g-value of 2.0051 and a peak-to-peak linewidth of 10.5 G (in good agreement with the results presented here), and has an asymmetric lineshape. The spectral properties of A_1^- are examined in more detail in chapter 5.

There are two reports in the literature of g-values for A_0^-. Gast, et al. [13] report a g-value for A_0^- of 2.0017 ±.0006 for PS1 particles prepared with Triton X-100 and a value of 2.0033 for PS1 particles prepared with lithium dodecyl sulfate (LDS particles). These authors obtained the value of 2.0017 by deconvoluting the g 2.0 signal from reduced PS1 particles. To do this they had to assume a particular lineshape and power dependence for both the A_0^- and A_1^- species. A similar deconvolution was performed by Bonnerjea and Evans [22] and a g-value of 2.0024 was obtained. In both of these procedures, errors

could be significant if the lineshapes are asymmetric and the asymmetry is not properly treated.

In one of these reports [13], the authors showed that the CIDEP data for randomly oriented chloroplasts (Fig. 4-2) could be accounted for if the g-value of A_0^- was 2.0017. However, the model used in their simulations did not include dipolar coupling so that: (a) it does not account for the orientation dependence of the signals; and (b) a negative g-value difference between P-700$^+$ and A_0^- had to be used to predict the asymmetry of the P-700$^+$ contribution to the spectrum. The inclusion of dipolar coupling in the model makes it possible to simulate the data using a g-value consistent with A_0^- being a Chl a or pheophytin anion. The reason for this is that dipolar coupling causes a significant amount of mixing between the singlet state and the T_{+1} and T_{-1} triplet sublevels. This mixing drastically alters the skewing of the P-700$^+$ spectrum. The effects of dipolar coupling on the development of CIDEP will be examined in more detail in section 4.4.

Several sets of experiments have been reported in the literature where attempts were made to correlate the appearance of g 2.0 EPR signals with changes in the primary photochemistry of PS1 [13,22,31,32]. In all of these attempts, PS1 particles were prepared in a reduced state and an attempt was made to correlate the amplitude of the g 2.0 EPR signals with the amplitude of the triplet P-700 EPR signal indicative of electron transfer in PS1 [16,33]. In

only two of these experiments was it demonstrated that the appearance of a g 2.0 signal accompanied a significant reduction in the amplitude of the ^3P-700 EPR signal, thus indicating that the g 2.0 signal was due primarily to A_0^- [13,31]. Both of these experiments were done on PS1 particles prepared with lithium dodecyl sulfate and the g-value of the signals was approximately 2.0033. This value is in excellent agreement with the value obtained in the above analysis of the CIDEP data.

4.4 The Effects of Electron-Electron Magnetic Dipole Coupling on the Development of CIDEP

The work presented above represents the first time that an electron-electron magnetic dipole coupling interaction has been used to describe the development of CIDEP in a spin system. This is because nearly all of the previous experimental and theoretical work done in this area concerned chemical reactions that take place in solution where anisotropic spin-spin interactions are averaged out. In this section, the effects of the interaction on the observed polarization patterns will be examined in detail using the same approach that one generally uses to describe triplet EPR spectra. This approach is to examine the effects by looking separately at the predicted outputs in the three canonical orientations: H_0 parallel to the z axis of the PAS of the dipolar coupling tensor; H_0 parallel to X; and H_0 parallel to Y. This treatment will point out two major

effects of dipolar coupling: that both the sign and the magnitude of the polarization are orientation dependent; and that the skewing of multiplet spectra (Figs. 2-3 and 2-4) is drastically affected by $S\text{-}T_{\pm1}$ mixing. The first effect arises because both the sign and the magnitude of the exchange field in Fig. 2-1 are orientation dependent.

A. The Z Canonical Orientation

In the z canonical orientation, the hamiltonian matrix of Fig. 4-9 simplifies greatly. In this orientation, $H_z=H_0$ and $H_x=H_y=0$. There is no longer mixing between the $|S\rangle$ state and $|T_{\pm1}\rangle$ so that the radical-pair wavefunction is composed of an admixture of the $|S\rangle$ and $|T_0\rangle$ states. Using the notation of chapter 2, the time dependent radical-pair wavefunction is given by

$$|\psi(t)\rangle = [(\omega-J-D/3)/2\omega]^{1/2}\, e^{-i(-D/3+\omega)t}\,|\phi_+\rangle + [(\omega+J+D/3)/2\omega]^{1/2}\, e^{-i(-D/3-\omega)t}\,|\phi_-\rangle \qquad (4\text{-}15)$$

where

$$\omega = [(J+D/3)^2 + H_1^{\,2}]^{1/2}$$

$$H_1 = \langle S\,|H_{RP}\,|T_0\rangle$$

$$|\phi_+\rangle = [(\omega-D/3-J)/2\omega]^{1/2}\,|S\rangle - [(J+D/3+\omega)/2\omega]^{1/2}\,|T_0\rangle$$

$$|\phi_-\rangle = [(\omega+J+D/3)/2\omega]^{1/2}\,|S\rangle + [(\omega-J-D/3)/2\omega]^{1/2}\,|T_0\rangle$$

The polarization on the donor cation can be determined by

using Eqn. 4-15 in Eqn. 2-16 and is given in Eqn. 4-16.

$$\rho_D(t) = 2[H_1(D/3 + J)/\omega^2] \sin^2\omega t \qquad (4\text{-}16)$$

Time averaging Eqn. 4-16 over the radical pair lifetime, τ, as in Eqn. 2-20 yields the time averaged polarization:

$$\overline{\rho}_D(\tau) = 4H_1(D/3+J)\tau^2/(1+4\omega^2\tau^2) \qquad (4\text{-}17)$$

Eqn. 4-17 is nearly identical to Eqn. 2-20, which was the expression developed without the dipolar coupling term in the radical-pair hamiltonian. The interaction enters into the expression for the z canonical orientation as just a modification of the spin-spin coupling constant, J. Thus, the polarization developed in this orientation is mathematically isomorphic to the simple isotropic exchange case considered in chapter 2. The skewing of the multiplet spectra is controlled by the $S\text{-}T_0$ mixing term, H_1,

$$H_1^{(i)} = [(g_D-g_A)\beta H_0 + A_i^{(D)} m_{iz}]/2 \qquad (4\text{-}18)$$

which is identical to that of the isotropic exchange case of chapter 2 (see Eqn. 2-24).

An additional point which should be made here is that the hamiltonian used to obtain Eqn. 4-17 assumes that J is negative and D is positive. If both coupling constants have the same sign (as with the cases discussed above), the two interactions will be dependent on one another to the point that for any D, a J can be found which will keep Eqn. 4-17 a constant. This is why unique values for these two parameters

could not be found in the above simulations.

B. The X and Y Canonical Orientations

Examination of the hamiltonian matrix (Fig. 4-9) shows that in the x and y canonical orientations a significant amount of mixing between the |S> state and all three triplet sublevels occurs. The effects of $S\text{-}T_{\pm 1}$ mixing on radical pair CIDEP spectra have been examined experimentally by Trifunac and coworkers [34-36] and theoretically by Adrian and Monchick [37]. This experimental work was done on radical pairs generated in solution where the amount of $S\text{-}T_{\pm 1}$ mixing was varied by changing the viscosity of the solvent. The effects observed by these authors were that as the viscosity of the samples increased, the skewing or asymmetry of the observed multiplet CIDEP patterns became significantly altered. In many cases, spectra that had multiplet patterns in low viscosity media (see Fig. 2-3) gave rise to mixed multiplet or nearly net-effect spectra in highly viscous solvents. Trifunac and Nelson [35] also saw similar effects when the radicals of interest were incorporated into micelles.

The changes in predicted CIDEP spectra caused by $S\text{-}T_{\pm 1}$ mixing in radical pairs generated in viscous media were analyzed theoretically by Adrian and Monchick [37]. These authors used a stochastic-Liouville equation for modeling $S\text{-}T_{\pm 1}$ mixing. In their treatment the mixing occurs because hindrance of diffusion in highly viscous solvents causes the

radical pair to remain for a relatively long time in the S-T_{+1} or S-T_{-1} level crossing region during the singlet-triplet mixing process. In the treatment presented in this chapter, diffusion is not important and the S-$T_{\pm 1}$ mixing is driven by the dipole-dipole coupling interaction. The effects of this mixing on the predicted CIDEP spectra can be understood by examining the singlet-triplet matrix elements of the radical pair hamiltonian in the case where H_z=0. They are:

$$\langle T_0 | H_{RP} | S \rangle = A_i^{(D)} m_{iz}/2$$

$$\langle T_{+1} | H_{RP} | S \rangle = [(-g_D+g_A)\beta(H_x-iH_y)]/(2\sqrt{2})$$

$$\langle T_{-1} | H_{RP} | S \rangle = [(g_D-g_A)\beta(H_x+iH_y)]/(2\sqrt{2}) \qquad (4\text{-}19)$$

where the $\langle T_0 | H_{RP} | S \rangle$ element generates multiplet effect spectra and the other two elements cause the mixing of net effects with multiplet effects. The differences between this case and the z canonical orientation are not readily apparent, because analytical solutions are difficult to develop here. However, the effects can be examined numerically using computer simulation, and the results of these calculations are that the skewing of the polarization pattern by the net effect terms has the opposite sense to those obtained using the isotropic exchange model of chapter 2. This result is shown in Fig. 4-16. Fig. 4-16a is a field profile obtained using the isotropic exchange model and Fig

Fig. 4-16. Simulations showing the effects of dipolar coupling on the skewing of mixed multiplet polarization patterns. The skewing is nearly identical for the two patterns; however, for the isotropic exchange model (trace a) $\Delta g = +.0005$; but for the dipolar coupling model (trace b) $\Delta g = -.0005$. The common parameters used in these simulations are: microwave frequency, 9.222 GHz; g_D, 2.0026; linewidth of the donor ion, 8G; and radical pair lifetime, 2 μsec. For trace (a): g_A=2.0021, J=9.5G; and for trace (b), g_A=2.0031, J=-9.5G, D=-50G, and E=0G.

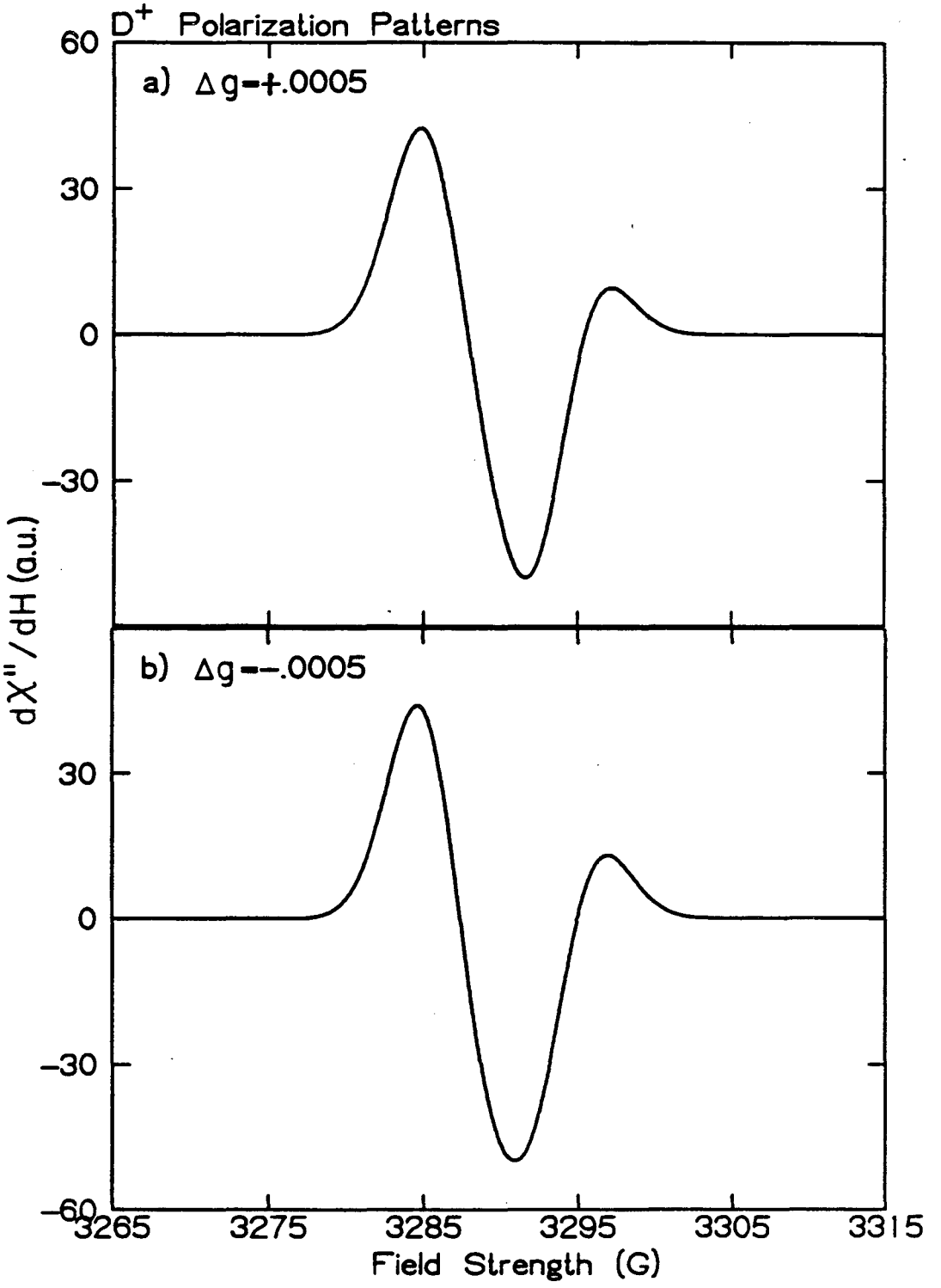
D+ Polarization Patterns
a) Δg=+.0005
b) Δg=−.0005
60
30
0
−30
30
0
−30
−60
dχ''/dH (a.u.)
3265
3275
3285
3295
3305
3315
Field Strength (G)

XBL 835-9842

Fig. 4-17. Effects of changing the sign of the $\langle S | H_{RP} | T_{+1} \rangle$ matrix element of the hamiltonian matrix of Fig. 4-9 on the skewing of mixed multiplet lineshapes for the donor ion. The parameters common to both traces are: g_D, 2.0026; g_A, 2.0031; linewidth of D^+, 8G; J, -9.35G; D=-50G; E=0; and microwave frequency, 9.193 GHz. In trace (a) the matrix is as in Fig. 4-9 and in trace (b) the sign of the $\langle S | H_{RP} | T_{+1} \rangle$ element is changed.

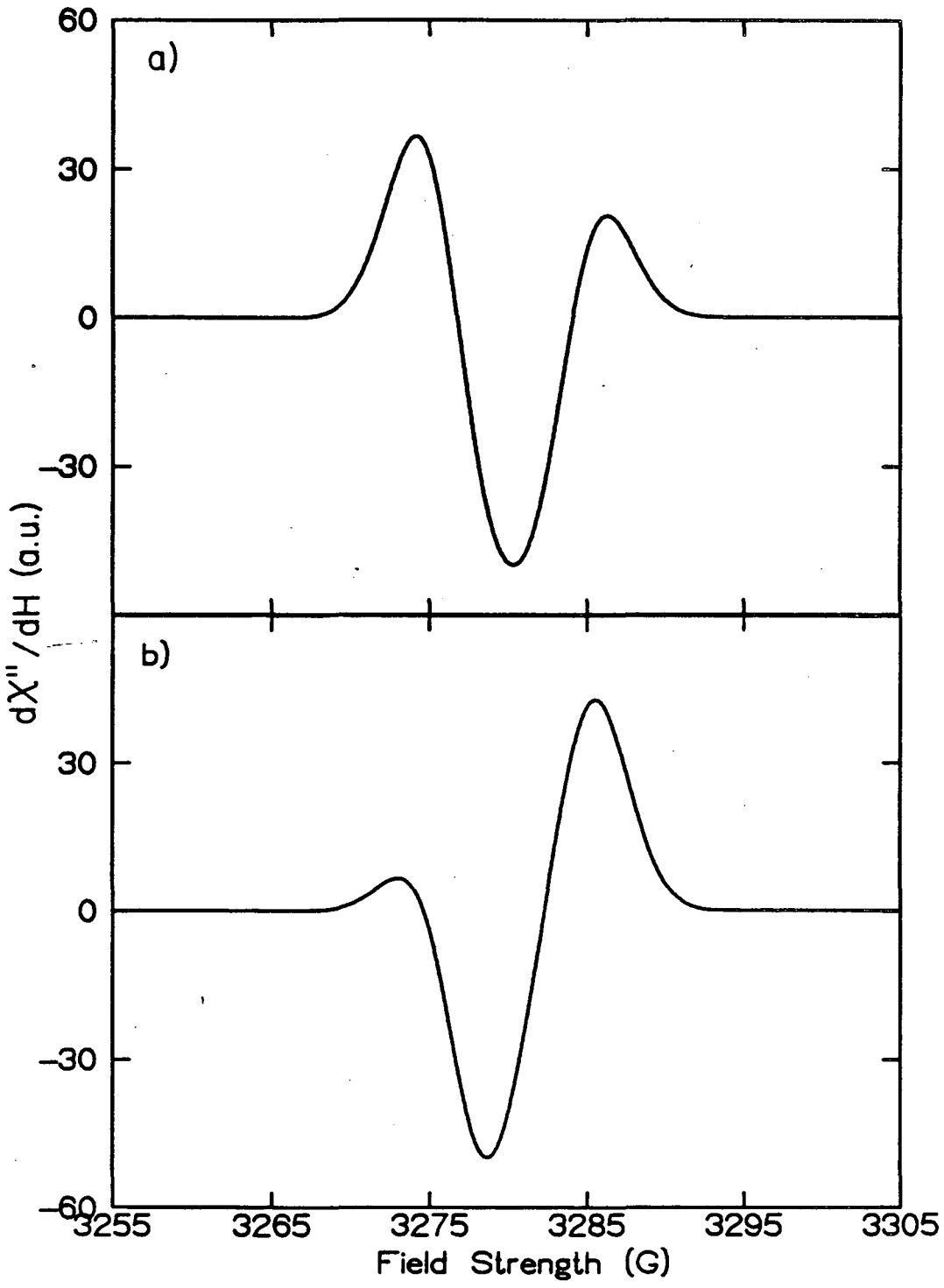
60
30
0
-30
a)
b)
30
0
-30
-60
dχ''/dH (a.u.)
3255
3265
3275
3285
3295
3305
Field Strength (G)

XBL 835-9841

4-16b is a spectrum obtained using the model with dipolar coupling added. In both cases, the skewing of the multiplet pattern is a function of the relation of $\Delta g\beta H$ to the magnitude of the hyperfine fields. However, in the top trace $\Delta g = g_D - g_A = +.0005$ and in the bottom trace, $\Delta g = -.0005$. The reason for this difference may be due to the sign difference between the $\Delta g\beta H$ term in the $\langle T_{+1}| H_{RP}| S\rangle$ and the $\langle T_{-1}| H_{RP} | S\rangle$ matrix elements (Eqn. 4-19). Fig. 4-17 shows that if the sign of the $\langle T_{+1}| H_{RP} | S\rangle$ matrix element is changed, the skewing of the predicted CIDEP spectrum is reversed.

4.5 The Two-site Model

During the course of the work presented in this chapter, several different models were used in attempts to analyze the data. Most of these models had shortcomings which kept them from being able to predict even the random spectrum. One model which successfully predicts the random spectrum and may be a viable alternative to the model used in the above analysis is a "two-site" model similar to that developed by Friesner, et al. [4]. This model is similar to the one-site model described above in that it requires the existence of an A_0 and A_1 in the primary acceptor complex. It is different in that an isotropic exchange interaction between P-700$^+$ and A_1^- is included. Thus, the polarization develops on P-700$^+$ due to two separate radical pair interactions: the first being between P-700$^+$ and A_0^-,

involving both dipolar coupling and isotropic exchange; and the second being between P-700$^+$ and A_1^- after electron transfer from A_0^- to A_1 has occurred. Because of its potential usefulness, this model will be described in detail below and its predictions concerning the random spectrum of Fig. 4-2 will be presented.

The quantum mechanics of the two-site model is an extension of the procedure used for developing the one-site model presented above. The spin-spin interactions are considered sequentially, and the time evolution of the radical pair wavefunction is determined. This wavefunction is then used to calculate the time dependence of the spin polarization on a given radical species using Eqn. 2-16. The hamiltonian that describes the energetics of the first radical pair is identical to that used in the above model and given in Eqn. 4-1. At the birth of the first radical pair, P-700$^+$ A_0^-, $|\psi(0)\rangle = |S\rangle$. The radical pair wavefunction at the time t_1, of electron transfer from A_0^- to A_1, is as in Eqn. 4-9 and can be written in the form:

$$|\psi(t_1)\rangle = C_S(t_1)|S\rangle + C_T(t_1)|T_0\rangle + C_+(t_1)|T_{+1}\rangle + C_-(t_1)|T_{-1}\rangle. \quad (4\text{-}20)$$

The hamiltonian that describes the energetics of the P-700$^+$ A_1^- radical pair is

$$H = H_{zee}^D + H_{zee}^A + H_{hf}^D + H_{hf}^A - J_2(2\underset{\sim}{S}_D \cdot \underset{\sim}{S}_A + 1/2) \quad (4\text{-}21)$$

where the Zeeman and hyperfine hamiltonians have the same form as in Eqns. 2-7 and 2-8. The hamiltonian matrix in the singlet-triplet basis is given below.

$$\begin{array}{c} \\ \langle S| \\ \langle T_0| \\ \langle T_{+1}| \\ \langle T_{-1}| \end{array} \begin{array}{c} \begin{array}{cccc} |S\rangle & |T_0\rangle & |T_{+1}\rangle & |T_{-1}\rangle \end{array} \\ \begin{bmatrix} J_2 & H_2 & 0 & 0 \\ H_2 & -J_2 & 0 & 0 \\ 0 & 0 & E_{+1} & 0 \\ 0 & 0 & 0 & -E_{+1}-2J_2 \end{bmatrix} \end{array}$$

H_2 in this matrix is given by

$$H_2 = [(g_D-g_A)\beta H + A_i^{(D)}m_{iz} - A_j^{(A)}m_{jz}]/2 \qquad (4\text{-}22)$$

and E_{+1} is given by

$$E_{+1} = [(g_D+g_A)\beta H + A_i^{(D)}m_{iz} + A_j^{(A)}m_{jz}]/2 - J_2.$$

The above matrix is easily diagonalized and the time evolution of the radical pair wavefunction is given by

$$|\psi(t_1,t_2)\rangle = \sum_{k=1}^{4} \langle\phi_k|\psi(t_1)\rangle\, e^{-iE_k t_2'}\, |\phi_k\rangle \qquad (4\text{-}23)$$

where the $|\phi_k\rangle$ and E_k are the eigenstates and eigenvalues obtained by diagonalizing the above matrix(t_2' contains $\hbar$). $|\psi(t_1)\rangle$ in Eqn. 4-23 is given in Eqn. 4-20. Substituting the $|\phi_k\rangle$ and E_k into Eqn. 4-23 one finds that

$$|\psi(t_1,t_2)\rangle = \{C_S(t_1)[(\omega_2-J_2)/2\omega_2]^{1/2}$$

$$-C_T(t_1)[(\omega_2+J_2)/2\omega_2]^{1/2}\}e^{-i\omega_2 t_2}|\phi_1\rangle$$

$$+\{C_S(t_1)[(\omega_2+J_2)/2\omega_2]^{1/2}$$

$$+C_T(t_1)[(\omega_2-J_2)/2\omega_2]^{1/2}\}e^{i\omega_2 t_2}|\phi_2\rangle$$

$$+C_+(t_1)e^{-iE_+t_2}|T_{+1}\rangle + C_-(t_1)e^{-iE_-t_2}|T_{-1}\rangle \qquad (4\text{-}24)$$

where

$$|\phi_1\rangle = [(\omega_2-J_2)/2\omega_2]^{1/2}|S\rangle - [(\omega_2+J_2)/2\omega_2]^{1/2}|T_0\rangle$$

$$|\phi_2\rangle = [(\omega_2+J_2)/2\omega_2]^{1/2}|S\rangle + [(\omega_2-J_2)/2\omega_2]^{1/2}|T_0\rangle$$

$$\omega_2 = (H_2^2 + J_2^2)^{1/2} .$$

Substituting $|\phi_1\rangle$ and $|\phi_2\rangle$ into Eqn. 4-24 yields

$$|\psi(t_1,t_2)\rangle = (C_S\cos\omega_2 t_2 + i[(C_S J_2 + C_T H_2)/\omega_2]\sin\omega_2 t_2)|S\rangle$$

$$+\{i[(C_S H_2 - C_T J_2)/\omega_2]\sin\omega_2 t_2 + C_T\cos\omega_2 t_2\}|T_0\rangle$$

$$+C_+e^{-iE_+t}|T_{+1}\rangle + C_-e^{-iE_-t}|T_{-1}\rangle \qquad (4\text{-}25)$$

where the C's are functions of t_1. Using Eqn. 4-25 in Eqn. 2-16, the spin polarization developed on the electron donor ion can be determined. The expression, which is identical to the result of Friesner, et al. [4], is

$$\rho_D(t_1,t_2) = (C_S^* C_T + C_T^* C_S + |C_+|^2 - |C_-|^2)$$
$$-2J_2^2[(C_T^* C_S + C_S^* C_T)/\omega_2^2]\sin^2\omega_2 t_2$$
$$+2J_2 H_2[(|C_S|^2 - |C_T|^2)/\omega_2^2]\sin^2\omega_2 t_2$$
$$+iJ_2[(C_S C_T^* - C_S^* C_T)/\omega_2]\sin 2\omega_2 t_2 \qquad (4\text{-}26)$$

The time averaging for Eqn. 4-26 is done over two radical pair lifetimes, τ_1 and τ_2, and is found using the following expression,

$$\rho_D(\tau_1,\tau_2) = (\tau_1\tau_2)^{-1}\int_0^\infty\int_0^\infty \rho_D(t_1,t_2)e^{-t/\tau_1}e^{-t/\tau_2}\,dt_1 dt_2 \qquad (4\text{-}27)$$

Before Eqn. 4-27 can be used, the coefficients for $|\psi(t_1)\rangle$ in Eqn. 4-26; $C_S(t_1)$, $C_T(t_1)$, $C_+(t_1)$, and $C_-(t_1)$ must be found in terms of the coefficients for the eigenstates of the first radical pair. This procedure involves a fair amount of algebra and is similar to that outlined in appendix A. Following the above procedure, the polarization on A_1^- may be found. It is given by:

$$\rho_A(t_1,t_2) = 2\langle\psi(t_1,t_2)|S_{Az}|\psi(t_1,t_2)\rangle$$
$$= -\rho_D(t_1,t_2) + 2(|C_+(t_1)|^2 - |C_-(t_1)|^2)\,. \qquad (4\text{-}28)$$

A listing of the computer program subroutine used to calculate these polarizations along with a description of how it is incorporated into the program described in section

Fig. 4-18. Simulation of the random spectrum of Fig. 4-2 using a two-site model. The simulation parameters are: g_D, 2.0026; g-value of A_0^-, 2.0029; g-value of A_1^-, 2.0035; J1, -5G; J2, -.01G; D, -50G; E, -3G; τ_1, 20 nsec; τ_2, 20 μsec; linewidth of P-700$^+$, 8G; linewidth of A_1^-, 12G; and microwave frequency, 9.11 GHz. The simulation is a sum of contributions from statically polarized P-700$^+$ and dynamically polarized A_1^- as in Figs. 4-12 and 4-15.

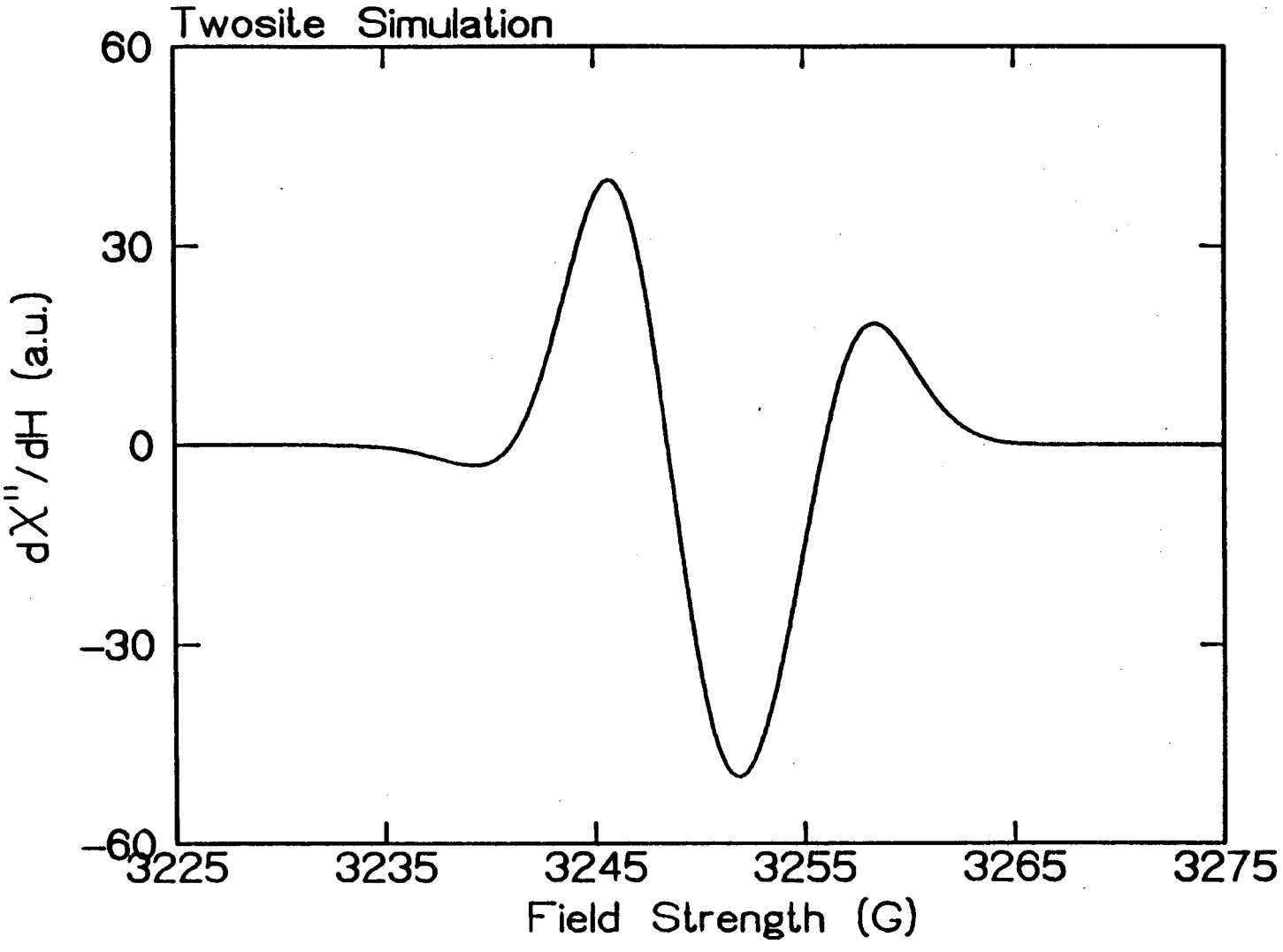
Twosite Simulation
60
30
0
-30
-60
dχ''/dH (a.u.)
3225
3235
3245
3255
3265
3275
Field Strength (G)

XBL 835-9822

4.3C is given in appendix B.

An example of a typical random spectrum simulation is shown in Fig. 4-18. The g-values of the peaks and the relative peak amplitudes are nicely predicted. However, it was found that simulations of this type could only be obtained if J_2 was less than J_1 by a factor of 500 - 1000. Because this interaction must be weak to obtain reasonable results, the one-site model used in the analysis of section 4.3 provides an adequate description of the development of electron spin polarization in PS1 under these experimental conditions.

REFERENCES

1. Blankenship, R., McGuire, A.E. and Sauer, K. (1975) Proc. Natl. Acad. Sci. USA 72, 4943-4947.
2. Dismukes, G.C., McGuire, A.E., Blankenship, R. and Sauer, K. (1978) Biophys. J. 21, 239-256.
3. Shuvalov, V.A., Dolan, E. and Ke, B. (1979) FEBS Lett. 100, 5-8.
4. Friesner, R., Dismukes, G.C. and Sauer, K. (1979) Biophys. J. 25, 277-294.
5. Goldman, S., Bruno, G., Polnaszek, C. and Freed, J.H. (1972) J. Chem. Phys. 56, 716-735.
6. Poole, C.P.,"Electron Spin Resonance," Wiley-Interscience, NY, 1967, pp. 406-408.
7. Arnon, D.I. and Chain, R.K. (1975) Proc. Natl. Acad. Sci. USA 72, 4961-4965.
8. Prince, R., Crowder, M.S. and Bearden, A.J. (1980) Biochim. Biophys. Acta 592, 323-337.
9. Blum, H., Harmon, H.J., Leigh, J.S., Salerno, J.C. and Chance, B. (1978) Biochim. Biophys. Acta 502, 1-10.
10. Geacintov, N.E., Van Nostrand, F., Becker, J.F. and Tinkel, J.B. (1972) Biochim. Biophys. Acta 267, 65-79.
11. Malkin, R. and Bearden, A.J. (1978) Biochim. Biophys. Acta 505, 147-181.
12. Dismukes, G.C. and Sauer, K. (1978) Biochim. Biophys. Acta 504, 431-445.
13. Gast, P., Swarthoff, T., Ebskamp, F.C.R. and Hoff, A.J.

(1983) Biochim. Biophys. Acta 722, 163-175.

14. Friesner, R., McCracken, J.L. and Sauer, K. (1981) J. Magn. Resonance 43, 343-356.
15. Hore, P. and McLauchlan, K.A. (1981) Mol. Phys. 42, 533-550.
16. Frank, H.A., McLean, M.B. and Sauer, K. (1979) Proc. Natl. Acad. Sci. USA 76, 5124-5128.
17. Golbeck, J.H., Lien, S. and San Pietro, A. (1977) Arch. Biochem. Biophys. 178, 140-148.
18. McIntosh, A.R., Manikowski, H., Wong, S., Taylor, C.P.S. and Bolton, J.R. (1979) Biochem. Biophys. Res. Commun. 87, 605-612.
19. Evans, M.C.W., Sihra, C.K. and Cammack, R. (1976) Biochem. J. 158, 71-77.
20. Commoner, B., Heise, J.J. and Townsend, J. (1956) Proc. Natl. Acad. Sci. USA 42, 710-718.
21. Pedersen, J.B. (1979) FEBS Lett. 97, 305-310.
22. Bonnerjea, J. and Evans, M.C.W. (1982) FEBS Lett. 148, 313-316.
23. Roelofs, M., Chidsey, C.E.D. and Boxer, S.G. (1982) Chem. Phys. Lett. 87, 582-588.
24. Norris, J.R., Bowman, M.K., Budil, D.E., Tang, J., Wraight, C.A., and Closs, G. (1982) Proc. Natl. Acad. Sci. USA 79, 5532-5536.
25. Gast, P. and Hoff, A.J. (1979) Biochim. Biophys. Acta 548, 520-535.
26. Gast, P., Mushlin, R.A. and Hoff, A.J. (1982) J. Phys.

Chem. 86, 2886-2891.

27. Scheer, H., Katz, J.J. and Norris, J.R. (1977) J. Am. Chem. Soc. 99, 1372-1381.
28. Lubitz, W., in "Proceedings of the International Conference on Electron Spin Resonance of Radicals in Organic and Bio-Organic Systems," Nottingham University Press, Nottingham, England, 1982.
29. Blum, H., Salerno, J.C. and Leigh, J.S. (1978) J. Magn. Resonance 30, 385-391.
30. Boxer, S.G., Chidsey, C.E.D. and Roelofs, M.G. (1982) Proc. Natl. Acad. Sci. USA 79, 4632-4636.
31. Rutherford, A.W. and Mullet, J.E. (1981) Biochim. Biophys. Acta 635, 225-235.
32. McLean, M.B. and Sauer, K. (1982) Biochim. Biophys. Acta 679, 384-392.
33. Blackwell, M.F., "Electron Paramagnetic Resonance Studies of Triplet States in Photosystem 1 of Chloroplasts," Ph.D. Thesis, University of California, Berkeley, 1982, Lawrence Berkeley Laboratory Report, LBL-15012.
34. Trifunac, A.D. and Nelson, D.J. (1977) J. Am. Chem. Soc. 99, 289.
35. Trifunac, A.D. and Nelson, D.J. (1977) Chem. Phys. Lett. 46, 346-348.
36. Trifunac, A.D. (1977) Chem. Phys. Lett. 49, 457-458.
37. Adrian, F.J. and Monchick,L. (1979) J. Chem. Phys. 71, 2600-2610.

CHAPTER 5

LOW TEMPERATURE CIDEP FROM PHOTOSYSTEM 1 - PART 2

5.1 Introduction

In chapter 4, the spin polarized EPR signals that are a result of Photosystem 1 electron transport were examined in detail for broken spinach chloroplasts poised in a redox state where Fe-S centers A and B were reduced prior to application of an actinic flash. In this chapter, the CIDEP signals from PS1 are examined for chloroplasts poised at lower redox potentials so that the species X and possibly A_1 are reduced prior to flash stimulation.

The purpose of this set of experiments was to determine if one could learn anything about the role of X in PS1 electron transport using time resolved EPR and to attempt to probe the EPR properties of A_1^- without interference from spin-polarized P-700$^+$. The latter idea involved trying to study polarization transfer from A_0^- to A_1^- using conditions similar to those used by Gast, et al. on bacterial reaction centers [1-3]. In those experiments, the authors took bacterial reaction centers which contained the primary electron donor, P, the primary acceptor, I, and the secondary acceptor, U; and redox poised them so that U was reduced. When a laser flash was applied to the sample, spin polarized EPR signals due to U^- were observed. The authors

concluded that spin-spin coupling between I^- and U^- caused spin polarization to be transferred from I^- to U^- after the primary radical ion pair (P^+I^-) was created. The reaction sequence for these experiments was proposed to be:

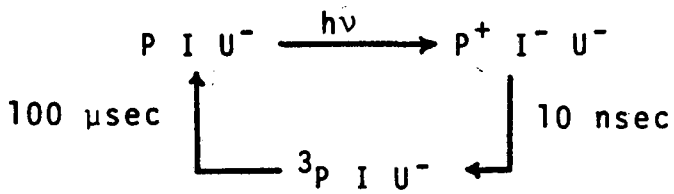

where the rise and decay times of the ^3P species are known from previous studies [4-6]. This type of experiment provides a means by which the spectrum of U^- can be examined in a polarized state without interference from P^+ or I^-, because they decay to ^3P on a time scale that is fast compared to that of an EPR experiment. In bacterial reaction centers one does not need to go to these extremes to examine the EPR spectrum of U^- because the species can be studied using steady state spectroscopy without interference from other radicals. However, in PS1 the sample preparations that contain A_1 are crude and as mentioned in chapter 1 there can be interference from other EPR signals occurring in the same region that could hinder steady-state measurements. Therefore, experiments of the type described above allow one to examine the EPR properties of A_1^- without interference from P-700$^+$ and A_0^-.

In this chapter, attempts at studying the EPR properties of A_1^- using the above approach will be

described. The experiments were performed on broken spinach chloroplasts poised at low redox potentials at 10K. Both random and oriented thylakoids were studied in an attempt to determine whether the disappearance of the low field portion of the CIDEP spectrum of Fig. 4-2 (attributed to A_1^-) was due to g-anisotropy on A_0^- or an anisotropic property of the A_1^- species.

5.2 Materials and Methods

The spectrometer and equipment configurations, the spinach chloroplast preparation, and the sample orientation procedures were identical to those described in chapter 4. The sample treatments used for poising the PS1 reaction center at low oxidation-reduction potentials were as follows.

1. Treatment with ascorbate. Broken spinach chloroplasts were suspended in 50mM Tris buffer, pH=8.0 containing 10mM NaCl, 0.1mM EDTA and an initial ascorbate concentration of 50 mM. If the sample was to be randomly oriented, the above suspension was mixed with an equal volume of glycerol. If oriented samples were desired, orientation was achieved by partial dehydration of the above suspension on mylar as described in chapter 4.

2. Treatment with dithionite. Broken spinach chloroplasts were suspended in 0.2M glycine buffer, pH=10

containing 0.1mM EDTA, 10 μM methyl viologen, 1 mg/ml glucose, 0.2 mg/ml glucose oxidase, 0.2 mg/ml catalase, and an initial sodium dithionite concentration of 50 mM. This suspension was then mixed with an equal volume of glycerol. Oriented samples for this treatment were prepared using the field alignment technique described in chapter 4.

Samples prepared using both of the above treatments were poised at low redox potentials by illuminating them at high light intensity (700 W/m^2) for 20 sec at room temperature and then rapidly immersing them in liquid N_2 and illuminating for another 20 sec at the same intensity. A tungsten lamp filtered with a heat reflection filter was used as a light source for these experiments.

5.3 Results

A. Samples Prepared with Ascorbate and Illumination While Cooling

As in chapter 4, the steady-state EPR spectra of the various samples examined in these experiments were used as an assay of the redox state of the PS1 reaction center and for determining the degree of orientation for the oriented samples. The EPR spectra obtained for samples prepared by treatment with ascorbate and illuminated during cooling are shown in Fig. 5-1. These spectra are of oriented samples and were taken at 10K. The top trace (Fig. 5-1a) was taken for

Fig. 5-1. Steady state EPR spectra of oriented chloroplast thylakoids treated with ascorbate and illuminated while freezing. Trace (a) is the spectrum obtained when the thylakoid membrane normals are parallel to the DC field direction and trace (b) is for the perpendicular orientation. The spectrometer settings were: microwave frequency, 9.19 GHz; microwave power, 10 mW; sample temperature, 13K; field modulation amplitude, 12.5 G; and modulation frequency, 100 KHz.

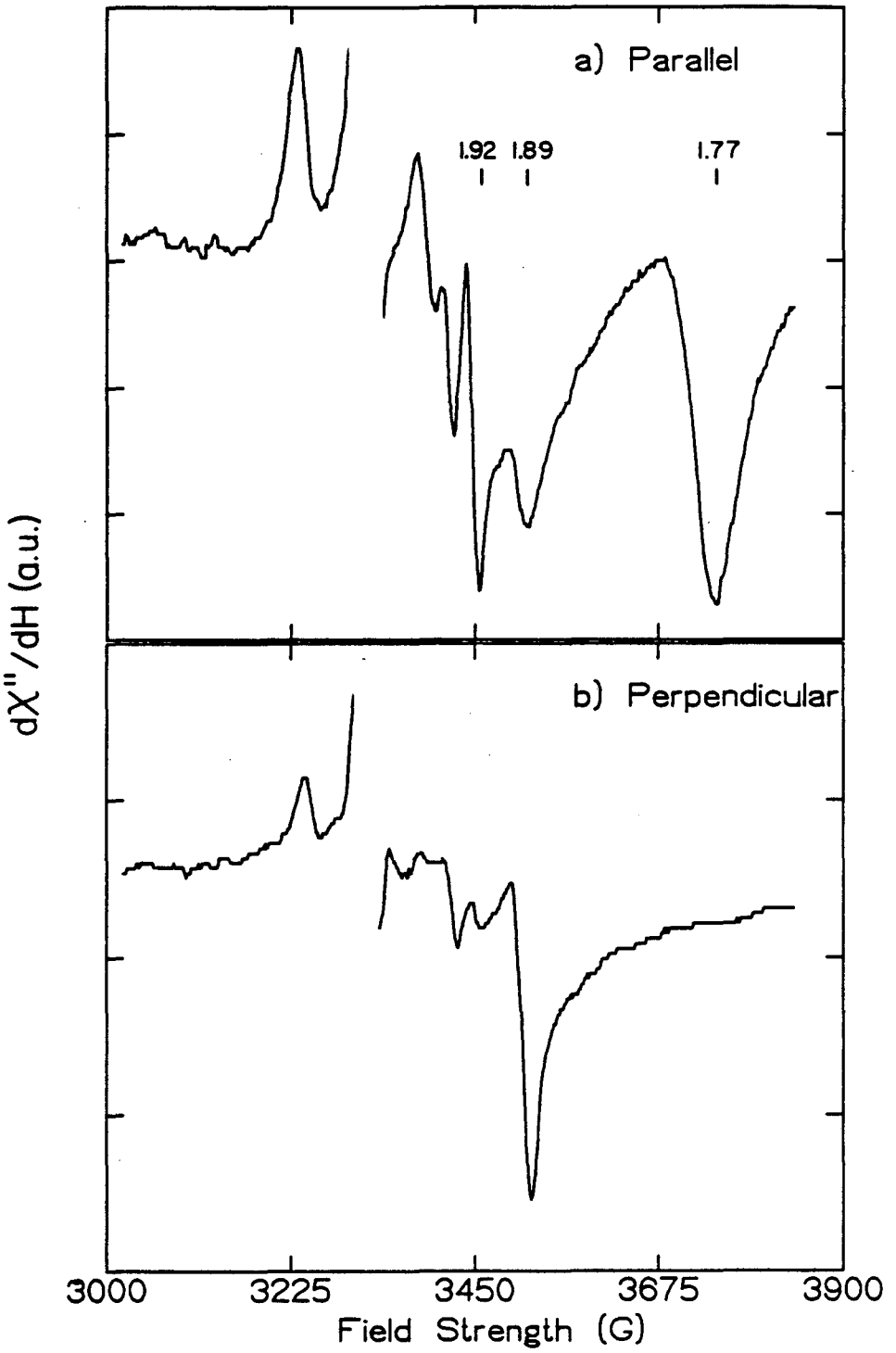
a) Parallel
1.92
1.89
1.77
b) Perpendicular
dχ''/dH (a.u.)
3000
3225
3450
3675
3900
Field Strength (G)

XBL 835-9815

oriented thylakoids positioned so that the thylakoid membrane normals were coincident with the direction of the Zeeman field (the parallel orientation), while the bottom trace (Fig. 5-1b) was taken for oriented thylakoids in the perpendicular orientation. The peaks due to Fe-S centers A and B at g 1.89 and 1.92 show an orientation dependence identical to that obtained when the X species was not reduced (Fig. 4-1). The large peak at g 1.77 is due to X^- and has its maximum amplitude in the parallel orientation (Fig. 5-1a). In the perpendicular orientation, the EPR absorption at g 1.77 vanishes (Fig. 5-1b). This result is similar to that obtained by Dismukes and Sauer [7] using thylakoids oriented in a 9 kG magnetic field, but shows a higher degree of order.

The ascorbate samples treated so that X was reduced prior to flash stimulation gave rise to biphasic EPR transient signals in the g 2.0 region. The lifetimes (1/e times) of these two phases were approximately 3 μsec and 30 μsec. The relative amplitude of each component depends on both orientation and field position. When the sample is in the perpendicular orientation, the fast (3 μsec) component nearly vanishes, whereas in intermediate and parallel orientations, it dominates the decays at some field positions. The effect of reducing X on the EPR transient signals is demonstrated in Fig. 5-2 by plotting a kinetic trace obtained for oriented chloroplasts (parallel orientation) with X not reduced (trace a) and a kinetic

Fig. 5-2. Kinetic traces for oriented thylakoids prepared using ascorbate treatment. The top trace (a) is of a sample where X is not reduced by the treatment and illumination procedure; and trace (b) is for a sample where X is reduced. Measurement conditions were: g=2.0041; parallel orientation; sample temperature, 15 K; field modulation frequency, 1 MHz; modulation amplitude, 2.5 G; and microwave power, 0.05 mW. Each trace is the average of 500 events.

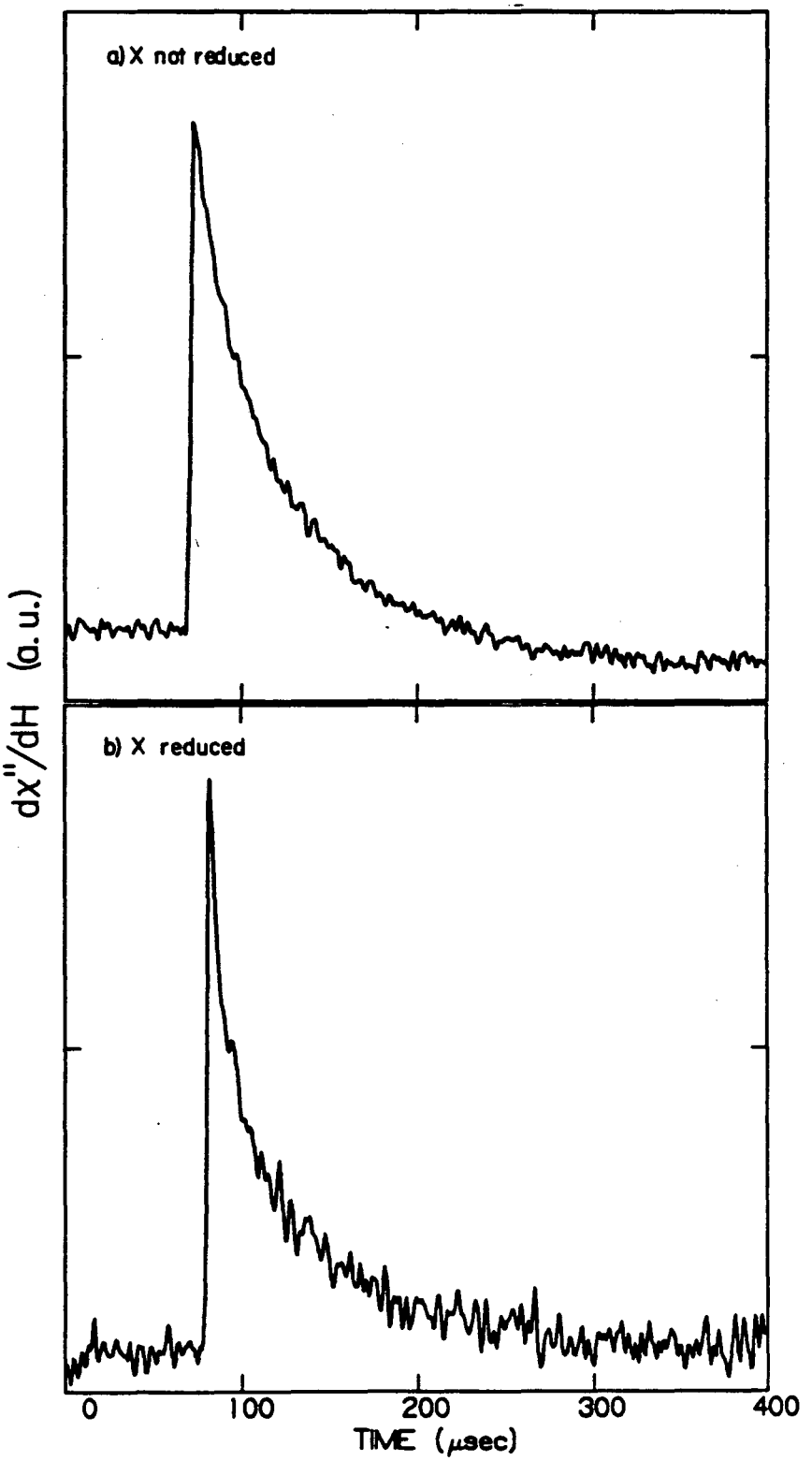

XBL 831-7504

trace obtained for chloroplasts in the same orientation and at the same field position, but with X reduced (trace b).

For randomly oriented chloroplasts, prepared with X reduced using ascorbate treatment, the field profile of both kinetic components combined is similar to that obtained in the X not reduced case (Fig. 4-2). This time resolved EPR spectrum is plotted in Fig. 5-3. For randomly oriented samples, the signal-to-noise ratio was too low to separate the two kinetic components and plot them separately with any accuracy. However, it was possible to achieve this separation with the oriented samples. Fig. 5-4 shows the combined amplitude of both components plotted versus field position for oriented thylakoids in the parallel orientation. Fig. 5-5 shows the same data, only with the amplitudes of the two kinetic components plotted separately. These figures show that the lineshapes of both kinetic components are identical in this orientation and very similar to that obtained for oriented chloroplasts under the same conditions with X not reduced prior to flash stimulation (Fig. 4-3). When the sample was rotated to the perpendicular orientation, very little fast component was present and the field profile of the slow (30 μsec) component (Fig. 5-6) was identical to that obtained in the X not reduced case (Fig. 4-4). Fig. 5-7 shows the field profile of both kinetic components combined when the sample is positioned so that the thylakoid membrane normals are at approximately 45^{o} to the Zeeman field direction. Profiles of

the separated components (Fig. 5-8) show that the lineshapes are different in this orientation. The fast component has an emissive-absorptive shape similar to the lineshape in the parallel orientation. The slow component has a lineshape which is similar to that of both components combined (Fig. 5-7).

B. Samples Prepared with Dithionite and Illumination While Cooling

Samples that were reduced by treatment with sodium dithionite and illumination while freezing gave rise to results which are significantly different from those presented above. The steady state spectra of a typical oriented sample (magnetic field alignment is used with this treatment) are shown in Fig. 5-9. Fig. 5-9a was taken for oriented thylakoids with their membrane normals parallel to the direction of the Zeeman field and shows a prominent peak at g 1.77 indicative of X^-. When the sample is rotated to the perpendicular orientation (Fig. 5-9b), the signal at g 1.77 becomes small, and a signal at g 1.86 due to the g_y peak of X^- centered at g 1.88 [7,8] grows in. The relative amplitudes of the signals due to reduced Fe-S centers A and B at g 1.89 and 1.92 along with the signal at g 1.77 due to X^- indicate that alignment of the thylakoid membranes in these samples is not so good as that obtained with the partial dehydration technique. An interesting observation is that the peak at g 1.86 due to X^- is much more prominent in

Fig. 5-3. A plot of the amplitude of both kinetic components combined for randomly oriented chloroplasts prepared by ascorbate treatment as described in the text. The sample was illuminated while freezing so that the X species was reduced prior to doing flash studies. The measurement conditions were: microwave frequency, 9.220 GHz; microwave power, 0.05 mW; sample temperature, 11.5K; modulation frequency, 1 MHz; and field modulation amplitude, 2.5 G. Each point is the average of 750 passes.

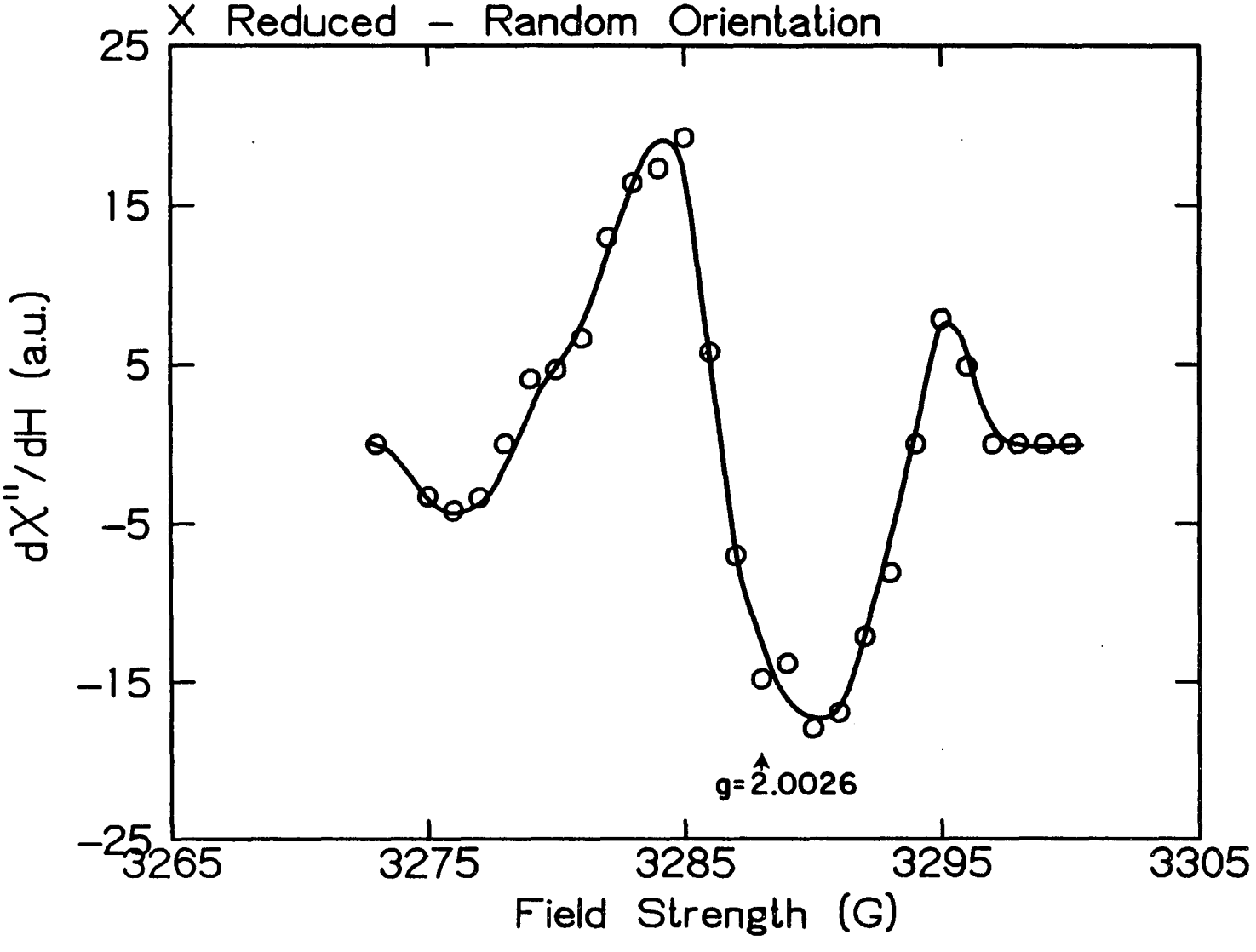
X Reduced – Random Orientation
25
15
5
-5
-15
-25
dX''/dH (a.u.)
3265
3275
3285
3295
3305
Field Strength (G)
g=2.0026

XBL 835-9850

Fig. 5-4. A plot of both kinetic components combined for oriented chloroplast thylakoids treated with ascorbate and frozen under illumination so that X was reduced. The measurement conditions were: sample orientation, parallel; microwave frequency, 9.165 GHz; microwave power, 0.05 mW; sample temperature, 9 K; modulation frequency, 1 MHz; and modulation amplitude, 2.5 G. Each point was the average of 500 events.

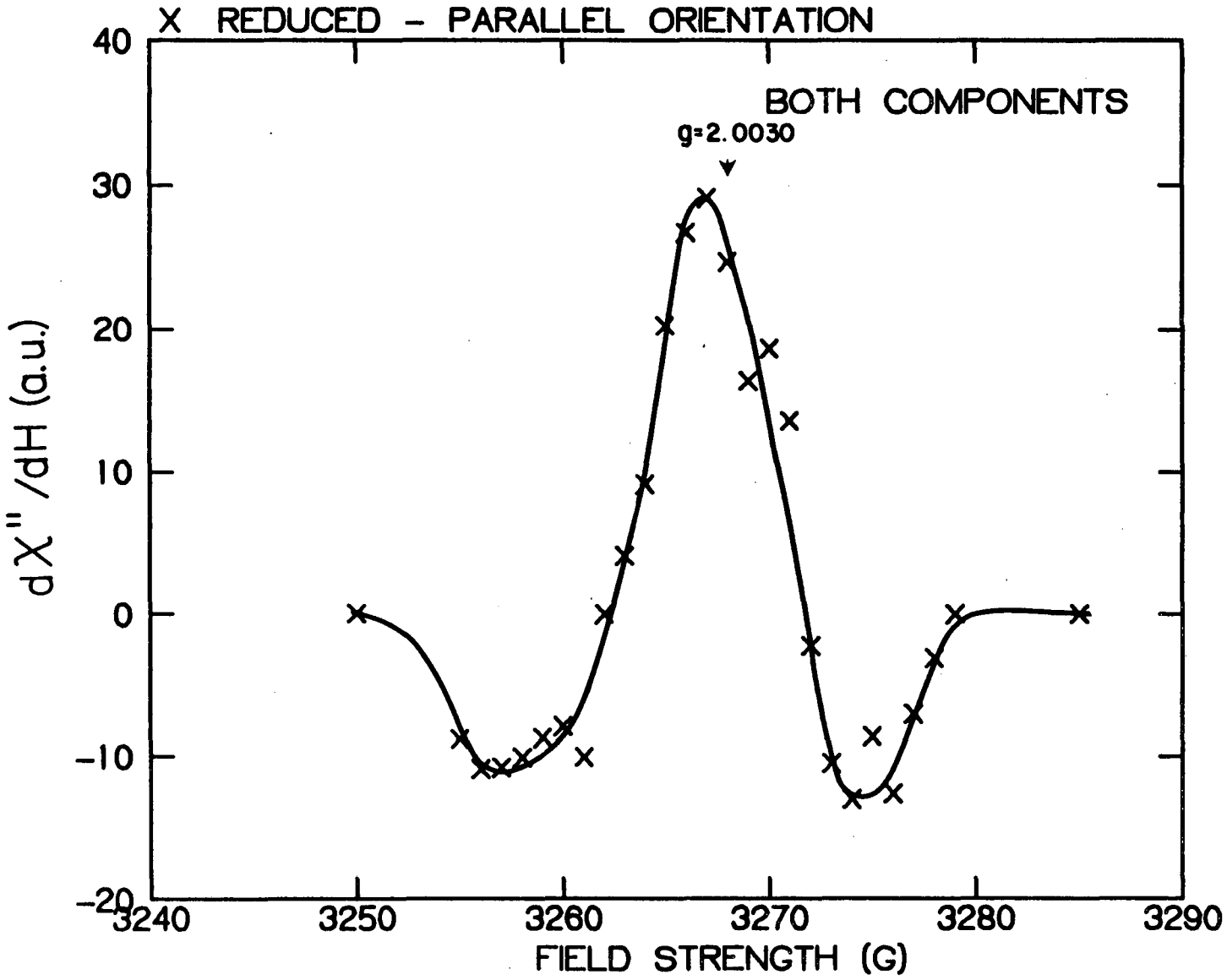
X REDUCED - PARALLEL ORIENTATION
BOTH COMPONENTS
g=2.0030
40
30
20
10
0
-10
-20
dX''/dH (a.u.)
3240
3250
3260
3270
3280
3290
FIELD STRENGTH (G)

XBL 835-9851

Fig. 5-5. Plots of the data of Fig. 5-4 for the separated kinetic components. Trace (a) is the field profile of the fast component and trace (b) is the field profile of the slow component. Conditions for the measurement are as given in Fig. 5-4.

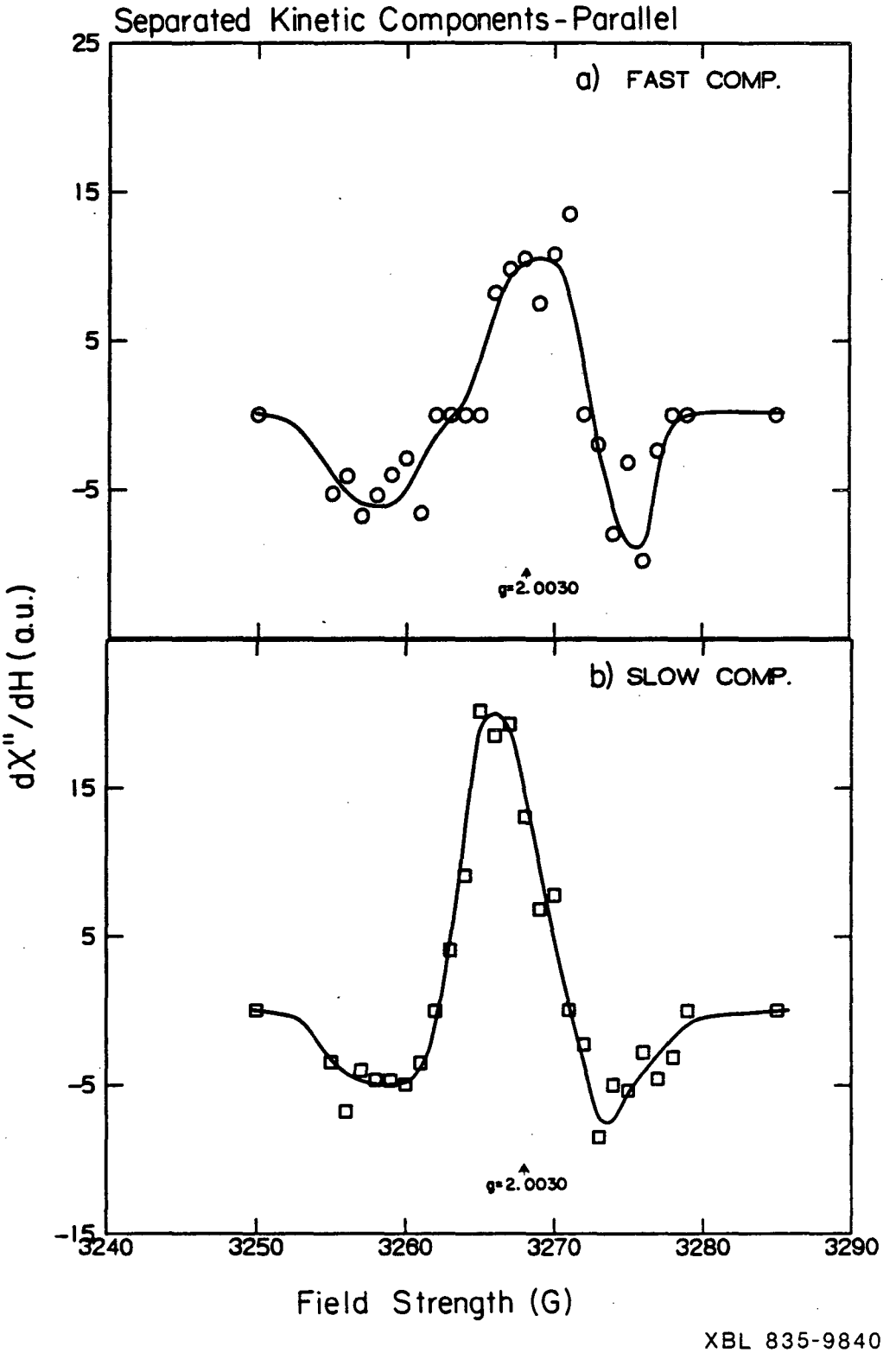
Separated Kinetic Components - Parallel
a) FAST COMP.
b) SLOW COMP.
g=2.0030
g=2.0030
dχ''/dH (a.u.)
Field Strength (G)
25
15
5
-5
15
5
-5
-15
3240
3250
3260
3270
3280
3290

XBL 835-9840

Fig. 5-6. A plot of the slow kinetic component for oriented thylakoids in the perpendicular orientation and prepared as in Fig. 5-1. The conditions for the measurement were: microwave frequency, 9.166 GHz; microwave power, 0.05 mW; sample temperature, 9 K; field modulation frequency, 1 MHz; and modulation amplitude, 2.5 G. Each point is the average of 500 passes.

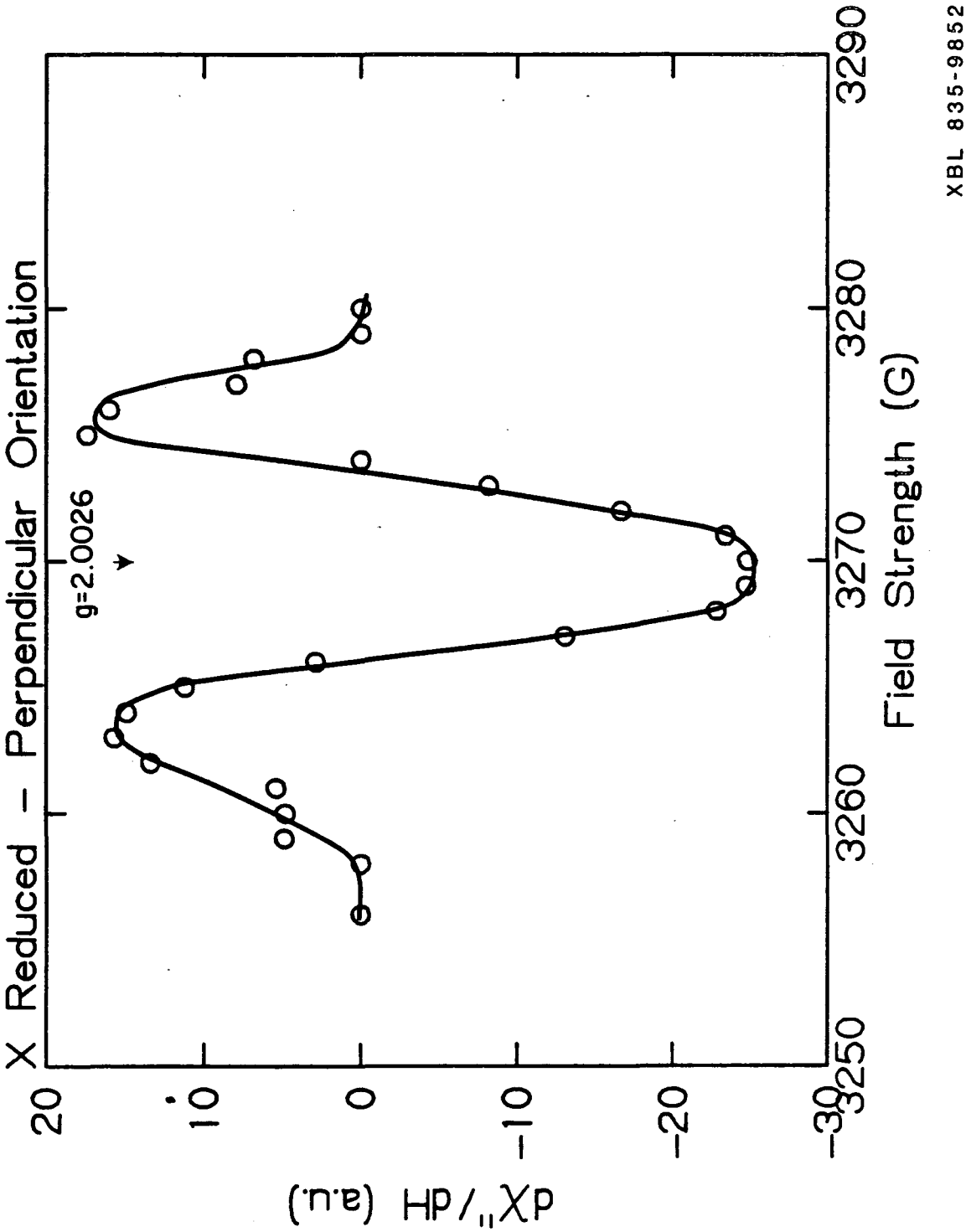
X Reduced – Perpendicular Orientation
g=2.0026
dX''/dH (a.u.)
Field Strength (G)
20
10
0
-10
-20
-30
3250
3260
3270
3280
3290

XBL 835-9852

Fig. 5-7. Field profile of both kinetic components combined for oriented chloroplasts prepared as in Fig. 5-1 and examined in the 45^{o} orientation. Measurement conditions were identical to those of Fig. 5-6.

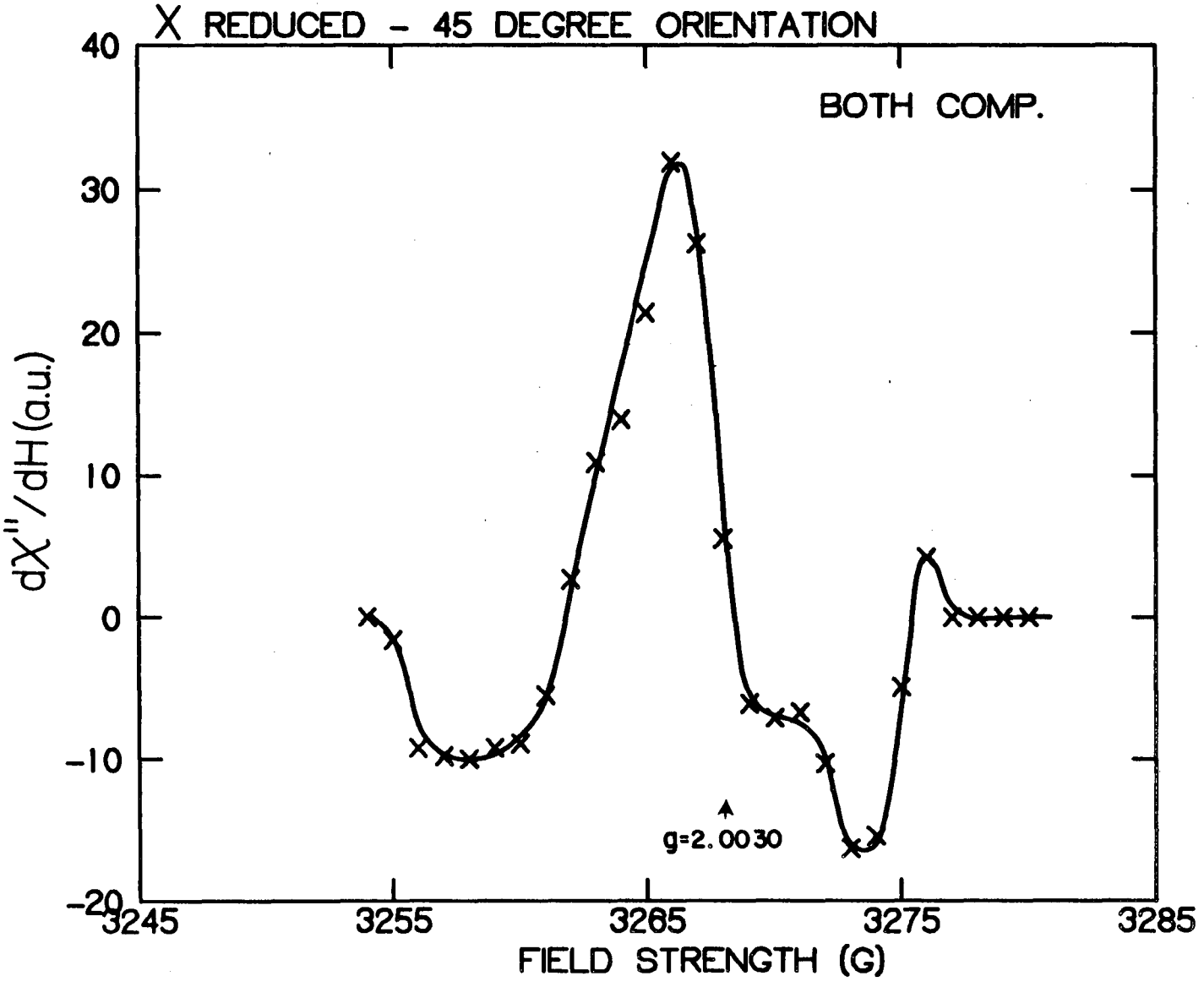
X REDUCED - 45 DEGREE ORIENTATION
BOTH COMP.
40
30
20
10
0
-10
-20
dχ''/dH(a.u.)
3245
3255
3265
3275
3285
FIELD STRENGTH (G)
g=2.0030

XBL 835-9853

Fig. 5-8. The data of Fig. 5-7 plotted for the separate kinetic components. Trace (a) is the field profile of the fast component and trace (b) is the field profile for the slow component.

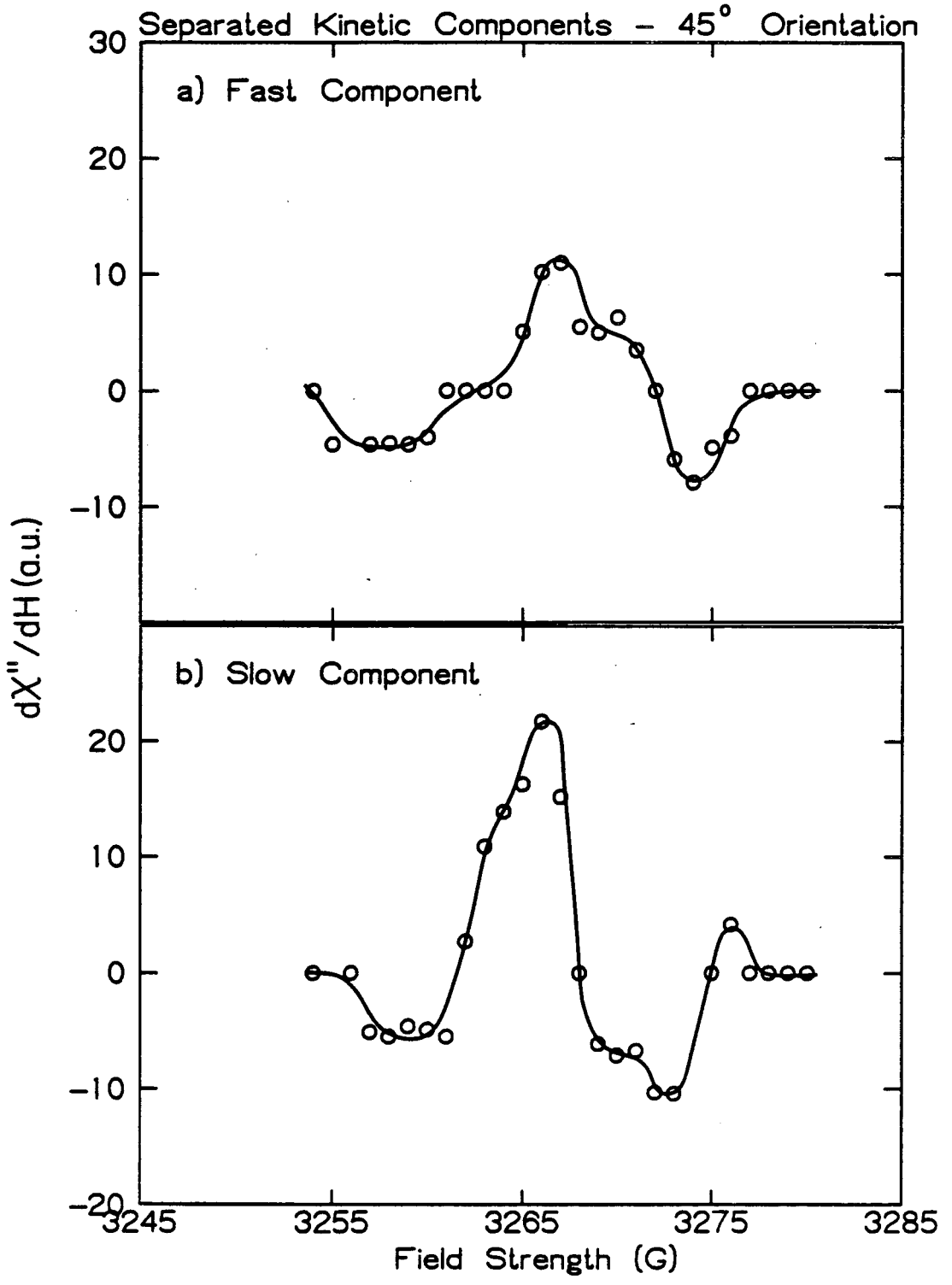
Separated Kinetic Components – 45° Orientation
a) Fast Component
b) Slow Component
dχ''/dH (a.u.)
30
20
10
0
-10
20
10
0
-10
-20
3245
3255
3265
3275
3285
Field Strength (G)

XBL 835-9839

Fig. 5-9. Steady state EPR spectra of oriented thylakoids prepared by treatment with dithionite and illumination while freezing in a 13.5 kG alignment field. Trace (a) is for thylakoids in the parallel orientation and trace (b) is for thylakoids in the perpendicular orientation. The measurement conditions were: microwave frequency, 9.220 GHz; microwave power, 10 mW; modulation frequency, 100 KHz; modulation amplitude, 12.5 G; and sample temperature, 11 K.

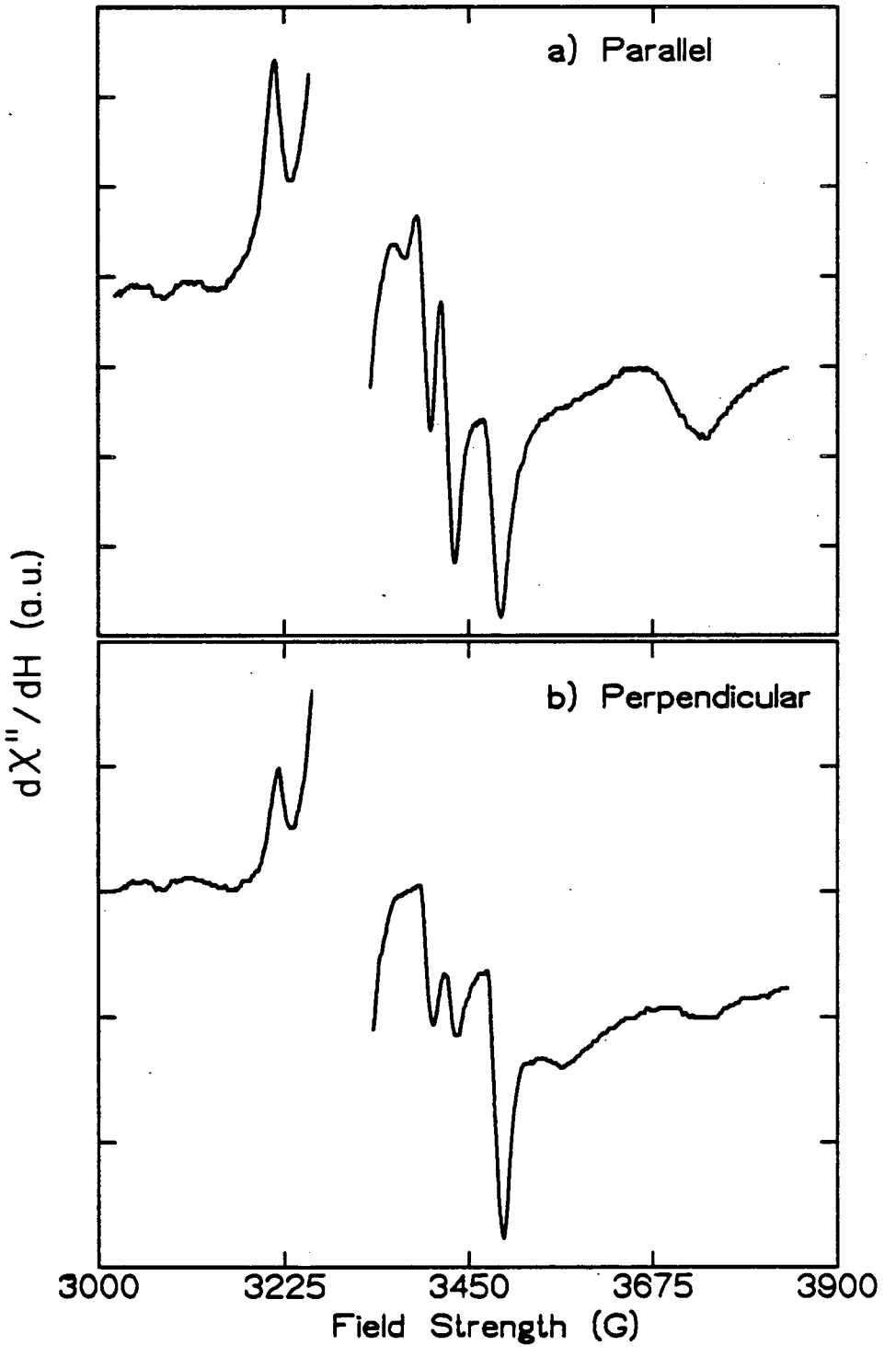
a) Parallel
b) Perpendicular
dχ''/dH (a.u.)
3000
3225
3450
3675
3900
Field Strength (G)

XBL 835-9816

the spectra of the field aligned samples than in the spectra of the samples oriented on mylar.

Samples prepared with dithionite treatment and illumination during freezing gave rise to EPR transient signals in the g 2.0 region that had a lifetime of approximately 5 μsec (Fig. 5-10) at 10-15K and a microwave power of 50 μW. The field profile of this kinetic component obtained using high frequency field modulation is shown in Fig. 5-11. The lineshape is an asymmetric or skewed, emissive-absorptive type which is typical for CIDEP of organic radicals (see chapter 2, Fig. 2-4). The field profiles of this 5 μsec component for oriented thylakoids are shown in Fig. 5-12 (parallel orientation) and Fig. 5-13 (perpendicular orientation). In the parallel orientation (Fig. 5-12) an emissive-absorptive lineshape which is skewed so that the net polarization is absorptive is observed. The intensity of this spin polarized spectrum is centered at g 2.0040. For the perpendicular orientation (Fig. 5-13), an absorptive-emissive pattern skewed towards absorption is observed. The center of intensity of this pattern is at g 2.0026; and, as was found with the samples with X not reduced prior to flash excitation, the intensity at low field is not present. Because the samples studied in this redox state had cylindrical symmetry, the amplitudes of the signals at the different orientations can be compared. Examination of Figs. 5-12 and 5-13 indicates that the intensity of the peaks in the perpendicular orientation is

Fig. 5-10. A kinetic trace for oriented chloroplasts treated with dithionite as in Fig. 5-9. The measurement conditions were: sample orientation, parallel; microwave frequency, 9.219 GHz; microwave power, 0.05 mW; modulation frequency, 1 MHz; modulation amplitude, 2.5 G; sample temperature, 19 K; and field position, 3290 G. This trace represents the average of 500 passes.

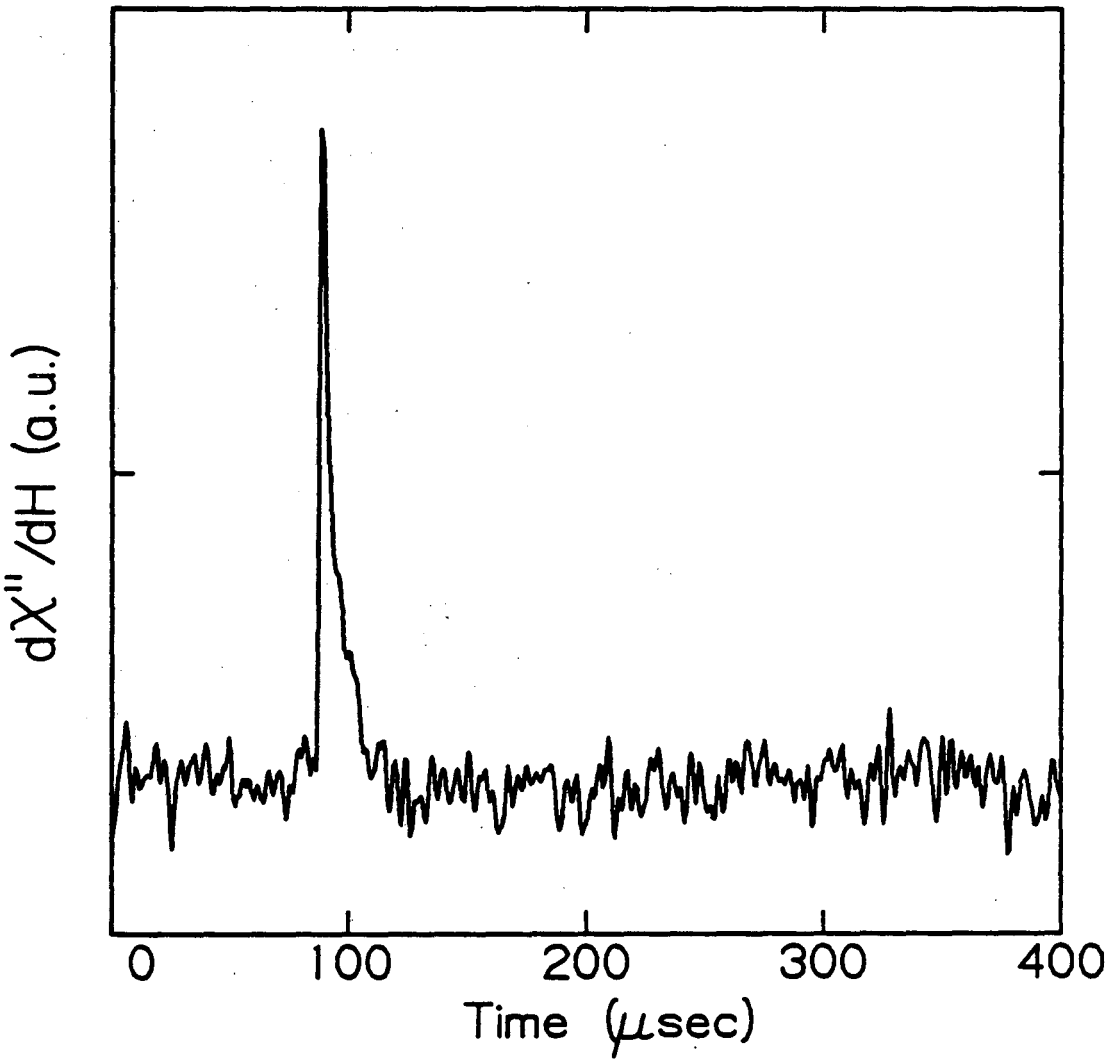

XBL 835-9830

Fig. 5-11. Field profile for the 5 μsec component of a sample of randomly oriented chloroplasts treated with dithionite and illuminated while freezing. The measurement conditions were identical to those of Fig. 5-10 except that the microwave frequency was 9.222 GHz, the temperature was 13 K, and the sample orientation was random.

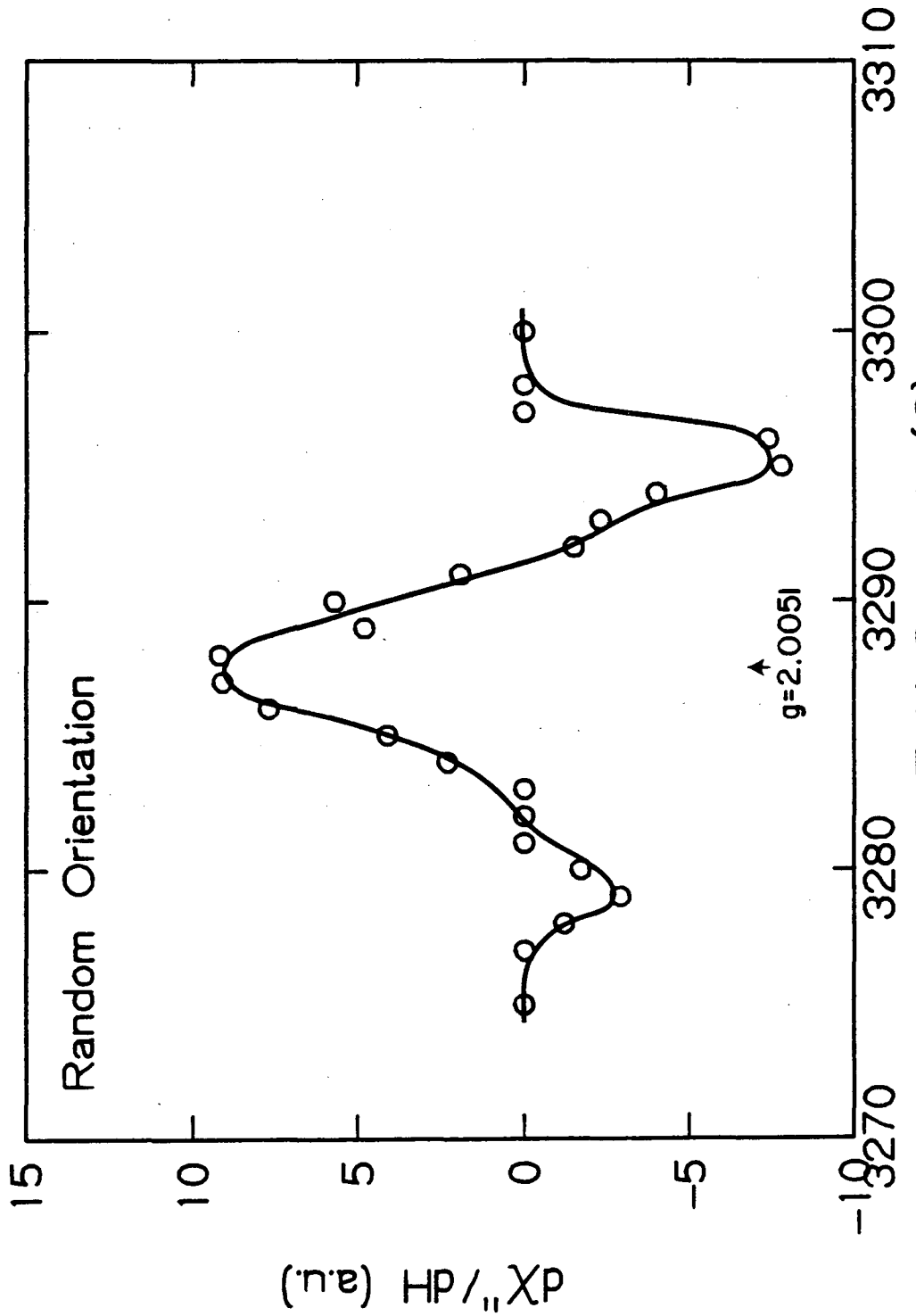
Random Orientation
g=2.0051
Field Strength (G)
dχ''/dH (a.u.)
15
10
5
0
-5
-10
3270
3280
3290
3300
3310

XBL 835-9831

Fig. 5-12. A field profile for oriented thylakoids treated with dithionite and prepared as in Fig. 5-9. The measurement conditions were: sample orientation, parallel; microwave frequency, 9.221 GHz; microwave power, 0.05 mW; modulation frequency, 1 MHz; modulation amplitude, 2.5 G; and sample temperature, 15 K. Each trace is the average of 500 events.

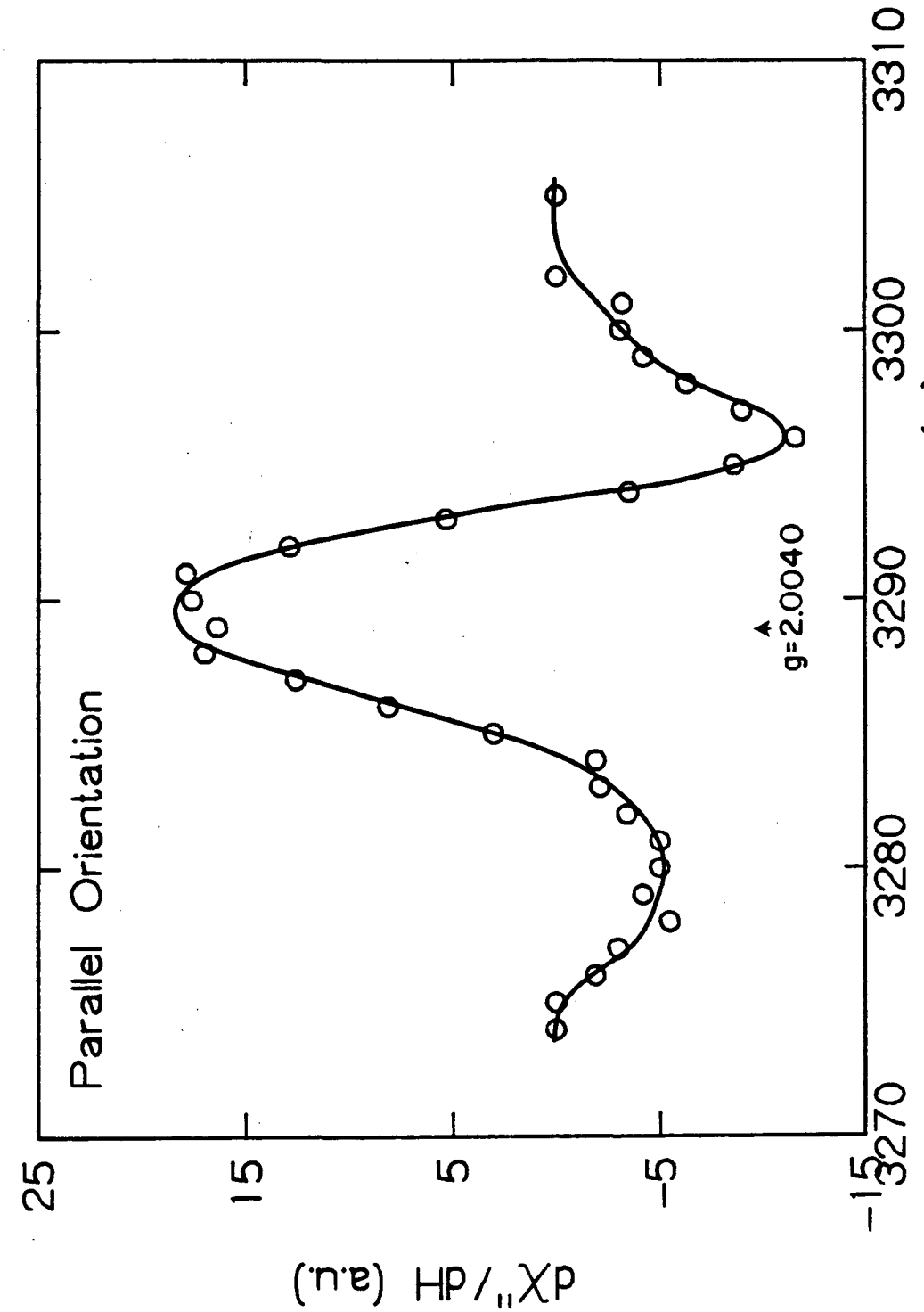
Parallel Orientation
g=2.0040
Field Strength (G)
3270
3280
3290
3300
3310
25
15
5
-5
-15
dχ''/dH (a.u.)

XBL 835-9832

Fig. 5-13. A field profile for oriented chloroplasts treated with dithionite as in Fig. 5-9. The measurement conditions were identical to those of Fig. 5-12 except that the microwave frequency was 9.220 GHz and the sample orientation was perpendicular.

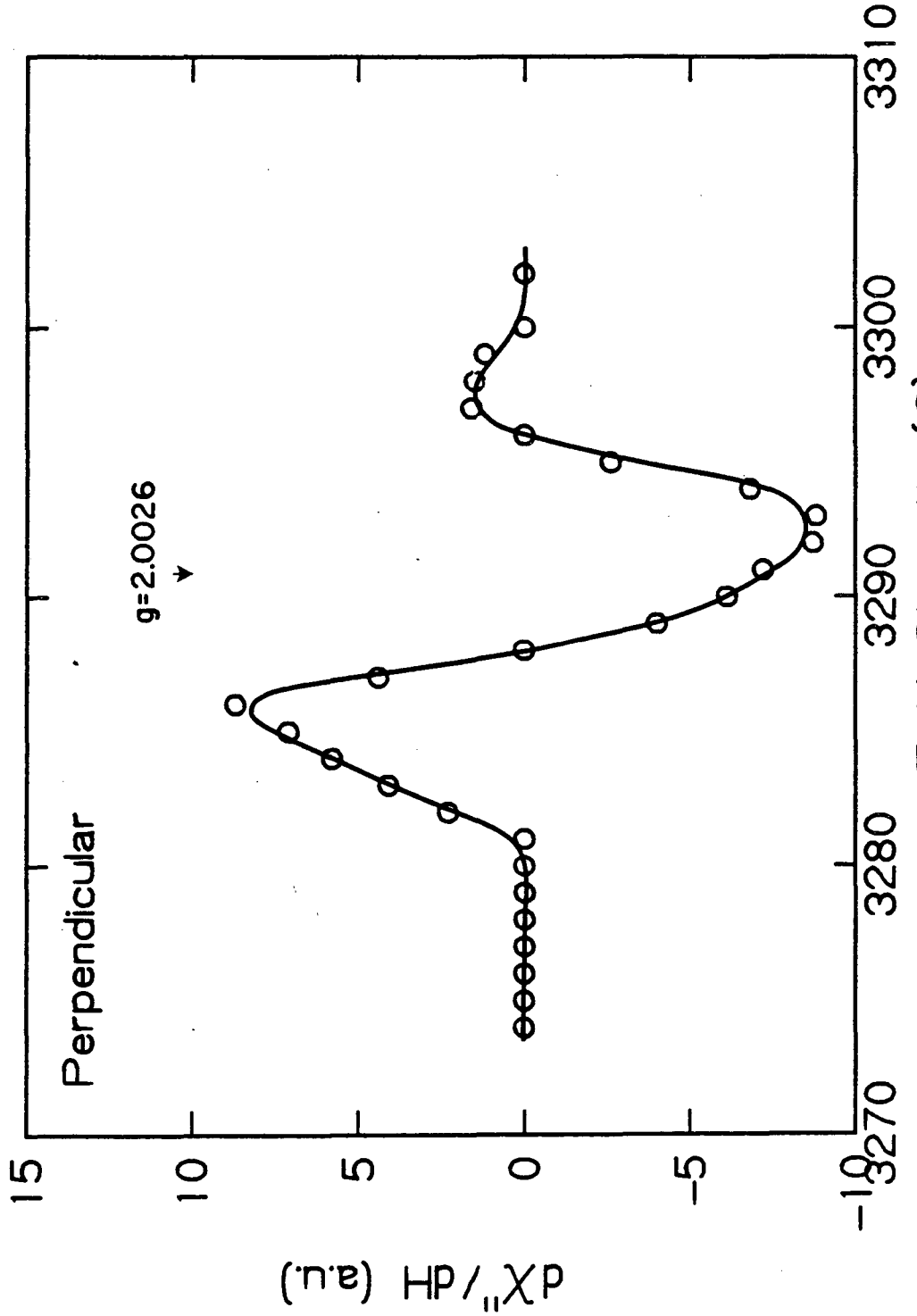
Perpendicular
g=2.0026
15
10
5
0
-5
-10
3270
3280
3290
3300
3310
Field Strength (G)
dχ''/dH (a.u.)

XBL 835-9833

about half of that found in the parallel orientation.

As in the previous chapter, the oriented samples were also examined using direct detection. The results of these measurements are shown in Fig. 5-14. They are in reasonable agreement with the data collected using field modulation (Fig. 5-12 and 5-13) considering that the sensitivity is lower with the direct detection system. Thus, the distortion of the amplitudes of the field-modulated data due to rapid passage is probably minimal.

5.4 Discussion

The data obtained from broken chloroplasts treated with ascorbate and illuminated while freezing probably represents CIDEP signals from PS1 reaction centers poised in two different redox states. One piece of evidence that suggested this was that the slow (30 μsec) component gave rise to spin polarized EPR lineshapes that were identical to those obtained for random and oriented chloroplast samples prepared with X not reduced prior to flash stimulation, while the fast (3 μsec) component gave rise to field profiles that were similar to those obtained in the case where dithionite treatment and illumination during freezing was used. Because the amplitude of the CIDEP signals for samples prepared with dithionite was small in the perpendicular orientation, little fast component was seen in the ascorbate treated samples in this orientation. In addition to these observations, little or no radical pair

triplet due to charge recombination between P-700$^+$ and A_0^- was observed when samples were reduced with ascorbate treatment [9], despite the presence of large EPR signals from X^- (Fig. 5-1). According to the work of Gast, et al. [10] and the analysis of chapter 4, radical-pair triplet signals on P-700 are expected only from reaction centers where A_1 is reduced prior to illumination, so that the reaction sequence is:

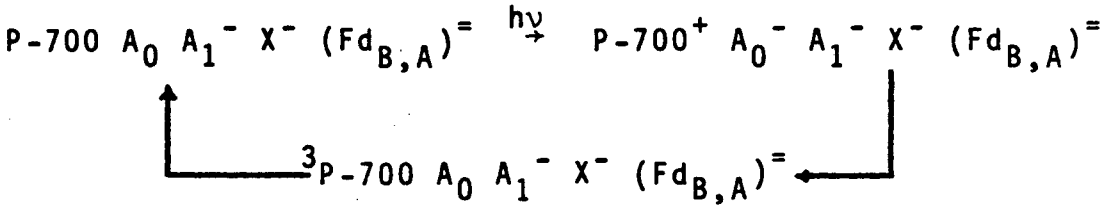

Therefore, treatment with ascorbate and illumination while freezing probably poises PS1 in a mixture of two redox states: P-700 A_0 A_1^- X^- $(Fd_{B,A})^=$; and P-700 A_0 A_1 X^- $(Fd_{B,A})^=$. The relatively small amplitude of radical pair polarized triplet from P-700 in these samples compared to that obtained if treatment with dithionite and illumination during freezing is used [11,12] indicates that the latter state, P-700 A_0 A_1 X^- $(Fd_{B,A})^=$, was prevalent.

In contrast to ascorbate treatment, treatment of broken spinach chloroplasts with dithionite and illumination during freezing poises the PS1 reaction center in a redox state where the dominant photochemistry at 10K involves formation of the spin-polarized ^{3}P-700 species [11-13]. This redox configuration according to the model presented in chapter 4

will be P-700 A_0 A_1^- X^- $(Fd_{B,A})^=$. The reaction sequence by which the P-700 triplet species is generated is given above. Under these conditions, the radical pair $P\text{-}700^+A_0^-$, which is responsible for the development of spin polarization in PS1, will decay to form ^{3}P-700 A_0. The triplet P-700 species will not contribute significantly to the observed spin polarization of Figs. 5-10 through 5-14, because this signal is small in the g 2.0 region and has a lifetime (1/e time) of nearly 1 msec [14]. There is some evidence that the $P\text{-}700^+$ A_0^- radical pair decays too quickly to be the species observed in our experiments. Setif, et al. [14] report that the risetime of the P-700 triplet (detected optically) is < 1 μsec. Sonneveld, et al. [15] studying luminescence in PS1 particles prepared using Triton X-100 attributed a signal which had a lifetime of 200 nsec at 77K to the decay of the $P\text{-}700^+A^-$ radical pair. Their assignment of this luminescence phase was strengthened by the observations that its amplitude was altered in the presence of small magnetic fields and that it was observed only under strongly reducing conditions (dithionite and background illumination). In light of these findings, it is probable that the signals observed in the measurements of Figs. 5-11 through 5-14 are due to spin polarization that develops on A_1^- due to spin-spin interactions with polarized A_0^-. The mechanism of this development is identical to that described qualitatively in the introduction to this chapter [1-3] and will be examined in more detail below.

The spectrum shown in Fig. 5-11 from randomly oriented chloroplasts poised at a low potential with dithionite treatment and illumination while freezing, has been reported previously [16]. The experimental apparatus used to collect those data was inferior to that used in the study presented above in two ways: the sensitivity was not high enough to detect an appreciable orientation dependence; and the uncertainty in g-values measured from the experiments was high, ± .0010. Because the signals were not orientation dependent, the 'static' polarization theory of chapter 2 was used to analyze the data. The analysis was based on the assumption that only polarized P-700$^+$ was being observed and that the signal from the primary electron acceptor was broadened by interactions with X^- to the extent that it was not observable in the experiments. From Fig. 5-11, one finds that the g-values of the low, middle, and high field peaks are 2.0102, 2.0051, and 2.0004, respectively. The splitting between the low and high field peaks of the derivative spectrum is 16 G and the ratio of the low field peak amplitude to that at high field is about 1:2.5. Attempts at simulating this signal (Fig. 5-11) using the theory of chapter two, a g-value of 2.0026 for P-700$^+$ and a linewidth of 8 G were made. In these simulations, the g-value of A_0^- was adjusted to give the predicted P-700$^+$ polarized EPR spectrum the proper asymmetry. The result of this calculation is shown in Fig. 5-15. This simulation shows that although the general features of the lineshape can be

simulated, the g-values and peak splittings are considerably different from those obtained experimentally. These findings support the idea that the observed CIDEP under these conditions can not be from P-700$^+$ alone.

Further evidence that the CIDEP signals of Fig. 5-11 through 5-14 are due to A_1^- concerns the structure and position of the low field lobe in the random spectrum and the behavior of this low field component as a function of orientation. Examination of the random spectrum of Fig. 5-11 shows that the low field lobe is centered at g 2.0102 (±.0010) and that there is a 'leveling off' or shoulder in the signal between the low field and the middle lobes of the spectrum. The shoulder was very reproducible. The simulation of the CIDEP spectrum for randomly oriented chloroplasts where X was not reduced prior to flash excitation of the sample (Fig. 4-12) shows that the low field lobe of this spectrum is centered at g 2.0107 and that there is disagreement between experiment and simulation at the field positions between the low field lobe and the rise of the adjacent positive lobe. Fig. 4-12 also indicates that the low field lobe of the spectrum is entirely due to A_1^- in this model. It is possible that the shoulder observed experimentally in Fig. 5-11 represents a structural feature of the lineshape of A_1^- and that this feature may account for the discrepancy between experiment and theory shown in Fig. 4-12 and mentioned above.

Another piece of evidence that supports the idea that

Fig. 5-15. An attempt at simulating the random spectrum of Fig. 5-11 using the one-site isotropic exchange model given in chapter 2 and assuming that the signal was due to P-700$^+$. The simulation parameters were: g-value of P-700$^+$, 2.0026; P-700$^+$ linewidth, 8 G; J, -9.5G; g-value of A_0^-, 2.0029; and microwave frequency, 9.222 GHz.

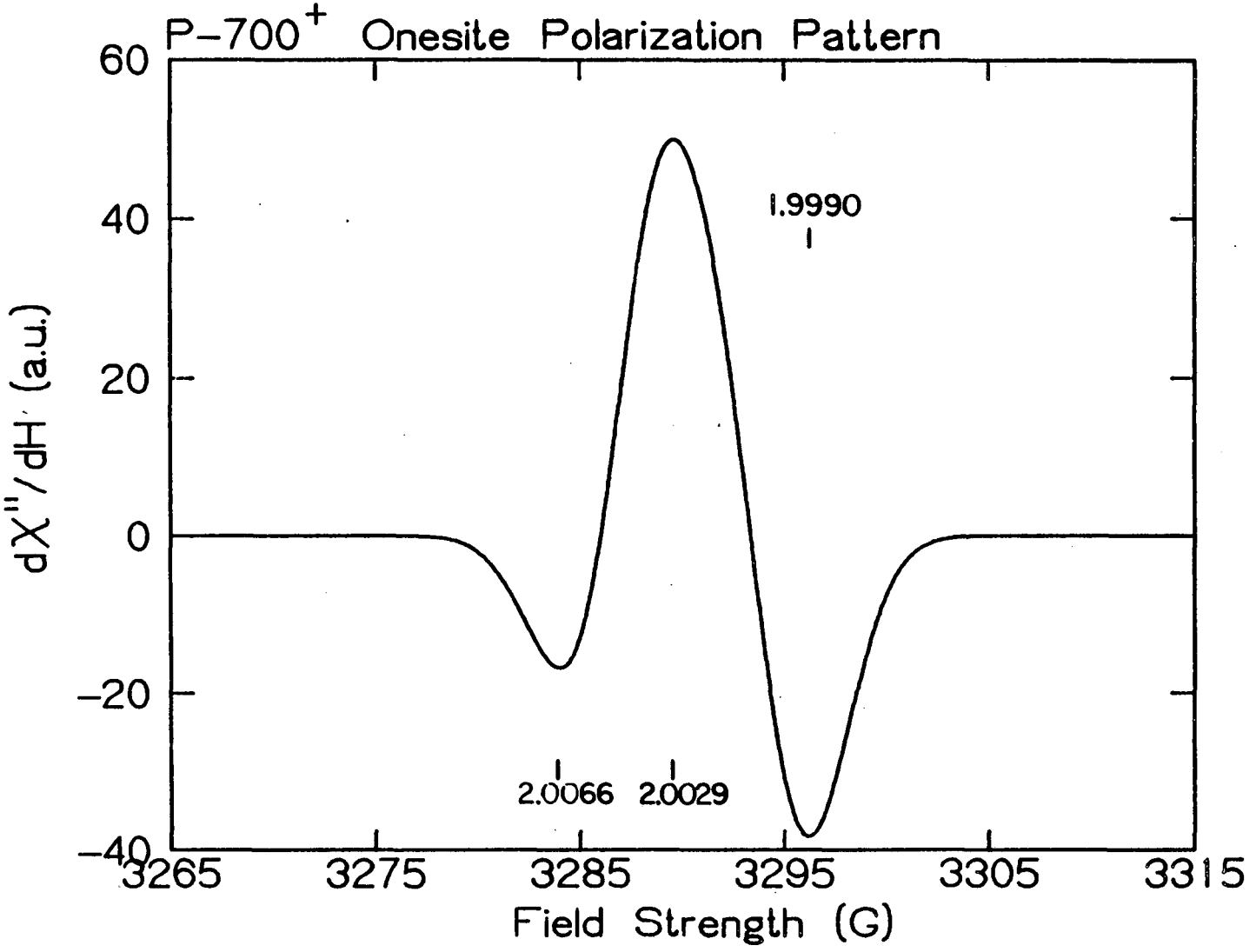
P–700+ Onesite Polarization Pattern
60
40
20
0
–20
–40
dχ''/dH (a.u.)
1.9990
2.0066
2.0029
3265
3275
3285
3295
3305
3315
Field Strength (G)

XBL 835-9834

the CIDEP signals of Figs. 5-11 through 5-14 are due to polarization transfer to A_1^- is that the low field lobe of the spectrum is prominent in the parallel orientation, but not present in the perpendicular orientation (see Figs. 5-12 and 5-13). This observation is consistent with what was thought about the contributions of the A_1^- spectrum to the CIDEP data collected in the X not reduced case presented in chapter 4. In chapter 4, it was concluded that either the spectrum of A_1^- was not spin polarized in the perpendicular case (because the g-value of A_0^- was equal to that of P-700$^+$ in this orientation) or that an anisotropic property of A_1^- caused the intensity at low field to vanish in the perpendicular orientation. If this second idea is correct, one could parameterize the lineshape of A_1^- in the perpendicular orientation using the spectrum of Fig. 5-13 and then use the parameters to repeat the simulation presented in Fig. 4-15b.

Before parameterizing the lineshape of Fig. 5-13, a brief description of the lineshape analysis and the development of spin polarization on A_1^- when the species is reduced prior to light excitation of the sample should be given. The mechanism of development of spin polarization on A_1^- is expected to be quite different from the case where it is polarized by an electron transfer reaction as described in chapter 4. Pedersen's mechanism [17] describes a situation where polarization is transferred to a radical that was formed from an electron transfer reaction with a

spin-polarized radical. In this case only 'net effect' type spin-polarized lineshapes are possible. The spectra, obtained when A_1 is reduced prior to flash excitation, that are being attributed to polarized A_1^- (Figs 5-11 through 5-14) develop polarization as a result of a completely different set of interactions. What occurs in this redox state is that the light flash generates the primary radical ion pair, P-700$^+A_0^-$, on which the spin polarization develops via the radical pair mechanism. Spin polarization on A_1^- develops from spin-spin interactions with polarized A_0^-. Thus, there are two separate, static radical-pair interactions occurring simultaneously; that between P-700$^+$ and A_0^-, and that between A_0^- and A_1^-. Because of these interactions, the polarization that develops on A_1^- while the P-700$^+A_0^-$ radical pair exists, could have characteristics of a static polarization pattern. There is some experimental evidence that supports this idea in the literature [3].

Parameterization of the spectral properties of A_1^- in a particular orientation involves analysis of the lineshape to determine a g-value and a peak-to-peak, first derivative linewidth of the species in that orientation. This is a "zero order" parameterization and is all that can really be done until the quantum mechanics of the problem described above is worked out in detail. The goal of this procedure is to determine if these properties of A_1^- can account for the gross features of the spin polarized EPR spectrum obtained

in the perpendicular orientation for the X not reduced case (Figs. 4-4 and 4-15b). This would relieve the constraint that the g-value of A_0^- must equal that of P-700$^+$ in this orientation. The parameterization is done using the static polarization model of chapter 2 and determining what g-value and linewidth are needed to give rise to the peak positions and relative peak amplitudes of the spectrum of Fig. 5-13. The results of this procedure are that the effective g-value of A_1^- in the perpendicular orientation is 2.0026 and the peak-to-peak, first derivative linewidth is approximately 8 G.

In chapter 4, it was stated that one way in which the constraint that the g-tensor of A_0^- be anisotropic could be lifted was if the EPR spectrum of A_1^- lies on top of that due to P-700$^+$ in the perpendicular orientation. If one uses the above A_1^- parameters in the orientational averaging procedure described in chapter 4, the CIDEP spectrum for the perpendicular orientation of Fig. 4-15b can be simulated satisfactorily (Fig. 5-16). This simulation is performed with the g-value of A_0^- set at 2.0031; the same value used in the random, parallel and 45^o orientation spectra simulations shown in Figs. 4-12, 4-15a and 4-15c, respectively. Therefore, if the interpretation of the data presented in this chapter is correct, the model by which CIDEP develops in PS1 when Fe-S centers A and B are reduced is as follows.

Fig. 5-16. Simulation of the CIDEP spectrum of Fig. 4-4 using the parameters for A_1^- in the perpendicular orientation obtained from the data of Fig. 5-13. The points represent the data obtained in this orientation with X not reduced, and the line is the simulation. The simulation conditions were: g-value of $P\text{-}700^+$, 2.0026; $P\text{-}700^+$ linewidth, 8 G; g-value of A_0^-, 2.0031; g-value of A_1^-, 2.0026; linewidth of A_1^-, 8 G; J, -9.5G; D, -50G; E, 0G; theta, 90^o; phi, 10^o; mosaic spread, 20^o; and microwave frequency, 9.143 GHz.

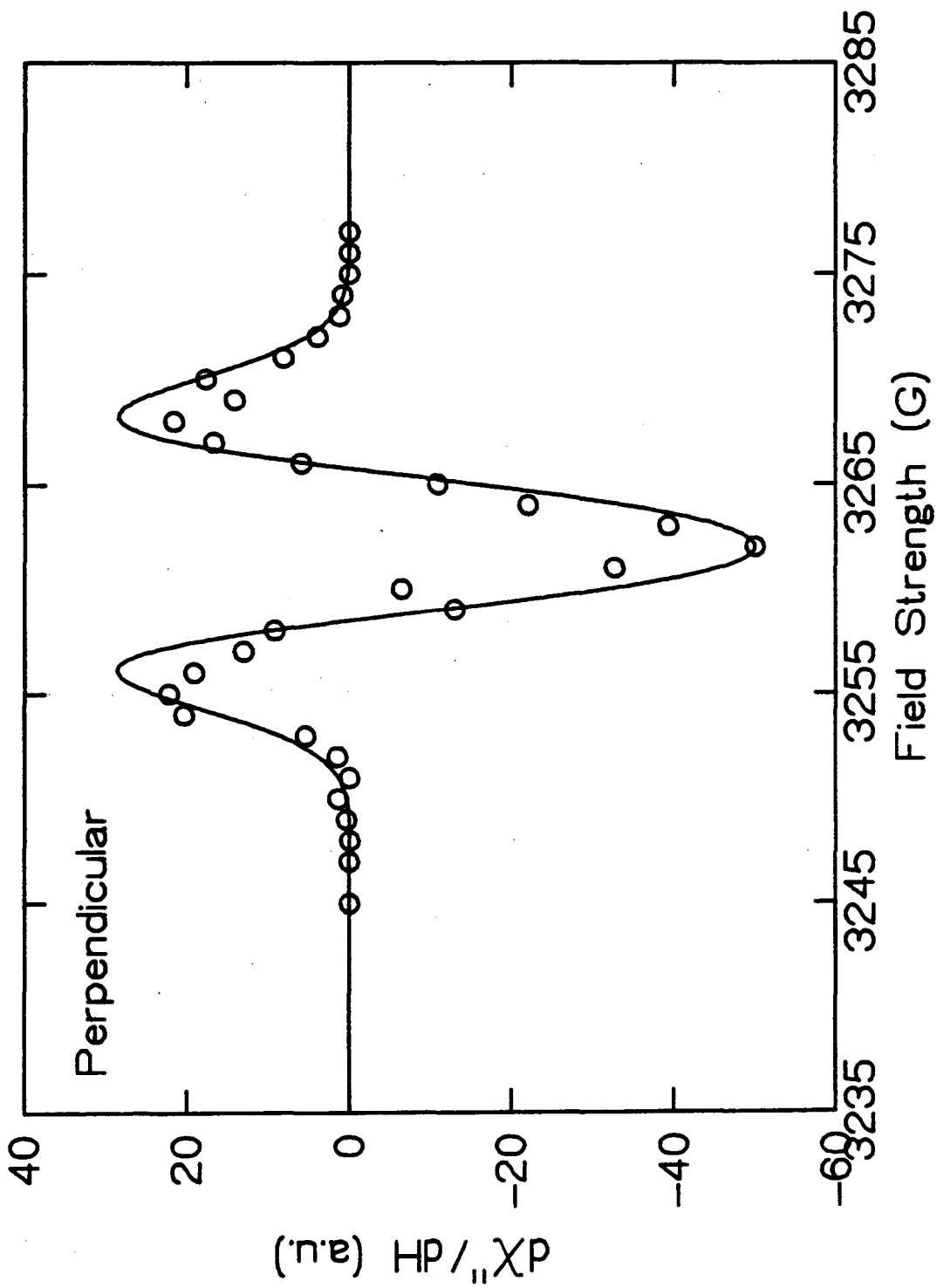
Perpendicular
dχ''/dH (a.u.)
40
20
0
-20
-40
-60
3235
3245
3255
3265
3275
3285
Field Strength (G)

XBL 835-9835

1. The light flash generates the radical pair, P-700$^{+}A_0^{-}$. Spin polarization develops on these radicals via a static radical pair mechanism where the spin-spin interaction can be modeled with an electron-electron magnetic dipole interaction and an isotropic exchange interaction.

2. The g-value of A_0^{-} is $2.0031 \pm .0003$ and is isotropic.

3. A_1 is a secondary electron acceptor that is dynamically polarized due to electron transfer from statically polarized A_0^{-} (when it is not reduced prior to application of the actinic flash). The lineshape of A_1^{-} is complex and gives rise to some of the structure seen in the spectra of oriented thylakoids.

4. In the random and parallel orientations, A_1^{-} can be modeled using a structureless gaussian lineshape centered at $2.0054 \pm .0010$ having a peak-to-peak, first derivative linewidth of 8-10.5 G. In the 45^{o} and perpendicular orientations, this parameterization of A_1^{-} is no longer very good, and in the perpendicular orientation a g-value of 2.0026 and a linewidth of 8 G provides a better description of the radical.

A final point about the orientation dependence of the CIDEP signals from chloroplasts that are redox poised by dithionite treatment and illuminated while freezing is that

the net polarization transferred to A_1^- is also orientation dependent. This is expected because the amount of spin polarization that develops on A_0^- will be orientation dependent due to the dipolar coupling interaction. In addition, the spin-spin coupling between A_0^- and A_1^- that drives the polarization transfer may be orientation dependent.

REFERENCES

1. Gast, P. and Hoff, A.J. (1979) Biochim. Biophys. Acta 548, 520-535.
2. Hoff, A.J. and Gast, P. (1979) J. Phys. Chem. 83, 3355-3358.
3. Gast, P., Mushlin, R.A. and Hoff, A.J. (1982) J. Phys. Chem. 86, 2886-2891.
4. Kaufmann, K.J., Dutton, P.L., Netzel, T.L., Leigh, J.S. and Rentzepis, P.M. (1975) Science 188, 1301-1304.
5. Rockley, M.G., Windsor, M.W., Cogdell, J.R. and Parson, W.W. (1975) Proc. Natl. Acad. Sci. USA 72, 2251-2255.
6. Gast, P. and Hoff, A.J. (1978) FEBS Lett. 85, 183-188.
7. Dismukes, G.C. and Sauer, K. (1978) Biochim. Biophys. Acta 504, 431-445.
8. Evans, M.C.W., Sihra, C.K. and Cammack, R. (1976) Biochem. J. 158, 71-77.
9. This effect has also been observed by S. Tabbutt, Univ. of California, Berkeley (private communication).
10. Gast, P., Swarthoff, T., Ebskamp, F.C.R. and Hoff, A.J. (1983) Biochim. Biophys. Acta 722, 163-175.
11. Frank, H.A., McLean, M.B. and Sauer, K. (1979) Proc. Natl. Acad. Sci. USA 76, 5124-5128.

12. McLean, M.B. and Sauer, K. (1982) Biochim. Biophys. Acta 679, 384-392.
13. Blackwell, M.F., "Electron Paramagnetic Resonance Studies of Triplet States in Photosystem 1 of Chloroplasts," Ph.D. Thesis, University of California, Berkeley, 1982, Lawrence Berkeley Laboratory Report LBL-15012.
14. Setif, P., Quaegebeur, J.P. and Mathis, P. (1982) Biochim. Biophys. Acta 681, 345-353.
15. Sonneveld, A., Duysens, L.N.M. and Moerdijk, A. (1981) Biochim. Biophys. Acta 636, 39-49.
16. McCracken, J.L., Frank, H.A. and Sauer, K. (1982) Biochim. Biophys. Acta 679, 156-168.
17. Pedersen, J.B. (1979) FEBS Lett. 97, 305-310.

CHAPTER 6

THE EFFECTS OF MAGNETIC FIELD MODULATION ON THE DYNAMICS OF CIDEP SIGNALS FOR INHOMOGENEOUSLY BROADENED LINES

6.1 Introduction

In general, there are three processes which may contribute to the dynamics of spin-polarized EPR signals. These processes are: decay of the polarization due to spin relaxation; decay of the polarization due to stimulated emission or absorption because the microwave field is resonant with the spin system during the time of observation; and decay of the EPR intensity due to chemical decay of the radical species being observed. Mathematical treatments of these processes have been reported by several investigators interested in analyzing time-resolved EPR data to extract spin-lattice and spin-spin relaxation times (T_1 and T_2, respectively) and in separating these processes from the chemical decay process. Atkins, et al. [1] ignored chemical decay and used transient solutions to the Bloch equations to determine T_1 and T_2 for benzophenone ketyl radical in liquid paraffin at different viscosities. Hore and McLauchlan [2] and Pedersen [3] incorporated chemical decay dynamics into a modified set of Bloch equations; in the former case, the results were used to interpret the

dynamics of CIDEP signals from the durosemiquinone radical [4].

The experimental work of Atkins, et al. [1] and Hore and McLauchlan [4] differed from that presented in chapters 4 and 5 of this thesis in that the chemical systems they studied were such that the experiments could be done without the use of magnetic field modulation. In contrast, the work on photosynthetic systems, presented above, required the use of high frequency field modulation to achieve adequate sensitivity for obtaining both amplitude and dynamical information. Incorporation of magnetic field modulation into the Bloch equations increases the difficulty of the determination of the transient solutions and was left out of the above analyses [1-3]. However, transient solutions to the Bloch equations under the conditions of magnetic field modulation have been obtained by Pasimeni [5]. Unfortunately, these solutions were derived assuming that the resonance condition was always satisfied exactly. This condition is:

$$\gamma H_0 = \omega_0 \qquad (6\text{-}1)$$

where $\gamma H_0 = \omega$ is the frequency of the probing microwave field and ω_0 is the Larmor frequency of the spin packet of interest. In most biological systems, Eqn. 6-1 is rarely satisfied because the EPR signals under investigation are inhomogeneously broadened by hyperfine interactions to the extent that individual spectral transitions are unresolved.

However, Pasimeni did determine that magnetic field modulation could substantially affect the dynamics of time-resolved EPR data for homogeneously broadened lines.

In light of Pasimeni's result, it was desirable to determine whether useful information concerning the spin relaxation times of the radicals giving rise to CIDEP signals in photosynthetic systems (chapters 4 and 5) could be obtained. To accomplish this task, the effects of magnetic field modulation on the dynamics of CIDEP signals for inhomogeneously broadened lines had to be determined. The analysis given below uses a numerical procedure for finding transient solutions to the Bloch equations which are modified to include the effects of magnetic field modulation. The solutions will be examined to determine the effects on both the dynamics of the transient EPR signals and their amplitudes under non-adiabatic rapid passage conditions that have not been described analytically.

6.2 Solution of the Bloch Equations

The Bloch equations in the rotating frame for a homogeneous ensemble of spin-1/2 systems can be written as:

$$\begin{aligned} dS_x/dt &= -S_x/T_2 + [\delta+(\gamma B_m \cos\omega_m t)/2]\cdot S_y \\ dS_y/dt &= -S_y/T_2 - [\delta+(\gamma B_m \cos\omega_m t)/2]\cdot S_x + \mu S_z \\ dS_z/dt &= -(S_z-S_0)/T_1 - \mu S_y \quad . \end{aligned} \tag{6-2}$$

Where T_2 is the spin-spin relaxation time; T_1 is the

longitudnal or spin-lattice relaxation time; $\delta=\omega_0-\omega$ is the displacement or frequency offset of the packet from resonance; $\gamma=g_e\beta$ is the gyromagnetic ratio of the paramagnetic species; B_m is the modulation field amplitude; ω_m is the modulation frequency; $\omega_0=\gamma H_0$ is the resonant frequency of the spin packet at Zeeman field strength H_0, ω is the frequency of the microwave field; $\mu=(\gamma H_1)/2$, where H_1 is the amplitude of the microwave magnetic field; and S_0 is the equilibrium z magnetization. Letting $H_m = (\gamma B_m)/2$ and rewriting Eqn. 6-2 as a matrix equation one finds:

$$d\underset{\sim}{S}/dt = [\underset{\approx}{A}_0 + \underset{\approx}{A}_1\cos\omega_m t]\cdot\underset{\sim}{S} + \underset{\sim}{\Gamma} \qquad (6\text{-}3)$$

where

$$\underset{\approx}{A}_0 = \begin{bmatrix} -1/T_2 & \delta & 0 \\ -\delta & -1/T_2 & \mu \\ 0 & -\mu & -1/T_1 \end{bmatrix} ,$$

$$\underset{\approx}{A}_1 = \begin{bmatrix} 0 & H_m & 0 \\ -H_m & 0 & 0 \\ 0 & 0 & 0 \end{bmatrix}$$

and

$$\Gamma = \begin{bmatrix} 0 \\ 0 \\ S_0/T_1 \end{bmatrix} .$$

This matrix equation is an inhomogeneous system of linear differential equations with periodic coefficients. It has a single, particular steady-state solution $\underset{\sim}{P}$, and three linearly independent transient solutions that go to zero as t goes to zero because of the real, negative diagonal elements of $\underset{\approx}{A}_0$. In this case, one is interested in describing experimental situations where the spin polarization is significantly larger than the steady-state solution and where the magnetization is being sampled at times short in comparison to the time required to attain thermal equilibrium. Thus, only the homogeneous portion of Eqn. 6-3 need be considered. For short times, one can write:

$$\underset{\sim}{S}(t) = \sum_{i=1}^{3} c_i \underset{\sim}{I}_i(t) \qquad (6\text{-}4)$$

where

$$d\underset{\sim}{I}_i/dt = [\underset{\approx}{A}_0 + \underset{\approx}{A}_1 \cos\omega_m t]\cdot\underset{\sim}{I}_i \quad . \qquad (6\text{-}5)$$

One can define a matrix, $\underset{\approx}{M}(t)$, such that

$$\underset{\approx}{M}(t) = \underset{\approx}{A}_0 + \underset{\approx}{A}_1 \cos\omega_m t \quad . \qquad (6\text{-}6)$$

$\underset{\approx}{M}(t)$ will be periodic in time, so that

$$\underset{\approx}{M}(t) = \underset{\approx}{M}(t+2\pi/\omega_m) \qquad (6\text{-}7)$$

where $2\pi/\omega_m$ is the period of oscillation. A theorem due to Floquet [6,7] states that the solutions to Eqn. 6-5 must have the form

$$\underset{\sim}{I}_i(t) = e^{-\alpha_i t}\underset{\sim}{Y}_i(t) \tag{6-8}$$

where $e^{-\alpha_i t}$ is a scalar function, α_i is a complex constant, and $\underset{\sim}{Y}_i(t)$ is periodic, with period $2\pi/\omega_m$.

One can expand the $\underset{\sim}{Y}_i(t)$ in a Fourier series of field modulation harmonics and obtain

$$\underset{\sim}{I}_j(t) = e^{-\alpha_j t}\sum_{k=-\infty}^{\infty}\underset{\sim}{Q}_k e^{i\omega_m k t} \tag{6-9}$$

where the vector Q_k is given by

$$\underset{\sim}{Q}_k = \begin{bmatrix} Q_k{}^x \\ Q_k{}^y \\ Q_k{}^z \end{bmatrix} . \tag{6-10}$$

The $\underset{\sim}{Q}_k$ represent the coefficients of the k^{th} field modulation harmonic. Substituting Eqns. 6-9 and 6-10 into Eqn. 6-5 and operating on both sides with

$$\int_0^{2\pi/\omega_m} e^{i\omega_m k' t}\,dt$$

yields an infinite set of coupled equations for the elements of $\underset{\sim}{Q}_k$:

$$-\alpha Q_{k'}{}^x + i\omega_m k' Q_{k'}{}^x = -Q_{k'}{}^x/T_2 + \delta Q_{k'}{}^y + H_m(Q^y{}_{k'+1} + Q^y{}_{k'-1})$$

$$-\alpha Q_{k'}{}^y + i\omega_m k' Q_{k'}{}^y = -Q_{k'}{}^y/T_2 - [\delta Q_{k'}{}^x + H_m(Q^x{}_{k'+1} + Q^x{}_{k'-1})] + \mu Q_{k'}{}^z$$

$$-\alpha Q_{k'}{}^z + i\omega_m k' Q_{k'}{}^z = -Q_{k'}{}^z/T_1 - \mu Q_{k'}{}^y \quad . \tag{6-11}$$

Eqn. 6-11 can be written in matrix form and yields:

$$\underset{\approx}{\alpha}\,\underset{\sim}{Z} = \underset{\approx}{U}\underset{\sim}{Z} \qquad (6\text{-}12)$$

where

$$\underset{\sim}{Z} = \begin{bmatrix} \vdots \\ Q_{-1}{}^{x} \\ Q_{-1}{}^{y} \\ Q_{-1}{}^{z} \\ Q_{0}{}^{x} \\ Q_{0}{}^{y} \\ Q_{0}{}^{z} \\ Q_{+1}{}^{x} \\ Q_{+1}{}^{y} \\ Q_{+1}{}^{z} \\ \vdots \end{bmatrix}$$

and

$$\underset{\approx}{U} = \begin{bmatrix} \ddots & & & & & & \\ & V_{-1} & W & & 0 & & \\ & W & V_{0} & W & & & \\ & & W & V_{+1} & W & & \\ & 0 & & W & \ddots & & \\ & & & & & \ddots & \end{bmatrix}.$$

The matrix $\underset{\approx}{U}$ in Eqn. 6-12 is a supermatrix whose elements are the 3x3 matrices:

$$\underset{\approx}{V}_k = -\underset{\approx}{A}_0 + i\omega_m k \underset{\approx}{I} \quad (\underset{\approx}{I} \text{ is the identity})$$
$$\underset{\approx}{W} = -\underset{\approx}{A}_1$$

Eqn. 6-12 has the form of an infinite dimension eigenvalue equation and can be solved approximately by using a limited set of Fourier harmonics. Eqn. 6-9 should be rewritten as

$$\underset{\sim}{I}_j(t) = e^{-\alpha_j t} \sum_{k=-N}^{N} \underset{\sim}{Q}_k e^{i\omega_m k t} \quad . \tag{6-13}$$

The $\underset{\sim}{I}_j(t)$ can be determined by setting up the matrix $\underset{\approx}{U}$, of Eqn. 6-12; diagonalizing it; and using the eigenvectors and corresponding eigenvalues to determine the approximate $\underset{\sim}{Q}_k$ and α_j, respectively. In the limit as N goes to infinity, only three solutions will be linearly independent. The remainder of the 3N eigenvectors, Z_j, can be written as combinations of the form

$$\underset{\sim}{Z}_j' = \sum_j c_j \underset{\sim}{Z}_j e^{-\alpha_j} e^{im\omega_m} \tag{6-14}$$

where m is an arbitrary integer.

Using the above results to determine experimentally observed quantities requires the specification of definite experimental conditions. The situation applicable to the experiments described in this thesis is one where radical pairs are produced by a delta function laser pulse, and the observed signal is averaged over several laser flashes. For a given flash, the instantaneous phase of the modulation field, ϕ, can assume any value. The signal averaging process

will average over ϕ in addition to other shot-to-shot fluctuations. The transient solution of interest is related to the output of the phase sensitive detection system used in a modulation experiment by a response function, $R(\delta,\phi)$. This response function is defined as an integral over a solution $S_y(\delta,\phi,t)$ of a modified form of Eqn. 6-5,

$$d\underset{\sim}{S}(\delta,\phi,t)/dt = [\underset{\approx}{A}_0+\underset{\approx}{A}_1\cos(\omega_m t+\phi)]\cdot\underset{\sim}{S}(\delta,\phi,t) \qquad (6\text{-}15)$$

where

$$\underset{\sim}{S} = [S_x(\delta,\phi,t),S_y(\delta,\phi,t),S_z(\delta,\phi,t)]$$

satisfies the initial conditions

$$\begin{aligned} S_x(\delta,\phi,0) &= 0 \\ S_y(\delta,\phi,0) &= 0 \\ S_z(\delta,\phi,0) &= \sigma_0(\delta) \quad . \end{aligned} \qquad (6\text{-}16)$$

The spin polarization is incorporated into the analysis using Eqn. 6-16. $\sigma_0(\delta)$ is the polarization of the spin packet of interest at frequency $\omega_0=\omega-\delta$ at t=0.

An additional assumption that will be made in characterizing the above equations is that recovery of the EPR signal is accomplished by phase sensitive detection of the first Fourier harmonic in the absorption mode. The phase angle between the transient signal and the field modulation reference signal to the lock-in amplifier is taken to be 0^o. The response function will be given by

$$R(\delta,\phi) = \int_0^{\tau_c} S_y(\delta,\phi,t)\cos\omega_m t \, dt \qquad (6\text{-}17)$$

where τ_c is the time constant of the lock-in amplifier. If relaxation processes are such that the spin polarization has decayed by time τ_c, then $R(\delta,\phi)$ will correspond to a transient "spike" in a plot of the instrument response versus time. The calculation of observed signal amplitude in a given time interval can be obtained by replacing the limits of integration in Eqn. 6-17 with the appropriate values. This will be useful in relating the transient solutions to experimentally observed kinetic traces. One should also note that higher order harmonics can be examined by replacing $\cos\omega_m t$ in Eqn. 6-17 by $\cos n\omega_m t$ where $n=1,2,3,\ldots$ denotes the harmonic desired. Also, dispersion or various mixtures of absorption and dispersion signals can be examined by selecting the appropriate component(s) of the transverse magnetization in the integrand of Eqn. 6-17 and by introducing a phase angle in the cosine function.

The determination of $S(\delta,\phi,t)$ is achieved by replacing the supermatrix, $\underset{\approx}{U}$ of Eqn. 6-12 with a new matrix, $\underset{\approx}{U}(\phi)$ in which the shot-to-shot fluctuations in the modulation field strength are taken into account. $\underset{\approx}{U}(\phi)$ is given by

$$\underset{\approx}{U}(\phi) = \begin{bmatrix} \underset{\approx}{V}_{-k} & \underset{\approx}{W}_{+1} & & & & \\ \underset{\approx}{W}_{-1} & \underset{\approx}{V}_{-k+1} & \ddots & & 0 & \\ & \ddots & \ddots & \ddots & & \\ & & \ddots & \underset{\approx}{V}_{0} & \ddots & \\ & 0 & & \ddots & \ddots & \underset{\approx}{W}_{+1} \\ & & & & \underset{\approx}{W}_{-1} & \underset{\approx}{V}_{k} \end{bmatrix} \qquad (6\text{-}18)$$

where

$$\underset{\approx}{V}_k = \underset{\approx}{V}_k$$
$$\underset{\approx}{W}_1 = -\underset{\approx}{A}_1 e^{i\phi}$$
$$\underset{\approx}{W}_{-1} = -\underset{\approx}{A}_1 e^{-i\phi}$$

The signal averaged response of a spin packet at displacement δ from resonance is then

$$\bar{R}(\delta) = \int_0^{2\pi} R(\delta, \phi)\, d\phi \quad . \qquad (6\text{-}19)$$

In appendix C it will be shown that $\bar{R}(\delta)$ is antisymmetric, i.e. $\bar{R}(-\delta) = -\bar{R}(\delta)$.

The amplitude of the observed transient signal at a fixed Zeeman field strength, H_0, is an ensemble average over the distribution of resonant frequencies. This average can be written as an ensemble average over a distribution of frequency offsets at a particular H_0 and is given by

$$I(H_0) = \int_{-\infty}^{\infty} \bar{R}(\delta)\, g(\omega - \delta)\, P(\omega - \delta)\, d\delta \qquad (6\text{-}20)$$

where $g(\omega-\delta)$ is the distribution of moments in the resonance line (the lineshape function) and $P(\omega-\delta)$ is the spin polarization at $\omega-\delta$ and t=0. For calculations, the integral of Eqn. 6-20 is replaced by a discrete sum

$$I(H_0) = \sum_{i=1}^{N} \bar{R}(\delta_i)\,[h(\omega-\delta_i)+h(\omega+\delta_i)]\cdot\Delta \qquad (6\text{-}21)$$

where the symmetry property of $\bar{R}(\delta)$ about $\delta=0$ has been utilized, $h(\omega-\delta) = g(\omega-\delta)P(\omega-\delta)$, and $\Delta = \delta_{i+1}-\delta_i$.

6.3 The Various Passage Cases - Definitions

As mentioned in the introduction, the treatment of the Bloch equations given above was used in this study to examine the effects of magnetic field modulation on the dynamics and lineshapes of CIDEP signals under various passage conditions. Before discussing the results of this study, a brief definition of these passage cases will be given.

Slow passage refers to cases where the time of passage of the magnetic field strength through the resonance of an individual spin packet is long compared to the packet's spin relaxation time. Thus, the system is in equilibrium at any given moment. The value of the DC (Zeeman) field is given by

$$H(t)=H_0+dH_0(t)/dt+H_m\cos\omega_m t \qquad (6\text{-}22)$$

where $dH_0(t)/dt$ is the Zeeman field sweep rate and the term $H_m\cos\omega_m t$ accounts for the contribution of the modulation field. In our experiments the Zeeman field is held constant

while signal averaging so that $dH_0(t)/dt=0$. The passage, or sweep rate of the DC magnetic field is given by

$$dH/dt = -\omega_m H_m \sin\omega_m t \quad . \tag{6-23}$$

The time of passage through each packet also depends on the magnitude of H_1, the microwave magnetic field. The case of slow passage has been treated by Portis [8] and is characterized by the conditions:

$$1/\gamma H_1 < \sqrt{T_1 T_2} < H_1/(\omega_m H_m) \tag{6-24}$$

Rapid passage describes a condition where the time in which each spin packet is swept through is short compared to the mean relaxation time, $\sqrt{T_1 T_2}$. This passage may be adiabatic, meaning that it is sufficiently slow so that the magnetization vector can follow the effective field ($\underset{\sim}{S}$ is either parallel or antiparallel to $\underset{\sim}{H}-\omega/\gamma+\underset{\sim}{H}_1$); or it can be non-adiabatic, meaning that passage through the packet is too rapid for the spins to be able to follow the effective field. In this case the magnetization vector will remain almost parallel to the DC field direction. The rapid adiabatic condition is described by the relations:

$$\begin{aligned} &\sqrt{T_1 T_2} > H_1/(\omega_m H_m) \\ &1/(\gamma H_1) < H_1/(\omega_m H_m) \\ &\sqrt{T_1 T_2} > (\gamma H_1)^{-1} \quad . \end{aligned} \tag{6-25}$$

Rapid, non-adiabatic passage is described by the relations:

$$\sqrt{T_1T_2} > H_1/(\omega_m H_m)$$
$$(\gamma H_1)^{-1} > H_1/(\omega_m H_m)$$
$$\sqrt{T_1T_2} > (\gamma H_1)^{-1} \quad . \tag{6-26}$$

The case of adiabatic rapid passage has been examined theoretically by Portis [8] and experimentally by Weger [9]. In many cases the result of adiabatic rapid passage is inversion of the absorption signal or the generation of dispersive type signals in phase with the modulation. These effects could easily be misinterpreted and attributed to CIDEP phenomena. Therefore, it is instructive to examine our experimental conditions to determine what the effects of rapid passage could be in the experiments presented above.

The microwave magnetic field, H_1, can be estimated for a TE_{102} cavity that is critically coupled and has the same cross section as the waveguide by the relation

$$\langle H_1^2 \rangle_c = 2 \cdot 10^{-3} \, (Q_L P_w)$$

where P_w is the incident microwave power in watts, and Q_L is the loaded Q of the cavity [10]. For a Q_L of 5000 and an incident microwave power of .05 mW, H_1 = .022G (or .06 MHz). The field modulation frequency was 1 MHz and the value of H_m was 1.25 G. Using these values we find:

$$H_1/(\omega_m H_m) = 0.017 \ \mu\text{sec} \quad \text{and} \quad (\gamma H_1)^{-1} = 16 \ \mu\text{sec}.$$

The "rapid" condition, $\sqrt{T_1T_2} > H_1/(\omega_m H_m)$ is probably always

satisfied at 10K, but the passage will always be non-adiabatic. Eqns. 6-25 and 6-26 point out that rapid passage effects are only operative under saturating conditions. The question to be answered is then:

$$\sqrt{T_1 T_2} \overset{?}{>} 16\ \mu\text{sec} \ . \qquad (6\text{-}27)$$

If the relation of Eqn. 6-27 is satisfied then the conditions of non-adiabatic rapid passage are fulfilled and lineshape distortion may result. Attempts at answering this question were made using both theoretical and experimental approaches.

The experimental approach to the above problem involved two types of measurements. The first experiment was to study the saturation behavior of the amplitudes of the transient signals discussed in chapter 4 and 5 as a function of incident microwave power. It was found that the transient signal amplitudes did not begin to 'level off' or saturate until incident powers of .2 mW were used. This is well above the .05 mW level used in the studies presented above. An interesting feature of this study was that, at approximately 2 mW incident power, the 50 μsec EPR transient signals studied in chapter 4 actually inverted, possibly an indication that rapid passage effects are starting to set in. A problem with these studies is that as the power is increased, the dynamics of the signals become faster. This is due to the effects of stimulated emission and absorption processes which become prominent at higher microwave power

levels. In the case of the rapid transient signals studied in chapter 5, these stimulated processes made the EPR transients almost impossible to detect owing to the time response limitations of the 1 MHz field modulation system. Because these effects will interfere with saturation studies; a second, independent test for rapid passage distortion is required. This second method involved repeating the measurement using direct detection. As stated in chapters 4 and 5, these measurements showed that distortion of the amplitudes of the transient EPR signals due to rapid passage is negligible.

The results of the theoretical approach to examining the effects of non-adiabatic rapid passage on the dynamics and amplitudes of transient EPR signals are given in section 6.4.

6.4 Theoretical Results and Predictions

Computation of the transient magnetization $S(\delta,\phi,t)$ using the procedure outlined in 6.2 requires diagonalization of the supermatrix of Eqn. 6-18. To ensure satisfactory performance of the matrix diagonalization routine, the number of Fourier harmonics utilized in the calculation had to be held at seven. The error in calculations was computed by substituting the solutions $S(\delta, \phi, t)$ back into Eqn. 6-15 and comparing left and right hand sides of the equality. Typical errors in calculating the response function, $\overline{R}(\delta)$, ranged from 3-10%. An increase in error was encountered when

more than seven harmonics were used, owing to limitations of the matrix diagonalization routine. When fewer than five harmonics are considered, proper convergence of the solutions is no longer assured.

As expected, the effect of magnetic field modulation on the transient magnetization is to impose oscillations. This effect is shown in Fig. 6-1. When the frequency offset, δ, is zero; the second order harmonic dominates $S_y(t)$. The amplitude of the odd harmonics are enhanced as δ moves away from zero. Higher order ($n > 2$) harmonics become significant when H_m becomes large. The periodicity of these oscillations is controlled by the field modulation frequency; and the phase angle, ϕ, used to average the shot-to-shot fluctuations in the values of H_m, affects both the amplitude and phase of $S_y(t)$. Also, the oscillations imposed by magnetic field modulation are not observable for short spin-spin relaxation times.

In a time-resolved EPR experiment utilizing magnetic field modulation, the relation between the transient magnetization discussed above and the signal averaged output of the phase sensitive detector is given by

$$R(\delta,t) = \int_0^{2\pi} \int_{t-\tau_c/2}^{t+\tau_c/2} S_y(\delta,\phi,t')\cos\omega_m t' dt' d\phi \quad . \quad (6\text{-}28)$$

Eqn. 6-28 assumes that the in-phase absorptive component of the magnetization is being observed, and that sufficient signal averaging has occured to average the spectrometer response over the instantaneous value of H_m.

Fig. 6-1. $S_y(t)$ calculated using frequency offsets of 0, 1, and 2 MHz. Conditions for these simulations were T_1=10 μsec, T_2=1 μsec, μ =0.05 MHz, H_m=2.0 MHz, ω_m=1 MHz. The phase angle of H_m as described in Eqn. 6-18 was 360^o.

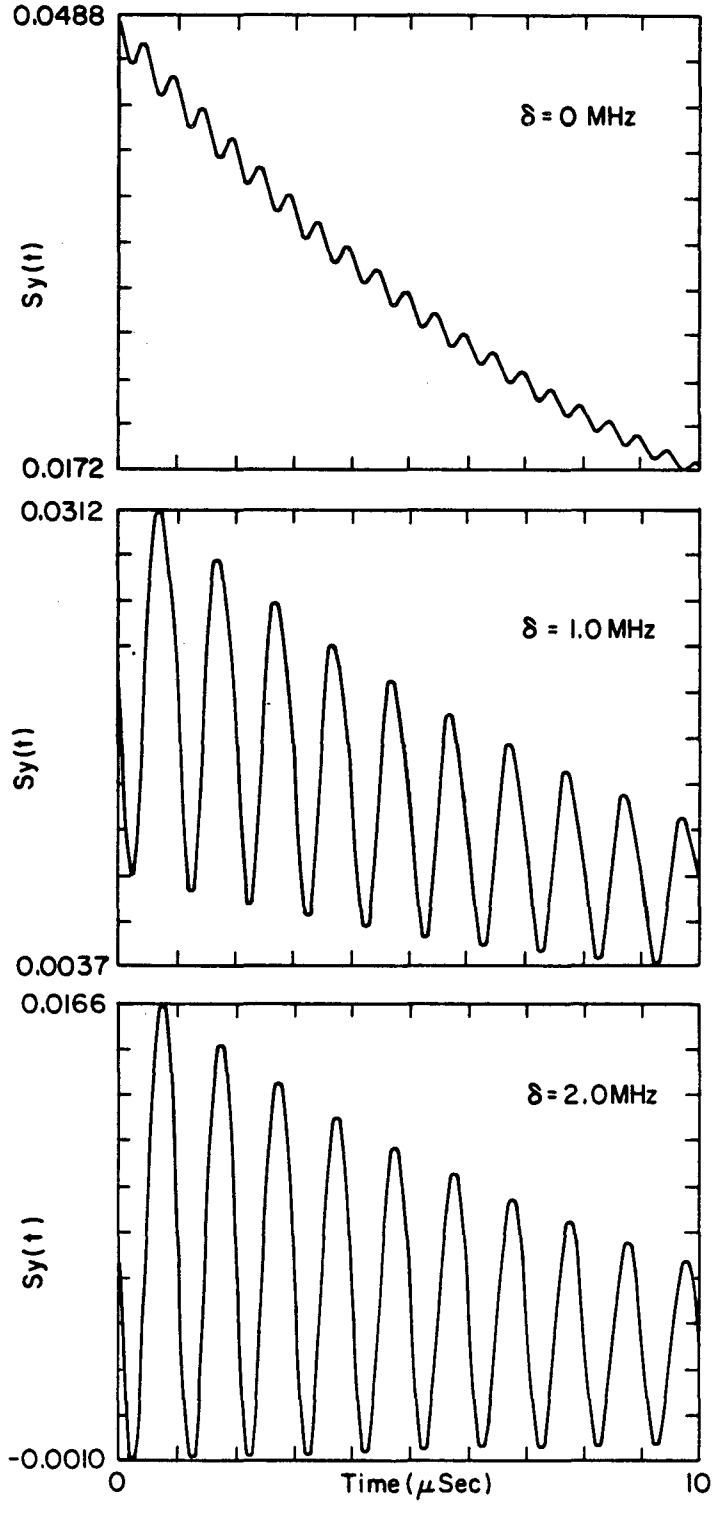
0.0488
δ = 0 MHz
Sy(t)
0.0172
0.0312
δ = 1.0 MHz
Sy(t)
0.0037
0.0166
δ = 2.0 MHz
Sy(t)
-0.0010
0
Time (μSec)
10

XBL 809-4343

Fig. 6-2. The signal averaged spectrometer response as a function of time for various values of H_1 and H_m. The fixed parameters for these calculations were T_1=10 μsec, T_2=1 μsec, ω_m=1.0 MHz, and δ=1.0 MHz. An instrument time constant of 2 μsec was utilized. The varied parameters were: (a)μ=0.05 MHz, H_m=0.01 MHz; (b) μ=0.5 MHz, H_m=0.1 MHz; (c) μ=0.5 MHz, H_m=6.0 MHz; and (d)μ=0.5 MHz, H_m=10.0 MHz.

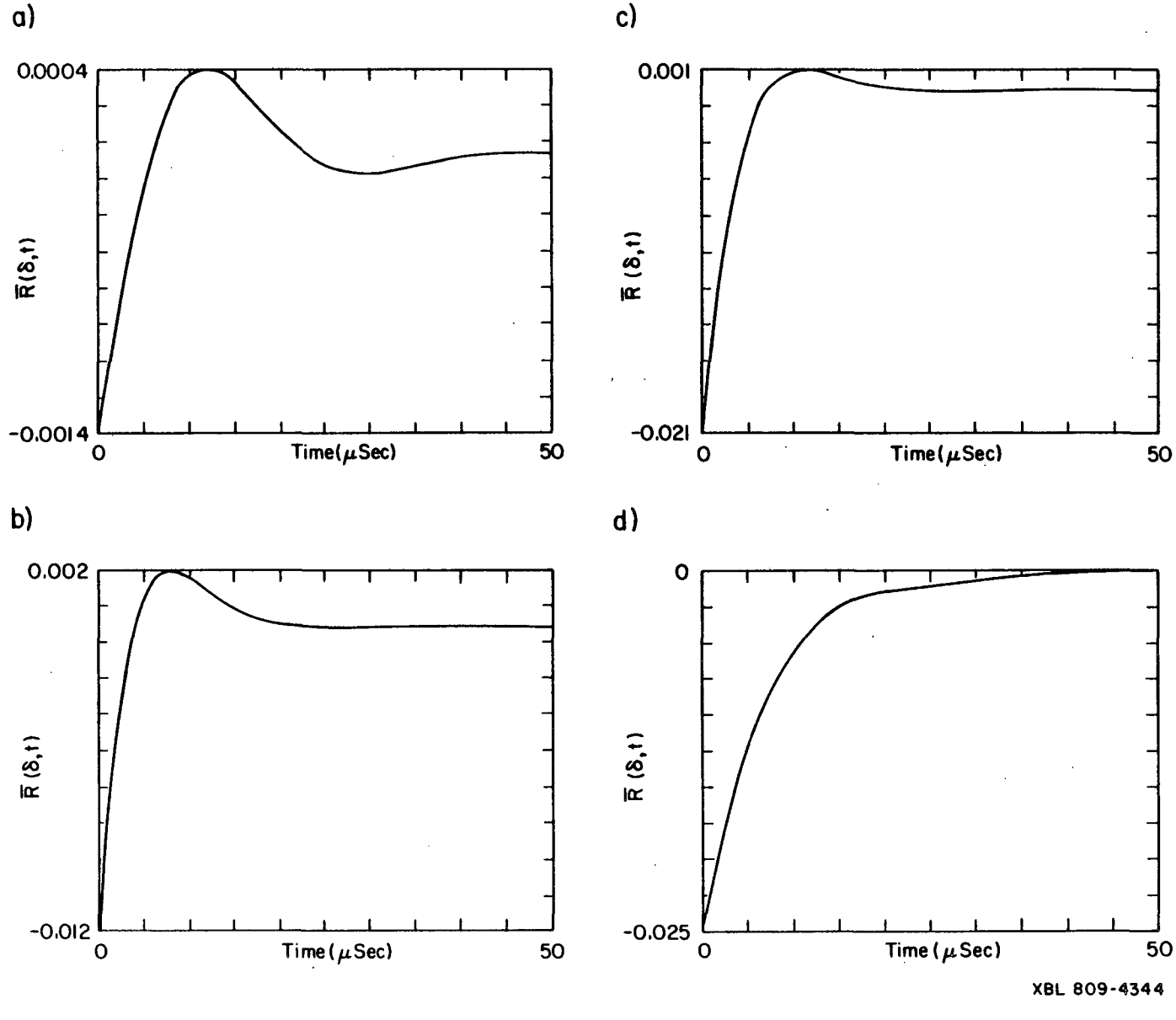
a)
0.0004
-0.0014
$\bar{R}(\delta,t)$
0
Time(μSec)
50
c)
0.001
-0.021
$\bar{R}(\delta,t)$
0
Time(μSec)
50
b)
0.002
-0.012
$\bar{R}(\delta,t)$
0
Time(μSec)
50
d)
0
-0.025
$\bar{R}(\delta,t)$
0
Time(μSec)
50
XBL 809-4344

Figure 6-2 shows the signal averaged response as a function of time for various conditions. In this figure the relaxation times, modulation frequency, frequency offset from resonance, and time constant are fixed; and H_1 and H_m are varied. In Fig. 6-2a the slow passage condition is satisfied and the resulting EPR transient is an oscillating function which has damped out in about 40 μsec. When μ is increased to 0.5 MHz (Fig. 6-2b), the decay of the transient magnetization is enhanced, as expected. When the modulation amplitude is increased (Figs. 6-2c,d), and the non-adiabatic rapid passage condition is fulfilled (Eqn. 6-26), the oscillation of the transient response ceases and the decays become biexponential. Further, as the passage goes from the moderate to the extreme rapid non-adiabatic case, the lifetime of the faster decay component lengthens, but the overall amplitude of the response does not change greatly. This result is significant, because the conditions of rapid, non-adiabatic passage are often difficult to avoid when doing time-resolved EPR work with an instrument that employs high frequency field modulation, as pointed out in 6.3. The onset of non-adiabatic rapid passage may affect the dynamics of the transient EPR signal without altering the amplitude appreciably.

The effects of various intermediate rapid passage conditions on the EPR lineshape can be examined by averaging the result of Eqn. 6-17 over ϕ according to Eqn. 6-19 and convoluting the response function for a range of δ's over a

distribution of resonant frequencies using Eqn. 6-21. The behavior of $\bar{R}(\delta)$ as a function of spin relaxation times, field modulation amplitudes, and microwave field strengths under slow passage conditions is as one might expect. As T_1 and T_2 are decreased, the response function broadens. Increasing the field modulation amplitude also serves to broaden the response. As H_m is increased the broadening observed after convolution of $\bar{R}(\delta)$ with a gaussian distribution of resonant frequencies is in agreement with that predicted in [10]. Response functions and resulting gaussian lineshapes under various non-adiabatic rapid passage conditions are plotted in Fig. 6-3. Under rapid passage conditions, the response function is either opposite in sign to that obtained in slow passage cases or has both positive and negative components. The latter case gives rise to mixed absorptive-emissive patterns (Figs. 6-3c,d) and the former case results in emissive lineshapes.

6.5 Conclusions

The results of the work presented in this chapter point out the complications involved in attempting to analyze the dynamics of spin polarized EPR signals obtained using magnetic field modulation. Certain passage cases that have little effect on the amplitudes of these signals may significantly alter the signal decay characteristics. The obvious solution to this dilemma is to collect the data using direct detection of resonance. In many systems this

Fig. 6-3(a-c). Plots of $\bar{R}(\delta)$ and corresponding Gaussian convolutions for various passage conditions. In all cases $\bar{R}(\delta)$ was convoluted with a Gaussian of 20 MHz half width (peak-to-peak). The parameters for each simulation are: (a) T_1=10 μsec, T_2=1 μsec, H_m=1 MHz, μ=1 MHz, ω_m=100 kHz, time constant=20 μsec; (b) T_1=10 μsec, T_2=3 μsec, H_m=2.0 MHz, μ=0.05 MHz, ω_m=1 MHz, time constant=20 μsec; and (c) T_1=10 μsec, T_2=1 μsec, H_m=0.5 MHz, μ=0.5 MHz, ω_m=1 MHz, time constant=2 μsec.

a) slow passage

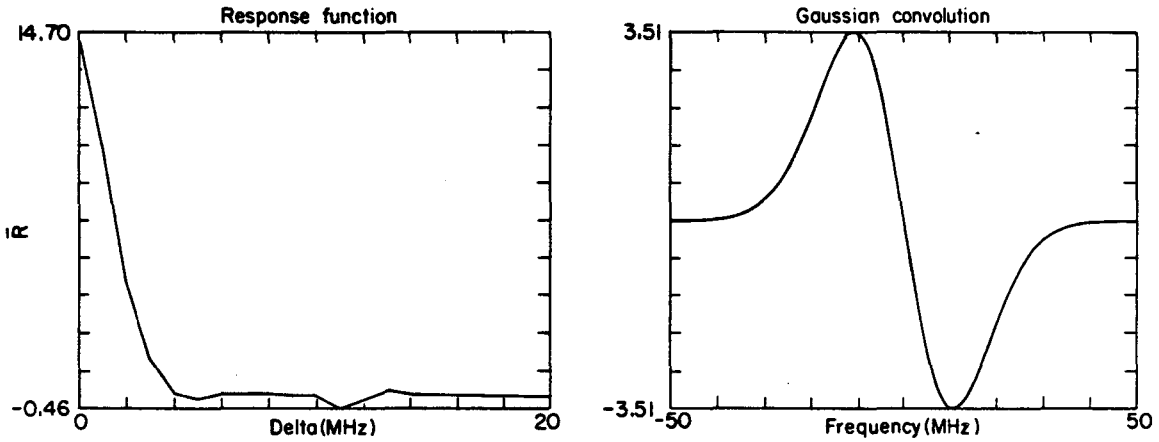

b) rapid passage, γH_1 not saturating

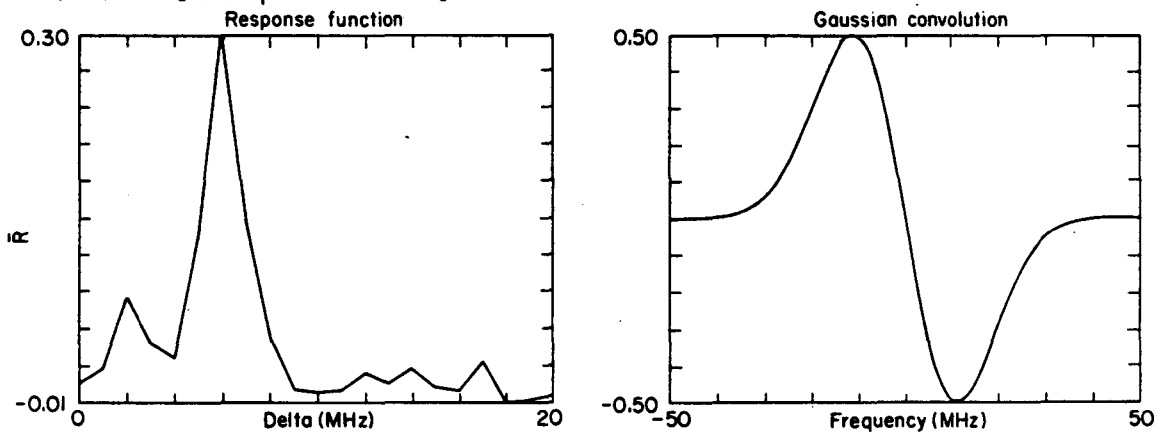

c) nonadiabatic rapid passage (moderate)

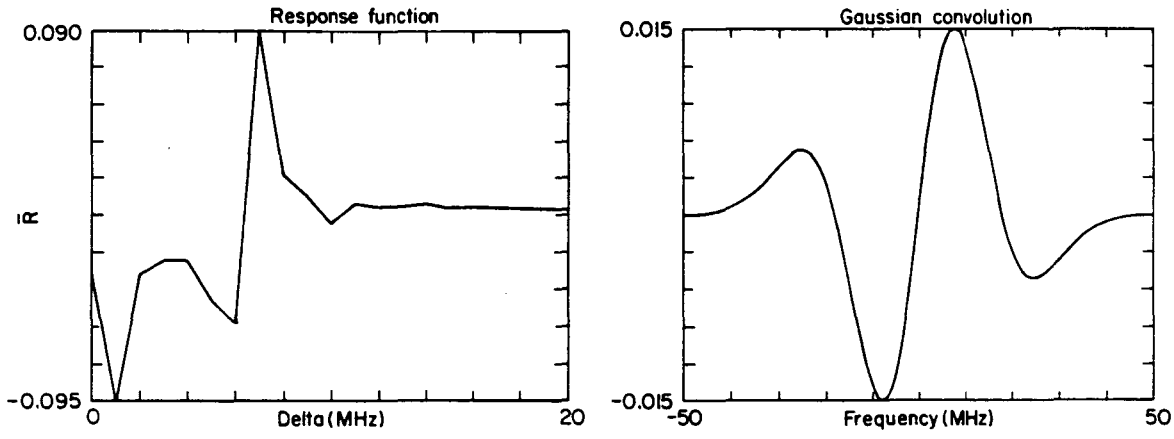

XBL 809-4341

Fig. 6-3(d-f). The parameters for each simulation are: (d) T_1=10 μsec, T_2=3 μsec, H_m=6.0 MHz, μ=1.0 MHz, ω_m=1 MHz, time constant=2 μsec; (e) T_1=10 μsec, T_2=3 μsec, H_m=10.0 MHz, μ=0.5 MHz, ω_m=2 MHz, time constant=2 μsec; and (f) T_1=10 μsec, T_2=3 μsec, H_m=1 MHz, μ=2 MHz, ω_m=1 MHz, time constant=2 μsec.

d) nonadiabatic rapid passage

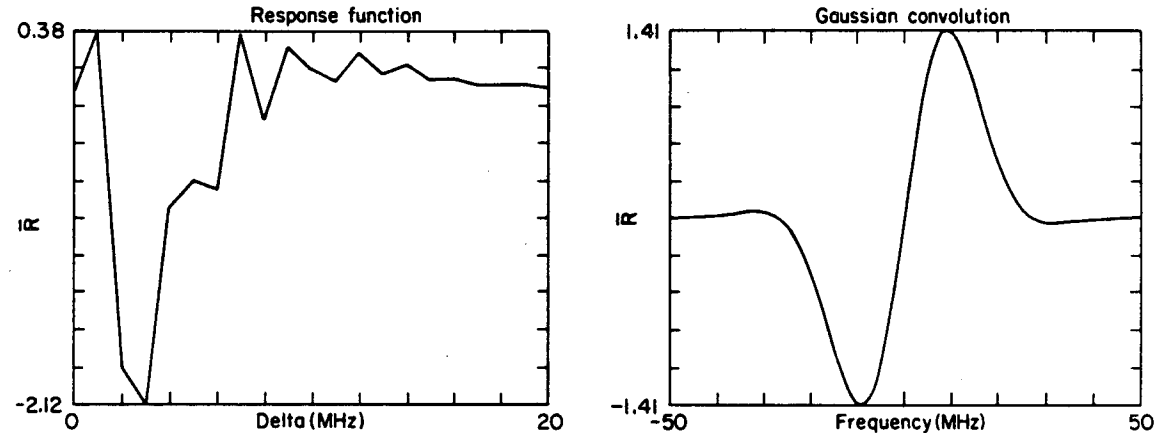

e) nonadiabatic rapid passage (extreme)

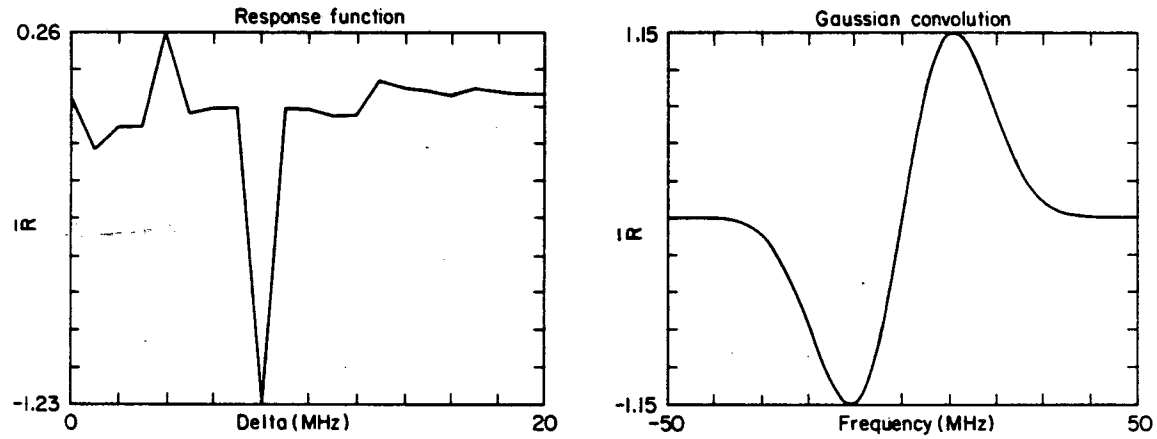

f) adiabatic rapid passage

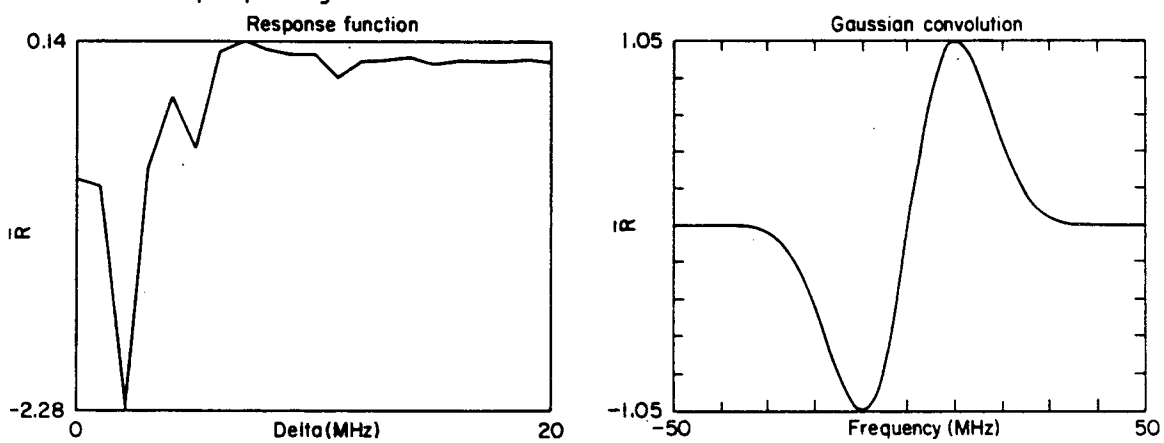

XBL 809-4342

has been possible [1,4,11]. However, in the studies on chloroplasts in chapters 4 and 5 the sensitivity with direct detection was not adequate to study the dynamics in a manner that would yield good values for the spin relaxation times. This is often the case in biological systems. These studies could probably be done on more concentrated reaction center preparations. In any case, the usefulness of magnetic field modulation techniques in determining spin relaxation times from CIDEP signals for inhomogeneously broadened lines is probably best summarized by a quote due to Abragam and given in the conclusion of the paper by Weger [9]. Abragam states that "...whenever the methods of observation are such that a complicated mathematical treatment is required to establish a relationship between the data (signals) and the physical nature of the system studied, the methods of observation are inadequate and must be changed, whenever possible."

Figure 6-3 raises an interesting question, "why aren't the CIDEP lineshapes obtained using 1 MHz field modulation and reported in chapters 4 and 5 distorted from non-adiabatic rapid passage processes?" The answer to this question in light of the discussion presented in 6.3 is probably that under the experimental conditions used to collect the data, the saturation condition was not fulfilled. A final point concerning testing for rapid passage distortion of lineshapes is that if one wishes to test for the effects using a field modulation system; either ω_m, H_m or H_1 may have to be changed by one to three orders

of magnitude before a definitive conclusion can be drawn. This is often not possible because of sensitivity constraints. Therefore, the only definitive test is to repeat the measurements using direct detection.

REFERENCES

1. Atkins. P.W., McLauchlan, K.A. and Percival, P.W. (1973) Molec. Phys. 25, 281-296.
2. Hore, P.J. and McLauchlan, K.A. (1981) Molec. Phys. 42, 533-550.
3. Pedersen, J.B. (1973) J. Chem. Phys. 59, 2656-2667.
4. Hore, P.J. and McLauchlan, K.A. (1981) Molec. Phys. 42, 1009-1026.
5. Pasimeni, L. (1978) J. Magn. Resonance 30, 65-73.
6. Birkoff, G. and Rota, G.,"Ordinary Differential Equations," Blaisdell, Boston, 1969.
7. Cesari, L., "Asymptotic Behavior and Stability Problems in Ordinary Differential Equations," Springer-Verlag, NY, 1971.
8. Portis, A.M., "Magnetic Resonance in Systems with Spectral Distributions," Technical Note No. 1 of the Sarah Mellon Scaife Laboratory, University of Pittsburgh, Nov. 15, 1955.
9. Weger, M. (1960) Bell. Syst. Tech. J. 39, 1013-1112.
10. Poole, C.P.,"Electron Spin Resonance," Wiley-Interscience, NY, 1967.
11. Trifunac, A.D., Thurnauer, M.C. and Norris, J.R. (1978) Chem. Phys. Lett. 57, 471-473.

CHAPTER 7

CONCLUSION

As mentioned in chapters 1 and 4, recent steady-state EPR measurements on PS1 reaction center particles have led to the postulation that there are two electron acceptors with g-values in the free electron region and operating in series between P-700 and X [1,2]. The results presented in this thesis are in good agreement with these findings. Further, in the course of analyzing the data presented in chapters 4 and 5, a model capable of predicting the spin-polarized EPR lineshapes of $P\text{-}700^{+}$ and A_1^{-} for both random and oriented thylakoids was developed. This model provided a means by which the EPR properties of A_0^{-} and A_1^{-} could be more fully characterized than in previous reports [1,2]. In addition, the nature of the spin-spin interactions which are a natural consequence of PS1 electron transport could be probed.

The results presented above indicate that the g-tensor of A_0^{-} is probably isotropic with a g-value of $2.0031 \pm .0003$. This g-value is consistent with A_0^{-} being a chl a or pheophytin a species. The g-tensor of A_1^{-} is probably anisotropic. In addition, this species may have an anisotropic nuclear hyperfine coupling tensor. The species can be characterized in the random and parallel orientations

as having a g-value of 2.0054± .0010 and a peak-to-peak, first derivative linewidth of 8-10.5 G. In the perpendicular orientation, A_1^- has a g-value of 2.0026 and an 8 G linewidth. These properties are consistent with A_1^- being some type of quinone species, but further characterization of A_1's spectral properties are needed before speculation about its identity can be made. These results are summarized in Fig. 7-1.

Time-resolved EPR experiments at Q-band would help pin down the EPR properties of A_1^- more fully. At Q-band the contributions from the two radicals would be almost completely separated in the random and parallel orientations if the above analysis is correct. Another feature of these experiments would be that at 12.5 kG the $\Delta g\beta H$ term would be large enough so that only net-effect spectra would be observed. This would simplify the lineshape analysis. These effects are shown in Fig. 7-2; where the random spectrum, obtained with Fe-S centers A and B reduced and X not reduced, is simulated assuming the microwave frequency to be 35 GHz. The hamiltonian and lineshape parameters in this figure are identical to those used in Fig. 4-12, only the microwave frequency has been changed. A second way in which the properties of A_1^- could be probed without interference from $P\text{-}700^+$ was presented in chapter 5. Better quality data and an adequate theoretical description of spin polarization transfer under these conditions are needed before this line of experiments can be fully exploited.

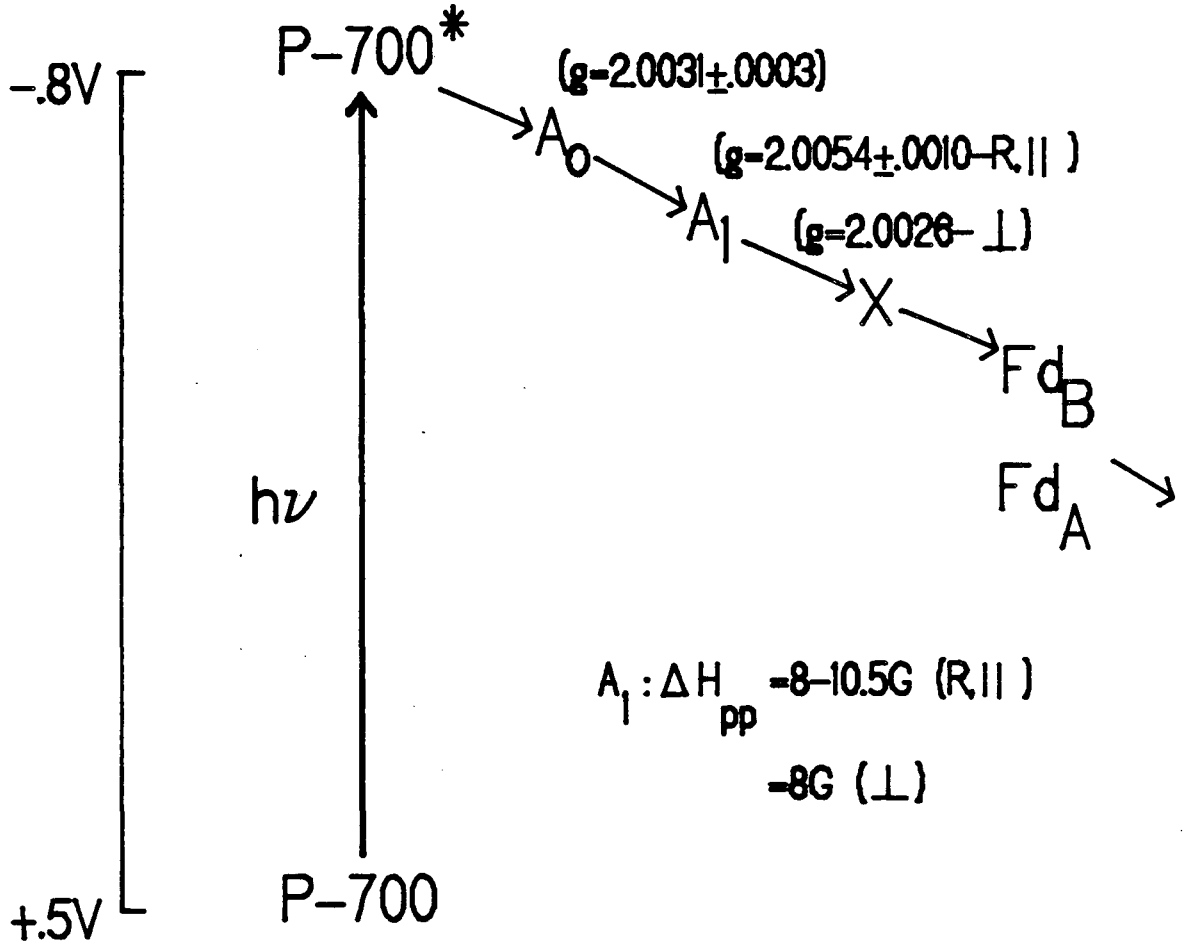

XBL 835-9844

Fig. 7-1. The photosystem 1 electron transport chain showing the addition of the A_0 species. The redox potentials of A_0 and A_1 are more negative than that of X, but are not known. [R=random, || = parallel, ⊥ = perpendicular]

Fig. 7-2. Simulation of the random spectrum of Fig. 4-12 for chloroplasts treated with ascorbate and frozen under illumination so that Fe-S centers A and B are reduced, but X is not reduced. Trace (a) shows contributions of both P-700$^+$ and A_1^- to the spectrum, and trace (b) shows the contribution of P-700$^+$ alone. The simulation conditions were: g-value of P-700$^+$, 2.0026; linewidth of P-700$^+$, 8 G; g-value of A_0^-, 2.0031; g-value of A_1^-, 2.0054; linewidth of A_1^-, 9 G; D, -50 G; J, -9.35 G; E, 0 G; and microwave frequency, 35.0 GHz.

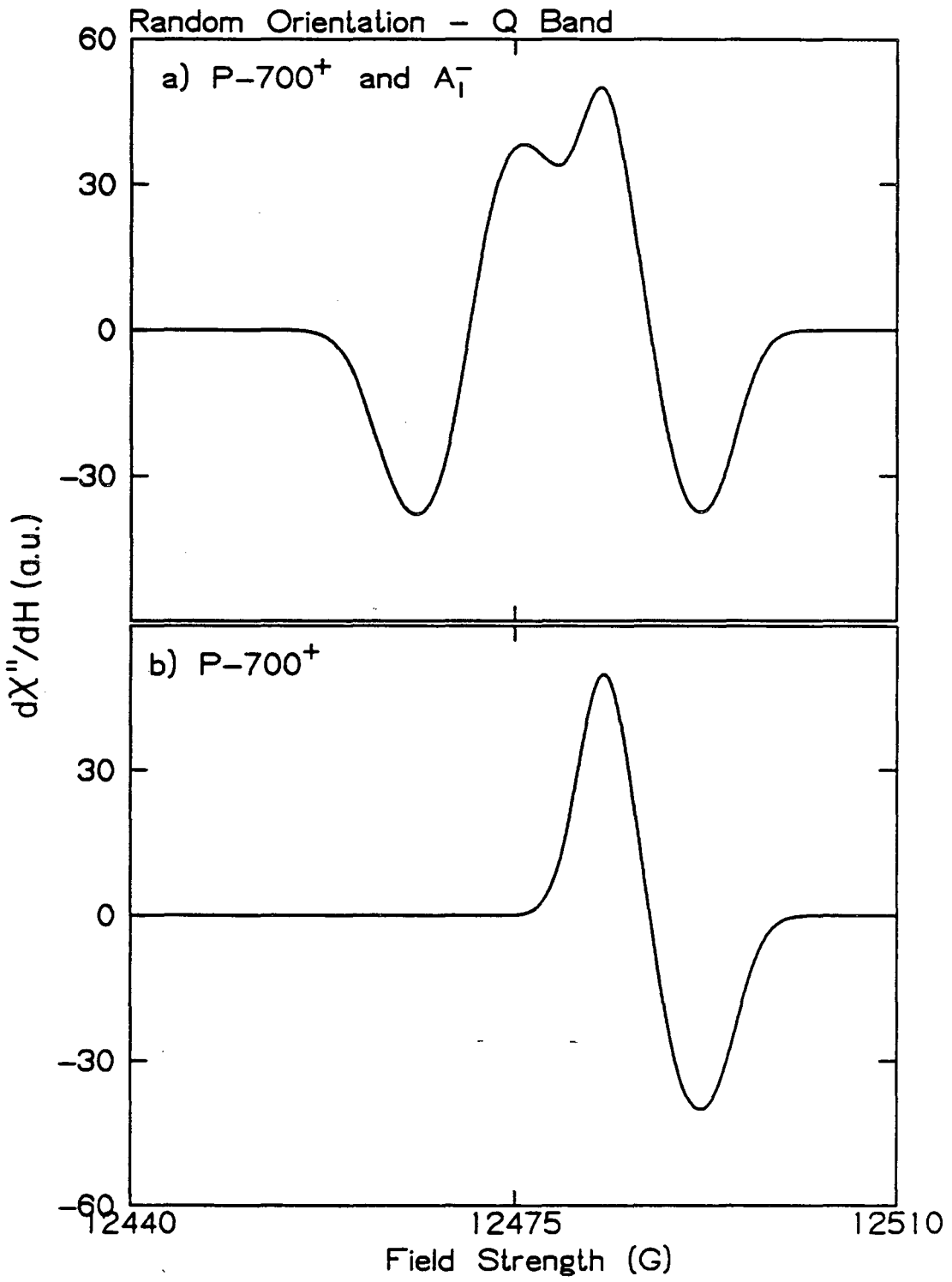
Random Orientation – Q Band
a) P–700+ and A1−
b) P–700+
60
30
0
–30
30
0
–30
–60
dX''/dH (a.u.)
12440
12475
12510
Field Strength (G)

XBL 835-9837

In addition to obtaining information about the spectral properties of A_0^- and A_1^-, information regarding the spin-spin interactions between the primary electron donor and acceptor species was also extracted from the data. In chapter 4 it was shown that the low temperature CIDEP data from PS1 was consistent with the idea that there is an electron-electron magnetic dipole interaction and an isotropic exchange interaction between P-700$^+$ and A_0^-. The values of D and J used in our simulations were in the ranges of those found for the primary radical ion pair of bacterial photosynthetic systems. However, these values were not unique, as discussed in chapter 4. A good measure of the values of D and J could be obtained by studying magnetic field effects on the yield of ^{3}P-700 [3] and by using the reaction yield detected magnetic resonance technique (RYDMAR) [4]. These experiments along with the CIDEP measurements presented in this thesis would provide a complete description of the magnetic properties associated with PS1 electron transport.

Another interesting result obtained in this work concerns the orientation of the PAS of the dipolar coupling tensor relative to the thylakoid membrane normal. It was found that the Z axis of the tensor was perpendicular to the membrane normal. This information provides an important piece to the puzzle of how the primary donor and acceptor molecules are situated with respect to each other and the membrane surface. To answer this question, additional pieces

of information must be obtained. One experiment that would help solve this problem would be to determine how the PAS of the dipolar coupling interaction involved in the ^{3}P-700 species is oriented relative to the membrane normal. Analogous experiments on bacterial photosystems have been done [5].

In 4.5 the significance of the two-site model used to describe the development of CIDEP in PS1 for experiments done at ambient temperature was examined [6,7]. It was concluded that although the model was capable of analyzing the low temperature data (considering the acceptors were A_0 and A_1 instead of A_1 and X), the magnitude of the second coupling constant was small enough that a one-site model was adequate for describing the experiments. The room temperature experiments [6] could also be described using a one-site model if the effects of an anisotropic spin-spin interaction were incorporated. The results of this work indicate that the magnetic interaction between P-700$^+$ and A_1^- is too weak to be important in the development of CIDEP in PS1.

The work presented in chapter 5 indicates that there is another spin-spin interaction that could give us information concerning PS1 reaction center structure. This is the interaction between A_0^- and A_1^-, when A_1 is reduced prior to flash excitation of the sample. Although this interaction is non-existent in normal PS1 electron transport, it could provide information concerning the structural relation

between these two acceptor species. Further characterization of this interaction will require an adequate theory of polarization transfer under these conditions.

In chapter 6, the possibility of obtaining dynamical information from time resolved EPR data was examined. The conclusion was that, for polarized radicals, the only reliable way to accomplish this task would be to use direct detection. However, the usefulness of continuous wave direct detection techniques for the study of biological samples is questionable. There are two problems which must be overcome: the low sensitivity of the technique, and the complex analysis required if the lines of interest are inhomogeneously broadened. This second problem may have the most severe consequences since it will require extension of the analyses developed for previous studies [8]. An alternative method for obtaining spin relaxation data and properly dealing with inhomogeneously broadened lines is to use pulsed EPR techniques [9]. These measurements may prove to be more useful than those made with continuous wave techniques.

REFERENCES

1. Bonnerjea, J. and Evans, M.C.W. (1982) FEBS Lett. 148, 313-316.
2. Gast, P., Swarthoff, T., Ebskamp, F.C.R. and Hoff, A.J. (1983) Biochim. Biopys. Acta 722, 163-175.
3. Roelofs, M., Chidsey, C.E.D. and Boxer, S.G. (1982) Chem. Phys. Lett. 87, 582-588.
4. Norris, J., Bowman, M., Budil, D., Tang, J., Wraight, C. and Closs, G. (1982) Proc. Natl. Acad. Sci. USA 79, 5532-5536.
5. Frank, H.A., Friesner, R., Nairn, J.A., Dismukes, G.C. and Sauer, K. (1979) Biochim. Biophys. Acta 547, 484-501.
6. Dismukes, G.C., McGuire, A.E., Blankenship, R. and Sauer, K. (1978) Biophys. J. 21, 239-256.
7. Friesner, R., Dismukes, G.C. and Sauer, K. (1979) Biophys. J. 25, 277-294.
8. Hore, P. and McLauchlan, K.A. (1981) Molec. Phys. 42, 533-550.
9. "Time Domain Electron Spin Resonance," Kevan, L. and Schwartz, R.N. eds., Wiley-Interscience, NY, 1979.

APPENDIX A

The purpose of this appendix is to show how one uses the eigenstates and eigenvalues of the hamiltonian matrix of Fig. 4-9 to calculate the time-averaged polarization on the donor cation species (Eqn. 4-10). The procedure is essentially an algebra problem and was, therefore, left out of the text of chapter 4. At the end of this appendix, a listing of the subroutines used to perform the polarization calculation and the integration of Eqn. 4-12 will be given.

Diagonalization of the hamiltonian matrix of Fig. 4-9 yields four eigenstates and eigenvalues. The eigenstates are given by:

$$
\begin{aligned}
|\phi_1\rangle &= C(1,1)\,|S\rangle + C(2,1)\,|T_0\rangle + C(3,1)\,|T_{+1}\rangle + C(4,1)\,|T_{-1}\rangle \\
|\phi_2\rangle &= C(1,2)\,|S\rangle + C(2,2)\,|T_0\rangle + C(3,2)\,|T_{+1}\rangle + C(4,2)\,|T_{-1}\rangle \\
|\phi_3\rangle &= C(1,3)\,|S\rangle + C(2,3)\,|T_0\rangle + C(3,3)\,|T_{+1}\rangle + C(4,3)\,|T_{-1}\rangle \\
|\phi_4\rangle &= C(1,4)\,|S\rangle + C(2,4)\,|T_0\rangle + C(3,4)\,|T_{+1}\rangle + C(4,4)\,|T_{-1}\rangle
\end{aligned}
\qquad \text{(A-1)}
$$

where the 'C' matrix is the matrix of eigenstate coefficients returned by the diagonalization routine (the j^{th} column of the array represents the j^{th} eigenvector). The corresponding eigenvalues are E_1 through E_4. Since $|\psi(0)\rangle = |S\rangle$, the time-dependent radical pair wavefunction is given by

$$
|\psi(t)\rangle = \sum_j \langle\phi_j|S\rangle e^{-iE_j t/\hbar} |\phi_j\rangle
$$

$$= C(1,1)e^{-iE_1 t'}|\phi_1\rangle + C(1,2)e^{-iE_2 t'}|\phi_2\rangle + C(1,3)e^{-iE_3 t'}|\phi_3\rangle + C(1,4)e^{-iE_4 t'}|\phi_4\rangle \qquad (A\text{-}2)$$

where $t'=t/\hbar$. The spin polarization on the donor cation species will be given by:

$$\rho_D(t) = 2\langle\psi(t)|S_{Dz}|\psi(t)\rangle \quad . \qquad (A\text{-}3)$$

Substituting Eqns. A-1 into A-2 and performing the operation of Eqn. A-3 yields:

$$\rho_D(t) = X_1 + \sum_{j=2}^{7} [X_j e^{i\omega_j t} + X_j^* e^{-i\omega_j t}] \qquad (A\text{-}4)$$

where

$$\omega_2 = E_1 - E_2$$
$$\omega_3 = E_1 - E_3$$
$$\omega_4 = E_1 - E_4$$
$$\omega_5 = E_2 - E_3$$
$$\omega_6 = E_2 - E_4$$
$$\omega_7 = E_3 - E_4$$

and the X_j are given by:

$$X_2 = C(1,1)^*C(2,1)^*(C(1,2))^2 + (C(1,1)^*)^2C(2,2)C(1,2) + C(3,2)C(3,1)^*C(1,2)C(1,1)^* - C(4,2)C(4,1)^*C(1,2)C(1,1)^*$$

$$X_3 = C(2,1)^*C(1,1)^*(C(1,3))^2 + (C(1,1)^*)^2C(2,3)C(1,3) + C(3,3)C(3,1)^*C(1,3)C(1,1)^* - C(4,3)C(4,4)^*C(1,3)C(1,1)^*$$

$$X_4 = (C(1,4))^2 C(1,1)^* C(2,1)^* + (C(1,1)^*)^2 C(2,4)C(1,4)$$
$$+C(3,1)^* C(3,4)C(1,1)^* C(1,4) - C(4,4)C(4,1)^* C(1,4)C(1,1)^*$$

$$X_5 = (C(1,3))^2 C(2,2)^* C(1,2)^* + (C(1,2)^*)^2 C(2,3)C(1,3)$$
$$+C(3,3)C(3,2)^* C(1,3)C(1,2)^* - C(4,3)C(4,2)^* C(1,3)C(1,2)^*$$

$$X_6 = (C(1,4))^2 C(2,2)^* C(1,2)^* + (C(1,2)^*)^2 C(2,4)C(1,4)$$
$$+C(3,4)C(3,2)^* C(1,4)C(1,2)^* - C(4,4)C(4,2)^* C(1,4)C(1,2)^*$$

$$X_7 = (C(1,4))^2 C(2,3)^* C(1,3)^* + (C(1,3)^*)^2 C(2,4)C(1,4)$$
$$+C(3,4)C(3,3)^* C(1,4)C(1,3)^* - C(4,4)C(4,3)^* C(1,4)C(1,3)^*$$

$$X_1 = X_0 + X_0^* + |C(1,1)|^2 [\,|C(3,1)|^2 - |C(4,1)|^2\,]$$
$$+ |C(1,2)|^2 [\,|C(3,2)|^2 - |C(4,2)|^2\,]$$
$$+ |C(1,3)|^2 [\,|C(3,3)|^2 - |C(4,3)|^2\,]$$
$$+ |C(1,4)|^2 [\,|C(3,4)|^2 - |C(4,4)|^2\,]$$

where

$$X_0 = |C(1,1)|^2 C(1,1)C(2,1)^* + |C(1,2)|^2 C(2,2)^* C(1,2)$$
$$+ |C(1,3)|^2 C(1,3)C(2,3)^* + |C(1,4)|^2 C(1,4)C(2,4)^* \quad .$$

Eqn. A-4 can be rearranged to the form:

$$\rho_D(t) = X_1 + \sum_{j=2}^{7} [(X_j + X_j^*)\cos\omega_j t + i(X_j - X_j^*)\sin\omega_j t] \quad (A\text{-}5)$$

Time averaging Eqn. A-5 over the radical pair lifetime, τ, is accomplished by the following integral.

$$\rho_D(\tau) = \tau^{-1} \int_0^\infty \rho_D(t) e^{-t/\tau}\, dt \quad (A\text{-}6)$$

The result of this integration is:

$$\rho_D(\tau) = X_1 + \sum_{j=2}^{7} [X_j + X_j^* + i(X_j - X_j^*)\omega_j \tau](1+\omega_j^2\tau^2)^{-1} \quad (A\text{-}7)$$

which is identical to Eqn. 4-11. The subroutine used to perform the above calculation is listed below. The routine is supplied with the hamiltonian parameters, the resonant field position, and the current values of the direction cosines through common blocks. It returns the value of the spin polarization on the donor species for the input parameter set that it receives. A flow diagram is given in Fig. 4-11.

In addition to the DIPOL subroutine, the subroutine (EPRFCN) used to perform the integration of Eqn. 4-12 for the orientation averaging is also listed.

```
      SUBROUTINE DIPOL(RHO)
C
C     CALCULATES POLARIZATION ON THE DONOR RADICAL
C     ASSUMING DIPOLAR AND EXCHANGE INTERACTIONS ARE
C     ACTIVE BETWEEN THE DONOR AND PRIMARY ACCEPTOR
C
      COMMON/HAMBLK/G1,G2,G3,J1,T1,FREQ,D1,E1,J2,T2
      COMMON/EPRBLK/ERES(100),OSC(100),H(3)
      COMMON/AA/AM,MHF,MHF2,AM2
      COMPLEX A(10),C(4,4),CN,X(7),XX,CRHO
      DIMENSION D(4),WK(32),W(7)
      REAL DCC,J1,DEN,RHO
C
C     SET UP THE HAMILTONIAN MATRIX
C
      HX=ERES(1)*H(1)
      HY=ERES(1)*H(2)
      HZ=ERES(1)*H(3)
C
      DZZ=-2.0*D1/3.0
      DXX=D1/3.0-E1
      DYY=D1/3.0+E1
C
      A(1)=J1
      A(2)=0.5*((G1-G2)*HZ+AM-AM2)
      A(3)=-J1-DXX-DYY
      A(4)=0.354*(G2-G1)*HX+(0.0,1.0)*0.354*(G1-G2)*HY
      A(5)=0.354*(G1+G2)*HX-(0.0,1.0)*0.354*(G1+G2)*HY
      A(6)=0.5*((G1+G2)*HZ+AM+AM2-DXX-DYY)-J1-DZZ
      A(7)=0.354*(G1-G2)*HX+(0.0,1.0)*0.354*(G1-G2)*HY
      A(8)=0.354*(G1+G2)*HX+(0.0,1.0)*0.354*(G1+G2)*HY
      A(9)=0.5*(-DXX+DYY)
      A(10)=-0.5*((G1+G2)*HZ+AM+AM2+DXX+DYY)-J1-DZZ
C
C
C     DIAGONALIZE THE MATRIX
C
      CALL EIGCH(A,4,1,D,C,4,WK,IER)
C
C     NORMALIZE THE EIGENVECTORS
C
      DO 10 J=1,4
         CN=(0.0,0.0)
         DO 20 I=1,4
   20       CN=CN+C(I,J)*CONJG(C(I,J))
         CN=CSQRT(CN)
         DO 30 I=1,4
   30       C(I,J)=C(I,J)/CN
   10    CONTINUE
C
```

```
C
C       SET UP CONSTANTS TO COMPUTE POLARIZATION
C
        W(2)=D(1)-D(2)
        W(3)=D(1)-D(3)
        W(4)=D(1)-D(4)
        W(5)=D(2)-D(3)
        W(6)=D(2)-D(4)
        W(7)=D(3)-D(4)



C
        TAU=T1*8.83E+06
C
        XX=C(1,1)**2*CONJG(C(1,1))*CONJG(C(2,1))
       1+C(1,2)**2*CONJG(C(2,2))*CONJG(C(1,2))
       2+C(1,3)**2*CONJG(C(1,3))*CONJG(C(2,3))
       3+C(1,4)**2*CONJG(C(1,4))*CONJG(C(2,4))
C
        X(1)=XX+CONJG(XX)+C(1,1)*CONJG(C(1,1))
       1*(C(3,1)*CONJG(C(3,1))-C(4,1)*CONJG(C(4,1)))
       2+C(1,2)*CONJG(C(1,2))*(C(3,2)*CONJG(C(3,2))
       3-C(4,2)*CONJG(C(4,2)))+C(1,3)*CONJG(C(1,3))
       4*(C(3,3)*CONJG(C(3,3))-C(4,3)*CONJG(C(4,3)))
       5+C(1,4)*CONJG(C(1,4))*(C(3,4)*CONJG(C(3,4))
       6-C(4,4)*CONJG(C(4,4)))
C
        X(2)=CONJG(C(1,1))*C(1,2)**2*CONJG(C(2,1))
       1+(CONJG(C(1,1)))**2*C(2,2)*C(1,2)+C(3,2)
       2*CONJG(C(3,1))*C(1,2)*CONJG(C(1,1))-C(4,2)*
       3CONJG(C(4,1))*C(1,2)*CONJG(C(1,1))
C
        X(3)=CONJG(C(2,1))*CONJG(C(1,1))*C(1,3)**2
       1+(CONJG(C(1,1)))**2*C(2,3)*C(1,3)+C(3,3)
       2*CONJG(C(3,1))*C(1,3)*CONJG(C(1,1))
       3-C(4,3)*CONJG(C(4,1))*C(1,3)*CONJG(C(1,1))
C
        X(4)=C(1,4)**2*CONJG(C(1,1))*CONJG(C(2,1))
       1+(CONJG(C(1,1)))**2*C(2,4)*C(1,4)+CONJG(C(3,1))
       2*C(3,4)*CONJG(C(1,1))*C(1,4)-C(4,4)*CONJG(C(4,1))
       3*C(1,4)*CONJG(C(1,1))
C
        X(5)=C(1,3)**2*CONJG(C(2,2))*CONJG(C(1,2))
       1+(CONJG(C(1,2)))**2*C(2,3)*C(1,3)+C(3,3)
       2*CONJG(C(3,2))*C(1,3)*CONJG(C(1,2))
       3-C(4,3)*CONJG(C(4,2))*C(1,3)*CONJG(C(1,2))
C
        X(6)=C(1,4)**2*CONJG(C(2,2))*CONJG(C(1,2))
       1+(CONJG(C(1,2)))**2*C(2,4)*C(1,4)+C(3,4)
       2*CONJG(C(3,2))*C(1,4)*CONJG(C(1,2))
       3-C(4,4)*CONJG(C(4,2))*C(1,4)*CONJG(C(1,2))
C
C
C
```

```
C
C
C
      X(7)=C(1,4)**2*CONJG(C(2,3))*CONJG(C(1,3))
      1+(CCNJG(C(1,3)))**2*C(2,4)*C(1,4)+C(3,4)
      2*CONJG(C(3,3))*C(1,4)*CONJG(C(1,3))
      3-C(4,4)*CONJG(C(4,3))*C(1,4)*CONJG(C(1,3))
C
      CRHO=X(1)
      DO 100 K=2,7
         DEN=1.0+(W(K)*TAU)**2
         CRHO=CRHO+(X(K)+CONJG(X(K)))/DEN+(0.0,1.0)*
      1        (X(K)-CONJG(X(K)))*W(K)*TAU/DEN
  100    CONTINUE
C
      RHO=-REAL(CRHO)
      RETURN
      END
```

```
      SUBROUTINE EPRFCN(NPNTS)
C
C
C
C       THIS ROUTINE CONTROLS THE SIMULATION.
C
C
C
      COMMON/CUTBLK/IOUT(15),ISPEC,IPT
      COMMON/TOTHFI/NTOT,NTOT2,NTOT3
      COMMON/BLK1/NSETS,IHAM,IHF,IPOL,ISHP,NTR
      COMMON/AA/AM,MHF,MHF2,AM2
      COMMON/FXSPC/HMIN,HMAX,NW,NPT,DELTA(10)
      COMMON/EPRBLK/ERES(100),OSC(100),H(3)
      COMMON/PTBLK/HPNT(20),AMPL(20),DPDH(1000)
      COMMON/SPECBL/ABSP(1000),DIDH(1000)
        COMMON/WW/WEIGHT,WT1,WT2,WT3
        COMMON/HAMBLK/G1,G2,G3,J1,T1,FREQ,D1,E1,J2,T2
        COMMON/ANGBLK/THETA,PHI,SPANG,FIXOM,NOR1,NOR2
        REAL J1,J2,PROB,COVAL
C
C
C       ZERO THE ABSORPTION AND DERIVATIVE ARRAYS.
      DO 1 I=1,1000
      ABSP(I)=0.0
      DIDH(I)=0.0
    1 CONTINUE
        PROB=1.0
        RHOSUM=0.0
        PI=3.14159
        ERES(2)=0.0
        OSC(2)=0.0
        IF(IHAM.LT.3) THEN
           NOR1=1
           NOR2=1
        END IF
        C1=PI/(6.0*FLOAT(NOR1))
        C2=PI/(6.0*FLOAT(NOR2))
C       NOW LOOP OVER HYPERFINE STATES OF RADICAL
        DO 40 MHF=1,NTOT
           ERES(1)=(7.1455E-07*FREQ)/G1
           OSC(1)=1.0
           WEIGHT=1.0
           CALL HFSET
           WEIGHT=WT1
C          CORRECT ERES W/HYPERFINE ENERGY
           CALL HFEN
C
C
C
C
C
```

```
C
C          WEIGHT OSCILLATOR STRENGTHS OF HF LINE
C          BY POLARIZATION IF NECCESSARY
C          INTEGRATE OVER THETA AND PHI TO DETERMINE
C          POLARIZATION FOR THESE HF COMPONENTS
           IF(IHAM.EQ.1)THEN
              GO TO 29
           ELSE IF(IHAM.EQ.2)THEN
              RHOBAR=0.0
              DO 45 MHF2=1,NTOT2
                 CALL HFSET2
                 CALL SPOL(RHO)

   45            RHOBAR=RHOBAR+WT2*RHO
              OSC(1)=RHOBAR
C             SET RUNNING TOTAL OF RHO VALUES
              RHOSUM=RHOSUM+RHOBAR
              GO TO 29
           END IF
           CMWT=0.0
           DO 410 IOR1=1,NOR1
C             DIVIDE OMEGA INCR INTO EQUAL COS INTERVALS
              COVAL=1.0-FLOAT(IOR1-1)/FLOAT(NOR1-1)
              OMEGA=ACOS(COVAL)
C             COMPUTE MOSIAC SPREAD WEIGHTING
              IF(IPOL.EQ.2) THEN
                 PROB=(EXP(-1.0*(OMEGA-FIXOM)**2/SPANG**2))/SPANG
                 PROB=PROB*SIN(OMEGA)
              ELSE IF(IPOL.EQ.3) THEN
                 PROB=SIN(OMEGA)
              END IF
              AIWT=0.0
              DO 420 IOR2=1,NOR2
                 ALPHA=FLOAT(IOR2-1)*PI/(2.0*FLOAT(NOR2-1))
C                SET DIRECTION COSINES  FOR DIPOL ROUTINE
                    CALL ANGCALC(OMEGA,ALPHA,IPOL)
C                LOOP OVER HF STATES OF ACCEPTOR RADICAL TO
C                COMPUTE INTEGRAND
C
                 RHOBAR=0.0
                 DO 430 MHF2=1,NTOT2
                    CALL HFSET2
                    CALL DIPOL(RHO)
                    RHOBAR=RHOBAR+WT2*RHO
  430               CONTINUE
C                SUM OVER PHI
                 I2=IOR2-1
                 IF(I2.EQ.0.OR.IOR2.EQ.NOR2) THEN
                   AIWT=AIWT+RHOBAR
                   GO TO 420
                 ELSE IF(MOD(I2,2).EQ.1) THEN
                   AIWT=AIWT+4.0*RHOBAR
                   GO TO 420
                 ELSE
                   AIWT=AIWT+2.0*RHOBAR
                 END IF
  420            CONTINUE
```

```
C
              ALWT=C2*ALWT*PROB
              I1=ICR1-1
              IF(I1.EQ.0.OR.IOR1.EQ.NCR1) THEN
                  OMWT=OMWT+ALWT
                  GO TO 410
              ELSE IF(MOD(I1,2).EQ.1) THEN
                  OMWT=OMWT+4.0*ALWT
                  GO TO 410
              ELSE
                  OMWT=OMWT+2.0*ALWT
              END IF
  410         CONTINUE
C         STORE POLARIZATION FOR THIS HF COMBONATION


          OSC(1)=C1*OMWT
          WRITE(6,908)ERES(1),AM
  908     FORMAT('0ERES(1)=',F8.2,5X,'AM=',F8.4)
          WRITE(6,909)(OSC(I),I=1,NTR)
  909     FORMAT('0CSC(I)=',2(F8.4,5X))
          RHOSUM=RHOSUM+C1*OMWT
C         STORE THE RESULTS IN ABSP ARRAY
    29    IF(IOUT(9).EQ.3)GO TO 40
          CALL SPCTRM
          IF(IPT.NE.1)CALL PTAMP
    40    CONTINUE
C
C         GENERATE SPECTRUM OF DYNAMICALLY POLARIZED
C         COUNTER RADICAL IF DESIRED
C
          IF(IHF.EQ.4.AND.IOUT(9).NE.2)CALL DYNSPC(RHOSUM)
C
C         GENERATE DERIVATIVE SPECTRUM
C
          IF(IOUT(10).EQ.1) THEN
          NPTS=NPNTS-4
          DO 110 I=4,NPTS
             DIDH(I)=(ABSP(I+3)-ABSP(I-3))/2.0
  110        CONTINUE
          ELSE IF(IOUT(10).EQ.2)THEN
             NPTS=NPNTS-5
             DO 111 I=5,NPTS
  111           DIDH(I)=(ABSP(I+4)-ABSP(I-4))/2.0
          ELSE IF(IOUT(10).EQ.3)THEN
             NPTS=NPNTS-8
             DO 112 I=8,NPTS
  112           DIDH(I)=(ABSP(I+8)-ABSP(I-8))/2.0
          END IF
  999  CONTINUE
       RETURN
         END
```

APPENDIX B

The time-dependent polarization on the donor cation for the two-site model described in chapter 4 is given in Eqn. 4-26. To determine the time-averaged polarization, the expression must be integrated over time using Eqn. 4-27. Before this integration can be done the radical pair wavefunction coefficients, $C_S(t_1)$, $C_T(t_1)$, $C_+(t_1)$, and $C_-(t_1)$, must be determined in terms of the eigenvalues and eigenvectors of the hamiltonian that described the first radical pair, $P\text{-}700^+A_0^-$. This hamiltonian is identical to the one used in the one-site case, so that the procedure for doing this is identical to that outlined in appendix A. The time-averaged polarization for the two-site model is given by:

$$\begin{aligned}\rho_D(\tau_1,\tau_2) = K_{10} &+ \sum_{j=1}^{6} [(K_{1j}+K_{1j}^*)+i\varepsilon_j\tau_1(K_{1j}-K_{1j}^*)]/D(1) \\ &-4J_2{}^2\tau_2{}^2/D(2) \\ &\cdot[K_{20}+ \sum_{j=1}^{6} (K_{2j}+K_{2j}^*+i\varepsilon_j\tau_1(K_{2j}-K_{2j}^*))/D(1)] \\ &+4J_2H_2\tau_2{}^2/D(2) \\ &\cdot[K_{30}+ \sum_{j=1}^{6} (K_{3j}+K_{3j}^*+i\varepsilon_j\tau_1(K_{3j}-K_{3j}^*))/D(1)] \\ &+2iJ_2\tau_2/D(2) \\ &\cdot[K_{40}+ \sum_{j=1}^{6} (K_{4j}+K_{4j}^*+i\varepsilon_j\tau_1(K_{4j}-K_{4j}^*))/D(1)]\end{aligned}$$

where

$$D(1) = 1 + \varepsilon_j^2 \tau_1^2$$
$$D(2) = 1 + 4\omega_2^2 \tau_2^2$$

and the K_{1j} are constants which consist of linear combinations of the eigenvector coefficients obtained from diagonalization of the hamiltonian matrix of Fig. 4-9. The K_{1j} are defined in the program listing below. The ε_j are the eigenvalue differences and are identical to the ω_j of Eqn. A-4. The subroutine that was incorporated into the simulation program to evaluate the above expression and also calculate the polarization on the secondary acceptor species, A_1^-, was named TWODIPOL and is listed below.

To incorporate this routine into the simulation program described in chapter 4, the subroutine which performs the integration needed for the orientation averaging was modified so that two integrations, one for the donor cation and a second for the acceptor anion, could be performed simultaneously. The two-site model differs from the one-site model in that the polarization is calculated for each species simultaneously according to Eqns. 4-26 and 4-28 (in the one-site case the net polarization on the donor ion must be determined before the acceptor ion spectrum can be simulated).

```
      SUBROUTINE TWODIPOL(RHOD,RHOA)
C
C     THIS ROUTINE CALCULATES THE SPIN POLARIZATION
C     ON BOTH THE DONOR AND SECONDARY ACCEPTOR
C     WHEN DIPOLAR COUPLING EXISTS BETWEEN THE FIRST
C     RADICAL PAIR IONS.
C
      COMMON/HAMBLK/G1,G2,G3,J1,T1,FREQ,D1,E1,J2,T2
      COMMON/EPRBLK/ERES(100),OSC(100),H(3)
      COMMON/AA/AM,MHF,MHF2,AM2
      COMMON/AA3/MHF3,AM3
C
      COMPLEX A(10),C(4,4),CN,K(5,7),KK,RHO(5),CDEN,CRHOD
      DIMENSION D(4),WK(32),W(7)
      REAL J1,J2,RHOD,RHOA
C
C     SET UP HAMILTONIAN MATRIX OF THE FIRST RADICAL
C     PAIR
C
      HX=ERES(1)*H(1)
      HY=ERES(1)*H(2)
      HZ=ERES(1)*H(3)
C
      DZZ=-2.0*D1/3.0
      DXX=D1/3.0-E1
      DYY=D1/3.0+E1
C
      A(1)=J1
      A(2)=0.5*((G1-G2)*HZ+AM-AM2)
      A(3)=-J1-DXX-DYY
      A(4)=.354*(G2-G1)*HX+(0.0,1.0)*0.354*(G1-G2)*HY
      A(5)=.354*(G1+G2)*HX-(0.0,1.0)*0.354*(G1+G2)*HY
      A(6)=0.5*((G1+G2)*HZ+AM+AM2-DXX-DYY)-J1-DZZ
      A(7)=.354*(G1-G2)*HX+(0.0,1.0)*0.354*(G1-G2)*HY
      A(8)=0.354*(G1+G2)*HX+(0.0,1.0)*0.354*(G1+G2)*HY
      A(9)=0.5*(-DXX+DYY)
      A(10)=-0.5*((G1+G2)*HZ+AM+AM2+DXX+DYY)-J1-DZZ
C
C     DIAGONAIZE MATRIX
C
      CALL EIGCH(A,4,1,D,C,4,WK,IER)
C
C     NORMAIZE THE EIGENVECTORS
C
      DO 10 J=1,4
         CN=(0.0,0.0)
         DO 20 I=1,4
20          CN=CN+C(I,J)*CONJG(C(I,J))
         CN=CSQRT(CN)
         DO 30 I=1,4
30          C(I,J)=C(I,J)/CN
10       CONTINUE
C
```

```
C
C       SET UP CONSTANTS TO COMPUTE POLARIZATION
C
        W(2)=D(1)-D(2)
        W(3)=D(1)-D(3)
        W(4)=D(1)-D(4)



        W(5)=D(2)-D(3)
        W(6)=D(2)-D(4)
        W(7)=D(3)-D(4)
C
        TT1=T1*6.83E+06
        TT2=T2*6.83E+06
        H2=0.5*((G1-G3)*ERES(1)+AM-AM3)
        W2=SQRT(H2**2+J2**2)
        ST1=TT1**2
        ST2=TT2**2
        SW2=W2**2
        DEN2=1.0+4.0*SW2*ST2
C
C       SET UP THE K ARRAY OF CONSTANTS
C
        KK=(0.0,0.0)
        DO 55 I=1,4
           KK=KK+(CONJG(C(1,I)))**2*C(1,I)*C(2,I)
   55      CONTINUE
        K(1,1)=KK+CONJG(KK)
        DO 60 II=1,4
           K(1,1)=K(1,1)+CONJG(C(1,II))*C(1,II)*(CONJG(C(3,II))
        1          *C(3,II)-CONJG(C(4,II))*C(4,II))
   60      CONTINUE
C
        K(1,2)=CONJG(C(1,1))*C(1,2)*(CONJG(C(1,1))*C(2,2)
        1       +CONJG(C(2,1))*C(1,2)+CONJG(C(3,1))*C(3,2)
        2       -CONJG(C(4,1))*C(4,2))
C
        K(1,3)=CONJG(C(1,1))*C(1,3)*(CONJG(C(1,1))*C(2,3)
        1       +CONJG(C(2,1))*C(1,3)+CONJG(C(3,1))*C(3,3)
        2       -CONJG(C(4,1))*C(4,3))
C
        K(1,4)=CONJG(C(1,1))*C(1,4)*(CONJG(C(1,1))*C(2,4)
        1       +CONJG(C(2,1))*C(1,4)+CONJG(C(3,1))*C(3,4)
        2       -CONJG(C(4,1))*C(4,4))
C
        K(1,5)=CONJG(C(1,2))*C(1,3)*(CONJG(C(2,2))*C(1,3)
        1       +CONJG(C(1,2))*C(2,3)+CONJG(C(3,2))*C(3,3)
        2       -CONJG(C(4,2))*C(4,3))
C
        K(1,6)=CONJG(C(1,2))*C(1,4)*(CONJG(C(1,2))*C(2,4)
        1       +CONJG(C(2,2))*C(1,4)+CONJG(C(3,2))*C(3,4)
        2       -CONJG(C(4,2))*C(4,4))
C
        K(1,7)=CONJG(C(1,3))*C(1,4)*(CONJG(C(1,3))*C(2,4)
        1       +CONJG(C(2,3))*C(1,4)+CONJG(C(3,3))*C(3,4)
        2       -CONJG(C(4,3))*C(4,4))
C
C
```

```
C
      K(2,1)=KK+CONJG(KK)
      K(2,2)=CONJG(C(1,1))*C(1,2)*(CONJG(C(1,1))*C(2,2)
     1       +CONJG(C(2,1))*C(1,2))
      K(2,3)=CONJG(C(1,1))*C(1,3)*(CONJG(C(1,1))*C(2,3)
     1       +CONJG(C(2,1))*C(1,3))
      K(2,4)=CONJG(C(1,1))*C(1,4)*(CONJG(C(1,1))*C(2,4)
     1       +CONJG(C(2,1))*C(1,4))
      K(2,5)=CONJG(C(1,2))*C(1,3)*(CONJG(C(1,2))*C(2,3)


     1       +CONJG(C(2,2))*C(1,3))
      K(2,6)=CONJG(C(1,2))*C(1,4)*(CONJG(C(1,2))*C(2,4)
     1       +CONJG(C(2,2))*C(1,4))
      K(2,7)=CONJG(C(1,3))*C(1,4)*(CONJG(C(1,3))*C(2,4)
     1       +CONJG(C(2,3))*C(1,4))
C
C
      K(3,1)=(0.0,0.0)
      DO 70 I=1,4
         K(3,1)=K(3,1)+(CONJG(C(1,I))*C(1,I))**2
     1          -CONJG(C(1,I))*C(1,I)*CONJG(C(2,I))*C(2,I)
   70    CONTINUE
C
      K(3,2)=CONJG(C(1,1))*C(1,2)*(CONJG(C(1,1))*C(1,2)
     1       -CONJG(C(2,1))*C(2,2))
      K(3,3)=CONJG(C(1,1))*C(1,3)*(CONJG(C(1,1))*C(1,3)
     1       -CONJG(C(2,1))*C(2,3))
      K(3,4)=CONJG(C(1,1))*C(1,4)*(CONJG(C(1,1))*C(1,4)
     1       -CONJG(C(2,1))*C(2,4))
      K(3,5)=CONJG(C(1,2))*C(1,3)*(CONJG(C(1,2))*C(1,3)
     1       -CONJG(C(2,2))*C(2,3))
      K(3,6)=CONJG(C(1,2))*C(1,4)*(CONJG(C(1,2))*C(1,4)
     1       -CONJG(C(2,2))*C(2,4))
      K(3,7)=CONJG(C(1,3))*C(1,4)*(CONJG(C(1,3))*C(1,4)
     1       -CONJG(C(2,3))*C(2,4))
C
C
      K(4,1)=CONJG(KK)-KK
      K(4,2)=CONJG(C(1,1))*C(1,2)*(CONJG(C(2,1))*C(1,2)
     1       -CONJG(C(1,1))*C(2,2))
      K(4,3)=CONJG(C(1,1))*C(1,3)*(CONJG(C(2,1))*C(1,3)
     1       -CONJG(C(1,1))*C(2,3))
      K(4,4)=CONJG(C(1,1))*C(1,4)*(CONJG(C(2,1))*C(1,4)
     1       -CONJG(C(1,1))*C(2,4))
      K(4,5)=CONJG(C(1,2))*C(1,3)*(CONJG(C(2,2))*C(1,3)
     1       -CONJG(C(1,2))*C(2,3))
      K(4,6)=CONJG(C(1,2))*C(1,4)*(CONJG(C(2,2))*C(1,4)
     1       -CONJG(C(1,2))*C(2,4))
      K(4,7)=CONJG(C(1,3))*C(1,4)*(CONJG(C(2,3))*C(1,4)
     1       -CONJG(C(1,3))*C(2,4))
C
```

```
C
      K(5,1)=(0.0,0.0)
      DO 72 I=1,4
         K(5,1)=K(5,1)+CONJG(C(1,I))*C(1,I)*(CONJG(C(3,I))
     1          *C(3,I)-CONJG(C(4,I))*C(4,I))
   72    CONTINUE
C
      K(5,2)=CONJG(C(1,1))*C(1,2)*(CONJG(C(3,1))*C(3,2)
     1       -CONJG(C(4,1))*C(4,2))
      K(5,3)=CONJG(C(1,1))*C(1,3)*(CONJG(C(3,1))*C(3,3)
     1       -CONJG(C(4,1))*C(4,3))
      K(5,4)=CONJG(C(1,1))*C(1,4)*(CONJG(C(3,1))*C(3,4)
     1       -CONJG(C(4,1))*C(4,4))
      K(5,5)=CONJG(C(1,2))*C(1,3)*(CONJG(C(3,2))*C(3,3)
     1       -CONJG(C(4,2))*C(4,3))
      K(5,6)=CONJG(C(1,2))*C(1,4)*(CONJG(C(3,2))*C(3,4)
     1       -CONJG(C(4,2))*C(4,4))



      K(5,7)=CONJG(C(1,3))*C(1,4)*(CONJG(C(3,3))*C(3,4)
     1       -CONJG(C(4,3))*C(4,4))
C
C     CALCULATE DONOR RADICAL POLARIZATION
C
      DO 75 I=1,5
   75    RHO(I)=K(I,1)
      DO 80 I=1,5
         DO 90 J=2,7
            CDEN=1.0+W(J)**2*ST1
            RHO(I)=RHO(I)+(K(I,J)+CONJG(K(I,J))+(0.0,1.0)
     1             *W(J)*TT1*(K(I,J)-CONJG(K(I,J))))/CDEN
   90       CONTINUE
   80    CONTINUE
C
      CRHOD=RHO(1)-4.0*J2**2*ST2*RHO(2)/DEN2+4.0*J2*H2*ST2
     1      *RHO(3)/DEN2+(0.0,1.0)*2.0*J2*TT2*RHO(4)/DEN2
      RHOD=REAL(CRHOD)
      RHOA=-RHOD+2.0*REAL(RHO(5))
      RHOD=-RHOD
      RHOA=-RHOA
      RETURN
      END
```

APPENDIX C

In this appendix it will be shown that the average response function, $\bar{R}(\delta)$, of Eqn. 6-19 is antisymmetric, i.e. $\bar{R}(\delta) = -\bar{R}(-\delta)$. If one sets $\Delta(\delta,t) = \delta + H_m \cos \omega_m t$, the Bloch equations can be rewritten as

$$\begin{aligned} dS_x/dt &= -S_x/T_2 + \Delta(\delta,t)S_y \\ dS_y/dt &= -S_y/T_2 - \Delta(\delta,t)S_x + \mu S_z \\ dS_z/dt &= -(S_0 - S_z)/T_1 - \mu S_y \quad . \end{aligned} \tag{C-1}$$

If $\underset{\sim}{S}(t) = (S_x(t), S_y(t), S_z(t))$ is a solution to the above equations then $\underset{\sim}{S}'(t) = (-S_x(t), S_y(t), S_z(t))$ is a solution when Δ goes to $-\Delta$. In other words

$$\begin{aligned} dS_x'/dt &= -S_x'/T_2 - \Delta(\delta,t)S_y' \\ dS_y'/dt &= -S_y'/T_2 + \Delta(\delta,t)S_x' + \mu S_z' \\ dS_z'/dt &= (S_0 - S_z')/T_1 - \mu S_y' \end{aligned} \tag{C-2}$$

making the subtitutions $S_x' = -S_x$, $S_y' = S_y$, and $S_z' = S_z$ one obtains Eqn. C-1. Utilizing the properties of the cosine function one finds

$$\begin{aligned} -\Delta(\delta,t) &= -\delta - H_m \cos \omega_m t \\ &= -\delta + H_m \cos \omega_m t' \end{aligned}$$

where $t' = t + \pi/\omega_m$. Then $-\Delta(\delta,t) = \Delta(-\delta, t+\pi/\omega_m)$ and

$$S_y(\delta,\phi,t) = S_y(-\delta,\phi,t+\pi/\omega_m) \quad . \tag{C-3}$$

The response function at a given δ and ϕ is given by

$$R(\delta,\phi) = \int S_y(\delta,\phi,t)\cos\omega_m t \, dt \tag{C-4}$$

where the phase angle between the reference and signal at the phase sensitive detector is taken to be 0^o as discussed in chapter 6. For $-\delta$ one obtains

$$R(-\delta,\phi) = \int S_y(-\delta,\phi,t)\cos\omega_m t \, dt \quad . \tag{C-5}$$

Substituting Eqn. C-3 into C-4 and using Eqn. C-5 one finds

$$\begin{aligned} R(-\delta,\phi) &= \int S_y(-\delta,\phi,t+\pi/\omega_m)\cos(\omega_m t+\pi)\, dt \\ &= \int S_y(\delta,\phi,t)\cos(\omega_m t+\pi)\, dt \\ &= -\int S_y(\delta,\phi,t)\cos\omega_m t \, dt \\ &= -R(\delta,\phi) \end{aligned}$$

Integration over ϕ yields the result,

$$\bar{R}(\delta) = -\bar{R}(-\delta) \quad . \tag{C-6}$$

TECHNICAL INFORMATION DEPARTMENT
LAWRENCE BERKELEY LABORATORY
UNIVERSITY OF CALIFORNIA
BERKELEY, CALIFORNIA 94720